Functionalized Conjugated Polymers for Signal Amplifying Biosensors and Sensor Arrays

by

Kangwon Lee

A dissertation submitted in partial fulfillment
of the requirements for the degree of
Doctor of Philosophy
(Materials Science and Engineering)
in The University of Michigan
2008

Doctoral Committee:

Assistant Professor Jinsang Kim, Chair
Professor Erdogan Gulari
Professor David C. Martin
Associate Professor Megan S. Lim

To my family for their support and love

ACKNOWLEDGMENTS

It is really difficult to list all the people who have helped me along the way during the long journey toward this point of my academic career. First of all, I would like to give my sincere acknowledgements to my supervisor, Professor Jinsang Kim for his guidance, support, and especially patience during my whole doctoral study. He led me to this fabulous world of photophysics and conjugated polymers, which I hardly knew anything about before I joined his group. His enthusiasm in science always encouraged me to keep on pursuing many interesting research topics. I also would like to appreciate my committee members; Professor Erdogan Gulari, Professor David Martin, and Professor Megan, S. Lim for their valuable suggestions and comments on my research. I thank Ilju foundation, Korea for Ilju fellowship for last four years.

I really want to thank microarray team including Dr. Jean-Marie Rouillard, Trinn Pham and Dr. Suparna Mandal. Especially, Jean-Marie greatly helped me study DNA microarray technique with valuable suggestions. I also appreciate the invaluable help of Kojo Elenitoba-Johnson, Charles Seiler and Adam Kronk in pathology department regarding cell-staining test. I have enjoyed collaborating with Professor Darrin Pochan and Tuna Yucel in polymer characterization. I also would like to thank current and past group members. Kim group is a great group to work in. All of them always gave me their support and advice. Korean graduate students of MSE, Macro and ChemE departments at Michigan have made my time profitable.

I owe a great deal to my Lord, Jesus Christ. I also thank all of my friends of Korean Bible Church of Ann Arbor for their love and support. Especially, I will not forget enjoyable time with Seunghyun, Ilju, and Taeil family eternally.

Finally, I would love to thank all my family members including my parents, my sister, my parents in law and two sisters in law. Without unconditional love, support, and prayer from all of my family members, I could never have achieved this goal. Finally, I deeply thank my lovely wife, Eunjoo, my son, Minseo, and my cute daughter, Yeseo for their love, patience and support. I specially dedicate this work to Eunjoo with love from the bottom of my heart.

TABLE OF CONTENTS

DEDICATION..... ii

ACKNOWLEDGMENTS..... iii

LIST OF FIGURES……..…….....x

LIST OF SCHEMES…….……..…….xviii

LIST OF TABLES……...xx

ABSTRACT…….xxi

CHAPTER 1. Introduction and Background……...……..1

1.1. Conjugated Polymers……...…….…….……...2

1.2. Optoelectronic Property of CPs……...……..…...4

1.3. Sensory Signal Amplification of CPs……...……7

1.4. Energy and Electron Transfer of CPs……...…8

1.5. Signal Transduction Modes of CPs……...……..14

1.5.1. Turn-on Mode……...…….15

1.5.2. Turn-off Mode……...…19

1.5.3. Fluorescence Color Change Mode…….…22

1.6. Objectives…….……..29

1.7. References……...……31

CHAPTER 2. Modulating the Side-chain Design of Poly(*p*-phenyleneethynylene) Derivatives to Make Water-Soluble and Highly Emissive Conjugated Polyelectrolytes……....35

2.1. Abstract……...……..……..36

2.2. Introduction……...……..37

2.3. Experimental Section..……..……..39

2.3.1. General Methods……...…….39

2.3.2. Synthesis and Characterization……...……...…… 41

2.4. Results and Discussion……....……...……49

2.5. Conclusion.……...……..60

2.6. References……...……....61

CHAPTER 3. Synthesis and Functionalization of a Highly Fluorescent and Completely Water Soluble Poly(*para*-phenyleneethynylene) Copolymer for Bioconjugation……..……...66

3.1. Abstract……...……....67

3.2. Introduction……...……..68

3.3. Experimental Section……..……69

3.3.1. Materials and Methods……..69

3.3.2. Synthesis of 2,5-Diiodo-1,4-dimethoxybenzene……...70

3.3.3. Synthesis of 1,4-Diiodo-2,5-hydroquinone……71

3.3.4. Synthesis of 1.3-Bis(3,6,9-trioxadecanyl)glycerol-2-toluenesulfonic ester……..……..71

3.3.5. Synthesis of 1,4-Bis(1,3-bis(3,6,9-trioxadecyl)-2-glyceryl)2,5-diiodobenzene……...……..72

3.3.6. Synthesis of (2,5-Bis(2,5,8,11,15,18,21,24-octaoxapentacosan-13-yloxy)-1,4-phenylene)bis(ethyne-2,1-diyl)bis(trimethylsilane)……....73

3.3.7. Synthesis of Monomer……...……...73

3.3.8. Synthesis of 1,4-Disodiumpropanesulfonoxy-2,5-diiodobenzene…....74

3.3.9. Synthesis for PPE-R_1 and PPE-R_1-COOH……75

3.4. Results and Discussion……..……75

3.5. Conclusions……...…….…….82

3.6. References……...82

CHAPTER 4. Label-Free and Self-Signal Amplifying Molecular DNA Sensors Based on Bioconjugated Polyelectrolytes …….……..…...85

4.1. Abstract…….……..86

4.2. Introduction……...……..……87

4.3. Experimental Section.....91

4.4. Results and Discussion……...……...…….....94

4.5. Conclusion.……...……..…….…107

4.6. References……...……..……107

CHAPTER 5. Conjugated Polyelectrolyte-Antibody Hybrid Molecules for Live Cell-Imaging……...112

5.1. Abstract……..……...……..……..113

5.2. Introduction……...……...……...……..114

5.3. Experimental Section.…….……...……..…116

5.4. Results and Discussion…….126

5.5. Conclusion...……...……..142

5.6. References……...……..142

CHAPTER 6. Chemically and Photochemically Stable Conjugated Poly(oxadiazole) Derivatives: A Comparison with Polythiophenes and Poly(*p*-phenyleneethynylenes)……...145

6.1. Abstract……...……..146

6.2 Introduction……....147

6.3. Experimental Section...……...……...…149

6.4. Results and discussion……...……..153

6.5. Conclusion.……...…..……...165

6.6. References……...……..….166

CHAPTER 7. Signal-Amplifying Conjugated Polymer-DNA Hybrid Chips….....170

7.1. Abstract……..……...171

7.2. Introduction……...……...…….172

7.3. Experimental Section……...……173

7.3.1. **P1** Synthesis…….……...……173

7.3.2. DNA Chip Fabrication……...……..179

7.3.3. Hybridization Test……...…...181

7.4. Results and Discussion……..…...184

7.5. Conclusion…...……...…….191

7.6. References……...……..192

CHAPTER 8. Sensitive and Selective Label-free DNA Detection by Conjugated Polymer-based Microarray and Intercalating Dye…….....195

8.1. Abstract…….……...……..……...196

8.2. Introduction……...……...…….197

8.3. Experimental Section……...……199

8.4. Results and Discussion……...……...…...202

8.5. Conclusion…...……...…….211

8.6. References……...……..211

CHAPTER 9. Label-Free and Self-Signal Amplifying "Molecular Beacon" Biosensors using Conjugated Polymers……..….....213

9.1. Abstract……...…….……..……...214

9.2. Introduction……...……...…….215

9.3. Experimental Section……...…….217

9.4. Results and Discussion……...……...…...224

9.5. Conclusion…...……...…….…238

9.6. References……...……..240

CHAPTER 10. Label-Free Identification of Prostate-Specific Antigen using Conjugated Polymer-Peptide Hybrid Chips……..….....242

10.1. Abstract……...…….……..……...243

10.2. Introduction……...……..……...…….244

10.3. Experimental Section……...……..…….246

10.4. Results and Discussion……...……..……...…...250

10.5. Conclusion…...……...……..…….257

10.6. References……...……..……..258

CHAPTER 11. Summary and Future Prospective….…...……...….....260

11.1. Research Summary…..……..……..……...261

11.2. Future Consideration…….…...……...…….265

LIST OF FIGURES

Figure 1-1. Chemical structure of various conjugated polymers ……...….....3

Figure 1-2. Examples of water-soluble CPs used in biosensor applications …….....….4

Figure 1-3. Jablonski diagram ……..……..5

Figure 1-4. Factors governing the optoelectronic properties of CPs ….……...……..7

Figure 1-5. Signal amplification of CPs ……..……...8

Figure 1-6. Photo-induced electron transfer …….9

Figure 1-7. Energy transfer mechanism ……..……..…10

Figure 1-8. Schematic representation of the FRET spectral overlap integral ……...…12

Figure 1-9. Schematic representation of a molecular beacon…….....13

Figure 1-10. Synthesis of quenched peptide fluorogenic substrate ……...……..16

Figure 1-11. Schematic representation of the PPE-labeled molecular beacon……...…..17

Figure 1-12. Schematic description of the formation of polythiophene/single-stranded nucleic acid duplex and polythiophene/hybridized nucleic acid triplex forms ….19

Figure 1-13. General scheme for the quencher-tether-ligand (QTL) protease assay...….20

Figure 1-14. Schematic illustration of exciton quenching by bound dye molecules. (a) high polymer/dye concentration ratio. Some excitons are quenched rapidly and others more slowly due to the exciton diffusion time along the chain. (b) Low polymer/dye concentration ratio. All excitons are in close proximity to the quenching region and quenching is dominated by a rapid process involving intra- and interchain exciton diffusion……..……...…22

Figure 1-15. Schematic representation for the use of a water-soluble CPs with a specific PNA-C* optical reporter probe to detect a complementary ssDNA sequence..... 24

Figure 1-16. Modified schematic DNA-C*/DNA sensor operation ……...…...…..24

Figure 1-17. (a) Schematic representation of the SNP assay. (b) polymer structure of PFP and dGTP-Fl. (c) DNA sequences used in the study ……...…….....26

Figure 1-18. Schematic representation of DNA sequence detection by FRET from the polymer to intercalating dyes in the absence (A) and presence (B) of the FRET gate. (C) Chemical structure of CPs (PFP), FL and EB ……28

Figure 1-19. (a) Chemical structure of the polymers used in this study. (b) Visualization of mutant, left, and mannose-binding, right, E. coli strains after incubation with mannosylated polymer **2a** ……29

Figure 2-1. Polymer (**P1**-**P5**) Structures ……39

Figure 2-2. Photoluminescence of **P1** before (red, in chloroform) and after (black, in water) the cleavage of the ethylhexyl protecting group (**P1** conc. = 5 mgL^{-1})…..52

Figure 2-3. Photoluminescence spectra of **P1** in various water/methanol mixture solvents (**P1** conc. = 0.7 $mgml^{-1}$, excitation wavelength: 365 nm)…….....53

Figure 2-4. Photoluminescence profile of **P1** in water by adding different types of surfactants (a) SDS, negative, (b) tween20, neutral, (c) DTAB, positive (**P1** conc. = 5 $mgmL^{-1}$)……53

Figure 2-5. Schematic illustration of surfactant effect on **P1** in water ...……54

Figure 2-6. TEM micrograph of (a) 1 w% **P1** in water (b) 0.1 w% **P2** in water (c) 0.1 w% **P4** in methanol, (figure in middle) Proposed mechanism for the aggregation of PPEs in a poor solvent …… 55

Figure 2-7. Absorption and Emission spectra of (a) **P2** (10 mgL^{-1}) and (b) **P3** (7 mgL^{-1}) in water (excitation at 365 nm)……..58

Figure 2-8. UV and PL spectra (5 mgL^{-1}) for **P5-A** and **P5-B** (Polymers are excited at 365 nm)……59

Figure 3-1. ^{1}H NMR spectra in D_2O of **PPE-R_1** (a) before and (b) after end-capping ...77

Figure 3-2. Normalized absorption (a) and emission (b) spectra of the polymers: **PPE-R_1** (solid); **PPE-R_1-COOH** (dotted); **PPE-R_2** (dashed)……...78

Figure 3-3. Molecular modeling of **PPE-R_1** simulated by Materials Studio 3.0 (Accelrys®). The purple chain indicates the polymer backbone (left: side view, right: edge view)……...79

Figure 3-4. ^{1}H-NMR spectrum of pentatyrosin-PPE in DMSO (left) and a confocal image of pentatyrosine-PPE (right, scale-bar: 20 um)……...82

Figure 4-1. Chemical Structure of PPE-R_1 and PPE-R_1-COOH ……..88

Figure 4-2. Polymer-oligonucleotide bioconjugation to form PPE-DNA (top) to demonstrate signal amplifying property by FRET and PPE-DNA beacon (bottom), demonstrating self-signal amplifying label-free detection ……...…90

Figure 4-3. Gel electrophoresis of DNA (lane 1), PPE-R_1-COOH (lane 2), and PPE-DNA (lane 3) in the presence of c-DNA ……...…….97

Figure 4-4. Normalized UV/PL spectra of PPE-R_1-COOH and HEX: absorption (■) and emission (□) spectrum of PPE, absorption (▲) and emission (○) spectrum of HEX……..… 98

Figure 4-5. Emission spectra of PPE-DNA (1.0×10^{-7} M) upon hybridization with a complementary target HEX-DNA (4.0×10^{-7} M) when HEX was directly excited at 500 nm (dotted line) and when the PPE was excited at 365 nm (solid line) followed by FRET to HEX…….…….……100

Figure 4-6. Comparison of PL change before (□) and after hybridization between HEX-labeled complementary target (excitation at 365 nm ■ ; at 500 nm ▲) and non-labeled complementary target (○)……...…….101

Figure 4-7. Chemical structure of positively charged PPE (PPE-$N(CH_3)_3^+$)……..…102

Figure 4-8. Comparison PL enhancement of HEX before (□) and after (○) adding HEX-labeled ssDNA in positively charged PPE (PPE-$N(CH_3)_3^+$). Compared with the PPE-DNA/DNA-HEX complex case (▲), increment of HEX emission in PPE-$N(CH_3)_3^+$/DNA-HEX are negligible……..……..103

Figure 4-9. Excitation spectrum of PPE-DNA/HEX-DNA (solid) and HEX-labeled DNA only (dotted) corresponding to the emission wavelength of 556 nm ……..103

Figure 4-10. UV absorbance of PPE-DNA beacon (1.0×10^{-6} M)…….……105

Figure 4-11. Overall fluorescence enhancement in polymer-beacon (1.0×10^{-6} M) after hybridization: complementary ssDNA (4×10^{-6} M, □), 1-mismatch (○), non-complementary ssDNA (▲), Excitation wavelength was 420 nm. Measurements were performed in Tris-HCl buffer (Tris-HCl 20 mM, NaCl 50 mM, $MgCl_2$ 5 mM, EDTA 2 mM). All curves are background (prehybridization) subtracted. Inset: Normalized fluorescence increase in 1-mismatch and perfect target DNA with respect to the emission in non-complementary DNA……..……106

Figure 5-1. Overall strategy of cell imaging with water-soluble fluorescent polymer-antibody conjugates ……...…….116

Figure 5-2. Chemical structure of PPE derivatives containing benzothiadiazole unit ...129

Figure 5-3. (a) UV absorption and (b) photoluminescence spectra of PPE-BT_x ……...130

Figure 5-4. UV absorption and photoluminescence spectra of PPE-B (UV:black/PL:blue) and PBZ2 (UV:green/PL: red). PPE-B (100 nM) and PBZ (150 nM) in deionized water was excited at 365 nm and 540 nm, respectively ….……...……..131

Figure 5-5. UV/PL spectra of PBZ-NBoc in chloroform (black/yellow) and DMF (blue/red) at 2 mg/L. Its quantum yields in chloroform and DMF are 92 % and 15 % respectively ……..……...132

Figure 5-6. Coomassie Blue-stained 10% SDS-PAGE analysis of CD3 and PPE-B-CD3 conjugates having varying stoichiometric amount of PPE-B per antibody. Lane A: only CD3, no polymer, lane B-D corresponds to 5:1, 10:1, 50:1, 100:1 (PPE-B:CD3), respectively. Bands located at the bottom of the gel are corresponding to the F_{ab} light chain of 23 KDa……..…….134

Figure 5-7. Fluorescence microscope images of live cells after the incubation with PPE-B-CD3 (a: Jurkat and b: B-cell) and PBZ2-CD20 (c: B-cell and d: T-cell) for 30 min. Differential interference contrast (DIC) images are shown in the left column and fluorescence images are in the right column. The images in the a and b low were obtained upon excitation at 470 nm and the images in the lows c and d were from 560 nm excitation. Scale bar: 20 μm……..……..…136

Figure 5-8. Confocal images of Jurkats stained with PPE-B-CD3. The cells were stained before fixation (a, b, c) and after fixation (d,e,f) with 3 % formaldehyde ……..137

Figure 5-9. Fluorescence microscope images of the mixed Jurkat and SUDHL-4 after incubation with PPE-B-CD3 (1.0 μM) and PBZ2-CD20 (1.0 μM) together. Panel a shows blue emission (excitation: 395-415 nm, emission: 435-485 nm) of PPE-B-CD3-stained Jurkat. Panel b shows PBZ2-CD20-stained SUDHL-4 having red emission (excitation: 540-580 nm, emission: 590-650 nm). The panel c image shows both Jurkat and SUDHL-4 having difference emission color. The image was obtained by using a wideband emission filter (> 500 nm), exposure of wide excitation filter (450-490 nm), and an external incandescent light….....138

Figure 5-10. The correlation between the ratio (the number of stained SUBHL-4/total number of stained cells) and the cell mixing ratio ……..……..…..139

Figure 5-11. Cell viability and proliferation of (a) SUDHL-4 and (b) Jurkat incubated with different concentrations of PPE-B for 3 days. The concentration of PPE-B in the media was varied from 0.05 to 500 μg/mL (in μg/mL, 500: Black, 50: red, 5: blue, 0.5: turquoise, 0.05: pink, 0: khaki (positive control)). Trypan blue reagents were added to small aliquot of sample, and the number of dead cells and live cells were counted by a hemacytometer in every 24 hrs after the incubation with PPE-B. Relative cell growth (%) was calculated as (the number of live cells) / (the number of live cell in control) × 100. (c) A cell proliferation curve of SUDHL-4 (black) and Jurkat (red) upon incubation with the highest concentration of PPE-B (500 μg/mL). (d) A fluorescence microscope image of SUDHL-4 after 1 hr from the incubation with PPE-B. 100 μl of SUDHL-4 cell media (1 millions cells) was incubated with10 μl of 3 μM PPE-B. The image was obtained after unbound PPE-B was washed off by spinning with fresh cell media (500 × g, 6 min) several times. (Inset) An optical image corresponding to the fluorescence image.…....141

Figure 6-1. (a) UV-Vis and (b) PL spectrum profiles of **M1** in chloroform upon TFA treatment. (c) Fluorescence life time results of **M1** (1mg/L) characterized by time-resolved fluorescence spectroscopy before (□, emission at 413 nm) and after (○, emission at 468 nm) adding 10 μl of TFA in 3 ml of chloroform upon excitation at 386 nm. The protonation of the aromatic dioxadiazole unit induces the planarization of the structure by forming a stable 6-membered ring structure and causes the blue to green fluorescence shift ……...……..156

Figure 6-2. A proposed planarization mechanism induced by TFA……...……...….156

Figure 6-3. The chemical structure of poly(*p*-phenyleneethynylene)s (**PPE**) and polythiophene (**P3HT**)……...……...…158

Figure 6-4. UV-Vis (■: solution, □: film) and PL (●: solution, ○: film) spectra of (a) **PO1**, (b) **PPE** (c) **P3HT** in solution and in the film……..... 160

Figure 6-5. (a) UV-Vis and (b) PL spectra of the polymer films before (■: **PO1**, ●: **PPE**, ▲: **P3HT**) and after (□: **PO1**, ○: **PPE**, Δ: **P3HT**) the HCl treatment. All polymer-coated slides were dipped in 1 M HCl solution at room temperature for 1 hr 161

Figure 6-6. Change in (a) UV and (b) PL spectra before (■: **PO1**, ●: **PPE**, ▲: **P3HT**) and after (□: **PO1**, ○: **PPE**, Δ: **P3HT**) UV irradiation (254 nm, 6W, 1hr) in the presence of photogenerated acid (PGA), UV irradiation condition: 254 nm, 6W, 1hr. (Inset) patterned images of **PO1** after 1 hr UV exposure. The area of the character "UM" was exposed to 254 nm of UV light for 1 hour…….....163

Figure 6-7. (a) UV-Vis and (b) photoluminescence spectra of **PO1** solution in chloroform (1 mg/L) upon addition of TFA, (c) Reversible feature of the emission change of **PO1** in chloroform by adding and removing of TFA (TFA was added and removed by vacuum repeatedly)……..……..…165

Figure 7-1. Schematic representation of the signal-amplifying conjugated polymer based DNA chip. a) **P1**-coated glass slide by covalent bonding, b) light-directed on-chip oligonucleotide synthesis, c) hybridization with a target DNA results in large emission enhancement of the fluorescent dye through efficient Förster resonance energy transfer……..……..……172

Figure 7-2. Schematic representation of light directed on-chip oligonucleotide synthesis …….…….181

Figure 7-3. UV absorbance for DMT quantification ……...…….....183

Figure 7-4. Profile of fluorescence intensity upon change of target DNA concentration…

…….……184

Figure 7-5. UV and PL spectra of **P1** in chloroform (black = UV, blue = PL) and solid film (green = UV, red = PL)……...…186

Figure 7-6. A fluorescence image of a patterned signal-amplifying DNA microarray with two different DNA sequences after hybridization with a mixture of c-DNA-HEX (green) and c-DNA-Cy5 (red; scale bar: 200 um)……..…… 188

Figure 7-7. PL emission spectra of P1 substrate before (black) and after hybridization when excited at 380 nm (red) and 535 nm (blue); PL emission of the control (pink, excited at 535 nm). Note that the blue and pink lines are essentially superimposed and appear around 550-625 nm. Inset: comparison of fluorescence intensity upon excitation at 535 nm (left) and 405 nm (right). Scale bar: 25 μm…….…..189

Figure 7-8. Selectivity test: A) perfect match, B) one mismatch, and C) random sequence. Inset: A microscanned image, from the top row down: perfect match, one mismatch, and random sequence. The spot diameter is 55 μm. I_f = fluorescence intensity……..……..……191

Figure 8-1. The chemical structures of POX1 and SYBR green I ……...…….....203

Figure 8-2. UV-Vis/PL spectra (black/blue for POX1 and green/red for SYBR green I) in the solid film (POX1) and in 0.5 μM 6 x SSPE solution at pH = 7.4 (SYBR green I)……...203

Figure 8-3. Selectivity test of conventional control slides without POX1. A: perfect match (5'-ACA CAT CAC GGA TGT-3'), B: 1-mismatch (5'-ACA CAT CTC GGA TGT'3'), C: random sequence (5'-TGT GTA GTG CCT ACA -3')……..205

Figure 8-4. Emission profile in various SYBR green I concentrations. The excitation wavelength was 380 nm ……..…….…...206

Figure 8-5. Normalized photoluminescence of SG1 solution (5 μM) in the presence of 15 base-pair ssDNA (0.1 nM; pink, 0.05 nM; green, 0.02 nM; blue, 0.01 nM; red, noDNA; black) in 6×SSPE buffer (pH = 7.4)……..207

Figure 8-6. PL emission spectra of SYBR green I after hybridization with a target DNA ([c-DNA] = 1.0 x 10-5 M, 5'-ACA CAT CAC GGA TGT-3', [SYBR green I] = 50 nM) when excited at 380 nm (solid), 490 nm (dotted)...……..…….209

Figure 8-7. Excitation spectrum for the SYBR green I emission at 525 nm …….....209

Figure 8-8. Selectivity test of the signal amplifying DNA microarray having the POX1 layer. A: perfect match (5'-ACA CAT CAC GGA TGT-3'), B: 1-mismatch (5'-ACA CAT CTC GGA TGT-3'), C: random sequence (5'-TGT GTA GTG CCT ACA-3'), D: prehybridized control, E: only POX1-coated slide. Hybridization condition: incubation in 6×SSPE at 37 °C for 20 min, each [DNA] = 1.0×10^{-5} M, [SYBR green I] = 50.0 nM…….....210

Figure 9-1. Schematic representation of label-free and signal amplifying DNA microarray using a molecular beacon ……..…...…..……217

Figure 9-2. Chemical Structure of **POX** ……..…..…218

Figure 9-3. UV absorption spectrum of POX-SH on glass substrate …… 229

Figure 9-4. PL spectrum of of POX-SH on glass substrate ……....…..229

Figure 9-5. UV absorption spectra after DNA synthesis on polymer coated surface …232

Figure 9-6. Polymer fluorescence before (square) and after hybridization (triangle) in various types of molecular beacons ...…….....233

Figure 9-7. Photoluminescence of polymer-DNA chips having two different probe (P1 and P2) upon hybridization with target complement C1 and C2 respectively....235

Figure 9-8. Schematic representation of turn-off sensor using fluorescence dye.…….....236

Figure 9-9. PL spectra in fluorescein dye case: Prehybridization state emission of (a) P1 and (c) P2 when excited at 380 nm (square) and 490 nm (triangle); relative fluorescence change after hybridization of P1 (b) and P2 (d) with target complement (C1 and C2, triangle) and random DNA (N1 and N2, circle) (excitation wavelength: 380 nm)……..……...……..237

Figure 9-10. PL spectra when HEX dye was used: (a) emission in prehybridization state when excited at 380 nm (square) and 535 nm (triangle); (b) fluorescence change after hybridization with target DNA (triangle) and non-complementary DNA (circle) (square: prehybridization state, excitation wavelength: 380 nm).....…238

Figure 10-1. Schematic representation of PSA detection using conjugated polymer-peptide hybrid chips ……..……...……...…….246

Figure 10-2. Chemical structure of P1…….……...… 251

Figure 10-3. The synthetic procedure of the on-chip peptide synthesis on the P1-coated substrate and the reagents used for the synthesis …….……...……...253

Figure 10-4. Photoluminescence spectra of P1-DABCYL system before (black) and after (red) PSA incubation. The slide was excited at 380 nm, a characteristic excitation wavelength of P1…….……....……..…….254

Figure 10-5. Photoluminescence of the same hexapeptide without DABCYL quencher on the P1-coated substrate as a control before and after the incubation with PSA. The excitation wavelength was 380 nm …..…….…...…255

Figure 10-6. Photoluminescence spectra of P1-fluorescein before (black) and after (red) the PSA incubation. The slide was excited at 380 nm, a characteristic excitation wavelength of polymer ……..……..…….……..255

Figure 10-7. Photoluminescence of the P1-fluorescein having the single-mismatch sequence QRY-SSN before and after the PSA incubation. Excitation wavelength: 380 nm for P1 excitation (black and blue lines) and 490 nm for direct fluorescein excitation (red)…….....……257

LIST OF SCHEMES

Scheme 1-1. Water soluble conjugated polymers and cationic dyes used in this study....21

Scheme 2-1. Synthesis of Monomer **M1** to **M4**…….....…….50

Scheme 2-2. Polymer synthesis (**P1** – **P5**)……...……...…..51

Scheme 2-3. *In-situ* end-capping reaction for **P5-B** ….……..……..60

Scheme 3-1. Polymer synthesis (a) DMF, K_2CO_3, 75 ºC, 72 hr; (b) THF, $Pd(PPh_3)4$, diisopropylamine (DIPA), CuI; (c) KOH, water/methanol.……..…….…...76

Scheme 3-2. Peptide-PPE coupling reaction …….…….…….…….80

Scheme 5-1. Monomer synthesis (a) I_2, H_2SO_4, acetic acid, water, 100 ºC (b) BBr_3, dichloromethane, -60 ºC → r. t., 48 hr (c) K_2CO_3, ethyl 4-bromobutyrate, dimethylformamide (DMF), 80 ºC, 48 hr (d) Bromine, hydrobromic acid, 100 ºC overnight (e) trimethylacetylene, Pd3(PPh3)4, CuI, triethylamine, toluene. 65 ºC, 7 hr. (f) potassium hydroxide, methanol:tetrahydrofuran (1:1 v/v), room temperature, 1 hr…….……..…127

Scheme 5-2. Synthesis of the CPEs (PPE-B and PBZ2)……...……...…129

Scheme 5-3. Synthetic route of PBZ-NBoc ……..…….....131

Scheme 6-1. Monomer and polymer synthesis for **PPE** ……...…….....……...151

Scheme 6-2. Monomer synthesis: (a) 2-Ethylhexylbromide (for R_1) or 1-bromohexadecane (for R_2), K_2CO_3, DMF, 80 °C, 48 h. (b) H_2NNH_2, ethanol, 78 °C, 24 h. (c) 4-bromobenzoyl chloride, triethylamine, chloroform, 12 h. (d) $POCl_3$, reflux, 12 h. (e) oxalyl chloride, methylene chloride, 0 °C → 25 °C, 12 h. (f) *t*-butanol, toluene, 0 °C → 40 °C, 15 min. (g) 1, 5-dibromopentane, *t*-BuOK, DMF, 40 °C, 1 h. (h) LiOH, THF, water, r. t., 3 h. (i) 2, 5-dibromohydroquinone, K_2CO_3, DMF, 70 °C, 48 h…….……..154

Scheme 6-3. Polymer synthesis (a) THF, water, $Pd(PPh_3)_4$, K_2CO_3, 80 °C, 36 h. (b) 50 % TFA in $CHCl_3$……..158

Scheme 7-1. Monomer synthesis: (a) Oxalyl chloride, methylene chloride, 0 °C → 25 °C, 12 h. (b) *t*-butanol, toluene, 0 °C → 40 °C, 15 min. (c) 1, 5-dibromopentane, *t*-BuOK, DMF, 40 °C, 1 h. (d) LiOH, THF, water, r. t., 3 h. (e) 2, 5-

dibromohydroquinone, K_2CO_3, DMF, 70 °C, 48 h. (f) 2-Ethylhexylbromide, K_2CO_3, DMF, 80 °C, 48 h. (g) H_2NNH_2, ethanol, 78 °C, 24 h. (h) 4-bromobenzoyl chloride, pyridine, NMP, 12 h. (i) $POCl_3$, reflux, 12 h..…....….174

Scheme 7-2. Light-directed parallel on-chip DNA synthesis on P1-immobilized glass: a) APTMS, b) 1,4-phenylenediisothiocyanate, c) polymer (**P1**), and d) cyclic procedures of oligo synthesis ……..…..……180

Scheme 7-3. Chemical structure of **P1**……...……..…. 185

Scheme 8-1. A label-free conjugated polymer-DNA hybrid microarray ……..….199

Scheme 8-2. Schematic illustration of the on-chip DNA synthesis…….....200

Scheme 9-1. Monomer synthesis for **M1**……..……...…..……225

Scheme 9-2. Polymerization for **POX-SH** ……..…….……..226

Scheme 9-3. Surface modification and polymer immobilization ……...……228

Scheme 9-4. SQ synthesis using trebler phosphorearmidite ...…..…….234

Scheme 10-1. Schematic representation of polymer immobilization onto glass substrate and on-chip peptide synthesis ……..…248

Scheme 10-2. Fmoc solid phase peptide synthesis ……..…249

LIST OF TABLES

Table 1-1. UV absorption and emission of conventional fluorophores quenchers used for molecular beacons ……..…….……..…14

Table 2-1. Physical properties of all polymers used in this study ……...…….…..52

Table 6-1. Photo-physical data of **PO1**, **PPE**, and **P3HT** used in this study ….……..159

Table 9-1. DNA hairpin probes, P1 and P2; their Target (C1 and C2) and non-complementary DNAs (N1 and N2) used in this study ……...……..224

Table 9-2. Monomer ratio and its corresponding molecular weight ……..…..227

ABSTRACT

Functionalized Conjugated Polymers for Signal Amplifying Biosensors and Sensor Arrays

by

Kangwon Lee

Chair: Jinsang Kim

Conjugated polymers (CPs) are great alternatives to the conventional fluorescence dyes as signaling reporters in biosensor design due to the fluorescent signal amplification property of CPs. Two series of CPs, poly(*p*-phenyleneethynylene) (PPE) and poly(*p*-oxadiazole-co-phenylene) (POX) derivatives, have been systematically designed, developed, and studied in this thesis to devise highly sensitive and selective novel molecular biosensors and sensor arrays for the detection of clinically important biological molecules. The key concept developed in the thesis work was the molecular design principles to combine biological receptor molecules for specific detection of target oligonucleotides and CPs as the signal transduction and amplification unit. To achieve this goal, a series of completely water-soluble and highly emissive conjugated polyelectrolytes (CPEs) were first developed through systematic investigation on the

correlation between the polymer structure and its water-solubility. We also developed a method to bioconjugate CPEs to peptides and DNA by end-modification of the CPEs with a carboxylic acid group to develop hybrid bio/-synthetic sensory CPs and to achieve selective detection of target with amplified fluorescence signal in aqueous solution. DNA detection results using the CPE-DNA hybrid system confirmed large signal amplification by means of efficient Förster energy transfer from the energy harvesting CPEs to the fluorescent dye attached to the complementary analyte DNA. To apply the signal amplification scheme to practically more useful solid-state microarray novel conjugated polymers, POXs, having unique photochemical stabilities were developed. By applying on-chip DNA synthesis on the POXs and achieving efficient Förster energy transfer from POXs to the dye-labeled target DNA we successfully developed signal amplifying DNA microarrays. The signal amplifying scheme was combined with a self-signaling concept by means of introducing intercalating dyes and molecular beacon into the CPs for label-free detection. As a result of sensitive and selective prostate specific antigen detection has been demonstrated. In addition to the biosensor development, the developed bioconjugation technique between biological molecules and CPEs was uniquely applied to the development of CPE-antibody for live cell imaging. Selective live cell imaging of human B-cell lymphoma and human T-cell leukemia having largely enhanced sensitivity and excellent selectivity was demonstrated by using the CPE-antibody.

CHAPTER 1

Introduction and Background

This chapter will describe the basic concept of conjugated polymers, their optoelectronic properties, the parameters influencing their signaling properties, the molecular wire approach for sensory signal amplification, and the charge and energy transport mechanism of conjugated polymers. Design strategy to generate sensory signal from conjugated polymer-based biosensors in the literature will be discussed in detail. These background concepts are essential to understand this Ph. D. dissertation on the development of highly sensitivity and selective conjugated polymer-based molecular biosensors and sensor arrays both in solution and in the solid state.

Parts of this chapter appear in: Lee, K.; Povlich, L. K.; Kim, J. manuscript in preparation.

1.1. Conjugated Polymers

Conjugated polymers (CPs) are macromolecules having alternating saturated and unsaturated bonds along the mainchain backbone. Saturated single bonds are σ-bonds while unsaturated double bonds are combination of a σ-bond and a π-bond. All CPs consist of a σ-bond through the overlapping sp^2 hybrid orbitals and the remaining out-of-plane p_z orbitals which overlaps with neighboring p_z orbitals and forms π-bonds. Therefore, the electrons that constitute the π-bonds are delocalized over the entire polymer backbone even though the chemical structures of CPs are presented as alternating single and double bonds. This continuous delocalized π-bonds along the backbone is the origin of the emissive property and conductive property of CPs. It was firstly discovered by Shirakawa, MacDiarmid, and Heeger that chemical doping of polyacetylenes caused increases in electronic conductivity over several orders of magnitude and this finding and their life-time contribution to the CP development lead them to the 2000 Nobel Prize in chemistry.[1,2] CPs have become emerging active materials in various applications such as light-emitting diodes (LEDs)[3,4,5], light-emitting electrochemical cells (LECs)[6,7,8,9], polymer actuators[10,11], field effect transistors (FETs)[12], plastic laser[13,14], batteries[15,16], photovoltaic cells[17], biomaterials[18,19] and sensors[20,21].

Many different conjugated backbones of CPs have been developed as some of them are shown in Figure 1-1. Most CPs are prepared by means of metal catalyzed polymerization methods in a mild reaction condition for example Sonogashira-Hagihara cross-coupling for poly(phenylene ethynylene)s (PPEs) through [22,23] Stille[24], Yamamoto[25] or Suzuki[26,27] couplings for poly(*p*-phenylene)s (PPPs) and poly(fluorine)s (PFs), Heck[28] coupling reaction for poly(phenylene vinylene)s (PPVs), and McCullough[29], Rieke[30] or electropolymerization[21] methods for poly(thiophene)s (PTs).

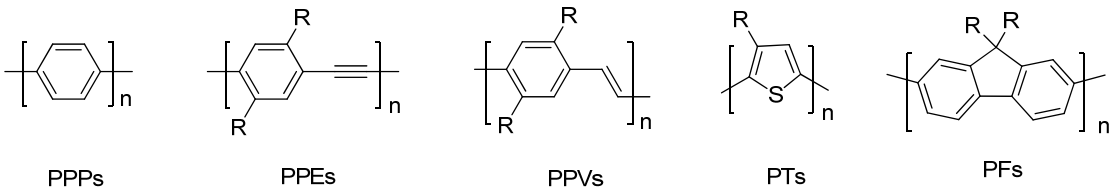

Figure 1-1. Chemical structure of various conjugated polymers.

Conjugated polyelectrolytes (CPEs) are π-conjugated polymers having a charged (anionic or cationic) side chains. Sulfonate (SO_3^-), carboxylate (CO_2^-), and phosphate (PO_4^{3-}) ions are negatively charged groups and a quaternary ammonium (NR_3^+) is a positively charged group mostly commonly used functional group to give water-solubility in the CPE design. These pendant groups, often combined with poly(ethylene oxide) side chains, help CPEs dissolve in water and prevent the aggregation of multiple chains. The water solubility of CPEs is a necessary property for conjugated polymers to be a good biosensor in homogeneous aqueous media because biological entities are present in aqueous environment. However, achieving complete water-soluble and highly emissive CPEs remains as a challenging task. The first CPEs were reported by Shi and Wudl in 1990 and others have been developed in recent years for biosensor applications.[31] Figure 1-2 shows the chemical structures of CPEs commonly used in the literature. A recent review published by Pinto and Schanze gives an in-depth overview of the synthetic methods to make conjugated polyelectrolyte, including those having poly(*p*-phenylene), poly(phenylene vinylene) and poly(phenyleneethynylene) backbone structures. [32]

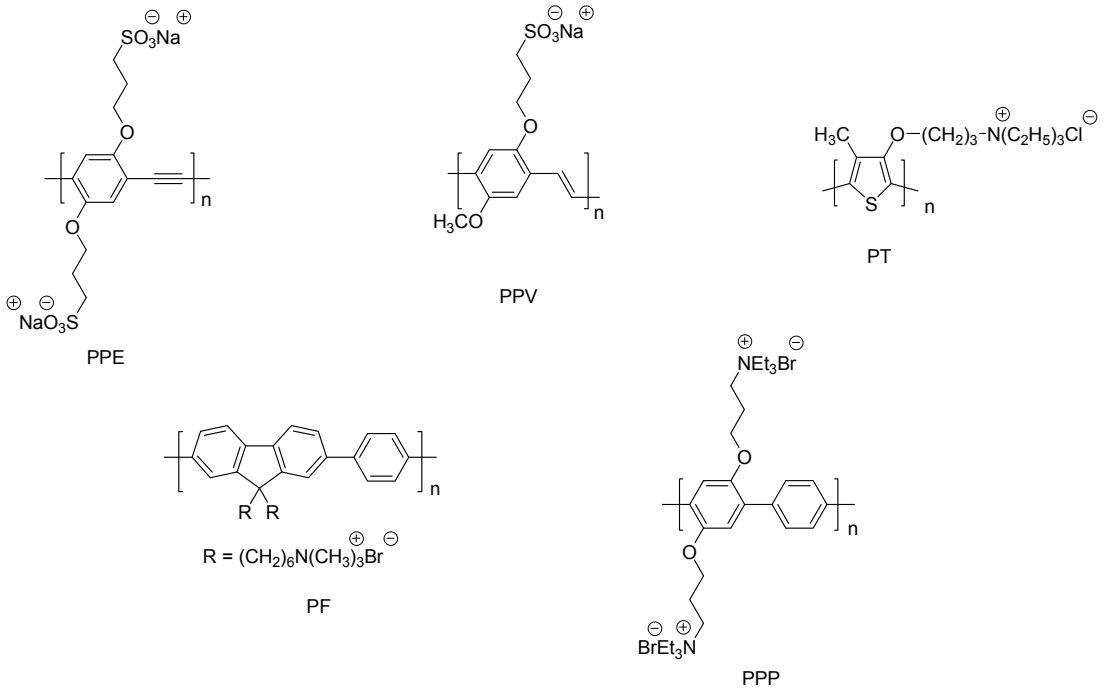

Figure 1-2. Examples of water-soluble CPs used in biosensor applications.

1.2. Optoelectronic Property of CPs

A molecule in an excited state can lose the absorbed energy in the following ways:

(a) radiationless transition, such as internal conversion or intersystem crossing (macroscopically observable by heat formation)

(b) emission of radiation (fluorescence and phosphorescence)

(c) photochemical reactions (*e.g.* rearrangements, dissociations, dimerizations, photoadditions, reactions with neighboring particles *etc*.)

Processes of type (a) and (b) which often happens in CPs are represented schematically in the so-called Jablonski diagram (Figure 1-3), which is a scheme of the essential levels: In Figure 1-3 the lowest vibration energy levels of electronic state are indicated by S_0; other horizontal lines represent associated vibrational levels.[33]

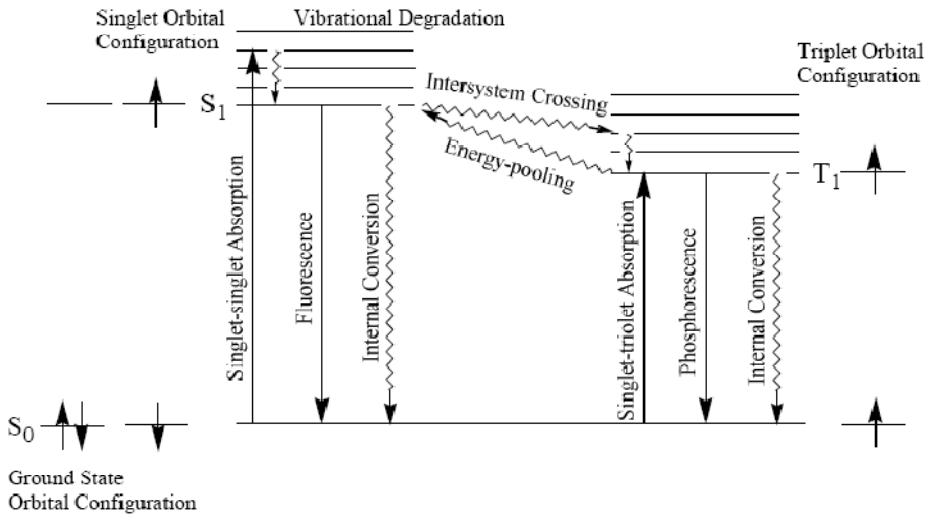

Figure 1-3. Jablonski diagram.

Vibrational deactivation (vertical wavy lines) leads to the lowest vibrational level of the respective excited singlet electronic state or to lower singlet states. Intersystem crossing (horizontal wavy lines) leads to triplet states. Emission of radiation from the lowest vibrational level of the excited state S_1 to any of the vibrational levels of the ground state S_0 is called fluorescence. The emission is called phosphorescence if the spin state of the initial is different from that of the final energy levels (e. g. $T_1 \rightarrow S_0$). The lifetime of the fluorescent state is very short (pico- to nano- second regime) but the phosphorescence lifetime is much longer (micro- to mili-second) since fluorescence is statistically much more likely than phosphorescence and phosphorescence is forbidden by the spin selection rule. If T_1 absorbs thermal energy T_1 can move back to S_1 and this process is referred to as energy-pooling. Extra excited singlet electrons provided by the energy pooling generate delayed fluorescence with a longer lifetime and the exactly same spectral distribution.

Most conjugated organic materials are commonly considered as a non-emissive in triplet-state. The nonradiative decay of triplet state in conjugated systems has been controlled by Franck-Condon overlap of wave functions. However, there has been considerable effort to prepare phosphorescent conjugated polymers although room-temperature luminescence from triplet-exciton in conjugated polymers is hardly reported. Conjugated polymers containing heavy metal like platinum in conjugated backbone shows a good phosphorescence property at room temperature.[34-36] Spin-orbit coupling happens by the heavy atoms in the backbone. Also, it enables the spin of the electron to flip or rephrase and transitions between the singlet and triplet manifolds can be achieved. Therefore, successful design highly phosphorescent conjugated polymers can be achieved by the introduction of heavy metal in aromatic hydrocarbon backbone.

Photophysical properties of CPs are strongly related with their polymer structure in solution and/or solid state. There are several factors governing their emissive properties such as chemical nature, effective conjugation length, intramolecular conformation and intermolecular packing. First of all, emission wavelength can be delicately tuned through the change in the charge density around the CP backbone. It can be achieved by replacing the side chain moieties of the polymers. For example, emission of the polymers was bathochromically shifted (red-shift) if the electron-donating moiety are attached to the backbone and vice versa. The emission wavelength is also dependent on the chain length of CPs. The longer chain generally shows the longer wavelength emission. However, the fluorescence wavelength of CPs does not change further when the length of CP exceeds the effective conjugation length. Systematic investigation regarding the optoelectronic properties of PPEs by Kim and Swager clearly showed that

the conformational change of the CP backbone and their intermolecular packing have dramatic influence on their emissive properties (Figure 1-4).[37]

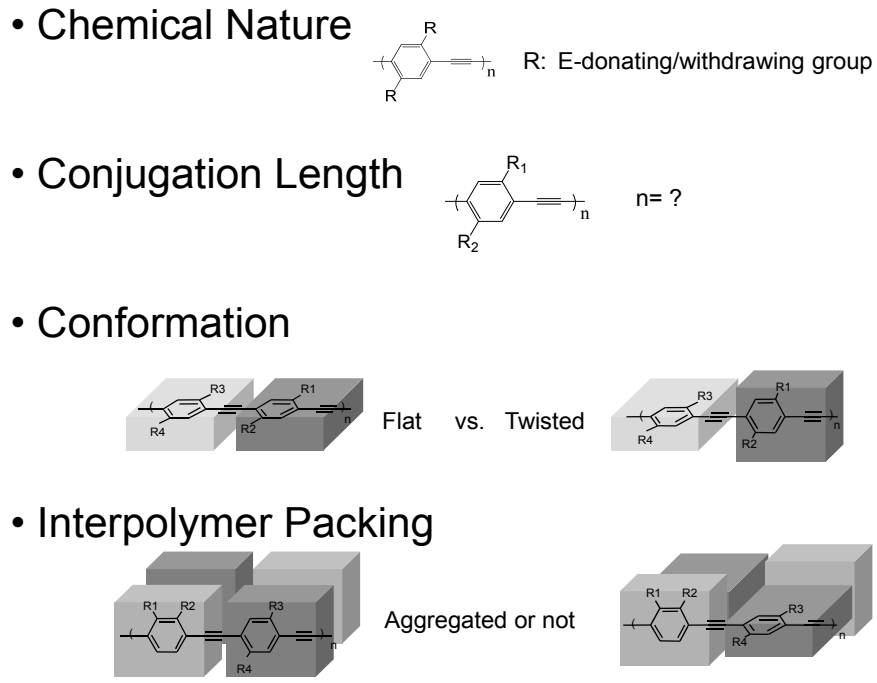

Figure 1-4. Factors governing the optoelectronic properties of CPs.[37]

1.3. Sensory Signal Amplification of CPs

CPs are more advantageous than small molecular sensors because they are able to amplify the signal from a binding event. The signal amplifying model of CPs was proposed by Swager group in 1995.[38] Figure 1-5 schematically illustrates the conceptual basis of the signal amplification of the fluorescence sensory signal generated by CP upon binding with a target analyte. When an analyte binds locally to a receptor on a CP repeat unit the entire conjugated backbone is affected due to its 1-dimensional wire-like property and the fluorescence of the entire polymer chain is altered. This results in an

amplification of fluorescence when compared to small molecule sensors because a binding event on a small molecule only causes a single chromophore to change its fluorescence, whereas a CP binding event affects the fluorescence of an entire chain of chromophores by energy migration through the conducting polymer backbone. This amplification of signals provided by CPs is important for biosensing applications because the molecules being analyzed are often present in extremely dilute concentrations.

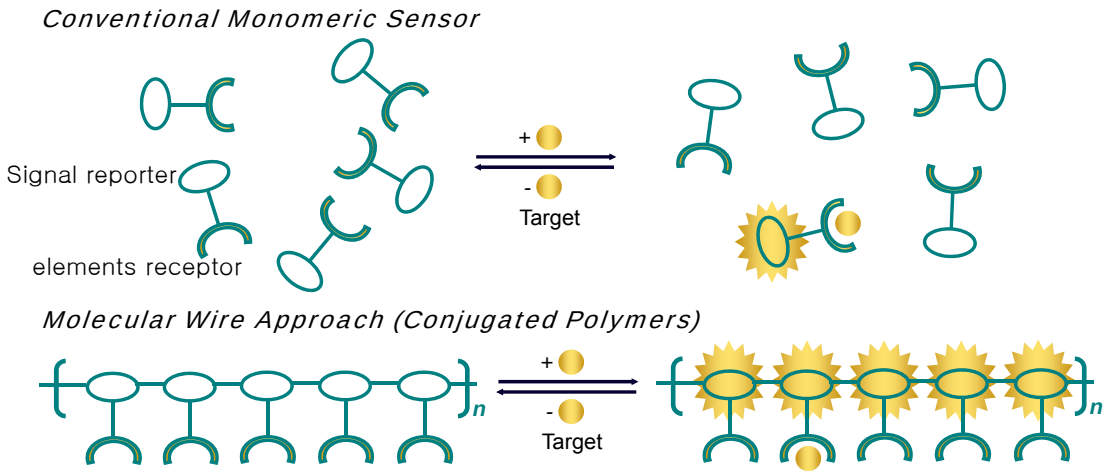

Figure 1-5. Signal amplification of CPs.[38]

1.4. Energy and Electron Transfer of CPs

Generally, following nomenclature describes electron or energy transfer process.

$D^+ + A \rightarrow D + A^+$ (hole transfer)

$D^- + A \rightarrow D + A^-$ (electron transfer)

$D^* + A \rightarrow D + A^*$ (energy transfer)

Where D and A are the donor and acceptor respectively and * represents an excited state molecule. Electron transfer (ET) is the process by which an electron moves from one

atom or molecule to another atom or molecule. ET is mechanistically described by the thermodynamic concept of redox, wherein the formal oxidation states of both reaction partners change. Similarly, the photoinduced electron transfer is an electron transfer which occurs when certain photoactive materials interact with light. As seen in Figure 1-6, the excited electron in the lowest unoccupied molecular orbital (LUMO) of a sensor is transferred into the highest occupied molecular orbital (HOMO) of a target through a nonradiative transfer. Therefore, the fluorescence from CPs is quenched by the analyte.

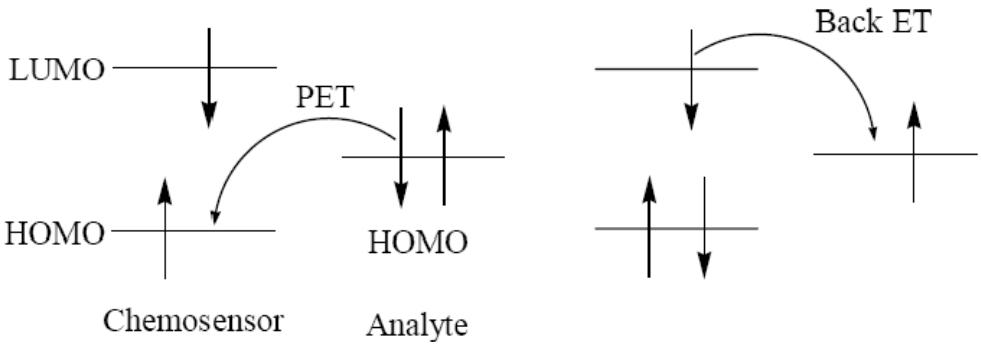

Figure 1-6. Photo-induced electron transfer.

Energy transfer consists of two types mechanism; Coulombic (Förster transfer) and exchange mechanisms (Dexter transfer) as shown in Figure 1-7.

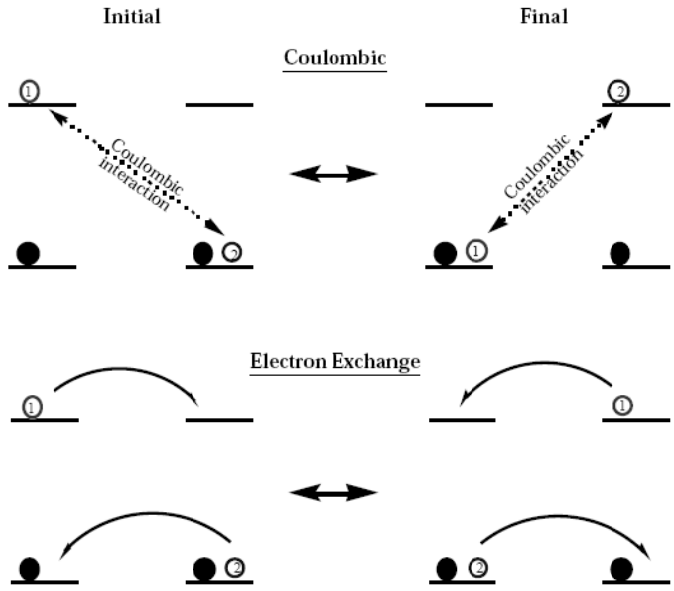

Figure 1-7. Energy transfer mechanism.

Electron exchange mechanism can be described by the following equation.

$$k_{ET}\,(\text{exchange}) = KJ\exp(-2r_{DA}/L)$$

where, K is related to specific orbital interactions.

J is the normalized spectral overlap integral, where normalized means that both the emission intensity and extinction coefficient have been normalized to unit area on the wavenumber scale.

r_{DA} is the donor-acceptor separation relative to their van der Waals radii L, which corresponds to the edge-to-edge separation.

Transfer rate of Dexter mechanism decreases as exp-(2r/L), This means that k_{ET} (exchange) drops to negligibly small values (relative to the donor lifetime) as the intermolecular (edge-to-edge) distance increases more than on the order of one or two molecular diameters (5-10 Å). Also, the transfer rate is independent of the oscillator strength of the D* → D and A → A* transitions.[39]

Coulombic mechanism representing a long range interaction by dipole-dipole oscillation interaction may be preferred to fluorescence resonance energy transfer (FRET) or Förster resonance energy transfer.[40,41,42] FRET is normally radiationless transfer of energy from a donor molecule to an acceptor molecule, therefore the signature of FRET is quenching of the high energy fluorophore followed by emission from the acceptor fluorophore of relatively low frequency of light. There are several requirements for FRET. First, donor and acceptor molecules must be in close proximity (typically 1-10 nm). The efficiency of FRET is dependent on the inverse sixth power of the intermolecular separation, making it useful over distances comparable with the dimensions of biological macromolecules. Magnitude of R_o is dependent on the spectral properties of the donor and acceptor dyes. Second, the fluorescence spectrum of the donor must be overlapped with the absorption spectrum of the acceptor (Figure 1-8). Finally, donor and acceptor transition dipole orientations should be preferably parallel. Therefore, when all conditions for FRET are considered, we can derive the following equations relating Förster radius (R_o). The distance for certain amount of FRET efficiency (i.e., 50 % efficiency means that 50% of excited donors are deactivated by FRET) is defined by the Förster radius.

$$R_0 = [8.8 \times 10^{23} \cdot \kappa^2 \cdot n^{-4} \cdot (QY_D) \cdot J(\lambda)]^{1/6} \; \mathring{A}$$

where κ^2 = dipole orientation factor. Range 0 to 4 : κ^2 =2/3 for randomly oriented donors and acceptors.

QY_D= fluorescence quantum yield of the donor in the absence of the acceptor.

n= refractive index

$J(\lambda)$ = spectral overlap integral

$$= \int \varepsilon_A(\lambda) \cdot F_D(\lambda) \cdot \lambda^4 d\lambda \, cm^3 M^{-1}$$

where ε_A : extinction coefficient of acceptor

F_D : fluorescence emission intensity of donor as a fraction of the total integrated intensity.

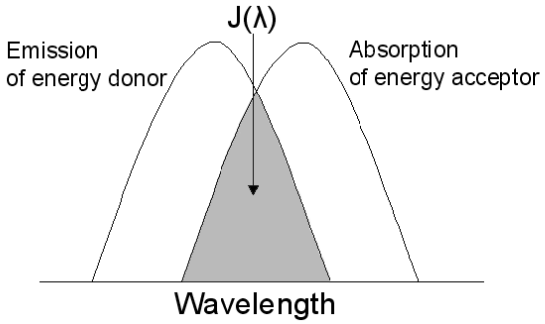

Figure 1-8. Schematic representation of the FRET spectral overlap integral.

While the efficiency of energy transfer by the exchange interaction cannot be directly related an experimental quantity, the efficiency of energy transfer by the dipole mechanism depends mainly on the oscillator strength of the A → A* transition since a smaller oscillator strength for D* → D is compensated by a slower radiative rate constant.

An interesting and well-design molecular switch to generate fluorescence signal in a sensor design by means of FRET concept is the molecular beacon that was invented by Tyagi et al[43]. Figure 1-9 shows the schematic operation of a molecular beacon. It is a single-stranded oligonucleotide which can form a stable hairpin-like stem-and-loop structure. The complementary sequence of a target DNA sequence is encoded into the loop sequence of a molecular beacon. The two chain ends are designed to self-recognize to close the molecular beacon to form the stable hairpin-like stem-and-loop structure. A fluorescent probe and a quencher molecule are covalently linked to each chain end of a molecular beacon so that the closed form is not emissive. In a hairpin shaped state (closed

form), the stem keeps these two moieties in close proximity to each other and fluorescent energy from a fluorophore was completely absorbed by non-fluorescent quencher to be completely quenched (FRET mechanism). However, when a target DNA is encountered to a system, it hybridizes with the loop of the beacon and opens up the molecular beacon (open form). The rigidity and the length of the resulting double helix DNA prevent the fluorophore and the quencher from being in the proximity. Thus, the molecular beacon undergoes a conformational reorganization that forces the stem apart and causes the fluorophore and the quencher to move away from each other. This phenomenon prevents FRET from restoration of fluorescence.

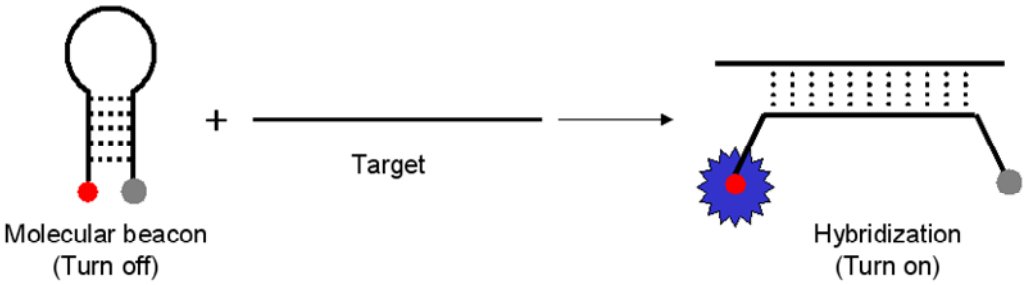

Figure 1-9. Schematic representation of a molecular beacon.

In order to detect multiple targets in the same solution, molecular beacon can be made in many different colors utilizing a broad range of fluorophore.[44] Table 1 summarizes the photophysical properties of fluorophores and quenchers commonly used in molecular beacons.

Table 1-1. UV absorption and emission of conventional fluorophores quenchers used for molecular beacons

Fluorophore	Ab. Max. (nm)	Em. Max. (nm)	Color	Quencher	Ab. Max. (nm)
Fluorescein	494	525	Green	DABCYL	478
Rhodamine Green	504	531	Green	Iowa Black FQ™	531
TET	521	536	Orange	BHQ™-1	534
Yakima Yellow	530	549	Yellow	BHQ™-2	578
HEX	535	556	Pink	Iowa Black FQ™	656
Cy3	546	563	Red		
TAMRA	565	580	Rose		
Redmond Red	579	595	Red		
Cy3,5	588	604	Purple		
Cy5	646	662	Violet		
Cy5.5	683	707	Dark Blue		

Currently, FRET are widely applied in both industrial and academic research. Followings are examples of bio-related applications of FRET: receptor/ligand interactions, immunoassays, probing interactions of single molecules, structure and conformation of proteins or nucleic acids, real-time PCR assays and SNP detection, detection of nucleic acid hybridization, primer-extension assays for detecting mutations, automated DNA sequencing, distribution and transport of lipids.

1.5. Signal Transduction Modes of CPs

Several detection modes have been developed for the sensing of biomolecules by CPs including fluorescence ‘turn-on’ and ‘turn-off’ and ‘fluorescence color change’ modes. When the turn-on mechanism is implemented perturbation of a CPs, such as

changes in the conjugation length or conformation of a polymer chain, upon a binding event causes fluorescence of CPs to be turned-on. Likewise, a binding event in a turn-off system makes the fluorescence of a CP to be effectively quenched through non-radiative relaxation pathways. Fluorescence color change mode is the most commonly used strategy in a sensor design and based on Förster energy transfer mechanism (FRET) from a CP to a reporting fluorophore or quencher. CPs in all of these fluorescence-based detection modes can provide signal amplification through efficient energy harvesting and effective energy transfer. Therefore, a CP-based sensory system is suitable a highly sensitive detection when only trace amount of analyte is available. Alternatively, a visible colorimetric detection through the conformation change of a CP upon binding events is also achievable for a convenient detection since the signal can be observed by the naked eye. Various fluorescent CP biosensors have been developed for many different specific biological targets such as DNA, proteins, and various small biological molecules. In the following section, each detection mode in the recent literatures are discussed in detail.

1.5.1. Turn-on Mode

CPE-based fluorogenic probes for proteases have been developed by Swager and co-workers.[45] They synthesized a set of carboxylic group-functionalized PPEs in which the carboxylic groups are separated from the polymer backbone by ethylene oxide spacers to make the polymer water-soluble (Figure 1-10). An oligopeptide that has a sequence specific to the protease trypsin was covalently bioconjugated to the carboxylic groups of PPE through the use of carbodiimide chemistry. Also, dinitroaniline quenchers added to the end of the peptide unit can effectively quench the fluorescence of the PPE.

After the peptide was cleaved by trypsin the PPE fluorescence was restored. Although the polymer was soluble in water and organic solvents, the quantum yield of the polymer in water was low presumably due to the limited solubility in water and resulting aggregation. The authors used a surfactant to improve the solubility of the polymer in water and achieved 3 times improvement in the fluorescence turn-on signal because the actual rate of enzymatic cleavage was not affected by the surfactant.

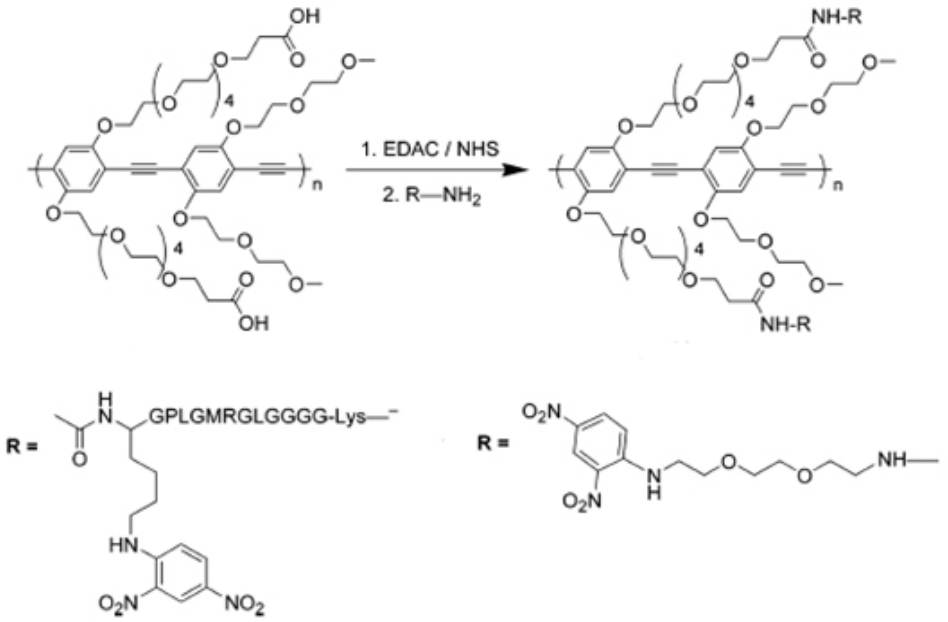

Figure 1-10. Synthesis of quenched peptide fluorogenic substrate.[45]

Tan and co-workers in 2005 reported a DNA-poly(phenylene ethynylene) (PPE) conjugate for label-free DNA detection (Figure 1-11).[46] An oligonucleotide unit that can form a molecular beacon hairpin loop was first synthesized on a fluorescent quencher (DABYCYL = 4-(4-(dimethylamino)phenyl-azo)benzoic acid)-terminated controlled pore glass (CPG). The oligonucleotide on CPG support was chemically modified with an

iodine group, making it suitable as a monomer for the polymerization of PPE. *In-situ* polymerization using two monomers, diethynylbenzene and diiodo-benzene with a sulfonated ionic pendent group, was achieved in the presence of the iodine-modified oligonucleotide CPG support. After the polymerization unbound PPE was easily separated from the DNA-PPE product by washing and centrifugation and the DNA-PPE hybrid materials were cleaved and deprotected to produce the final product. When the molecular beacon was in its closed state the polymer chain was close to the quencher and the emission from PPE was strongly suppressed. In the presence of complementary DNA the beacon opened and the PPE was able to emit an amplified fluorescence signal. Since PPEs aggregate in water and their emission was red-shifted due to the hydrophobic nature of the polymer backbone, non-ionic surfactant was needed to improve the water-solubility.

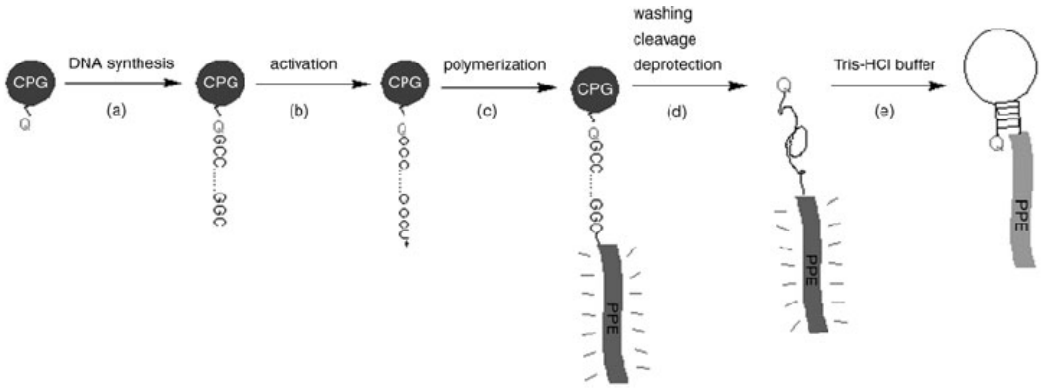

Figure 1-11. Schematic representation of the PPE-labeled molecular beacon.[46]

Another interesting turn-on sensor was actually developed as a colorimetric sensor based on poly(3-alkoxy-4-methylthiophene)s. These polymers change color when their conformation is altered and various derivatives have been synthesized to sense small

biological molecules along with large proteins and DNA. Fluorescent and colorimetric biosensing by means of poly(3-alkoxy-4-methylthiophene)s were first developed by Leclerc and co-workers. Initially, a water-soluble biotinylated polythiophene copolymer was synthesized, which has a violet color in solution but turns yellow when avidin is added.[47,48] When biotin binds to the large avidin protein the polymer main chain is twisted, which shortens the conjugation length of the backbone and changes the color of the solution. A similar concept was also applied to the colorimetric detection of DNA.[49,50] In this system a water-soluble cationic polythiophene is first exposed to single-stranded DNA, which forms a duplex with the polymer and causes the polymer chains to have an extended conformation (Figure 1-12). This change in conformation causes the polymer solution to turn from yellow to red due to the extended conjugation. After the complementary DNA strand is added, the solution turns back to yellow because of the formation of a triplex conformation. In this state, the polymer is less planar than in the duplex conformation, and thus has a shorter conjugation length and different absorption characteristics. Using simple electrostatic interactions and subsequent conformational changes the authors were able to colorimetrically detect oligonucleotides without any chemical labeling at the detection limit of 2×10^{-7} M. It is worth noting that the cationic polythiophene used in this experiment is also fluorescent and the fluorescence is quenched in the duplex (planar and aggregated) state. The fluorescence is mostly recovered in the triplex conformation and this fluorescence signal can be used to improve the detection limit as low as 2×10^{-14} M. Since the development of the colorimetric and fluorescent polythiophene DNA sensors, other derivatives of the water-soluble polythiophenes have been developed to sense proteins and small biological molecules.

Leclerc *et al* applied a similar concept to detect human α-thrombin using an aptamer that specifically binds to human α-thrombin and causes a cationic polythiophene to change conformation and subsequently change color.[51]

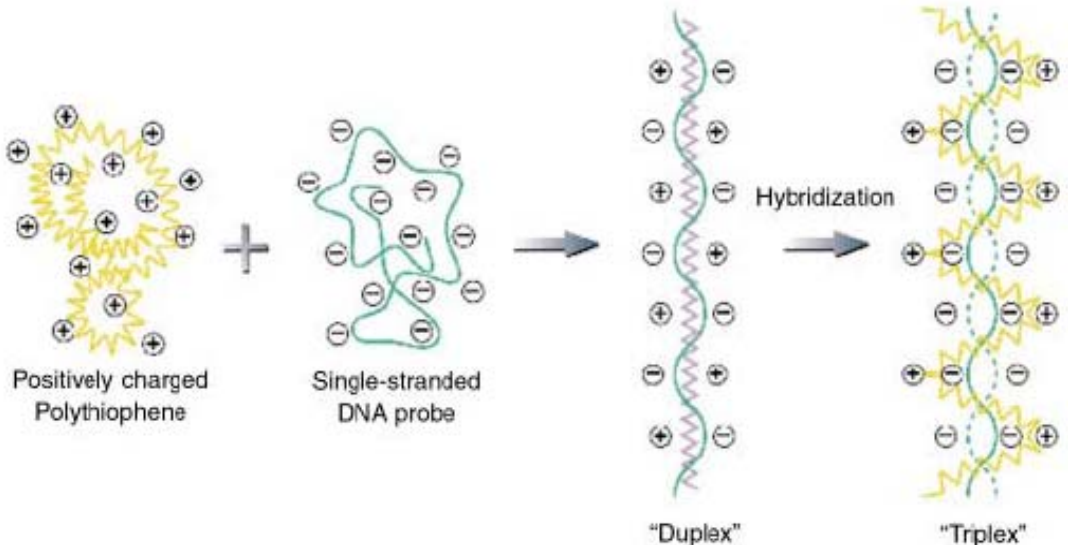

Figure 1-12. Schematic description of the formation of polythiophene/single-stranded nucleic acid duplex and polythiophene/hybridized nucleic acid triplex forms.[49]

1.5.2. Turn-off Mode

Fluorescence-based DNA or protein detection using polymer-grafted microparticles or microarrays is a growing development area in biosensor technologies. Especially, DNA or protein sensors having solid-support have many advantages such as fast and facile handling and low-cost when compared with homogeneous solution-based sensors that require fastidious isolation and purification steps. In 2004 Whitten and co-workers reported a highly sensitive protease sensor achieved by the superquenching techniques using fluorescent conjugated polyelectrolytes.[52] They prepared a synthetic

peptide substrate that contains a recognition and cleavage sequence and a non-fluorescent quencher (QSY-7 or Azo) and biotin at the two termini. Also, microsphere sensors were prepared by coating the surface of polystyrene microspheres with biotin binding protein (streptavidin or neutravidin) followed by additional coating of anionic biotin-functionalized PPEs or cationic PPEs. Initially, two types of experiments were conducted as indicated in the Figure 1-13. In the first approach, quencher and biotin tethered oligopeptides were incubated in an enzyme solution and the fluorescent polymer-coated microspheres were added after the enzymatic reaction. In the second approach, oligopeptides were first mixed with polymer-coated microspheres and then the enzyme was added. The first approach provided a very sensitive assay for cleavage in the presence of enzyme. Microspheres showed intense emission when enzymatic oligopeptide hydrolysis cleaved the tether between biotin and the quencher. The second approach, however, resulted in fluorescence quenching of the polymer because enzymatic cleavage was inhibited when the peptide was anchored on the microspheres.

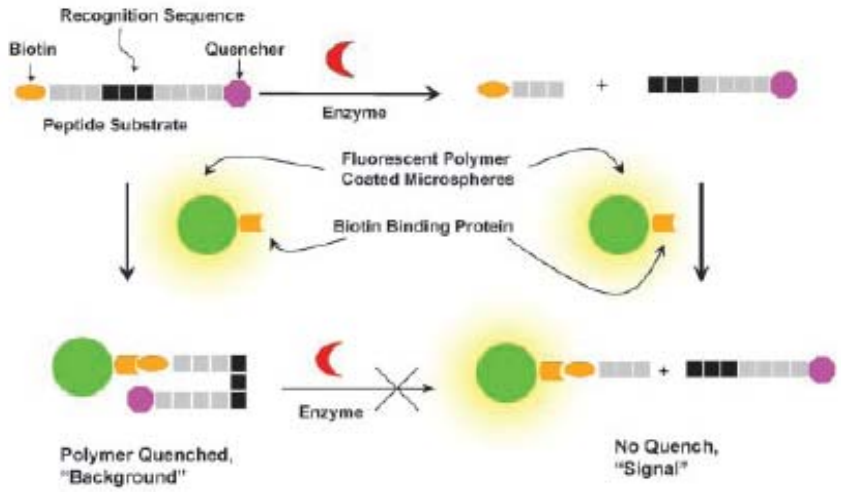

Figure 1-13. General scheme for the quencher-tether-ligand (QTL) protease assay.[52]

Schanze and co-workers have examined fluorescence quenching of the anionic conjugated polyelectrolyte with a series of cationic cyanine dyes to provide insight into the mechanism of amplified quenching (Scheme 1-1).[53] Amplified quenching by dipole-dipole interaction between the polymer and the dye was attributed to the energy transfer from the polymer to the dye acceptor. Fluorescence life-time experiments on the polymer/quencher system clearly indicated that the quenching efficiency was significantly dependent on the aggregation state of the conjugated polymers in solvents. Quenching mechanism for the slow energy transfer pathway primarily comes from intrachain diffusion of a singlet exciton, which is initially produced on a polymer chain at a site distant from the prompt quenching radius of the dye-binding site (Figure 1-14). As the dye concentration increased, the dynamics of this process accelerated due to the decrease of the average distance between the exciton and the nearest dye. However, the polymer aggregation which occurred at a higher dye concentration enhanced the possibility of interchain diffusion of excitons, resulting in the increase of the contributions of prompt and diffusional quenching to the overall quenching.

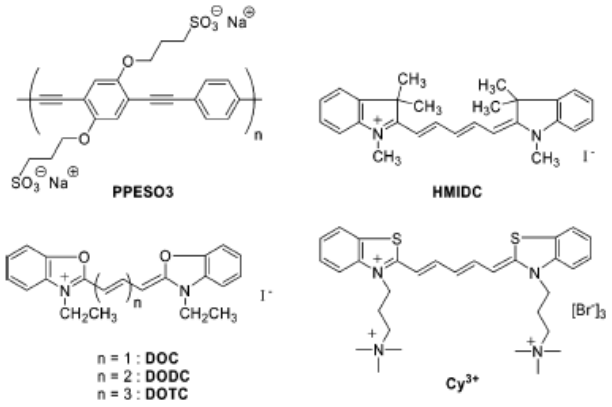

Scheme 1-1. Water soluble conjugated polymers and cationic dyes used in this study.[53]

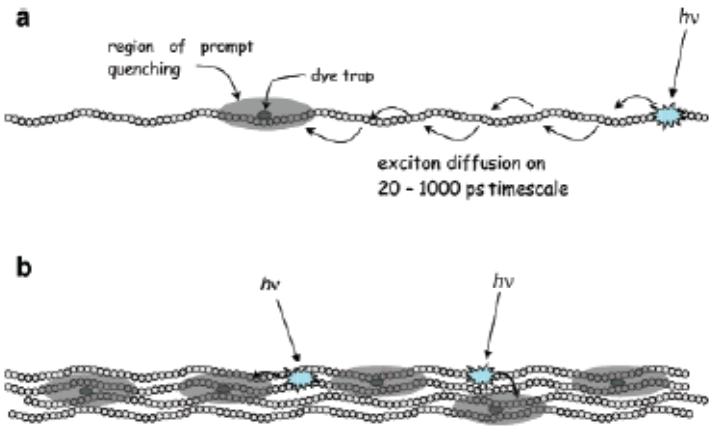

Figure 1-14. Schematic illustration of exciton quenching by bound dye molecules. (a) high polymer/dye concentration ratio. Some excitons are quenched rapidly and others more slowly due to the exciton diffusion time along the chain. (b) Low polymer/dye concentration ratio. All excitons are in close proximity to the quenching region and quenching is dominated by a rapid process involving intra- and interchain exciton diffusion.[53]

Recently, Shinkai *et al* at Kyushu University (Japan) used a cationic polythiophene to detect the anion adenosine triphosphate (ATP), a molecule that is vital for energy in living systems.[54] This technique was modified from the concept of colorimetric and fluorescent sensor mentioned above. This group showed that a solution containing the polymer changed from yellow to pink-red when ATP was added, due to the formation of π-stacking polymer aggregates. Using fluorescence spectroscopy ATP was detected in concentrations around 10^{-8} M.

1.5.3. Fluorescent Color Change Mode

A high extinction coefficient and effective one-dimensional migration of excitons throughout the backbone of CPs enable an exciton to move to a position on the chain

from which FRET can happen efficiently. Therefore, CPEs have the potential to be excellent energy donors in FRET-based DNA detection in aqueous media. Bazan and Heeger at University of California at Santa Barbara have developed a solution-based DNA sensor using water-soluble cationic conjugated poly(fluorene-co-phenylene)s. The strategy was first published in 2002 and used fluorescein-labeled peptide nucleic acid (PNA) to detect a target complementary DNA.[55] A PNA molecule is a synthetic DNA mimic having the same base units and neutral amide linkages rather than negatively charged phosphate linkages (Figure 1-15). PNA molecules can form a much more stable Watson-Crick base pairs with single-stranded DNA (ssDNA) than DNA-DNA double helix due to the charge neutrality of the PNA backbone. When the PNA is mixed with cationic conjugated polymers the average distance between the polymer and the PNA in aqueous solution is greater than the effective FRET distance because there is no electrostatic attraction between them. However, once a negatively charged complementary DNA is introduced to the solution, DNA hybridizes with PNA and the DNA/PNA complex electrostatically binds to the positively charged polymer, which brings the polymer and the dye attached to PNA close enough for FRET to happen. Therefore, in the present of a target DNA, a large amount of fluorescent energy from the polymer is efficiently transferred to the dye to provide strong signal from dye.

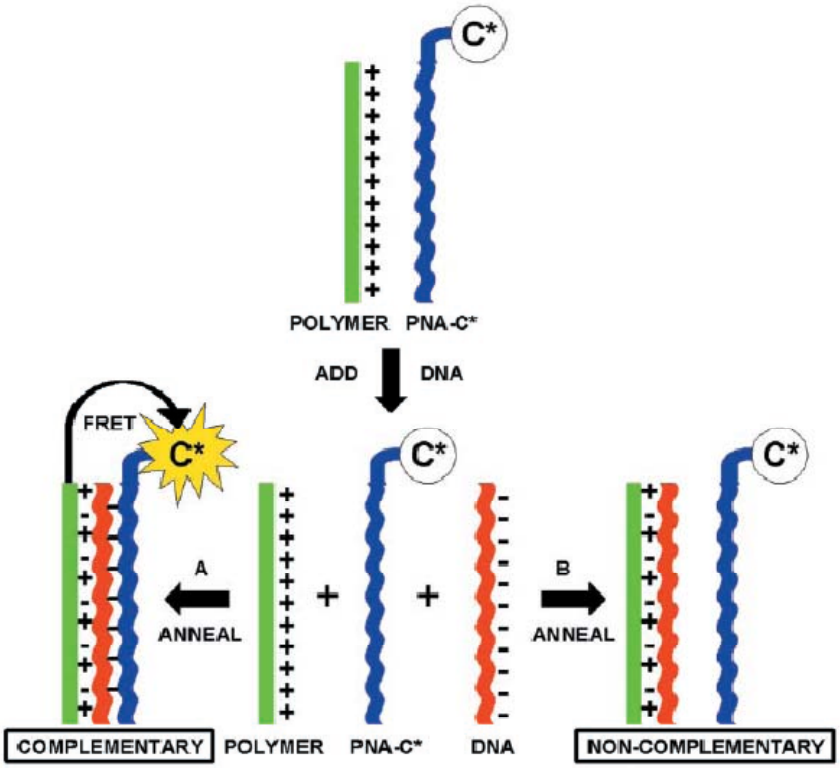

Figure 1-15. Schematic representation for the use of a water-soluble CPs with a specific PNA-C* optical reporter probe to detect a complementary ssDNA sequence.[55]

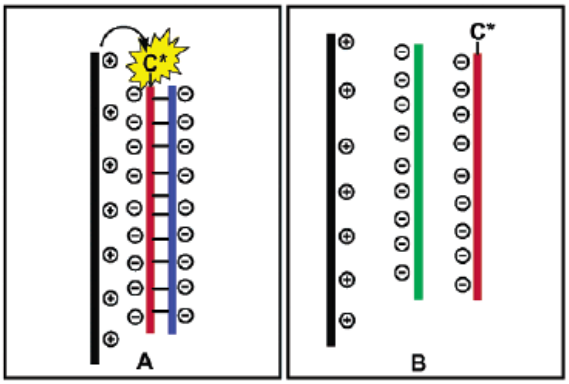

Figure 1-16. Modified schematic DNA-C*/DNA sensor operation.[56]

Later they have also developed a more conventional DNA/DNA duplex sensor based on the previous results of the PNA/DNA sensor but instead of using PNA, a tagged probe ssDNA strand was used (Figure 1-16).[56,57] When the polymer and dye-labeled DNA are incubated with target complement a stable polymer/DNA/DNA triplex is formed due to DNA/DNA hybridization and FRET from the polymer to the dye amplifies the fluorescent signal. The fluorescence intensity of the dye when the polymer was excited was 4-fold greater than that when the dye was directly excited. However, in the random-sequence case some dipole-dipole interaction existed between the dye-labeled probe DNA and the conjugated polymer. This problem due to non-specific interaction was reduced though because non-complementary ssDNA interferes with the electrostatic interaction between the dye-DNA and polymer, which results in a reduction of FRET. Partial screening of the probe-DNA from the polymer results in a 3-fold decrease in fluorescence intensity relative to when target DNA is present. Wang and co-workers also developed single nucleotide polymorphism (SNP) sensors using a similar concept developed by Bazan (Figure 1-17).[58] In the sensory system the target DNA was the mutant DNA fragment Arg282Trp, which has a nucleotide G instead of a specific A in the wild-type fragment as shown in Figure 1-17 (a). The nucleotide T located at the 3'-terminal base of the DNA probe is complementary to the mutant-type target sequence and is not complementary to the wild-type target. The probe was extended using Taq DNA polymerase and fluorescein labeled-dGTP on the G base. Therefore, the mutant target duplex has fluorescein at the end of 3'-terminus of the probe while the wild target does not. By adding a blue-emissive conjugated polyelectrolyte as an energy donor,

fluorescein, which accepts energy from the polymer, emitted an amplified signal only when the mutant target was present.

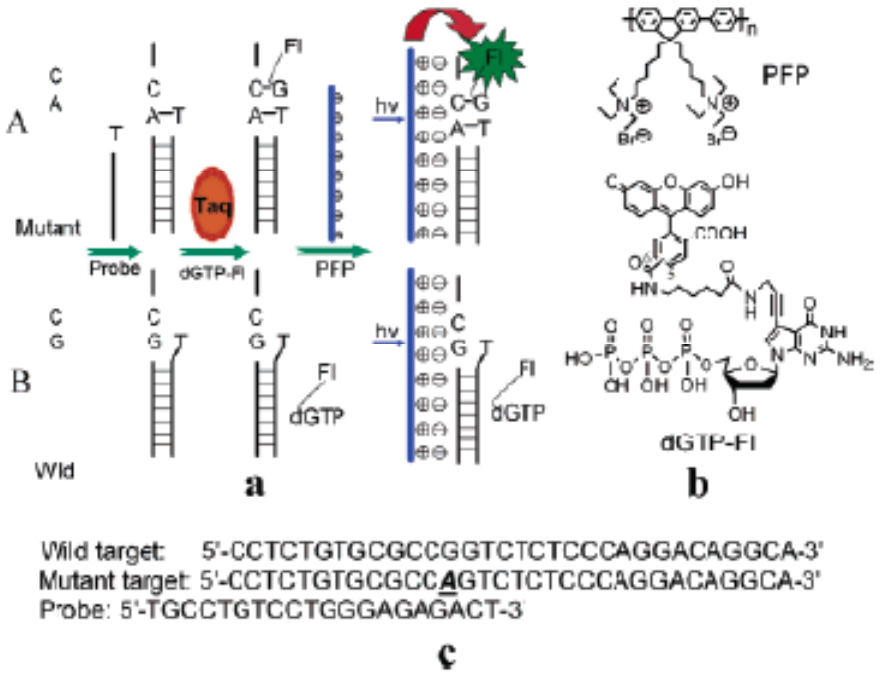

Figure 1-17. (a) Schematic representation of the SNP assay. (b) polymer structure of PFP and dGTP-Fl. (c) DNA sequences used in the study.[58]

Sensitivity and selectivity are often limited in the DNA/CP complex-based system because of the non-specific binding between dye-labeled anionic ssDNA and cationic polymer through electrostatic interactions. Wang *et al*. strived to improve the specificity of the polymer/DNA sensor by using a common intercalating dye, ethidium bromide (EB) (Figure 1-18).[59,60] The researchers used the same system as the previous polymer/DNA/DNA-dye triplex method except they added EB and monitored of the EB emission as the actual sensory signal. When target complement formed hybridization with the probe DNA, EB was selectively intercalated into the hydrophobic regions of the

double helix. Large signal amplification of EB was achieved by a stepwise energy-transfer process, which they called a fluorescence resonance gate (FRET gate), from polymer to fluorescein (FRET1) and then from fluorescein to EB (FRET2). The cascading energy-transfer process provides a substantial increase in EB emission through the light harvesting and signal amplifying properties of the conjugated polymer. Recently, they applied this concept to a G-quadruplex-to-duplex transition system by using a fluorescein-labeled guanine(G)-rich oligonucleotide probe. Before hybridization G-rich DNA forms a stable quadruplex with the aid of potassium ions and was attached to a cationic polymer through electrostatic interactions. Even though FRET1 from polymer to fluorescein happens, fluorescein and EB are not close enough for FRET2 to occur. However, the quadruplex-to-duplex transition in the presence of target complementary DNA enables EB to intercalate the double helix. Close proximity of the polymer/fluorescein-DNA to EB provides an effective FRET gate for the detection of amplified EB emission. The overall process provides substantial improvement in terms of specificity over previous homogeneous conjugated polymer-based DNA sensors that use FRET sensitization.

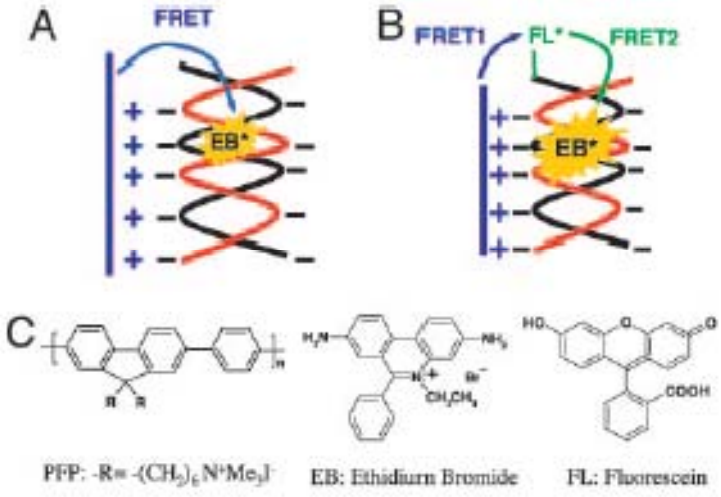

Figure 1-18. Schematic representation of DNA sequence detection by FRET from the polymer to intercalating dyes in the absence (A) and presence (B) of the FRET gate. (C) Chemical structure of CPs (PFP), FL and EB.[60]

In 2004 Seeberger and co-workers reported the detection of the bacteria *Escherichia coli* (*E. coli*) by using carbohydrate-functionalized PPE.[61]The design of the sensory system utilized the fact that carbohydrates expressed at the cell surface are commonly used as receptors by many kinds of pathogens that cause human infections. The authors polymerized water-soluble carboxylated PPE and through post-polymerization modification incorporated 2'-aminoethyl mannoside units, which was first used by Bunz *et al*.[62] When mannose-functionalized PPE was incubated in Alexa Fluor 594(yellow dye)-labeled concanavalin A (Con A), a lectin that binds mannose, the strong blue fluorescence from PPE was quenched by FRET from the polymer to the dye. A control galactose-functionlized PPE did not show any fluorescence quenching by FRET, confirming that mannose-functionalized PPE has the specificity toward the lectin. Interestingly, incubation of the mannose-functionalized PPE with *E. coli* yielded brightly fluorescent aggregates of bacteria. This aggregation was formed due to the multivalent

interactions between the carbohydrate receptors on the *E. coli* and the glycosylated PPE. Design of polymer-based detectors for other pathogens only requires information about the carbohydrates that they bind, which has been extensively reported in the literature.

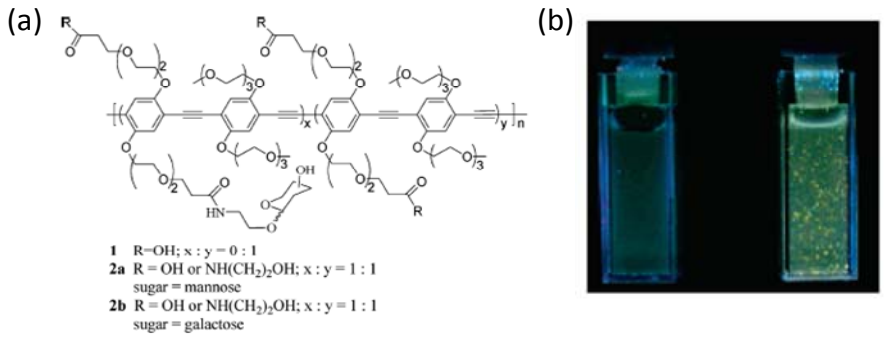

Figure 1-19. (a) Chemical structure of the polymers used in this study. (b) Visualization of mutant, left, and mannose-binding, right, E. coli strains after incubation with mannosylated polymer **2a**.[62]

1.6. Objectives

Conjugated polymer-based biosensors have drawn a great deal of interest from both academia and industry because conjugated polymers have several unique properties such as energy-harvesting ability and excellent emissive properties. As a result of the fact that the properties of conjugated polymers can be precisely modified by structural modifications, these polymeric materials have great potential as signal-reporting groups in design of novel sensory systems. In addition, the development of conjugated polymer-receptor hybrid system through the introduction of functionality to their chemical structures and efficient bioconjugation can lay a firm foundation for conjugated polymer-based biosensor development. This thesis focuses on the fabrication and optimization of the functionalized conjugated polymers for biosensory applications. Throughout this

thesis, important tuning parameters to optimize the sensitivity and selectivity of the conjugated polymer-based biosensor systems will be systematically addressed. In particular, it aims to address the diverse methods regarding chemical modification for bioconjugation and signal transduction for reporting a target-binding event.

Following chapters of this thesis mainly constitutes two categories; a) solution-state sensors using conjugated polyelectrolytes (Chapters 2 through 5), b) solid-state sensors using microarray technique (Chapters 6 through 10). In Chapter 2, insight into the optimization of the water-solubility and the emissive properties of conjugated polyelectrolytes by modulating the side-chain design of the polymers will be provided. Based on this design principle of the optimized polymer structure, Chapter 3 then elaborates on facile method for bioconjugation between conjugated polymers and probe molecules for sensory applications. Chapter 4 covers the development of hybrid bio/-synthetic sensory conjugated polyelectrolytes for signal amplification. Label-free method using molecular beacons will be also discussed. In Chapter 5, a new platform capable of live-cell imaging using water-soluble conjugated polymer-antibody hybrid conjugation materials will be demonstrated. For the application of conjugated polymers to on-chip oligonucleotide or peptide synthesis, highly fluorescent and uniquely stable conjugated polyoxadiazole derivatives were developed in Chapter 6. Chapter 7 describes a fast and readily applicable strategy to make a signal amplifying DNA microarray by means of the novel conjugated polymer developed in Chapter 6. Based on the solid-state signal amplifying result using conjugated polymers described in Chapter 7, efficient label-free detection methods using an intercalating dye and a molecular beacon in DNA microarray was introduced in Chapters 8 and 9, respectively. Finally, in Chapter 10, solid-state

microarray technique using conjugated polymers will be expanded to the development of sensor chips capable of highly sensitive and label-free detection of prostate specific antigen (PSA).

Parts of some chapters have been published previously as noted in respective chapters. The co-authors of the publications have contributed to the results in terms of materials preparations, experimentations, discussions, or manuscript preparation.

1.7. References

1. Shirakawa, H.; Louis, E. J.; MacDiarmid, A. G.; Chiang, C. K. and Heeger, A. J. *Chem. Commun*. **1977**, 578.

2. Service, R. F. *Science* **2000**, *290*, 425.

3. Kraft, A.; Grimsdale, A. C.; Holmes, A. B. *Angew. Chem. Int. Ed.* **1998**, *37*, 402.

4. Montali, A.; Smith, P.; Weder, C. *Synth. Met*. **1998**, *97*, 123.

5. Gustafsson, G.; Cao, Y.; Trecy G. M.; Klavetter, F.; Colaneri, N.; Heeger, A. J. *Nature* **1992**, *347*, 477.

6. Pei, Q.; Yang, Y.; Yu, G.; Zhang, C.; Heeger, A. J. *J. Am. Chem. Soc*. **1996,** *118*, 3922.

7. Cheng, C. H. W.; Lonergan, M. C. *J. Am. Chem. Soc*. **2004**, *126*, 10536.

8. Pei, Q.; Yu, G.; Zhang, C.; Yang, Y.; Heeger, A. J. *Science* **1995**, *269*, 1086.

9. Armstrong, N. R.; Wightman, R. M.; Gross, E. M. *Annu. Re*V. *Phys. Chem*. **2001**, *52*, 391-422.

10. Smela, E.; Ingana¨s, O.; Lundstro¨m, I. *Science* **1995**, *268*, 1735.

11. Baughman, R. H.; Shacklette, L. W.; Elsenbaumer, R. L.; Plichta, E. J.; Becht, C. In *Molecular Electronics*; Lazarev, P. I., Ed.; Kluwer Academic Publishers: Dordrecht, 1991; pp 267-289.

12. Stutzmann, N.; Friend, R. H.; Sirringhaus, H. *Science* **2003**, *299*, 1881.

13. Hide, F.; Diaz-Garcia, M. A.; Schwartz, B. J.; Heeger, A. J. *Acc. Chem. Res.* **1997**, *30*, 430.

14. McGehee, M. D.; Heeger, A. J. *Adv. Mater.* **2000**, *12*, 1655.

15. Torsi, L.; Dodabalapur, A.; Rothberg, L. J.; Fung, A. W. P.; Katz, H. E. *Science*, **1996**, *272*, 1462.

16. Novak, P.; Muller, K.; Santhanam, K. S. V.; Haas, O. *Chem. Rev*. **1997**, 97, 207.

17. Alam, M. M.; Jenekhe, S. A. *Chem. Mater*. **2004**, *16*, 4647.

18. McGinness, J.; Corry, P.; Proctor, P. *Science*, **1974**, *183*, 853.

19. Vogel, A.; Venugopalan, V. *Chem. Rev*. **2003**, *103*, 577.

20. Thomas, S. W., III; Joly, G. D.; Swager, T. M. *Chem. Rev.* **2007,** *107*, 1339.

21. McQuade, D. T.; Pullen, A. E.; Swager, T. M. *Chem. Rev*. **2000**, *100*, 2537.

22. Sonogashira, K.; Tohda, Y.; Hagihara, N. *Tetrahedron Lett.* **1975**, 4467.

23. Sonogashira, K. In *Handbook of Organopalladium Chemistry for Organic Synthesis*; Negishi, E., Ed.; Wiley-Interscience: New York, 2002; pp 493-529.

24. Stille, J. K. *Angew. Chem., Int. Ed. Engl*. **1986**, *25*, 1.

25. Yamada, J.; Yamamoto, Y. *J. Chem. Soc., Chem. Commun.* **1987**, 1302.

26. Miyaura, N.; Yamada, K.; Suzuki, A. *Tetrahedron Lett.* **1979**, 3437.

27. Miyaura, N.; Suzuki, A *Chem. Rev*. **1995**, 95, 2457.

28. Dieck, H. A.; Heck, F. R. *J. Organomet. Chem.* **1975**, *93*, 259.

29. McCullough, R. D.; Lowe, R. D. *J. Chem. Soc., Chem. Commun*. **1992**, 70.

30. Chen, T. A.; O'Brien, R. A.; Rieke, R, D. *Macromolecules* **1993**, *26*, 3462.

31. Shi, S.; Wudl, F. *Macromolecules* **1990**, *23*, 2119.

32. Pinto, M. R.; Schanze, K. S. *Synthesis-Stuttgart*. **2002**, *9*, 1293.

33. Turro, N. J. Modern *Molecular Photochemistry*: University Science Books: Sausalito, CA, 1991.

34. Wilson, J. S.; Dhoot, A. S.; Seeley, A. J. A. B.; Khan, M. S.; Köhler, A.; Friend, R. H. *Nature*, **2001**, *413*, 828.

35. Haskins-Glusac, K.; Pinto, M. R.; Tan, C.; Schanze, K. S. *J. Am. Chem. Soc*. **2004**, *126*, 14964.

36. Thomas, S. W., III; Yagi, S.; Swager, T. M. *J. Mater. Chem*. **2005**, *15*, 2829.

37. Kim, J.; Swager, T. M. *Nature* **2001**, *411*, 1030.

38. Zhou, Q.; Swager, T. M. J. Am Chem. Soc. **1995**, *117*, 12593.

39. Kavarnos, G. J. *Fundamentals of Photoinduced Electron Transfer*, VCH: Weinheim, New York, 1993.

40. Förster, T. *Ann. Phys*. **1948**, *2*, 55.

41. Stryer L.; Hauland R. P. *Proc. Natl. Acad. Sci*. **1967***, 58*, 719.

42. Wu, P.; Brand, L. *Anal. Biochem*. **1994**, *218*, 1.

43. Tyagi, S.; Kramer, F. R. *Nature Biotech*. **1996**, *14*, 303.

44. Tyagi, S.; Bratu, D. P.; Kramer, F. R. *Nature Biotech*. **1998**, *16*, 49.

45. Wosnick, J. H.; Mello, C. M.; Swager, T. M. *J. Am. Chem. Soc.***2005**, *127*, 3400.

46. Yang, C. J.; Pinto, M.; Schanze, K.; Tan, W. *Angew. Chem. Int. Ed*. **2005**, *44*, 2572.

47. Leclerc, M. *Adv. Mater*. **1999**, *11*, 1491.

48. Faïd, K.; Leclerc. M. *J. Am. Chem. Soc*. **1998**, *120*, 5274.

49. Ho, H.-A.; Boissinot, M.; Bergeron, M. G.; Corbeil, G.; Doré, K.; Boudreau, D.; Leclerc, M. *Angew. Chem., Int. Ed.* **2002**, *41*, 1548.

50. Ho, H.-A.; Béra-Abérem, M.; Leclerc, M. *Chem.-Eur. J.* **2005**, *11*, 1718.

51. Béra Abérem M.; Najari, A.; Hoang-Anh, H.; Gravel, J.-F.; Nobert, P.; Boudreau, D.; Leclerc, M. *Adv. Mater*. **2006**, *18*, 2703.

52. Kumaraswamy, S.; Bergstedt, T.; Shi, X.; Rininsland, F.; Kushon, S.; Xia, W.; Ley, K.; Achyuthan, K.; McBranch, D.; Whitten, D. *Proc. Natl. Acad. Sci. U.S.A.* **2004**, *101*, 7511.

53. Tan, C.; Atas, E.; Mu¨ller, J. G.; Pinto, M. R.; Kleiman, V. D.; Schanze, K. S. *J. Am. Chem. Soc.* **2004**, *126*, 13685.

54. Li, C.; Numata, M.; Takeuchi, M.; Shinkai, S. *Angew. Chem. Int. Ed*. **2005**, *44*, 6371.

55. Gaylord, B. S.; Heeger A. J.; Bazan G. C. *Proc. Natl. Acad. Sci.U.S.A.* **2002**, *99*, 10954.

56. Gaylord, B. S.; Heeger A. J.; Bazan, G. C. *J. Am. Chem. Soc*. **2003**, *125*, 896.

57. Liu, B.; Bazan, G. C. *Chem. Mater*. **2004**, *16*, 4467.

58. Duan, X.; Li, Z.; He, F.; Wang, S. *J. Am. Chem. Soc*. **2007**, *129*, 4154.

59. Wang, S.; Gaylord, B. S.; Bazan, G. C. *J. Am. Chem. Soc.* **2004**, *126*, 5446.

60. Xu, Q.-H.; Wang, S.; Korystov, D.; Mikhailovsky, A.; Bazan, G. C.; Moses, D.; Heeger, A. J. *Proc. Natl. Acad. Sci. U.S.A.* **2005**, *102*, 530.

61. Disney, M. D.; Zheng, J.; Swager, T. M.; Seeberger, P. H. *J. Am. Chem. Soc.* **2004**, *126*, 13343.

62. Erdogan, B.; Wilson, J. N.; Bunz, U. H. F. *Macromolecules* **2002**, *35*, 7863.

CHAPTER 2

Modulating the Side-chain Design of Poly(*p*-phenyleneethynylene) Derivatives to Make Water-soluble and Highly Emissive Conjugated Polyelectrolytes

Parts of this chapter appear in: Lee, K.; Yucel, T.; Kim, H.-J.; Pochan, D. J.; Kim, J. manuscript in preparation.

2.1. Abstract

The relationship between the molecular design of a conjugated polyelectrolyte (CPE), its aggregated structure and final fluorescence properties in water was systematically investigated by means of transmission electron microscopy, static and dynamic light scattering, and fluorescence spectrophotometry. Five different, rationally designed CPEs having carboxylic acid side chains for further functionalization were synthesized. All five conjugated polyelectrolytes were seemingly completely soluble in water in visual observation. However, their quantum yield was dramatically different, changing from 0.09 to 51.4 %. Morphological analysis by means of TEM and light scattering, combined with fluorescence spectrophotometry, revealed that the CPEs form self-assembled aggregates at the nanoscale depending on the nature of their side chains. This feature of the self-assembled aggregates directly determined the emissive property of the CPEs. The nature and the length of the spacer between the carboxylic acid group and the CPE backbone had a strong influence on the quantum yield of the CPEs. Our study demonstrates that bulky but hydrophilic side chains are required to achieve complete water-solubility and high quantum yield of CPEs in water, providing a molecular design principle to develop functional CPEs.

2.2. Introduction

A conjugated polyelectrolyte (CPE)[1], a conjugated polymer containing a charged (anionic or cationic) group, has received considerable attention as a biosensor such as solution-based DNA sensor[2-6], DNA microarray[7-9], protein sensor[10-16] in bioimaging[17] as well as optoelectronic materials such as an semiconductors[18], light-emitting device,[19,20] and actuators[21]. The ionic side group plays an important role to provide water-solubility to the polyelectrolytes. Control of the water solubility of CPEs is central to many biological applications due to their compatibility to aqueous environment. In addition, maintaining the highly emissive property of a conjugated polymer in aqueous solution is another requirement for biosensor applications because the merit of using conjugated polymers as a sensor is their amplified fluorescence signaling property upon environmental changes.[22-30] However, in this regard, CPE inherently has a critical problem originating from the fact that a π-conjugated polymer backbone is chemically hydrophobic and structurally rigid. It gives rise to polymer aggregation by intermolecular hydrophobic interaction among the polymer backbones in aqueous solutions.[24,25,31] Therefore, the solubility of CPE in water significantly decreases, consequently inducing a large drop of fluorescence quantum yield due to the aggregation-induced self-quenching. Moreover, once CPEs are completely dried, it is tremendously difficult to redissolve them in water due to the rigid hydrophobic nature of the backbone and ensuing strong, cohesive aggregation. Besides the solubility issue, for many biological applications an efficient and convenient functional group such as a carboxylic acid group or an amine group is also required to introduce a specific function to the CPE by means of bio-conjugation between the CPE and a biological molecule.[32,33]

Due to these demanding requirements, it remains a difficult task to develop highly emissive and completely water-soluble functional CPE. Several research groups have developed CPE-based functional systems by utilizing the emissive property of CPEs. Leclerc et al developed DNA sensors using cationically charged and water-soluble polythiophene derivatives. Charge-charge interaction between the cationic CPE and a single strand DNA and subsequent detection of the complementary DNA produces a conformation change of the CPE and consequent unique color change as a sensory signal.[2,10,34-37] Bazan and co-workers have reported signal amplifying biosensors based on cationically charged water-soluble CPEs and fluorescence resonance energy transfer (FRET).[4] Schanze *et. al.* investigated water-soluble CPE systems and reported amplified fluorescence quenching of sulfonated CPEs due to π-π aggregation of the rigid linear CPEs in aqueous media.[24,25,27] Recently, completely water-soluble CPEs have been also reported.[33,38] However, to our knowledge there has not been any article that comprehensively provides design principles to develop highly emissive and completely water-soluble CPEs systematically.

We have rationally designed and prepared a series of PPE-based CPEs and systematically investigated the effects of side chain structure on the solubility and fluorescence quantum yield in aqueous solution. Here, we report our comprehensive transmission electron microscopy (TEM) study, static and dynamic light scattering study, and quantum yield study to reveal the correlation between the chemical and structural characteristics of the side chain of the PPEs, their molecular assembly in water, and their emissive property. We chose carboxylic acid moiety for this study as a pendant ionic group considering the fact that it is the most convenient functional group for

bioconjugation with the ubiquitous amine group present in biological molecules. As molecular design parameters, we controlled the bulkiness of the side chain, the length of the linker molecule between the conjugated backbone and the carboxylic acid group, and the hydrophobic and hydrophilic property of the linker as illustrated in Figure 2-1.

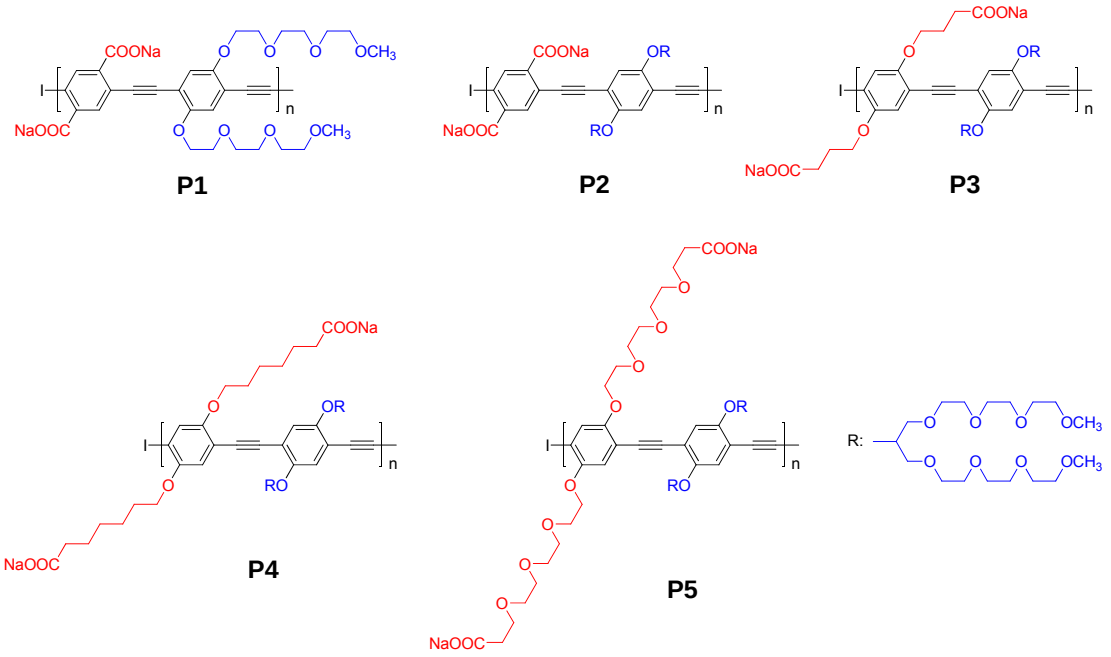

Figure 2-1. Polymer (**P1**-**P5**) Structures.

2.3. Experimental Section

2.3.1. General Methods

Materials and methods. All chemicals were purchased from Sigma-Aldrich, Inc. or Acros Organics, Inc. and used without further purification. Compound **1**[39,40], **2**[41,42], **M5**[33] and **M6**[33,38,43] in Scheme 1 and 2 were prepared according to the literature published previously. All polymers (**P1** to **P5-A** and **B**) were purified by dialysis against deionized water (molecular weight cut off : 12,000 – 14,000 $gmol^{-1}$) for 3 days, lyophilized to dry the polymer, and stored in the dried state at 4 °C. The molecular

weight of all PPE polymers except **P5-A** was determined by PS-GPC in THF before the cleavage of ethylhexyl protection group for the carboxylic acid group. Due to the limited solubility of **P5-A** in THF, its number-averaged molecular weight (M_n) was calculated by ^{1}H NMR end-group analysis.

Photophysical Experiments. UV/Vis absorption spectra of the conjugated polymer solutions were obtained on a Cary UV50 UV/Vis spectrometer (Varian, Inc.). Steady-state fluorescence spectra of the polymers were recorded on a PTI QuantaMaster spectrofluorometer™. The molar concentration of the polymer solutions was determined based on the repeat unit of the polymers. The true quantum yield of the polymers was measured with excitation at 365 nm in deionized water (1 mgL^{-1}) using an integrating sphere attached to the same spectrofluorometer.

Transmission Electron Microscopy. A copper TEM grid coated with a 20-30 nm film of pure carbon (purchased from Electron Microscopy Sciences, PA, USA) was held at the edge of a tweezer. A small drop of the polymeric solution was placed on the grid to form a bead. Excess sample was blotted off by touching with a filter paper and the sample was left to dry. Images were taken in bright-field mode with a Tecnai G2 12 Twin transmission electron microscope at 120 kV accelerating voltage. Structures were imaged at slight underfocus in order to enhance contrast.

Light Scattering Method. All solutions, except P4 (in pH=8), were in neutral (pH=7) deionized water and the solution concentrations were 0.05 wt%. This was the lowest concentration that gave enough signal to noise ratio in DLS experiments. All samples were filtered with 0.2 μm cellulose filter prior to the measurements. For dynamic

light scattering (DLS) experiments, polymer solutions were filtered into 1 cm diameter quartz cells. Samples were loaded in the thermostatted cell compartment of a Brookhaven Instruments BI200-SM goniometer, equipped with a diode laser operated at 532 nm wavelength. The temperature was controlled with 0.05 ^{o}C accuracy with a thermostatted recirculating bath at 22 ^{o}C. The time-averaged auto-correlation function (ACF) of the scattered intensity at 90^{o}, $g_2(q,t)$ was measured using a Brookhaven BI-9000 correlator. CONTIN regularization algorithm encoded by Provencher[44] was used for calculation of the mean hydrodynamic radius. We also carried out static light scattering measurement for **P1** using DAWN EOS (Wyatt Technology) to measure the radius of gyration of P1 in water. The detection angles range from 14° to 100° with 18 different angles and a solid-state laser with wavelength of 690 nm is employed. HPLC grade toluene filtered with a 0.02 μm syringe filter is passed through the flow cell for calibration; the software converts the raw voltage signal at 90° to the actual scattering intensity. And then, flow cell is filled with filtered (0.2 μm) Dextran (GPC grade, molecular weight: 25,000) in water and the voltage signal of each detector, which is corrected for the actual angle, is normalized to the 90° detector. Data are collected by injecting the polymer solution at 1 mg/ml using a 0.2 μm syringe filter.

2.3.2. Synthesis and Characterization

Synthesis of Bis(2-ethylhexyl) 2,5-diiodoterephthalate (**M1**) 2,5-diiodoterephthalic acid (**1**, 0.3 g, 0.72 mmol), 2-ethyl-1-hexanol (0.28 g, 2.16 mmol), toluene (20 ml), and 0.1 mL of concentrated H_2SO_4 were heated for 24 h to reflux, with separation of the water using a Dean-Stark trap. Reaction mixture was cooled down and

the organic layer was washed with water and dried with $MgSO_4$. Further purification was done by column chromatography (ethyl acetate: hexane = 1: 15 v/v) to get viscous yellow oil (0.14 g, 30 %). ^{1}H-NMR (500 MHz, $CDCl_3$): δ/ppm 8.26 (s, 2H, aromatic), 4.27 (d, 4 H, -OC$\underline{H}_2$-), 1.79 (m, 2H, -C$\underline{H}$-), 1.55-1.30 (m, 16H, -C$\underline{H}_2$-), 0.95 (m, 12H, C$\underline{H}_3$).

Diethyl 4,4'-(2,5-diiodo-1,4-phenylene)bis(oxy)dibutanoate (**M2**) To a solution of 2,5-diiodo-1,4-hydroquinone (**2**, 1.0 g, 2.76 mmol) were added a potassium carbonate (1.615 g, 8.28 mmol), ethyl 4-bromobutyrate (1.615 g, 8.28 mmol) and DMF (15 ml) and reaction mixture was stirred at 80 ºC for 48 hr. After the reaction, reaction mixture was cooled down and filtered. DMF was removed with rotary evaporator at reduced pressure. Crude mixture was re-dissolved in chloroform and extracted twice with deionized water. After drying over $MgSO_4$ and filtering, chloroform was removed in vacuo. Further purification was done by column chromatography (ethyl acetate : hexane = 1 : 1 v/v) and the following recrystallization in methanol at –18 oC to give white waxy powder (yield: 0.65 g, 41 %). ^{1}H-NMR (500 MHz, $CDCl_3$): δ/ppm 7.10 (s, 2H, aromatic), 4.20 (m, 4H, -OC$\underline{H}_2$CH$_3$), 4.01 (t, 4H, -OC$\underline{H}_2$-), 2.60 (t, 4H, -C$\underline{H}_2$COO-), 2.15 (m, 4H, -C$\underline{H}_2$-), 1.27 (t, 6H, -CH$_3$).

Diethyl 7,7'-(2,5-diiodo-1,4-phenylene)bis(oxy)diheptanoate (**M3**) Synthetic procedure for this compound is the same as that for **M2** except for using ethyl 7-bromoheptanoate (2 g, 8.43 mmol) as a reactant and different column eluent (ethyl acetate : hexane = 1 : 4 v/v) for column purification (yield: 0.89 g, 47 %). ^{1}H-NMR (500 MHz, $CDCl_3$): δ/ppm 7.18 (s, 2H, aromatic C-$\underline{H}$), 4.15 (m, 4H, COO-C$\underline{H}_2$-CH$_3$), 3.94 (t, 4H, O-C$\underline{H}_2$-), 2.33 (t, 4H, CH$_2$-C$\underline{H}_2$-CO-), 1.82 (m, 4H, -C$\underline{H}_2$-), 1.69 (m, 4H, -C$\underline{H}_2$-),

1.54 (m, 4H, -C<u>H</u>$_2$-), 1.42 (m, 4H, -C<u>H</u>$_2$-), 1.27 (t, 6H, -C<u>H</u>$_3$), Elemental analysis calcd; C 42.75, H: 5.38, obsd; C: 42.85, H: 5.40.

***Tert*-butyl 3-(2-(2-(2-hydroxyethoxy)ethoxy)ethoxy)propanoate** (**3**) This compound was prepared by procedure in a previous literature[32] through a slight modification. In 1000 ml of 2-necked round-bottomed flask, triethylene glycol (128 ml, 0.40 mol) is dissolved in 500 ml of THF. 0.34 g (14.8 mmol) of sodium lump was sliced and added to the solution under argon purging. The solution was vigorously stirred to dissolve sodium completely. After no more gas or bubble, *tert*-butyl acrylate (48 ml, 0.33 mol) was added to the solution. The reaction solution was stirred under argon atmosphere at room temperature for 20 h. The solution was neutralized with 1 M HCl and THF was evaporated at reduced pressure. Crude compound was suspended to saturated brine and extracted with ethyl acetate. Organic layer was washed with saturated NaCl solution and water again and dried over anhydrous $MgSO_4$ (yield: 58.5 g, 53 %). ^{1}H-NMR (500 MHz, $CDCl_3$): δ/ppm 3.75-3.21 (m, 14H, -OC<u>H</u>$_2$-), 2.69 (broad s, 1H, O<u>H</u>), 2.51 (t, 2H, -C<u>H</u>$_2$COO-), 1.45 (s, 9H, -C(CH_3)$_3$).

***Tert*-butyl 3-(2-(2-(2-(tosyloxy)ethoxy)ethoxy)ethoxy)propanoate** (**4**) Compound **3** (58.5 g, 0.21 mol) and triethylamine (171 ml) was dissolved in anhydrous dichloromethane (290 ml) and the solution was cooled down to 4 ºC using iced bath. *p*-toluenesulfonyl chloride (46.82 g, 0.245 mol) in 100 ml of dichloromethane was added dropwise. The temperature of reaction solution was slowly increased to room temperature and the solution was stirred overnight. After the reaction, the solution was poured into 1300 ml of 1 M HCl and the aqueous phase is removed. Organic phase was washed with saturated NaCl solution and dried over $MgSO_4$. The compound was purified by column

chromatography (ethyl acetate: hexane = 1: 1 v/v) (yield : 69.9 g, 77 %). ^{1}H-NMR (500 MHz, $CDCl_3$): δ/ppm 7.60 (d, J=5 Hz, 2H, aromatic H), 7.18 (d, J= 5 Hz, 2H, aromatic H), 3.97 (t, 2H, S-O-C$\underline{H}_2$), 3.58-3.31 (m, 12H, -O-C$\underline{H}_2$-), 2.29 (t, 2H, -C$\underline{H}_2$-COO), 2.25 (s, 3H, Ar-C$\underline{H}_3$), 1.25 (s, 9H, C(C$\underline{H}_3$)$_3$).

1,4-diiodo-2,5-bis(11-(*tert*-butoxycarbonyl)-3,6,9-trioxaundecyloxy)benzene (**5**) Compound **4** (11.28 g, 26.08 mmol), compound **2** (3.93 g, 10.87 mmol), potassium iodide (0.018 g, 0.11 mmol), potassium carbonate (9 g, 65.22 mmol) and 30 ml of 2-butanone were added to a 250 ml of two neck round-bottomed flask with condenser. Reaction solution was refluxed for 38 hr and 2-butanone was evaporated at reduced pressure. The crude mixture was suspended to methylene chloride and washed with 1 M HCl. The organic layer was again washed with saturated NaCl and dried over $MgSO_4$. Further purification was achieved by column chromatography on silica gel (ethyl acetate : hexanes =7:3 v/v). Compound was again chromatographed on silica gel (ethyl acetate : hexanes =1:1 v/v) (yield : 4.26 g, 44 %). ^{1}H-NMR (500 MHz, $CDCl_3$): δ/ppm 7.22 (s, 2H, aromatic), 4.15 (t, 4H, -OC$\underline{H}_2$-), 3.87 (t, 4H, -OC$\underline{H}_2$-), 3.8-3.6 (m, 20H, -OC$\underline{H}_2$-), 2.51 (t, 4H, -C$\underline{H}_2$COO-), 1.42 (s, 18H, -C(C$\underline{H}_3$)$_3$).

1,4-diiodo-2,5-bis(11-carboxy-3,6,9-trioxaundecyloxy)benzene (**M4**) To a 4.00 g (4.53 mmol) of compound 5 was added 85 ml of trifluoroacetic acid (CF_3COOH). As soon as trifluoroacetic acid was added, the color of reaction mixture turned red. The mixture was stirred at room temperature for overnight. The reaction mixture was evaporated at reduced pressure. The crude mixture was dissolved in chloroform and washed with water three times. Organic layer was dried over $MgSO_4$ and filtered. The filtrate was evaporated to dryness and the compound **M4** was further dried in vacuo and

solidified to white-yellow waxy powder (yield : 2.57 g, 74 %). ^{1}H-NMR (500 MHz, $CDCl_3$): δ/ppm 9.8 (broad s, 2H, -COO<u>H</u>), 7.22 (s, 2H, aromatic), 4.15 (t, 4H, -OC<u>H</u>$_2$-), 3.83 (t. 4H, -OC<u>H</u>$_2$-), 3.81-3.50 (m, 20H, -OC<u>H</u>$_2$-), 2.60 (t, 4H, -C<u>H</u>$_2$COOH).

Polymer synthesis P1: **M1** (65 mg, 0.14 mmol) and **M5** (90 mg, 0.14 mmol) were placed into a Schlenck flask (50 ml). Toluene (1.5 ml) and diisopropylamine (3 ml) were added. After complete dissolution of two monomers, the solution was degassed by three times of vacuum and argon purging. In a separate Schlenck flask, tetrakistriphenylphosphine palladium (0) and copper (I) iodide were dissolved in toluene (1.5 ml) under a nitrogen atmosphere in a glove box and degassed. The degassed solution containing catalyst was cannulated onto the monomer solution. After transfer of the catalysis solution to monomer solution, polymerization solution was finally degassed again and allowed to stir under argon purging at 55 ºC for 2 days. The reaction mixture filtered with 0.45 micrometer membrane syringe. The toluene solution was precipitated in methanol 2 times. For deprotection of ethylhexyl group of carboxylic group, the collected fluorescent yellow precipitate was redissolved in 100 ml of tetrahydrofuran (THF) and 1 M of NaOH (100 ml) was added. The solution was stirred overnight at 35 ºC. THF was evaporated at the reduced pressure, filtered and the water solution was dialyzed against deionized water for 3 days (membrane MW cut off: 12,000-14,000 $gmol^{-1}$, 10 x 4 L water exchanges). The polymer solution was lyophilized to yield a yellow solid (74 mg, 80 %). ^{1}H-NMR (500 MHz, D_2O): δ/ppm 7.60 (s, 2H, aromatic), 7.11 (s, 2H, aromatic), 4.13 (broad t, 4H, -OC<u>H</u>$_2$-), 3.90-3.30 (broad m, 20H, -OC<u>H</u>$_2$C<u>H</u>$_2$-), 3.15 (s, 6H, -OC<u>H</u>$_3$), Molecular weight based on PS-GPC in THF before hydrolysis of ethylhexylgroup M_n=163,700, M_w=624,600, PDI=3.82.

P2: Except **M6** (85 mg, 95.4 μmol) instead of **M5**, the polymerization step was followed by synthetic route of **P1** above. After polymerization, polymer solution was centrifuged to get the supernatant (3500 rpm). The supernatant solution was evaporated and redissolved in 10 ml tetrahydrofuran and 10 ml of 1 M NaOH solution. The solution was stirred overnight at 35 ºC and evaporated at reduced pressure. The solution was dissolved in deionized water and centrifuged to remove the impurity insoluble to water. The water solution was dialyzed against deionized water for 3 days. Centrifugation was again conducted to get supernatant after dialysis. The polymer solution was lyophilized to yield a yellow solid (91 mg, 87 %). ^{1}H-NMR (500 MHz, D_2O): δ/ppm 7.58 (s, 2H, aromatic), 7.12 (s, 2H, aromatic), 4.13 (m, 2H, -OC<u>H</u>-), 3.80-3.20 (broad m, 56H, -OC<u>H</u>$_2$-), 3.11 (s, 12H, -OCH_3). GPC-based molecular weight before the cleavage of protection group, M_n = 32,100 gmol^{-1}, M_w=105,900 gmol^{-1}, PDI = 3.3.

P3: A general procedure about polymerization is identical to the method for **P1**. Monomer **M2** (40.8 mg, 69.1 μmol), monomer **M6** (61.6 mg, 69.1 μmol), toluene (1.0 ml), and diisopropylamine (2 ml) are placed into a 50 ml of Schlenck flask. After complete dissolution of two monomers, the solution was degassed by three times of vacuum and argon purging. In a separate Schlenck flask, tetrakistriphenylphosphine palladium (0) (5 mol % of the monomer) and copper (I) iodide (5 mol % of the monomer) were transferred under a nitrogen atmosphere of a glove box and argon was purged in the Schlenck flask for 10 min. Two catalysts were dissolved in toluene (1.0 ml) and degassed by three times of vacuum and argon purging. The degassed solution containing catalyst was cannulated onto monomer solution. After transfer of the catalyst solution to monomer solution, three cycles of degassing to a polymer solution was finally done

again. The polymer solution was allowed to stir under argon purging at 55 ºC for 2 days. The reaction mixture was filtered with 0.45 micrometer membrane syringe. The mixture solution was concentrated at reduced pressure and precipitated in diethylether (15 ml). The crude polymer was redissolved in 15 ml of dioxane and the solution was mixed with 10 % aqueous NaOH solution (15 ml). Solution was stirred under argon atmosphere at room temperature for 12 h. Polymer solution was centrifuged and dialyzed against deionized water for 2 days (10 x 4 L water exchanges). The polymer solution was lyophilized to yield a yellow solid (51 mg, 60 %). ^{1}H-NMR (500 MHz, D_2O): δ/ppm 7.27 (s, 2H, aromatic), 7.15 (s, 2H, aromatic), 4.03 (broad m, 6H, -$CH_2C\underline{H}_2O$-, -$OC\underline{H}$-), 3.81-3.21 (broad m, 56H, -$OC\underline{H}_2C\underline{H}_2$), 3.18 (broad s, 12H, -$OC\underline{H}_3$), 2.25 (broad t, 4H, -$CH_2C\underline{H}_2COO$-), 1.87 (broad m, 4H, -$CH_2C\underline{H}_2CH_2$-), GPC (THF) based M_n= 73,100 $gmol^{-1}$, Mw= 214,200 $gmol^{-1}$, PDI = 2.93.

P4: Except **M3** (41.85 mg, 62 μmol) instead of **M2**, the polymerization step was conducted by synthetic route of **P3** above. After the polymerization, polymer mixture was centrifuged to get the supernatant (3500 rpm). The supernatant solution was concentrated at reduced pressure, precipitated in ether, and washed with acetone. The polymer was redissolved in 10 ml tetrahydrofuran and 10 ml of 1 M sodium hydroxide solution. The solution was stirred overnight at 35 ºC and evaporated at reduced pressure. The solution was dissolved in DI water and centrifuged to remove the unknown impurity. The water solution was dialyzed against deionized water for 3 days. During the dialysis, fibril type aggregations observed due to the hydrophobic long alkyl chain and the protonation of carboxylic group. The polymer solution was lyophilized to yield a yellow solid (46 mg, 57 %). A solid **P4**, of which a carboxylic group is protonated, was completely soluble in

water (pH=8). ^{1}H-NMR (500 MHz, D_2O): δ/ppm 7.01 (s, 2H, aromatic), 6.75 (s, 2H, aromatic), 4.41 (m, 2H, -OC<u>H</u>-), 3.95 (t, 4H, -OC<u>H$_2$</u>-), 3.80-3.23 (broad m, 56H, -OC<u>H$_2$</u>-), 3.15 (s, 12H, -OC<u>H$_3$</u>), 2.05 (t, 4H, -C<u>H$_2$</u>COO-), 1.78-1.10 (broad m, 16H, -C<u>H$_2$</u>-), GPC (THF) based M_n= 19,200 gmol^{-1}, Mw= 57,800 gmol^{-1}, PDI = 3.01.

P5-A: M4 (60.6 mg, 78.7 μmol) and **M6** (73.6 mg, 82.6 μmol) were placed into a 50 ml of Schlenck flask and DMF (2 ml) and diisopropylamine (1 ml) were added to the reaction vessel. After complete dissolution of two monomers, the solution was degassed by three times of vacuum and argon purging. In a separate Schlenck flask, tetrakistriphenylphosphine palladium(0) (1 mol % of the monomer) and copper(I) iodide (1 mol % of the monomer) were transferred under a nitrogen atmosphere of a glove box and argon was purged in the Schlenck flask for 10 min. Two catalysts were dissolved in morpholine (1 ml) and degassed by three times of vacuum and argon purging. The degassed solution containing catalyst was cannulated onto monomer solution. After transfer of the catalyst solution to monomer solution, three cycles of degassing to a polymer solution was finally done again. The polymer solution was allowed to stir under argon purging at 55 ºC for 2 days. The solvent was evaporated to dryness. The crude polymer was redissolved in 50 ml of 1 M sodium hydroxide solution and stirred under argon atmosphere at room temperature for 1 h. Polymer solution was centrifuged and the supernatant was dialyzed against deionized water for 2 days (10 x 4 L water exchanges). The polymer solution was lyophilized to yield a yellow waxy solid (77 mg, 67 %). ^{1}H-NMR (500 MHz, D_2O): δ/ppm 8.30 (broad s, 2H, -COO<u>H</u>), 7.25 (s, 2H, aromatic), 7.09 (s, 2H, aromatic), 4.16 (t, 4H, -OC<u>H$_2$</u>-), 4.08 (m, 2H, -OC<u>H</u>-), 3.8-3.2 (broad m, 80H, -

OC$\underline{H}_2$C$\underline{H}_2$O), 3.15 (s, 12H, -OC$\underline{H}_3$), 2.27 (s, 4H, -C$\underline{H}_2$COO-), molecular weight; M_n by ^{1}H-NMR end analysis = 14,200.

P5-B: End-capping reaction was conducted in-situ after polymerization of **P5-A** was finished. 4-ethynylbenzoic acid (11 mg, 79 μmol) as an end-capper was dissolved in DMF (0.5 ml) and DIPA (0.2 ml). End-capper solution was degassed and cannulated onto polymer solution. A trace amount of palladium catalyst and cupper iodide in DMF (0.5 ml) degassed by vacuum and argon purging recycles was also added to polymer solutions. The polymer solution was allowed to stir under argon purging at 55 ºC for an additional 24 hr. After the reaction, a work-up procedure for polymer recovery was same as **P5-A**. Two new peaks at ^{1}H-NMR analysis emerged at 7.78, 7.51 ppm corresponding to the aromatic protons of the end-capper, confirming that the carboxylic group was chemically attached.

2.4. Results and Discussion

Synthetic routes for the preparation of all monomers are described in Scheme 2-1 and 2-2. All polymers were prepared by the palladium-catalyzed Sonogashira-Hagihara copolymerization method. At first, we tried polymerization with a diiodophenyl unit having unprotected free carboxylic acid. However, reactions were not successful because it has been found out that carboxylic group in ortho-position caused a side reaction during the polymerization and results in the decrease of molecular weight.[45-47] **P1** and **P2** were prepared from the copolymerization of a diiodophenyl monomer having carboxylic groups protected with ethylhexyl chains. After polymerization, the ethylhexyl group was hydrolyzed by base treatment to give a negatively charged carboxylate ion to polymer

structure. A flexible and hydrophilic ethylene oxide unit was introduced in order to give water solubility to the hydrophobic polymer backbone by suppressing the hydrophobic aggregation. **P3** and **P4** were also prepared by polymerization of a diiodo monomer having ethyl-protected carboxylic group to avoid the solubility problem of the free carboxylic acid group in organic solvents.

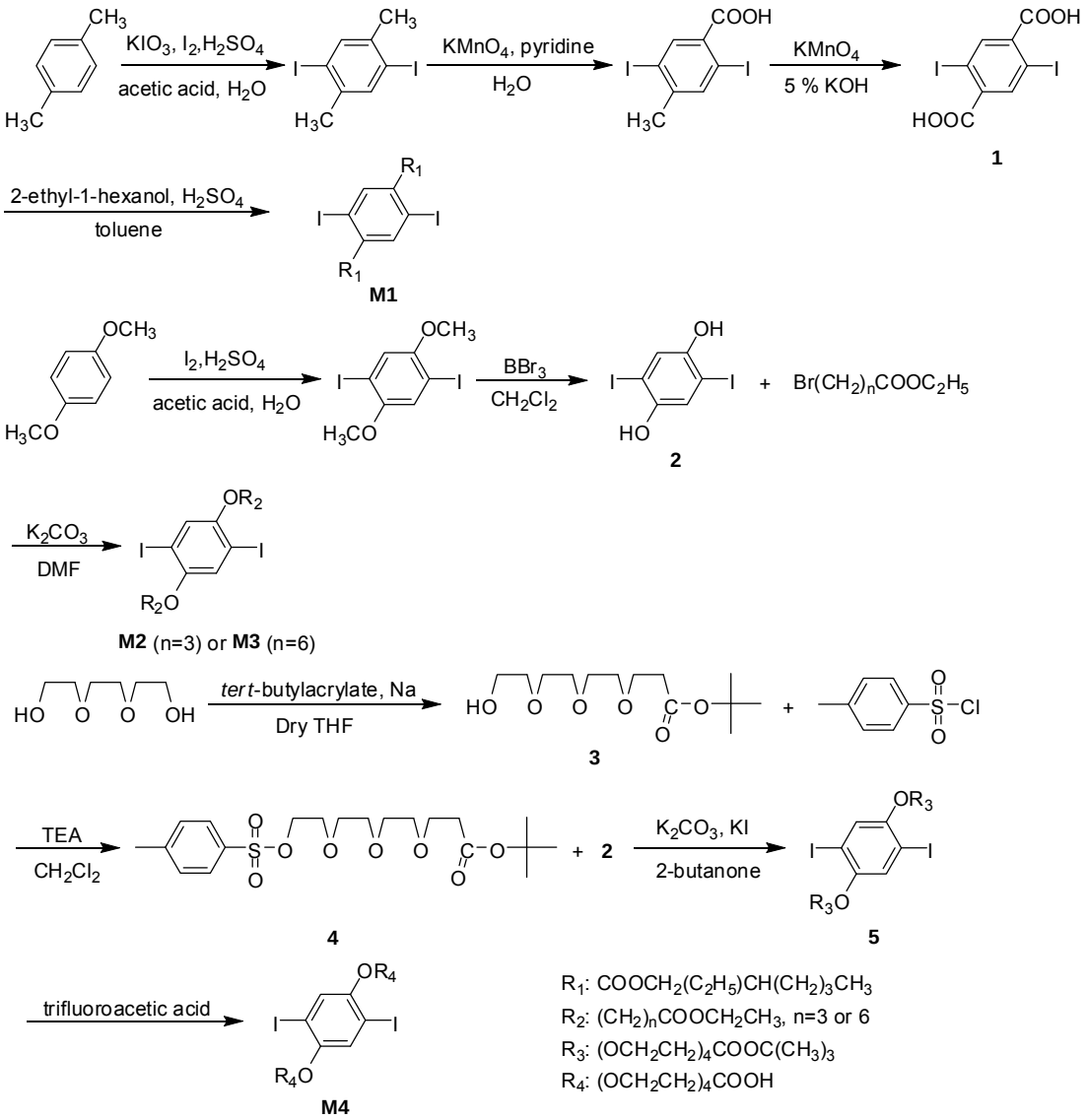

Scheme 2-1. Synthesis of Monomer **M1** to **M4**.

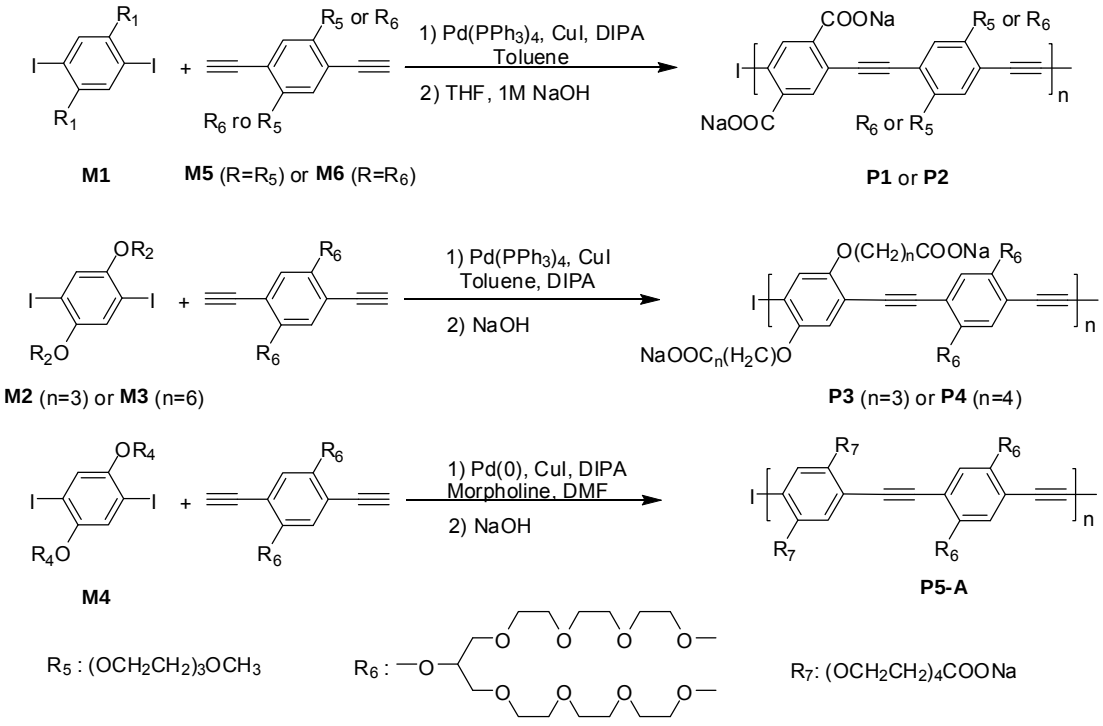

Scheme 2-2. Polymer synthesis (**P1** – **P5**)

Representative physical and photophysical data of all the CPEs described in this contribution are summarized in Table 2.1. All the CPEs were dissolved in water and showed blue-green emission having emission λ_{max} of about 460 nm. First, **P1** solution in water looked yellow and transparent in visual observation and its solubility in water is high enough to dissolve more than 1 mg of **P1** in 1 ml of deionized water. The precursor polymer of **P1** before the deprotection of the carboxylic acid group shows a well-defined 0-0 emission band at 487 nm and quantum yield of 45% in chloroform (Figure 2-2). However, **P1** in water after the deprotection shows a blue-shifted and much weaker emission. The quantum yield is only 0.45%.

Table 2-1. Physical properties of all polymers used in this study

poly	M_n/gmol^{-1} [a]	DP [b]	$\lambda_{max,abs/nm}$ $\lambda_{max,em/nm}$	Stokes shift cm^{-1} [c]	E_g/eV [d]	Φ_F (%, D_2O) [e]
P1	163,700	194	384	4110	2.14	0.45
			456			
P2	32,100	29	368	5430	2.18	0.09
			460			
P3	73,100	59	421	2150	2.54	31.6
			463			
P4	19,200	15	406	3080	2.52	5.3
			464			
P5-A (or **B**)	14,200	10	412	2390	2.64	51.4 (36.6)
			457			

[a] Molecular weight of all polymers except **P5** was measured by GPC before hydrolysis of ethylhexyl protection. M_n for **P5** was done by ^{1}H-NMR end analysis in D_2O. [b] Degree of polymerization (DP) was calculated from the M_n and the molar mass of the repeat unit. [c] The magnitude of the Stokes shift was calculated by $\Delta = \lambda_{max,em} - \lambda_{max,abs}$. [d] The optical HOMO-LUMO energy gap is based on the low-energy onset in the solution-state UV/Vis spectra. [e] Quantum yield is absolute quantum value measured by using an integrating sphere.

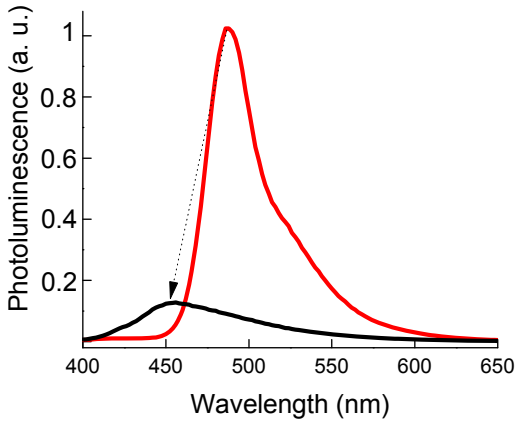

Figure 2-2. Photoluminescence of **P1** before (red, in chloroform) and after (black, in water) the cleavage of the ethylhexyl protecting group (**P1** conc. = 5 mgL^{-1}).

Even though the aqueous solution of **P1** looked to be transparent to the naked eye, our co-solvent study and surfactant study strongly implies that **P1** was aggregated in water. We examined photoluminescence properties of **P1** in water/methanol co-solvent system. As shown in Figure 2-3, the emission intensity of **P1** increased as the volume fraction of methanol increased in the water/methanol mixture because methanol is a

better solvent than water, implying **P1** aggregation in water. To further investigate the aggregation feature we conducted a surfactant study by using sodium dodecylsulfide (SDS, anionic), Tween 20 (non-ionic), and dodecyltrimethylammonium bromide (DTAB, cationic) and investigated their deaggregation capability for **P1** in water (Figure 2-4)**.**[48-52]

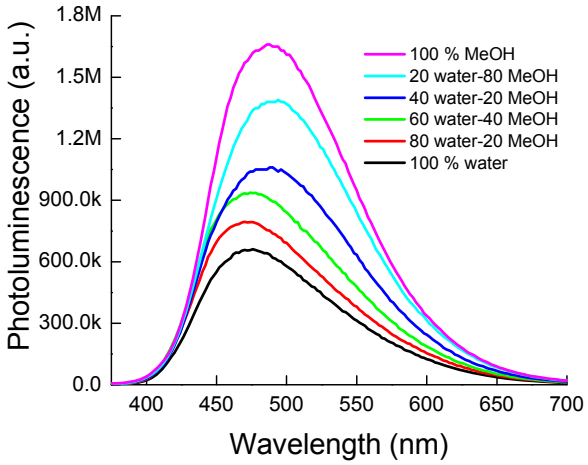

Figure 2-3. Photoluminescence spectra of **P1** in various water/methanol mixture solvents (**P1** conc. = 0.7 mgml^{-1}, excitation wavelength: 365 nm).

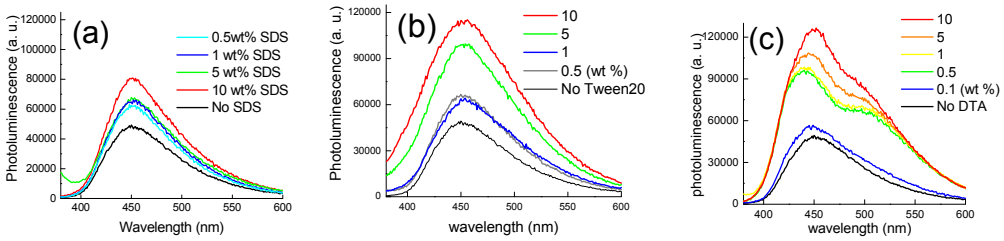

Figure 2-4. Photoluminescence profile of **P1** in water by adding different types of surfactants (a) SDS, negative, (b) tween20, neutral, (c) DTAB, positive (**P1** conc. = 5 mgmL^{-1}).

Fluorescence emission intensity of **P1** was enhanced as the surfactant concentration was increased in all three cases likely due to the deaggregation of polymer aggregates induced by the surfactants. The difference in the emission enhancement of **P1** at a given concentration of each surfactant indicates that the cationic surfactant DTAB most effectively dissemble **P1** aggregates. Considering the fact that **P1** is a negatively charged CPE, cationic surfactants should be more effective than nonionic or anionic surfactants. Note that the increase in the fluorescence intensity of **P1** with increasing concentration of added DTAB was most significant between 0.1 wt% of DTAB and 0.5 wt% of DTAB. Interestingly, our calculation showed that 0.4 wt% of DTAB is required to make 1:1 charge complex with carboxylic acid groups of **P1** as illustrated in Figure 2-5.[53] Distinct 0-0 and 0-1 emission bands are observed in Figure 2-4 (c) indicating that DTAB effectively dissembles **P1** aggregates.[33,54]

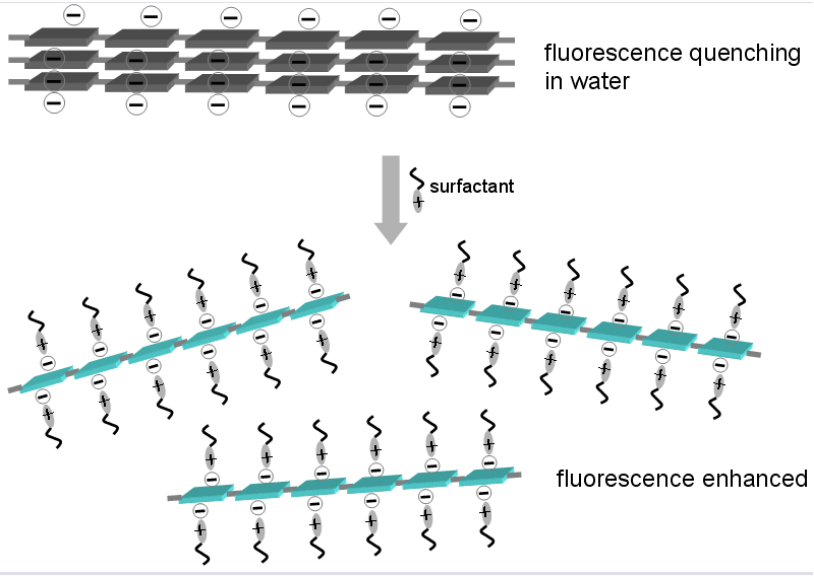

Figure 2-5. Schematic illustration of surfactant effect on **P1** in water.

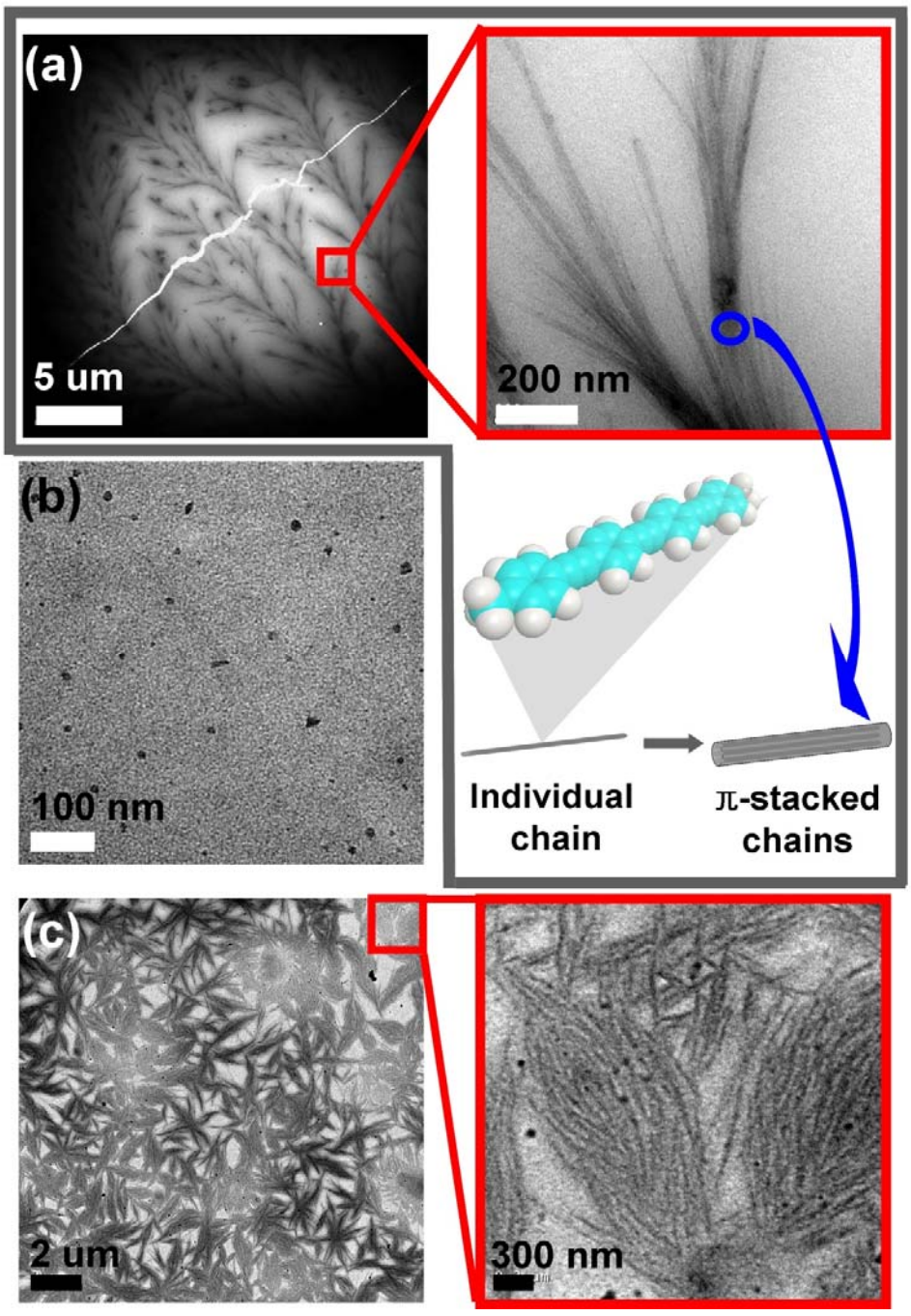

Figure 2-6. TEM micrograph of (a) 1 w% **P1** in water (b) 0.1 w% **P2** in water (c) 0.1 w% **P4** in methanol, (figure in middle) Proposed mechanism for the aggregation of PPEs in a poor solvent.

We investigated CPE aggregation in an aqueous environment by means of TEM.[55-59] The TEM micrographs of **P1** in water shown in Figure 2-6a revealed tree-like, fractal aggregation suggesting that **P1** was completely aggregated in water. The magnified transition region shows that rigid rod-like **P1** chains aggregated to form cylindrical aggregates. A few single **P1** chains could aggregate into a fibril by hydrophobic π- π stacking and several fibrils could agglomerate to form few tens of nanometers wide fibers. Therefore, even though **P1** was modified with water-soluble ionic and non-ionic side chains, **P1** molecules aggregate due to the rigidity and the hydrophobic nature of the main chain, resulting in a weakly fluorescent aqueous solution.

Dynamic (DLS) and static light scattering (SLS) studies were also conducted to estimate the mean size of the CPEs in aqueous solution. The lowest concentration regime to give strong enough signal was a few hundreds milligrams per liter that is almost hundred times larger than the concentration of the CPEs for UV and PL study. Therefore, we could not correlate the quantum yield data and the light scattering data systematically for all CPEs. However, the investigation of correlation between the radius of gyration (R_g) from SLS and hydrodynamic radius (R_h) from DLS clearly showed that **P1** aggregated into non-globular shapes. We calculated the hydrodynamic radius by DLS using CONTIN analysis. The ratio of the radius of gyration (R_g, 118.3 nm) to the hydrodynamic radius (R_h, 37.1 nm) was calculated to be 3.19, indicating a cylindrical morphology of the **P1** aggregates.[60-63] This is in good agreement with the TEM images of **P1** showing a few microns of rod-like aggregates.

We replaced the single strand ethylene oxide side chains of **P1** with a bulky bifurcated ethylene oxide chain and prepared **P2** to efficiently sheath the rigid

hydrophobic CPE backbone and minimize the π- π stacking (Figure 2-1).[33,38] Initially, we measured the size and the molecular weight of **P2** in DMF-based GPC after cleavage of carboxy-protecting group. However, the molecular weight of polymers was inflated up to a few millions ($gmol^{-1}$) due to the significant change of hydrodynamic volume following the limited solubility and aggregates in DMF. In the TEM micrograph of **P2** (Figure 2-6b), we could not observe any large aggregations that were observed from **P1** solutions. Instead, spherical particles of only a few tens of nanometers in size were observed. We did not observe any aggregation even in dried P2 sample in conventional TEM. It is fair to expect that P2 does not aggregate in water solution. Therefore, we could suppress aggregation of CPE through molecular design, by introducing the bulky nonionic ethylene oxide side chains. However, surprisingly even the non-aggregated **P2** aqueous solution has very low quantum yield of 0.9 % whilst the **P2** derivative having ethyl protected carboxylic acid side chains has 55 % quantum yield in chloroform. It is believed that carboxylic groups having sodium counter ions directly attached to CPE backbone induce photoluminescence quenching of CPE in water because we found emission enhancement of **P1** and **P2** in acidic water where the carboxylic group should be protonated. Fluorescence energy is likely dissipated by electron-deficient carboxylates through photon energy transfer.[64,65]

We put an alkyl spacer between the CPE backbone and carboxylic groups and prepared **P3** to exam this hypothesis. The absorption and emission spectra of **P2** and **P3** are presented in Figure 2-7. TEM micrographs of 1 wt% **P3** aqueous solution was essentially identical to that of **P2** having slightly larger size of spherical nanoparticles. The slightly larger sphere formation is believed to originate from the hydrophobic nature

of the propyl spacer. As we expected, **P3** aqueous solution has the quantum yield of 31.6 % that is dramatically improved from the 0.9 % of **P2** aqueous solution, proving that the directly attached carboxylic acid groups to **P2** backbone cause the quenching.

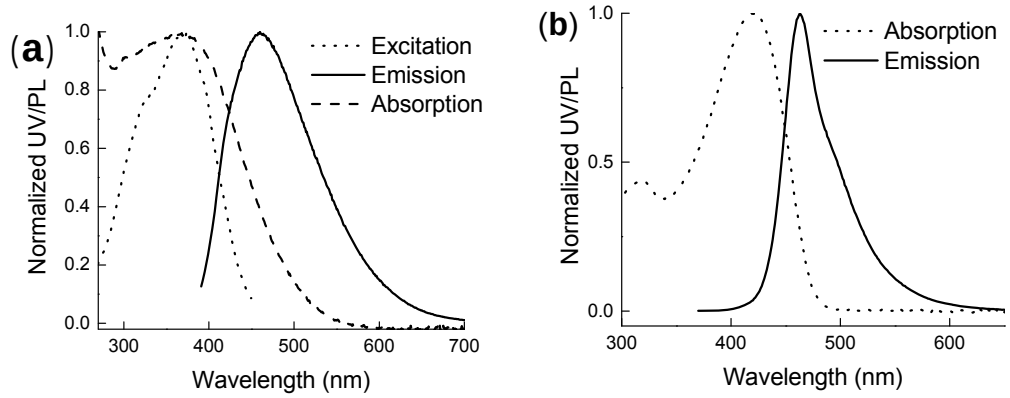

Figure 2-7. Absorption and Emission spectra of (a) **P2** (10 mgL^{-1}) and (b) **P3** (7 mgL^{-1}) in water (excitation at 365 nm).

We increased the length of alkyl spacer from C_3 to C_6 and prepared **P4** to test whether a long hydrophobic spacer would cause aggregation of CPE. As the TEM micrograph in Figure 6(c) shows, **P4** having hexyl spacers formed starfish-like self-assembled aggregates in water due to the hydrophobic long alkyl spacers.[66-70] Accordingly the quantum yield of **P4** aqueous solution dropped down significantly to 5.3 %. Dialysis purification of these CPEs also indicates that the longer hexyl hydrophobic chain lowers the solubility of **P4** in water. We did not observe any aggregation during dialysis of **P1**, **P2** or **P3** in water. They were completely soluble in deionized water and the solubility exceeded approximately 1 mg mL^{-1}. However, the protonation of carboxylic group of **P4** during dialysis induced precipitation of **P4**, indicating that the

long alkyl spaces reduced the water-solubility of **P4** compared to other CPEs. After giving negative charges to **P4** in phosphate buffer (pH=8) or basic water solution, the water-solubility of **P4** was significantly enhanced.

We used hydrophilic ethylene oxide linker to connect the carboxylic acid unit to the CPE backbone when we synthesized **P5-A** to prevent hydrophobic side chain-induced aggregation of CPE. **P5-A** completely dissolved in pure water (> 10 mg/mL) and its solubility is independent to the pH of the aqueous solution. Photoluminescence spectra of **P5-A** in Figure 2-8 are narrow with a well-defined 0-0 band at 457 nm. **P5-A** has the highest fluorescent emission quantum yield of 51.4 % among other CPEs and is over 110 times more emissive than **P1**. TEM analysis of P5-A did not show any aggregation, indicating that the hydrophilic nature of the side chain is necessary to prevent CPE aggregation in water.

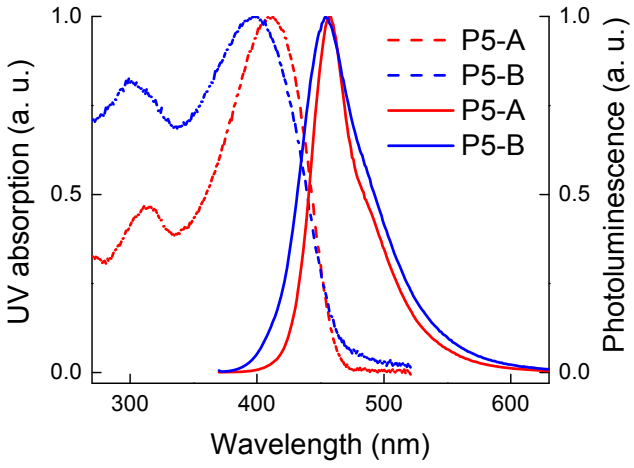

Figure 2-8. UV and PL spectra (5 mgL^{-1}) for **P5-A** and **P5-B** (Polymers are excited at 365 nm).

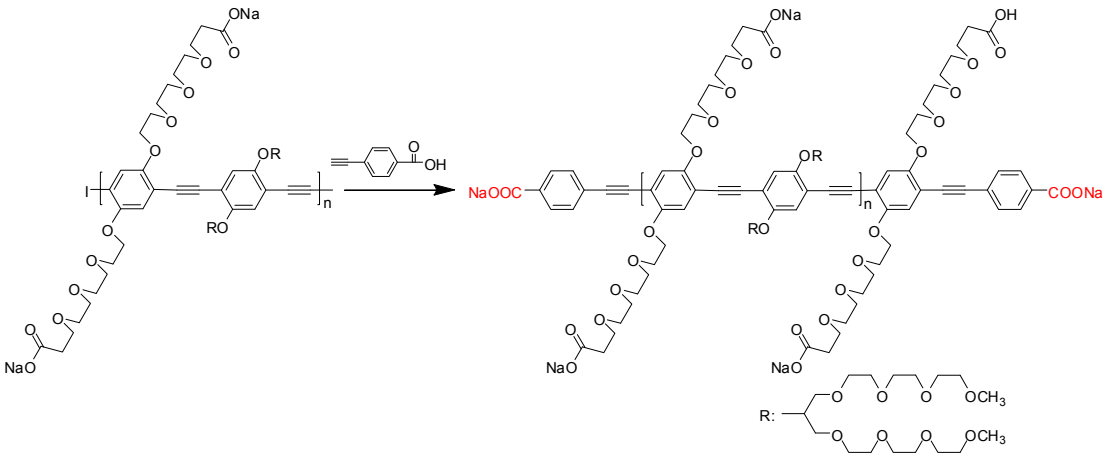

Scheme 2-3. *In-situ* end-capping reaction for **P5-B**.

Finally, we prepared **P5-B** which has two directly attached carboxylic acid unit at the two chain ends to confirm the influence of carboxylic acid group to the emissive property of CPEs. *In situ* end-capping reaction to **P5-A** during polymerization was undertaken by adding 4-ethynylbenzoic acid with an additional palladium catalyst (Scheme 2-3).[33,71-73] **P5-B** essentially has the same solubility in water as **P5-A** showed the identical TEM image as P5-A. However, the quantum yield of **P5-B** is largely reduced to 31.6 % that is 38.5% drop from that of **P5-A**, clearly demonstrating that directly connected carboxylic acid to the conjugated backbone of CPEs has a detrimental effect to the emission property of CPEs.

2.5. Conclusion

We investigated the effect of the chemical nature, shape, and length of the ionic and nonionic side chains on the water solubility and quantum yield of CPEs by means of TEM, static and dynamic light scattering, and spectroscopic analysis. Simple ionic and anionic decoration of CPEs did not warrant good water-solubility due to the rigid and

hydrophobic nature of the conjugated backbone of CPEs. TEM investigation revealed that unless CPEs are modified by attaching bulky hydrophilic ethylene oxide side chains CPEs form micellar aggregates in water and consequent fluorescence quenching. Carboxylic acid groups, which are commonly used, convenient functional groups for bioconjugation, turned out to have a detrimental influence on the emissive property of CPEs when they are connected directly to the CPE backbone. Placing a spacer linker between carboxylic acids and the CPE backbone solved the quenching problem. However, the nature and length of the spacer group determine the water-solubility of CPEs. When the alkyl linker was long, the hydrophobic nature of the linker induced self-assembled aggregates. This study reveals the effects of side chain design on the water-solubility and consequent emission property of CPEs and provides a molecular design principle to achieve highly emissive, completely water-soluble, and conveniently functionalized CPEs.

2.6. References

1. Pinto, M.; Schanze, K. S. *Synthesis* **2002**, *9*, 1293.

2. Ho, H.-A.; Béra-Abérem, M.; Leclerc, M. *Chem. Eur. J*. **2005**, *11*, 1718 and references therin.

3. Nilsson, K. P. R.; Inganäs, O. *Nat. Mater.* **2003**, *2*, 419.

4. Liu, B.; Bazan, G. C. *Chem. Mater*. **2004**, *16*, 4467 and references therein.

5. Yang, C. J.; Pinto, M.; Schanze, K.; Tan, W. *Angew. Chem. Int. Ed*. **2005**, *44*, 2572.

6. Lee, K.; Povlich, L. K.; Kim, J. *Adv. Funct. Mater*. **2007,** *17*, 2580.

7. Liu, B.; Bazan, G. C. *Proc. Natl. Acad. Sci. USA*. **2005**, *102*, 589.

8. Lee, K.; Rouillard, J.-M.; Pham, T.; Gulari, E.; Kim, J. *Angew. Chem. Int. Ed*. **2007**, *46*, 4667.

9. Pun, C.-C.; Lee, K.; Kim, H.-J.; Kim, J. *Macromolecules*, **2006**, *39*, 7461.

10. Abérem, M. B.; Najari, A.; Ho, H.-A.; Gravel, J.-F.; Nobert, P.; Boudreau, D.; Leclerc, M. *Adv. Mater*. **2006**, *18*, 2703.

11. Fan, C.; Plaxco, K. W.; Heeger, A. J. *J. Am. Chem. Soc*. **2002**, *124*, 5642.

12. Chen, L.; McBranch, D. W.; Wang, H.-L.; Helgeson, R.; Wudl, F.; Whitten, D. G. *Proc. Natl. Acad. Sci. USA*. **1999**, *96*, 12287.

13. Nilsson, K. P. R.; Herland, A.; Hammerström, P.; Inganäs, O. *Biochemistry* **2005**, *44*, 3718.

14. Song, X.; Wang, H.; Shi, J.; Park, J.-W.; Swanson, B. I. *Chem. Mater*. **2002**, *14*, 2342.

15. Kim, I.-B.; Dunkhorst, A.; Bunz, U. H. F. *Langmuir* **2005**, *21*, 7985.

16. Dwight, S. J.; Gaylord, B. S.; Hong, J. W.; Bazan, G. C. *J. Am. Chem. Soc*. **2004**, *126*, 16850.

17. Björk, P.; Herland, A.; Scheblykin, I. G.; Inganäs, O. *Nano Lett*. **2005**, *5*, 1948.

18. Wilson, J. S.; Frampton, M. J.; Michels, J. J.; Sardone, L.; Marletta, G.; Friend, R. H.; Samorí, P.; Anderson, H. L.; Cacialli, F. *Adv. Mater*. **2005**, *17*, 2659.

19. Ma, W.; Iyer, P. K.; Gong, X.; Liu, B.; Moses, D.; Bazan, G. C.; Heeger, A. J. *Adv. Mater*. **2005**, *17*, 274.

20. Yang, R.; Wu, H.; Cao, Y.; Bazan, G. C. *J. Am. Chem. Soc*. **2006**, *128*, 14422.

21. Smela, E. *Adv. Mater*. **2003**, *15*, 481.

22. Swager, T. M. *Acc. Chem. Res*. **1998**, *31*, 201.

23. McQuade, D. T.; Pullen, A. E.; Swager, T. M. *Chem. Rev*. **2000**, *100*, 2537.

24. Tan, C.; Atas, E.; Müller, J. G.; Pinto, M. R.; Kleiman, V. D.; Schanze, K. S. *J. Am. Chem. Soc*. **2004**, *126*, 13685.

25. Harrison, B. S.; Ramey, M. B.; Reynolds, J. R.; Schanze, K. S. *J. Am. Chem. Soc*. **2000**, *122*, 8561.

26. Kushon, S. A.; Ley, K. D.; Bradford, K.; Jones, R. M.; McBranch, D.; Whitten, D. *Langmuir* **2002**, *18*, 7245.

27. Tan, C.; Pinto, M. R.; Schanze, K. S. *Chem. Commun*. **2002**, 446.

28. Joly, G. D.; Geiger, L.; Kooi, S. E.; Swager, T. M. *Macromolecules* **2006**, *39*, 7175.

29. Pinto, M. R.; Kristal, B. M.; Schanze, K. S. *Langmuir* **2003**, *19*, 6523.

30. Jiang, H.; Zhao, X.; Schanze, K. S. *Langmuir* **2006**, *22*, 5541.

31. Wang, F.; Bazan, G. C. *J. Am. Chem. Soc*. **2006**, *128*, 15786.

32. Wosnick, J. H.; Mello, C. M.; Swager, T. M. *J. Am. Chem. Soc*. **2005**, *127*, 3400.

33. Lee, K.; Cho, J. C.; Deheck, J.; Kim, J. *Chem. Commun*. **2006**, 1983.

34. Ho, H.-A.; Leclerc, M. *J. Am. Chem. Soc*. **2004**, *126*, 1384.

35. Doré, K.; Dubus, S.; Ho, H.-A.; Lévesque, I.; Brunette, M.; Corbeil, G.; Boissinot, M.; Boivin, G.; Bergeron, M. G.; Doudreau, D.; Leclerc, M. *J. Am. Chem. Soc*. **2004**, *126*, 4240.

36. Ho, H. A.; Doré, K.; Boissinot, M.; Bergeron, M. G.; Tanguay, R. M.; Bourdreau, D.; Leclerc, M. *J. Am .Chem. Soc*. **2005**, *127*, 12673.

37. Ho, H.-A.; Boissinot, M.; Bergeron, M. G.; Corbeil, G.; Doré, K.; Bourdreau, D.; Leclerc, M. *Angew. Chem. Int. Ed*. **2002**, *41*, 1548.

38. Khan, A.; Müller, S.; Hecht, S. *Chem. Commun*. 2005, 584.

39. Häger, H.; Heitz, W. *Macromol. Chem. Phys*. **1998**, *199*, 1821.

40. Perry, R. J.; Wilson, B. D.; Turner, S. R.; Blevins, R. W. *Macromolecules* **1995**, *28*, 3509.

41. Zhang, J.; Cui. Y.; Wang, M.; Liu, J. *Chem. Commun*. **2002**, 2526.

42. Zhou, Q.; Swager, T. M. *J. Am. Chem. Soc*. **1995**, *117*, 12593.

43. Lauter, U.; Meyer, W. H.; Enkelmann, V.; Wegner, G. *Macromol. Chem. Phys*. **1998**, *199*, 2129.

44. Provencher, S. W. *Makromol. Chem*. **1979**, *180*, 201-209.

45. Liao, H.-Y.; Cheng, C.-H. *J. Org. Chem*. **1995**, *60*, 3711.

46. Subramanian, V.; Batchu, V. R.; Barange, D.; Pal, M. *J. Org. Chem*. **2005**, *70*, 4778.

47. Lambert, C.; Utimoto, K.; Nozaki, H. *Tetrahedron Lett*. **1984**, *25*, 5323.

48. There are several reports in the literature on the effects of surfactants on CPEs. Thünemann, A. F. *Adv. Mater*. **1999**, *11*, 127. Also, see refs. 47-50.

49. Lavigne, J. J.; Broughton, D. L.; Wilson, J. N.; Erdogan, B.; Bunz, U. H. F. *Macromolecules* **2003**, *36*, 7409.

50. Chen, L.; Xu, S.; McBranch, D.; Whitten, D. *J. Am. Chem. Soc*. **2000**, *122*, 9302.

51. Thünemann, A. F.; Ruppelt, D. *Langmuir* **2001**, *17*, 5098.

52. Burrows, H. D.; Lobo, V. M. M.; Pina, J.; Ramos, M. L.; Seixas de Melo, J.; Valente, A. J. M.; Tapia, M. J.; Pradhan, S.; Scherf, U. *Macromolecules* **2004**, *37*, 7425.

53. This value is calculated based on the molecular weight of polymer repeat unit (658.60 g/mol).

54. Kim, J.; Swager, T. M. *Nature* **2001**, *411*, 1030.

55. Talmon, Y. *Ber. Bunsenges. Phys. Chem*. **1996**, *100*, 364.

56. Danino, D.; Bernheim-Groswasser, A.; Talmon, Y. *Colloids Surf. A* **2001**, *183*, 113.

57. Li, Z.; Kesselman, E.; Talmon, Y.; Hillmyer, M. A.; Lodge, T. P. *Science* **2004**, *306*, 98.

58. Pochan, D. J.; Pakstis, L.; Ozbas, B.; Nowak, A. P.; Deming, T. J. *Macromolecules* **2002**, *35*, 5358.

59. Lamm, M. S.; Rajagopal, K.; Schneider, J. P.; Pochan, D. J. *J. Am. Chem. Soc.* **2005**, *127*, 16692.

60. Schanablegger, H.; Antonietti, M.; Göltner, C.; Hartmann, J.; Cölfen, H.; Samorí, P.; Rabe, J. P.; Häger, H.; Heitz, W. *J. Colloid Interface Sci*. **1999**, *212*, 24.

61. Kirkwood, J. G.; Riseman, J.; *J. Chem. Phys*. **1948**, *16*, 565.

62. Kok, C. M.; Rudin, A. *Makromol. Chem. Rapid Commun*. **1981**, *2*, 655.

63. Liu, Y.; Bo, S. *Chromatographia* **2004**, *59*, 299.

64. McQuade, D. T.; Hegedus, A. H.; Swager, T. M. *J. Am. Chem. Soc*. **2000**, *122*, 12389.

65. Murphy, C. B.; Zhang, Y.; Troxler, T.; Ferry, V.; Martin, J. J.; Jones, W. E. Jr. *J. Phys. Chem. B* **2004**, *108*, 1537.

66. There is research on π-π aggregation induced self-assembly of conjugated oligomer/polymers: Tan, C.; Pinto, M. R.; Kose, M. E.; Ghiviriga, I.; Schanze, K. S. *Adv. Mater*. **2004**, *16*, 1208. Also, see refs 65-68.

67. Moore, J. S. *Acc. Chem. Res*. **1997**, *30*, 402.

68. Nelson, J. C.; Saven, J. G.; Moore, J. S.; Wolynes, P. G. *Science* **1997**, *277*, 1793.

69. Brunsveld, L.; Folmer, B. J. B.; Meijer, E. W. *Chem. Rev*. **2001**, *101*, 4071.

70. Herz, L. M.; Daniel, C.; Silva, C.; Hoeben, F. J. M.; Schenning, A. P. H. J.; Meijer, E. W.; Friend, R. H.; Phillips, R. T. *Phys. Rev.* B **2003**, *68*, 045203.

71. Samorí, P.; Severin, N.; Müllen, K.; Rabe, J. P. *Adv. Mater*. **2000**, *12*, 579.

72. Samorí P.; Francke, V.; Müllen, K.; Rabe, J. P. *Chem. Eur. J.* **1999***, 5,* 2312.

73. Kuroda, K.; Swager, T. M. *Macromolecules* **2004**, *37*, 716.

CHAPTER 3

Synthesis and Functionalization of a Highly Fluorescent and Completely Water-Soluble Poly(*para*-phenyleneethynylene) Copolymer for Bioconjugation

Parts of this chapter appear in: Lee, K.; Cho, J. C.; DeHeck, J.; Kim, J. Published in *Chem. Commun*. **2006**, 1983.

3.1. Abstract

A simple and practical approach for the bioconjugation of a conjugated polyelectrolyte and a pentatyrosine, a model biological molecule was developed. Highly fluorescent and completely water-soluble conjugated poly(p-phenyleneethynylene) derivatives (**PPE-R_1** and **PPE-R_1-COOH**) having sulfonate ions and bifurcated ethylene oxide chains have been designed and prepared. To observe the effect of bulky ethylene oxide side chain in water-solubility and optoelectronic property, **PPE-R_2** having single ethylene oxide chain was prepared as a control polymer. All polymers are water-soluble and showed emission in pure water. UV/PL spectra of **PPE-R_2** showed an aggregation behavior in water while **PPE-R_1** and **PPE-R_1-COOH** did not. Fluorescent quantum yield of **PPE-R_1** and **PPE-R_1-COOH** was 53 % and 45 % respectively whereas that of **PPE-R_2** was only 19 %. End-functionalized **PPE-R_1-COOH** was attached to N-terminus amine of a model peptide, pentatyrosine on a 4-chloro-trityl polystyrene (PS) resin.

3.2. Introduction

Conjugated polymers are emerging materials for many modern technologies. One of the attractive applications of conjugated polymers is sensor design, because an environmental change at a single site can affect the properties of the collective system, producing large signal amplification.[1-5] In particular, the detection of biological analytes such as DNA, proteins and biological warfare agents has been receiving wide scale attention recently.[6-9] Receptors can be rationally designed and covalently connected to a conjugated polymer main chain.

A conjugated polymer should be water-soluble, highly fluorescent and have appropriate functional groups for conjugation with biological receptors to be a good molecular biosensor, because most target biological analytes are analyzed in an aqueous environment. However, by their nature, conjugated polymers have a hydrophobic and rigid main chain, which results in poor solubility in water and subsequent fluorescent quenching by micelle formation in an aqueous phase.[10-12] Even worse, once the polymer dries completely, it is extremely difficult to re-dissolve it in water again due to its strong aggregation. To address this problem, many research groups have been working on developing water-soluble conjugated polymers. Khan et al. very recently reported an effective method to suppress the aggregation of poly(*para*-phenyleneethynylene) s in water by introducing branched ethylene oxide units as a side chain.[13]

Here we describe the synthesis and functionalization of a completely water-soluble conjugated polymer, poly{[1,4-bis(1,3-bis(2-(2-(2-methoxyethoxy)ethoxy)ethoxy) propan-2-yloxy) benzene]-alt-[2,5-diethynylbenzene-2,4-(bis(3-propoxy-sulfonic acid)) sodium salt]} (PPE-R_1, Scheme 1), to improve the emissive property even further and

give bioconjugation capability. The copolymer, **PPE-R$_1$**, is composed of alternating ionic sulfonate units and bifurcated non-ionic ethylene oxide units on the main chain to provide water solubility and prevent micelle formation. Conventional palladium-catalyzed Sonogashira–Hagihara copolymerization was used. We developed a method to introduce a carboxylic acid group, a versatile functional group for bioconjugation, at the end of the PPE chain. The chemically modified polymer, with a carboxylic acid group at both ends, was subsequently conjugated with a model peptide, pentatyrosine.

3.3. Experimental Section

3.3.1. Materials and Methods. All chemicals were purchased from Sigma-Aldrich, Inc. or Acros Organics, Inc. and used without further purification. A diethynyl monomer having mono ethylene oxide side chain to prepare **PPE-R$_2$** was prepared in a same manner with monomer **1**. (characterization data: ^{1}H-NMR (500 MHz, $CDCl_3$): δ/ppm 7.01 (s, 2H, aromatic), 4.15 (t, 4H, -OC$\underline{H}_2$-), 3.87 (t, 4H, -OC$\underline{H}_2$-), 3.79 (t, 4H, -OC$\underline{H}_2$-), 3.67-3.65 (t, 8H, -OC$\underline{H}_2$-), 3.57 (t, 4H, -OC$\underline{H}_2$-), 3.39 (s, 6H, -C$\underline{H}_3$), 3.34 (s, 2H, -CC$\underline{H}$). ^{13}C-NMR (125 MHz, $CDCl_3$): δ/ppm 154.05, 118.26, 113.55, 82.81, 79.56, 71.95, 71.06, 70.71, 70.56, 69.59, 69.49, 59.03. HRMS (Electrospray with Na+ added, voltage ES+) : calculated m/z of [M+Na]+ 473.2151; measured m/z 473.2149.) All polymers were purified by dialysis against deionized water (molecular weight cut off : 12,000 – 14,000 gmol^{-1}) for 3 days, lyophilized to dry the polymer, and stored in the dried state at 4 °C. The molecular weight of all PPE polymers was determined by PS-GPC in DMF and the number-averaged molecular weight (M_n) was also calculated by ^{1}H NMR end-group analysis. There was a large deviation in the number of molecular weight measured by two

methods above because the large hydrodynamic volume of PPEs coming from the rigid rod shape resulted in the exaggeration of molecular weight of the polymers. UV/Vis absorption spectra of the conjugated polymer solutions were obtained on a Cary UV50 UV/Vis spectrometer (Varian, Inc.). Steady-state fluorescence spectra of the polymers were recorded on a PTI QuantaMaster spectrofluorometer™. The molar concentration of the polymer solutions was determined based on the repeat unit of the polymers. The true quantum yield of the polymers was measured with excitation at 365 nm in deionized water (1 mgL^{-1}) using an integrating sphere attached to the same spectrofluorometer. Confocal Images was obtained from a Leica TCS SP2 confocal microscope operating with a 63x oil immersion objective (numerical aperture 1.4). Molecular modeling for **PPE-R_1** was simulated by Materials Studio 3.0 (Accelrys®) with 10,000 iteration times.

3.3.2. Synthesis of 2,5-Diiodo-1,4-dimethoxybenzene This compound was prepared by the procedure reported in previous literature.[14] 10.00 g (72.4 mmol) of 1,4-dimethoxybenzene in 1000 ml 3-neck round bottom flask was dissolved in 220 ml acetic acid. Potassium Iodate (6.20 g, 28.96 mmol), iodine (40.04 g, 162.9 mmol), sulfuric acid (1.45 ml) and deionized (DI) water (25.4 ml) were added to the mixture. Reaction was refluxed for 18 hr with stirring. The solution was cooled down and 10 % sodium thiosulfate pentahydrate (40.0 g) in 360 g of DI water were slowly added to the solution to quench iodine. After 30 min with stirring, 220 ml of DI water was additionally added to the solution. The precipitated solid was collected by filtering. It is redissolved in 360 ml of methylene chloride and washed with 20 g of sodium thiosulfate pentahydrate in 180 ml water. The organic solution was washed with saturated brine and subsequent water again. It was dried over magnesium sulfate and filtered. Solvent was evaporated with a

rotary evaporator at reduced pressure. Additional purification was done by recrystallization with methylene chloride and methanol to get white needle. Yield: 19.8 g (70 %) ^{1}H-NMR (500 MHz, $CDCl_3$): δ/ppm 7.20 (s, 2H, aromatic), 3.84 (s, 46H, -OC<u>H</u>$_3$). ^{13}C-NMR (125 MHz, $CDCl_3$): δ/ppm 153.31, 121.59, 85.50, 57.21. HRMS (Voltage EI+) : calculated m/z of [M+] 389.8613; measured m/z 389.8605.

3.3.3. Synthesis of 1,4-Diiodo-2,5-hydroquinone To a solution of 2,5-diiodo-1,4-dimethoxybenzene (10.0 g, 25.6 mmol) in methylene chloride (200 ml) at 1000 ml 3 neck round bottom flask with condenser were added dropwise boron tribromide (1M, 14.1 ml) in methylene chloride (42.3 ml) at -70 ºC. Temperature gradually increased to room temperature and reaction was stirred for 48 hr.200 ml of water was dropped into solution. Organic layer was separated and kept it. Aqueous phase was extracted with 150 ml ether. Ether and methylene chloride solution were combined and extracted with 2N NaOH (28 g, 350 ml water). Aqueous layer was precipitated with HCl and crude solid product was filtered. Additional purification was done by recrystallization with benzene to get needle-type product. Yield: 5.6 g (60 %). ^{1}H-NMR (500 MHz, DMSO): δ/ppm 9.79 (s, 2H, hydroxy), 7.14 (s, 2H, aromatic). ^{13}C-NMR (125 MHz, $CDCl_3$): δ/ppm 150.84, 124.03, 84.79. HRMS (Voltage EI+) : calculated m/z of [M+] 361.8301; measured m/z 361.8314.

3.3.4. Synthesis of 1.3-Bis(3,6,9-trioxadecanyl)glycerol-2-toluenesulfonic ester 1,3-Bis(3,6,9-trioxadecanyl)glycerol (10.0 g, 26 mmol) prepared by the previous lieterature[15] and sodium hydroxide (1.57 g, 40 mmol) was dissolved in tetrahydrofuran (THF, 7 ml). *p*-toluenesulfonyl chloride (4.72 g, 24.8 mmol) in THF (7 ml) was added dropwise at 5 ºC. Reaction was stirred at 5 ºC for 12 hr. The mixture was transferred into

separation funnel and the upper layer (THF layer) was kept. The aqueous phase was extracted with small amount of ether. Organic phases were combined and washed with water 3 times (Be careful that the upper layer is organic layer). The solvents were evaporated and the compound was redissolved in MC. The solution was dried over $MgSO_4$ and filtered. The solvent was evaporated with a rotary evaporator at reduced pressure. Additional purification was done by silica-gel based column chromatography (ethyl acetate : hexanes = 10 : 1 v/v). Yield: white-yellow liquid, 6.3 g (45 %). ^{1}H-NMR (500 MHz, DMSO): δ/ppm 7.81 (dd, 2H, J=8 Hz, aromatic), 7.30 (dd, 2H, J = 8 Hz, aromatic), 4.67 (m, 1H, -C<u>H</u>-), 3.64-3.50 (m, 28H, -OC<u>H</u>$_2$C<u>H</u>$_2$-), 3.64 (s, 6H, -OC<u>H</u>$_3$), 2.78 (s, 3H, -C<u>H</u>$_3$). ^{13}C-NMR (125 MHz, $CDCl_3$): δ/ppm 144.51, 134,04, 129.59, 128.01, 79.63, 71.91, 70.88, 70.58, 70.50, 70.34, 69.65, 59.01, 21.62. HRMS (Voltage ES+) : calculated m/z of [M+Na]+ 561.2346; measured m/z 561.2342.

3.3.5. Synthesis of 1,4-Bis(1,3-bis(3,6,9-trioxadecyl)-2-glyceryl)2,5-diiodobenzene This compound was prepared by procedure in a previous literature[13] through a slight modification. In 100 ml of 2-necked round-bottomed flask, 1,4-diiodo-2,5-hydroquinone (1.43 g, 3.97 mmol) and 1.3-Bis(3,6,9-trioxadecanyl)glycerol-2-toluenesulfonic ester (4.36 g, 8.10 mmol), potassium carbonate (2.19 g, 15.88 mmol) and dimethylformamide (10 ml) were added. Reaction was stirred at 75 ºC for 72 hr. Mixture was diluted with methylene chloride (100 ml) and washed with saturated ammonium hydroxide solution, followed by saturated brine. The organic layer was dried over $MgSO_4$ and filtered. The solution was concentrated and purified by silica-gel column chromatography (ethylacetate : hexanes = 9 : 1 v/v). Yield: 2.2 g (white-yellow viscous liquid, 50 %). ^{1}H-NMR (500 MHz, $CDCl_3$): δ/ppm 7.40 (s, 2H, aromatic), 4.38 (m, 2H, -

C<u>H</u>-), 3.8-3.4 (m, 56H, -OC<u>H</u>$_2$C<u>H</u>$_2$-), 3.37 (s, 12H, -OC<u>H</u>$_3$). ^{13}C-NMR (125 MHz, $CDCl_3$): δ/ppm 153.30, 125.97, 87.91, 80.79, 71.92, 71.18, 70.80, 70.65, 70.62, 70.57, 70.50, 59.02. HRMS (Electrospray with Na+ added, voltage ES+) : calculated m/z of [M+Na]+ 1117.2706; measured m/z 1117.2700.

3.3.6. Synthesis of (2,5-Bis(2,5,8,11,15,18,21,24-octaoxapentacosan-13-yloxy)-1,4-phenylene)bis(ethyne-2,1-diyl)bis(trimethylsilane) In 50 ml of schlenck flask, 1,4-bis(1,3-bis(3,6,9-trioxadecyl)-2-glyceryl)2,5-diiodobenzene (0.5 g, 0.457 mmol), copper iodide (I) (0.0043 g, 0.05 x 0.457 mmol), $Pd_3(PPH_3)_4$ (0.016 g, 0.05 x 0.457 mmol), tetrahydrofuran (10 ml) and diisopropylamine (DIPA) were added. After 5 min, trimethylsilyl acetylene (0.142 ml, 2.2 x 0.457 mmol) was added to the solution and the reaction was stirred at 70 ºC for 24 hr. The solvent was evaporated by a rotary evaporator at reduced pressure. The crude product was extracted with chloroform and water 3 times and dried over $MgSO_4$. The solution was filtered and evaporated again. Additional purification was done by silica-gel based column chromatography (ethylacetate : hexanes = 9 : 1). Yield: 0.4 g (85 %, light-yellow viscous liquid). ^{1}H-NMR (500 MHz, $CDCl_3$): δ/ppm 7.07 (s, 2H, aromatic), 4.43 (m, 2H, -C<u>H</u>-), 3.77-3.55 (m, 56H, -OC<u>H</u>$_2$C<u>H</u>$_2$-), 3.38 (s, 12H, -OC<u>H</u>$_3$), 0.24 (s, 18H, -Si(C<u>H</u>$_3$)$_3$). ^{13}C-NMR (125 MHz, $CDCl_3$): δ/ppm 153.91, 121.35, 115.87, 101.08, 100.05, 79.82, 71.92, 71.17, 70.63, 70.62, 70.56, 70.51, 59.03. HRMS (Electrospray with Na+ added, voltage ES+) : calculated m/z of [M+Na]+ 1057.5563; measured m/z 1057.5571.

3.3.7. Synthesis of Monomer (**1**) In 50 ml 2 neck round-bottom flask with Ar purging, (2,5-bis(2,5,8,11,15,18,21,24-octaoxapentacosan-13-yloxy)-1,4-phenylene)bis-

(ethyne-2,1-diyl)bis(trimethylsilane) (0.5 g, 0.48 mmol), methanol (2 ml) and 1M potassium hydroxide (0.1 g in 2 ml DI water) were added and the reaction was stirred at room temperature for 1 hr. In thin layer chromatography, the peak corresponding to reactant disappeared, which means that the reaction completed. Solvent was evaporated and redissolved the crude product in chloroform. The solution was washed with water (3 times) and dried with $MgSO_4$. Solution was filtered and concentrated by a rotary evaporator at reduced pressure. The product was dried in vacuo to get light-yellow viscous liquid (yield : 0.41 g, 97 %). ^{1}H-NMR (500 MHz, $CDCl_3$): δ/ppm 7.16 (s, 2H, aromatic), 4.22 (m, 2H, -C<u>H</u>-), 3.75-3.63 (m, 48H, -OC<u>H$_2$</u>C<u>H$_2$</u>-), 3.55 (m, 8H, -OCH(C<u>H$_2$</u>)2-), 3.38 (s, 12H, -OC<u>H$_3$</u>), 3.22 (s, 2H, -CC<u>H</u>). ^{13}C-NMR (125 MHz, $CDCl_3$): δ/ppm 154.15, 121.51, 115.06, 82.72, 80.01, 79.23, 71.93, 71.15, 70.63, 70.60, 70.56, 70.50, 59.01. HRMS (Electrospray with Na+ added, voltage ES+) : calculated m/z of [M+Na]+ 913.4773; measured m/z 913.4771.

3.3.8. Synthesis of 1,4-Disodiumpropanesulfonoxy-2,5-diiodobenzene (**2**) 2,5-diiodohydroquinone (2.0 g, 5.53 mmol) was dissolved in 1 % sodium hydroxide (0.55 g, 13.83 mmol) aqueous solution under argon purging. 1,3-propanesultone (1.69 g, 13.83 mmol) in 1,4-dioxane (13.8 ml) was added at once. The resulting mixture was stirred at room temperature overnight. Solution became a thick pink surly. The reaction mixture was then stirred at 80-100 ºC for another 30 min and then cooled down in a water/ice bath. The obtained suspension was vacuum-filtered and retained solution was washed with cold water, followed by acetone. Additional purification was done by recrystallization twice from water. Yield: 2.2 g (white powder, 62 %). ^{1}H-NMR (300 MHz, DMSO-d_6):

δ/ppm 7.29 (s, 2H, aromatic), 4.04 (t, 4H, -OC$\underline{H}_2$-), 2.80 (t, 4H, -C$\underline{H}_2$-S-), 1.95 (m, 4H, -C$\underline{H}_2$-).

3.3.9. Synthesis for PPE-R_1 and PPE-R_1-COOH A 50 ml Schlenk flask equipped with a stir bar was charged with **1** (83.6 mg, 93.8 μmol, 1 eq.), **2** (61.0 mg, 93.8 μmol, 1 eq.), 1.0 ml of DMF and 1.5 ml of deionized water. The flask was placed under argon atmosphere and tetrakis(triphenylphosphine)palladium (0) (3.25 mg, 2.81 μmol, 0.03 eq.) copper(I) iodide (0.54 mg, 2.81 μmol, 0.03 eq.) and diisopropylamine (DIPA, 0.5 ml) in DMF (0.5 ml) were by cannular transfer and degassed by argon purging and vacuum recycles several times. The mixture was stirred at 50 °C for 24 hours. For *in-situ* end-capping reaction, 4-ethynylbenzoic acid (13.7 mg, 93.8 μmol) and Pd and CuI as a catalyst (trace amount) were additionally added. After degassing, reaction was stirred for additional 24 hr. The cooled polymer solution was filtered, concentrated, and precipitated in acetone. The polymer was washed with ethyl acetate and tetrahydrofuran. Polymer was dissolved in basic water (20 ml, pH=9) and dialyzed (Spectra/Por®, Spectrum Laboratories, Inc., 12-14,000 MWCO) against several changes of deionized water for 3 d. Lyophilization of the resulting yellow-orange solution gave **PPE-R_1-COOH** as a yellow-brown fiber. **PPE-R_2** were synthesized in a same manner. Molecular weight by NMR end-group analysis = 13,000.

3.4. Results and Discussion

Monomer synthesis for the PPE copolymer starts by reacting 1,4-dimethoxybenzene with I_2 (I_2, HIO_3, H_2SO_4, AcOH, 85%). Demethylation (BBr_3, CH_2Cl_2, -78 ºC to room temperature, 90%) was then achieved by means of BBr_3. The resulting

diiodohydroquinone was reacted with the tosylated bifurcated ethylene oxide molecule,[13,15] followed by the reaction with trimethylsilylacetylene and a subsequent deprotection reaction to give monomer **1**. A diiodo compound, **2**, having sulfonic acid sodium salt units, was prepared according to the literature[16,17] (Scheme 1).

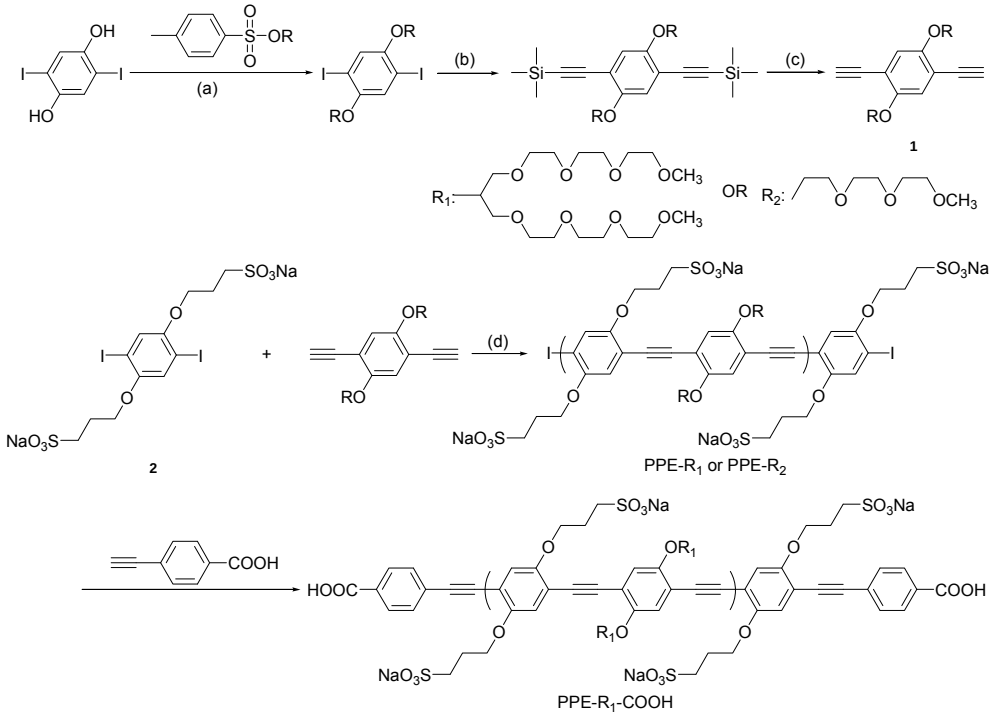

Scheme 3-1. Polymer synthesis (a) DMF, K_2CO_3, 75 ºC, 72 hr; (b) THF, $Pd(PPh_3)4$, diisopropylamine (DIPA), CuI; (c) KOH, water/methanol.

The copolymerization of **1** and **2** was carried out in the presence of a palladium catalyst (tetrakis(triphenylphosphine)palladium, $Pd(PPh_3)_4$) at 50 ºC in a water/DMF cosolvent system (50/ 50 v/v). The synthesized **PPE-R$_1$** showed excellent solubility in water or methanol but poor solubility in common organic solvents such as THF and chloroform. The *in situ* end-capping reaction was undertaken by adding 4-ethynylbenzoic

acid with additional palladium catalyst.[18] The crude polymer solution was precipitated in acetone, filtered, and washed with ethyl acetate and THF to remove diacetylene side product. Further purification of the polymer was achieved by dialysis against de-ionized water for 3 days. The *in situ* end-capping reaction of **PPE-R$_1$** with carboxylic groups was investigated by ^{1}H NMR spectroscopy (Fig. 1). Two aromatic proton peaks from the main chain of **PPE-R$_1$** appeared at 7.27 and 7.20 ppm. After the *in situ* end-capping reaction, two new peaks emerged at 7.73 and 7.49 ppm, corresponding to the aromatic protons of the end-capper, confirming that the carboxylic group was chemically attached. The molecular weight of the functionalized PPE (**PPE-R$_1$–COOH**), confirmed by ^{1}H NMR end-group analysis, was 13 000. We also prepared **PPE-R$_2$** as a control which does not have the bifurcated ethylene oxide units.

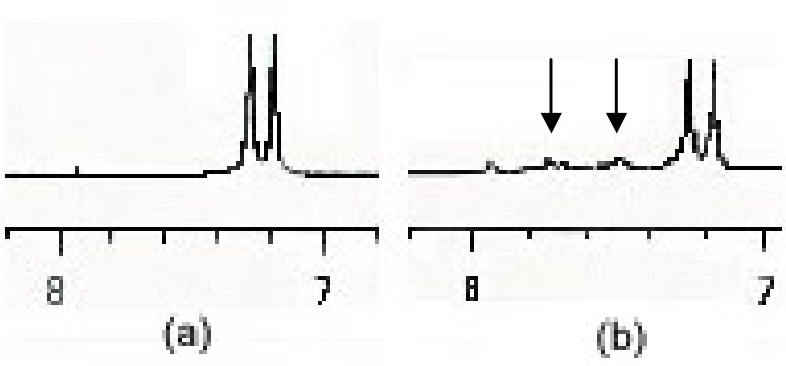

Figure 3-1. ^{1}H NMR spectra in D_2O of **PPE-R$_1$** (a) before and (b) after end-capping.

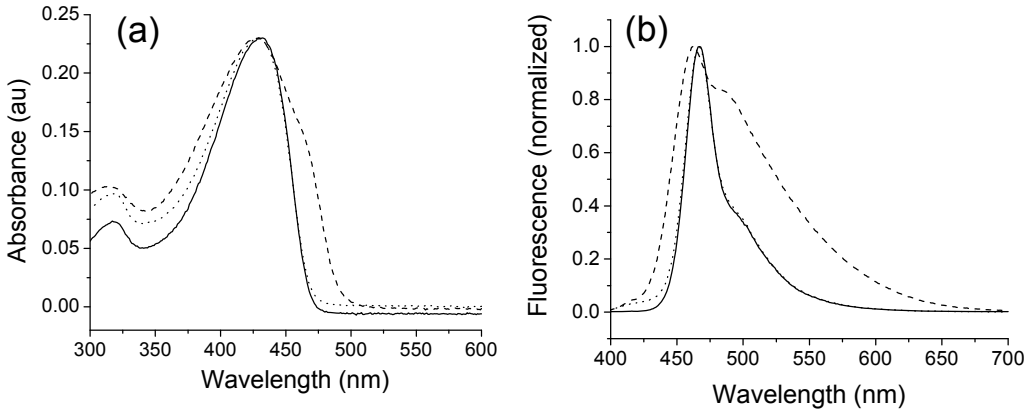

Figure 3-2. Normalized absorption (a) and emission (b) spectra of the polymers: **PPE-R$_1$** (solid); **PPE-R$_1$-COOH** (dotted); **PPE-R$_2$** (dashed).

Figure 3-2 illustrates the absorption and emission spectra of the prepared PPEs. The absorption spectra of **PPE-R$_2$**, unlike that of **PPE-R$_1$** and **PPE-R$_1$–COOH**, shows a pronounced shoulder in the longer wavelength region, typical of an aggregation band. **PPE-R$_2$** also shows a broad emission spectrum with the suppressed 0–0 band at λ_{max} = 460 nm and a long tail, a characteristic shape of excimer/aggregation-like emission caused by polymer aggregation, as expected.[19-21] On the contrary, the emission spectra of **PPE-R$_1$** and **PPE-R$_1$–COOH** are narrow with a well-defined 0–0 band at λ_{max} = 460 nm. We achieved a high quantum yield of PPE in water by adding ionic and bulky non-ionic side chains. The absolute quantum yield of **PPE-R$_1$** in water (1 mg L^{-1}) was 53%. Absolute quantum yield was measured with excitation at 365 nm in deionized water using PTI QuantaMaster® spectrofluorometers with an integrating sphere. Fully dried **PPE-R$_1$** completely dissolves in pure water with a solubility exceeding approximately 1 mg/ml. Until this paper, the best quantum yield of PPE-based polyelectrolyte was 57%, according to the previous literature.[22] While they introduced dendritic side chains into PPEs by a complicated synthetic route in order to overcome aggregation, we synthesized

PPEs using a simple method. To our knowledge, ours is the highest quantum yield ever reported of water-soluble conjugated polymers prepared through a simple synthetic route. Conversely, the absolute quantum yield of **PPE-R$_2$** in water (1 mgL^{-1}) was only 19%, suggesting that the ionic side chain, sulfonic acid sodium salts, provide additional water-solubility but that the bulky non-ionic side group is required to prevent aggregation. Recently, there is another method to overcome the aggregation of conjugated polyelectrolytes in water using surfactant.[10,23-25] However, unlike our polymers, this method was not enough to overcome an aggregated and emissive problem which polymers have inherently. Molecular modeling of PPE-R1, presented in Figure 3-3, shows that the hydrophobic PPE backbone is sheathed by the bulky ethylene oxide side chain, effectively preventing aggregation.

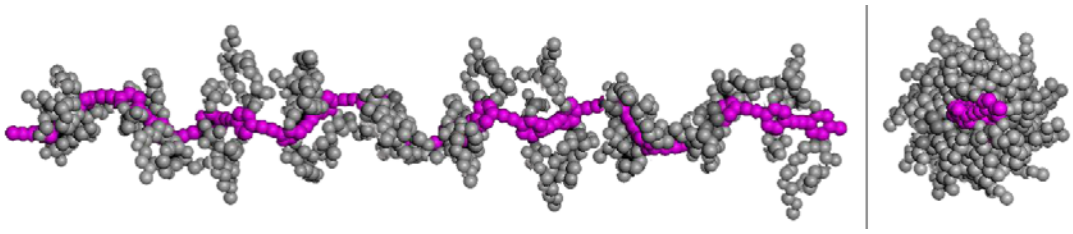

Figure 3-3. Molecular modeling of **PPE-R$_1$** simulated by Materials Studio 3.0 (Accelrys®). The purple chain indicates the polymer backbone (left: side view, right: edge view).

Chemical modification of **PPE-R$_1$** was done by an in situ endcapping reaction at the end of the copolymerization. We selected 4-ethynylbenzoic acid as an end-capper because a carboxylic group is of practical use for bioconjugation.[26] The absolute quantum yield of the resulting PPE-R1–COOH was 45%, lower than that of **PPE-R$_1$**. This drop in the quantum yield is believed to be due to the carboxylic acid group being directly

connected to the conjugated backbone. We have made various water-soluble PPE copolymers with carboxylic acid side chains in every other repeating unit. We consistently observed that the fluorescent quantum yields of PPEs with directly connected carboxylic acid side groups are always substantially lower than those of PPEs with carboxylic acid side chains connected to the conjugated backbone through a non-conjugated linker group.[27] The reason why **PPE-R$_1$-COOH** has only a slightly smaller quantum yield than **PPE-R$_1$** is likely to be because there are only two carboxylic acid groups at the ends of the conjugated backbone.

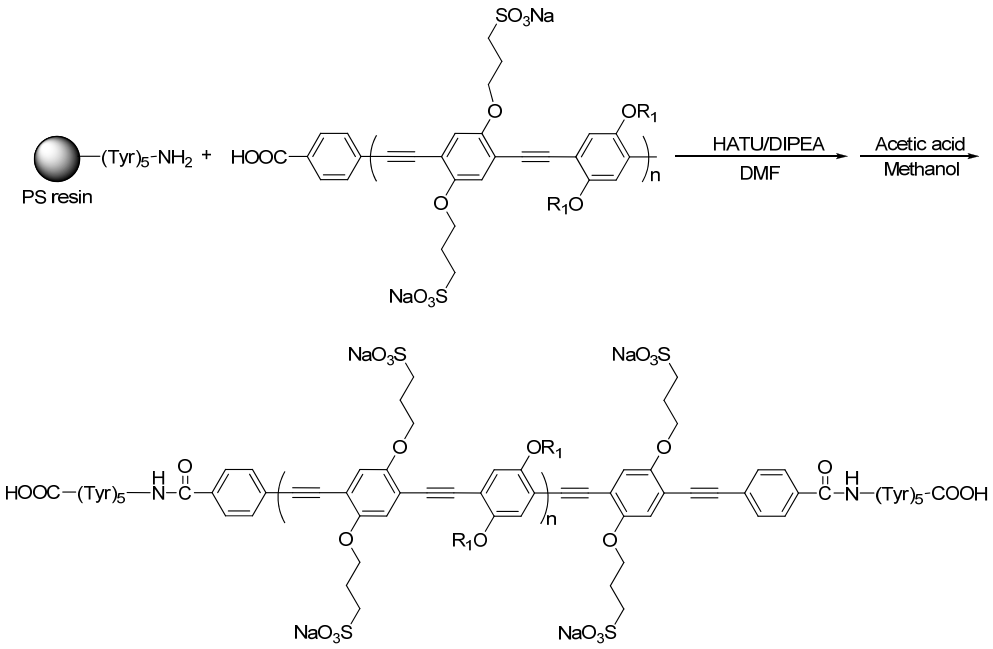

Scheme 3-2. Peptide-PPE coupling reaction.

We carried out the peptide conjugation reaction on the carboxylic acid groups of **PPE-R$_1$–COOH** by using 4-chlorotrityl resin bound with pentatyrosine as a model peptide (Scheme 3-2). We chose 4-chloro-trityl polystyrene (PS) resin because the

cleavage reaction can be undertaken using mild conditions, meaning that the PPE backbone is not damaged. After cleavage of the pentatyrosine from the resin, the quantitative coupling reaction of **PPE-R_1–COOH** with the pentatyrosine was confirmed by NMR. New aromatic proton peaks at 7.8–8.8 ppm, corresponding to pentatyrosine, are shown in Figure 3-4 (left). It was confirmed that pentatyrosine units were coupled at both ends of the **PPE-R_1–COOH** by end-group analysis. The ratio of the integration values in the 1H NMR corresponding to the phenyl rings in the PPE backbone and the tert-butyl group in pentatyrosine was in accordance with the calculated value. It is assumed that the polymer chains lay down on the large PS resin surface, such that every carboxyl group of the polymer has reacted with an amine group.[28] Figure 3-4 (right) shows a confocal microscope image of photoluminescent 4-chloro-trityl resin reacted with **PPE-R_1–COOH**. The image was taken after three stringent rinses of the resin with methanol, DMF, water and dichloromethane to remove any unreacted copolymers. The filtrate of the washing step to remove unbound polymers hardly showed any fluorescence, confirming that almost every polymer chain end has a carboxyl group that had reacted with the PS resin. After cleaving the pentatyrosine from the resin, the resulting peptide-conjugated PPE does not have any carboxylic acid directly bound to the conjugated backbone. Due to the hydrophobic tyrosine unit, solubility of the PPE–pentatyrosine bioconjugate in water significantly decreased. However, the PPE–peptide is completely soluble in DMSO and other organic solvents.

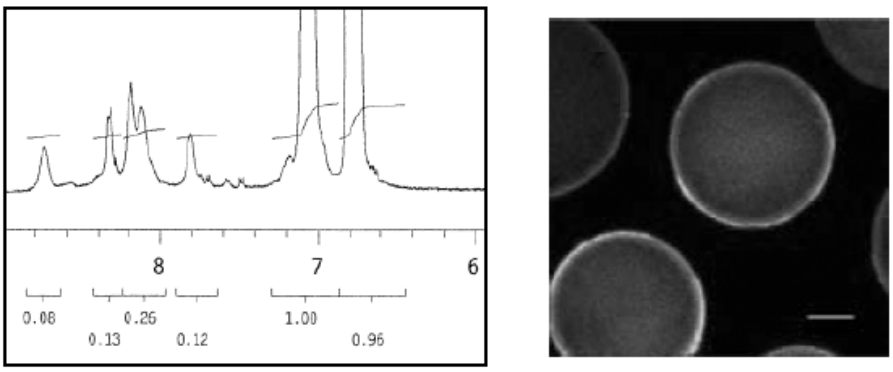

Figure 3-4. ^{1}H-NMR spectrum of pentatyrosin-PPE in DMSO (left) and a confocal image of pentatyrosine-PPE (right, scale-bar: 20 um).

3.5. Conclusion

We have established a simple and practical approach for the bioconjugation of a conjugated polyelectrolyte and a pentatyrosine, a model biological molecule. We designed and synthesized completely water-soluble and highly fluorescent sulfonated PPE with bifurcated ethylene oxide side chains. Endfunctionalized PPE, prepared by *in situ* chemical modification during polymerization, was successfully attached to a model peptide, pentatyrosine on a 4-chloro-trityl PS resin. This study provides a design principle for the preparation of functionalized, water-soluble, fluorescent, conjugated polymers for bioconjugation. Bio/synthetic hybrid conjugated polymers have a large potential as molecular biosensors to detect biological analytes quickly and selectively.

3.6. References

1. Liu, B.; Bazan, G. C. *Chem. Mater*. **2004**, *16*, 4467.

2. Pinto, M.; Schanze, K. S. *Synthesis* **2002**, *9*, 1293.

3. McQuade, D. T.; Pullen, A. E.; Swager, T. M. *Chem. Rev*. **2000**, *100*, 2537.

4. Wosnick, J. H.; Mello, C. M.; Swager, T. M. *J. Am. Chem. Soc*. **2005**, *127*, 3400.

5. Ho, H. A.; Doré, K.; Boissinot, M.; Bergeron, M. G.; Tanguay, R. M.; Bourdreau, D.; Leclerc, M. *J. Am .Chem. Soc*. **2005**, *127*, 12673.

6. Liu, B.; Bazan, G. C. *Proc. Natl. Acad. Sci. USA*. **2005**, *102*, 589.

7. Nilsson, K. P. R.; Inganäs, O. *Nat. Mater*. **2003**, *2*, 419.

8. Zhang, S.; Swager, T. M. *J. Am. Chem. Soc*. **2003**, *125*, 3420.

9. Ho, H.-A.; Boissinot, M.; Bergeron, M. G.; Corbeil, G.; Doré, K.; Bourdreau, D.; Leclerc, M. *Angew. Chem. Int. Ed*. **2002**, *41*, 1548.

10. Lavigne, J. J.; Broughton, D. L.; Wilson, J. N.; Erdogan, B.; Bunz, U. H. F. *Macromolecules* **2003**, *36*, 7409.

11. Tan, C.; Atas, E.; Müller, J. G.; Pinto, M. R.; Kleiman, V. D.; Schanze, K. S. *J. Am. Chem. Soc*. **2004**, *126*, 13685.

12. Chen, L.; McBranch, D. W.; Wang, H.-L.; Helgeson, R.; Wudl, F.; Whitten, D. G. *Proc. Natl. Acad. Sci. USA*. **1999**, *96*, 12287.

13. Khan, A.; Müller, S.; Hecht, S. *Chem. Commun*. 2005, 584.

14. Zhou, Q.; Swager, T. M. *J. Am. Chem. Soc*. **1995**, *117*, 12593.

15. Lauter, U.; Meyer, W. H.; Enkelmann, V.; Wegner, G. *Macromol. Chem. Phys*. **1998**, *199*, 2129.

16. Tan, C.; Pinto, M. R.; Schanze, K. S. *Chem. Commun*. **2002**, 446.

17. Chen, W.; Joly, A. G.; Malm, J.; Bovin, J.; Wang, S. *J. Phys. Chem. B* **2003**, *107*, 6544.

18. Samorí P.; Francke, V.; Müllen, K.; Rabe, J. P. *Chem. Eur. J.* **1999***, 5,* 2312.

19. Jenekhe, S. A.; *Adv. Mater*. **1995**, *7*, 309.

20. Kim, J.; Swager, T. M. *Nature* **2001**, *411*, 1030.

21. Kim, J.; Levitsky, I. A.; McQuade, T.; Swager, T. M. *J. Am. Chem. Soc*. **2002**, *124*, 7710.

22. Jiang, D.-L.; Choi, C.-K.; Honda, K.; Li, W.-S.; Yuzawa, T.; Aida, T. *J. Am. Chem. Soc*. **2004**, *126*, 12084.

23. Chen, L.; Xu, S.; McBranch, D.; Whitten, D. *J. Am. Chem. Soc*. **2000**, *122*, 9302.

24. Burrows, H. D.; Lobo, V. M. M.; Pina, J.; Ramos, M. L.; Seixas de Melo, J.; Valente, A. J. M.; Tapia, M. J.; Pradhan, S.; Scherf, U. *Macromolecules* **2004**, *37*, 7425.

25. Tapia, M. J.; Burrows, H. D.; Valente, A. J. M.; Pradhan, S.; Scherf, U.; Lobo, V. M. M.; Pina, J.; Seixas de Melo, *J. Phys. Chem. B* **2005**, *109*, 19108.

26. For comprehensive reading regarding conjugation techniques, Hermanson, *Bioconjugate Techniques*; Academic Press: San Diego, CA, 1996.

27. Lee, K.; Yucel, T.; Kim, H.-J.; Pochan, D. J.; Kim, J.; See Chapter 2 in this thesis.

28. Jo. S.; Shin, H.; Mikos, A. G. *Biomacromolecules* **2001**, *2*, 255.

29. Kong, X.; Jenekhe, S. A. *Macromolecules* **2004**, *37*, 8180.

CHAPTER 4

Label-Free and Self-Signal Amplifying Molecular DNA Sensors Based on Bioconjugated Polyelectrolytes

Parts of this chapter appear in: Lee, K.; Povlich, L. K.; Kim, J. Published in *Adv. Funct. Mater*. **2007**, *17*, 2580.

4.1. Abstract

Hybrid bio/-synthetic sensory conjugated polyelectrolytes were developed to achieve selective label-free detection of target oligonucleotides with amplified fluorescence signal in solution. A completely water soluble and highly fluorescent conjugated poly(p-phenyleneethynylene) (PPE) was rationally designed and synthesized as a signal amplifying unit and chemically modified with carboxylic functional groups at the ends of the polymer chains to bioconjugate with amine functionalized single stranded oligonucleotides as a receptor using carbodiimide chemistry. This approach allows the functional groups on the polymers to be effectively linked to DNA without any damage to the conjugated p-system of the polymers. DNA detection results using the PPE-DNA hybrid system confirmed large signal amplification by means of efficient Förster energy transfer from the energy harvesting PPE to the fluorescent dye attached to the complementary analyte DNA. To realize label-free detection, we also connected a DNA molecular beacon to the newly developed conjugated polymer as a self-signaling molecular switch. A DNA detection study by using the resulting PPE-DNA beacon and single strand analyte DNAs showed not only signal-amplification properties but also self-signaling properties.

4.2. Introduction

Conjugated polymers (CPs), pioneered by Shirakawa et al., have a framework of alternating single and double carbon-carbon bonds and are emerging materials for many modern technologies.[1] CPs have unique properties that are not exhibited by monomeric fluorophores such as amplified fluorescence through energy-harvesting,[2-9] excellent one-dimensional energy transport of electrons or holes,[10-19] and strong UV absorption. Among these properties, fluorescence is one of the most sensitive to environmental change and this allows conjugated polymers to be used as signaling reporter groups.[20-22] In monomeric fluorophore based sensors, only the receptors bound with target analyte can contribute to the sensory signal, which is a simple summation of the fluorescence emission from each bound receptor. On the contrary, any single binding event between receptor and target causes a change in the electronic environment of a conjugated polymer chain, resulting in an alteration of the emission of the entire polymer chain. In addition, the target receptor group can be rationally designed and covalently connected to the CP main chain in order to give eminent selectivity.[23-25] CPs have attracted great attention for sensor technologies including ion sensors,[26-31] pH sensors,[32-34] TNT sensors,[35-37] temperature sensors,[38] warfare agent sensors[39-40] and even recently developed biosensors.[7,41-47]

A conjugated polyelectrolyte (CPE) is a π-conjugated polymer that contains charged side chains to give it water-solubility.[48] The water-soluble pendent groups used most for CPEs are sulfonate (SO_3^-), carboxylate (CO_2^-), and phosphate (PO_4^{3-}) ions (negative) and quaternary ammonium (NR_3^+) ions (positive). Water-solubility of CPEs is difficult to achieve because of the hydrophobic nature of the CPE backbones and π-π

interactions between adjacent polymer main chains cause polymer aggregation. Even worse, it is almost impossible to redissolve a CPE in water once the polymer has been completely dried. Solving the problem of CPE aggregation in aqueous media remains a challenging task in many research groups.[46,49-51] For several years we have been systematically investigating the relation between water-solubility and the chemical structure of CPEs. In our previous research, we synthetically prepared completely water soluble and highly emissive conjugated poly(p-phenyleneethynylene) (PPE-R_1 and PPE-R_1-COOH, Figure 4-1).[52] We discovered that well-defined tuning of water-solubility can be achieved by precise control of the side chain shape and pendent ionic group of CPEs. Achieving the water solubility of CPEs should expand the applications of conjugated polymers to biological sensors for DNA and protein detection in aqueous media. By rendering largely amplified fluorescence signal through the signal amplifying property of CPs, trace amounts of target can be possibly detected.

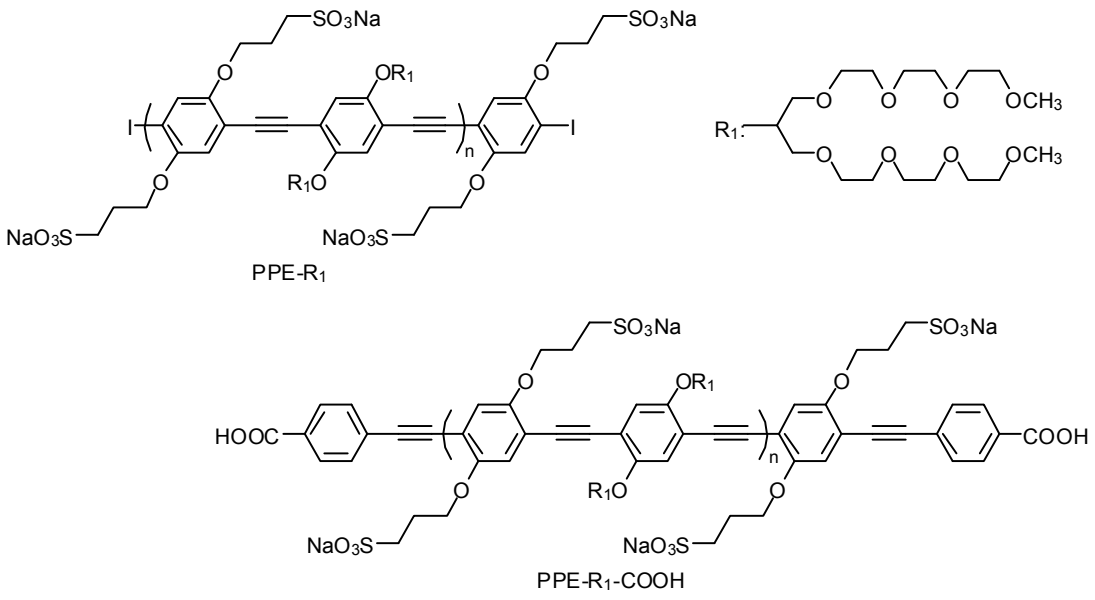

Figure 4-1. Chemical Structure of PPE-R_1 and PPE-R_1-COOH.

Many research groups have reported signal amplifying DNA sensors using various types of CPEs. Leclerc et al. have explored positively charged poly(thiophene) based DNA detection systems on the basis of conformational perturbations of polymer main chains and ensuing color change.[53-55] Bazan et al. used a fluorescence resonance energy transfer (FRET) mechanism to detect a target DNA through triplex formation of DNA/PNA or DNA/DNA with cationic poly(fluorene-cophenylene)s.[41,56-57] These methodologies used charge-charge interactions between cationically charged CPE and negatively charged oligonucleotide without requiring any chemical functionalization of polymer probes. Tan et al. recently reported an effective method for covalent conjugation of an oligonucleotide molecule to PPE by in-situ polymerization of PPE in the presence of an oligonucleotide linked to a CPG support and achieved self-signal amplifying DNA detection.[58] However, this system requires surfactants due to the limited solubility of the resulting polymer in water.

Herein, we describe a practical synthetic method for bio/-synthetic anionic poly(phenyleneethynylene)-DNA sensors for efficient self-signal amplifying DNA detection (Figure 4-2) in aqueous solution. By using a simple carboiimide chemistry, PPE was successfully conjugated to DNA molecules by amide bond formation. The resulting single stranded DNA (ssDNA) coupled at the end of the polymer chains selectively hybridized with HEX (hexachlorofluorescein, a fluorescent dye)-labeled target complementary DNA. A large amount of fluorescence energy from the PPE was efficiently transferred to the target HEX-DNA upon DNA/DNA hybridization, resulting in large signal amplification. Therefore, the PPE-DNA hybrid based DNA detection

system successfully showed large signal amplification through Förster type energy transfer mechanism (FRET). In addition, we also covalently connected the PPE with an oligonucleotide probe that has a quencher at the end. This oligonucleotide molecular beacon can form a hairpin-shape in buffer solutions resulting in the fluorescence quenching of the PPE but unfolds to form a DNA double helix upon addition of complementary DNA turning on the fluorescence emission of the PPE. Hence, in this molecular design the completely water-soluble and highly fluorescent conjugated polymer replaces a fluorescent dye of the conventional molecular beacon to allow label-free and self-signal amplifying detection of target DNA upon hybridization.

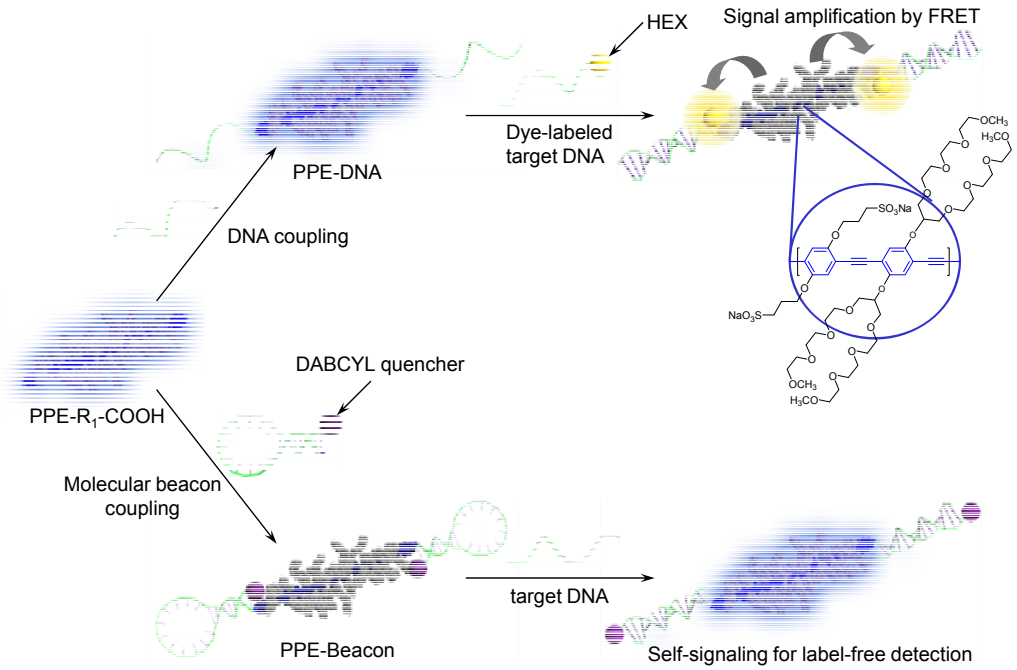

Figure 4-2. Polymer-oligonucleotide bioconjugation to form PPE-DNA (top) to demonstrate signal amplifying property by FRET and PPE-DNA beacon (bottom), demonstrating self-signal amplifying label-free detection.

4.3. Experimental Section

Materials and methods The synthesis and characterization of PPE-R_1 and PPE-R_1-COOH have been reported previously.[52] The polymer was purified by dialysis against deionized water (molecular weight cut off = 14 400 g mol^{-1}), lyophilized to dry the polymer, and it was stored in the dried state at 4 ºC. We tried to investigate the molecular weight of polymer using polystyrene-based GPC in DMF. However, the result was inflated and unreliable because the rigid rod backbone of the PPE resulted in a very large hydrodynamic volume. The number averaged molecular weight (M_n) of the functionalized PPE (PPE-R_1-COOH), confirmed by ^{1}H-NMR end-group analysis, was 13,000. The polymer solution was diluted as needed to prepare solutions used for spectroscopic experiments. Final concentrations of the diluted PPE-R_1-COOH solutions were determined on the basis of polymer repeat unit concentrations. All of the oligonucleotides were purchased from Integrated DNA Technologies, Inc. (Coralville, IA) and used without further purification. EDC (1-ethyl-3-[3-dimethylaminopropyl]carbodiimide hydrochloride) and sulfo-NHS were purchased from Fluka, Inc. and Pierce, Inc. respectively and used as received. Polymer-DNA bioconjugation samples were prepared by initially determining the DNA concentrations using standard UV absorption measurements with 200 μL samples. Microcentrifugal units for separation of unbound oligonucleotides were used with two molecular weight cut-offs available: 10 000 (purchased from Millipore Co), 12 000 (purchased from Whatman). Microcentrifugations were conducted with Eppendorf Minispin at 13,400 rpm (12,100 x G).

Polymer synthesis for PPE-$N(CH_3)_3$+ The synthesis and characterization of M1 and M2 have been reported previously.[19,52,59] A 50 ml Schlenk flask equipped with a stir

bar was charged with M1 (44.0 mg, 62.0 μmol, 1 eq.), M2(55.0 mg, 62.0 μmol, 1 eq.), and copper(I) iodide (0.35 mg, 1.86 μmol, 0.03 eq.). The flask was placed under argon atmosphere and tetrakis(triphenylphosphine)palladium (0) (2.15 mg, 1.86 μmol, 0.03 eq.) and DMF (1ml) were added. Degassed diionized water (1ml) and diisopropylamine (1ml) were successively added to the mixture by cannular transfer and degassed by argon purging and vacuum recycles several times. The mixture was stirred at 55 °C for 48 hours. The cooled polymer solution was filtered, concentrated, and precipitated in acetone and tetrahydrofuran. Then the compound was dissolved in diionized water (20 ml) and dialyzed (Spectra/Por®, Spectrum Laboratories, Inc., 12-14,000 MWCO) against several changes of deionized water for 2 d. Lyophilization of the resulting yellow-orange solution gave PPE-$N(CH_3)_3^+$ as a yellow-brown fiber. ^{1}H NMR (500MHz, D_2O) δ7.33 (s, 2H), 7.23 (s, 2H), 4.56 (m, 2H), 4.15 (t, 4H), 3.73 (m, 4H), 3.65-3.38 (broad m, 48H), 3.37 (m, 8H), 3.17 (s, 12H), 3.00 (s, 18H), 2.26 (t, 4H); Molecular weight by NMR end-analysis = 14,000.

Photophysical experiments UV/Vis absorption spectra of the solutions were obtained on a Cary UV50 UV/Vis spectrometer (Varian, Inc.). Steady-state fluorescence of the polymer and dye was recorded on a PTI QuantaMaster spectrofluorometer™ with a xenon lamp and a detector at an angle 90 degree. The absolute quantum yield of the polymer was measured with excitation at 365 nm in deionized water (1 mg L^{-1}) using an integrating sphere attached to the same spectrofluorometer.

Polymer-oligonucleotide bioconjugation PPE-R_1-COOH (0.13 mg), EDC (0.019 mg), and sulfo-NHS (0.0217 mg) were dissolved in 15 μl of DI water and incubated for 30 min in a dark room at room temperature. 1 mM (50 μl) of amino-

functionalized 15-base DNA (5'-ACA TCC GTG ATG TGT-3'-NH_2-3') was added to the polymer solution and the solution was stirred for 2 h. Unbound oligonucleotides from the PPE-DNA solution were removed by centrifugal washing with DI water several times using microcentrifuge tube (MWCO=10,000) until no change in characteristic UV absorbance (260 nm) from the filtrate solution was observed. After filtering, the polymer-DNA bioconjugate solution was lyophilized to allow preservation in a dried state at -20 °C. Coupling of DNA beacon to polymer **1** was also achieved in the same manner as the polymer-15-base DNA bioconjugate. Amine-functionalized oligonucleotides with DABCYL as a quencher (5'-NH_2-C_6-CGC TCG AAG GAG GAA GGA GGG AGC G-DABCYL-3') were used in the coupling reaction. Microcentrifuge tubes (MWCO=12,000) were used for the purification of polymer-beacon bioconjugates.

Analysis of polymer-DNA bioconjugates formation by gel electrophoresis To an each DNA, polymer, and polymer-DNA complex solution 4.8 μg of complementary DNA (c-DNA, 15 bp) was added. The mixture was diluted with 6×SSPE buffer to a final c-DNA concentration of 50 μg/mL, followed by incubation for 2 h at room temperature. The mixture was then analyzed by running it on a 4 % agarose gel (Nusieve® 3:1 Agarose, Cambrex Bio Science Rockland, Inc.) in 1× phosphate buffer (0.89 M Tris base, 0.89 M boric acid, and 0.02 M EDTA, pH = 8.3) at a constant voltage (60 V) for 90 min. The gel was then stained with ethidium bromide to visualize the DNA bands. Images were captured with a CCD camera in fluorescence mode with a band pass filter of 630 nm to remove fluorescence (460 nm) from polymer emission.

Hybridization Test All DNA hybridization tests were conducted at 25 °C. To 1.0 × 10^{-7} M polymer-DNA in 6×SSPE (900 mM sodium chloride, 60 mM sodium hydrogen

phosphate, 6 mM EDTA, pH 7.4) buffer solution, 4×10^{-7} M of HEX-labeled ssDNA (5'-HEX-ACA CAT CAC GGA TGT-3') was added. FRET tests were performed by checking UV absorbance and PL emission changes before and after hybridization upon excitation at 365 nm or 500 nm. In the polymer beacon case, Tris-HCl buffer (Tris-HCl 20 mM, NaCl 50 mM, $MgCl_2$ 5 mM, EDTA 2 mM) was used as the hybridization media. 2 equimolar amounts (4×10^{-6} M) of target DNA (5'-CGC TCC CTC CTT CCT CCT TCT TT-3') were added to the polymer-DNA beacon solutions for which the concentration (1×10^{-6} M) was determined by the UV absorption. Random sequence DNA (5'-GTG AGG GAG GAA GTA AAA AGA TT-3') and 1-mismatch (5'- CGC TCC CTC CAT CCT CCT TCT TT-3') tests were also done in the same manner.

4.4 Results and Discussion

Water solubility of the CPE Water soluble PPE-R_1 and its carboxylic acid-functionalized derivative (PPE-R_1-COOH) were previously reported in literature.[52] Homogeneous biological sensors must be water soluble or at least have entire compatibility with aqueous phase because most biological targets that we are interested in detecting exist in an aqueous environment. Another issue for sensor design is the need to develop fine selectivity to trace amounts of biological molecule. Therefore, it is indispensable for solution-state sensors to be water-soluble and highly sensitive to the binding event between receptor and target molecule. However, the hydrophobicity of conjugated polymer backbones causes aggregation between polymer chains in water and restricts aqueous dissolution of the polymers. Even worse, if rigid and hydrophobic polymers are dried, they are extremely difficult to re-dissolve in water. Many groups

have tried to de-aggregate the polymer chains by adding surfactant, however, this is not always the finest solution because, in some cases, surfactants may interfere with the sensing system.[49,58,60-62] To fulfill the requirements mentioned above, we strived to make completely water-soluble and highly fluorescent conjugated polymers for to biological sensor applications. Almost all the PPE polymers we initially made showed aggregation or fluorescence quenching in water.[27,63] Eventually, it was discovered that PPE-R_1-COOH was completely soluble in water. The ionic side chain (sulfonic acid sodium salt) provides the polymer with water-solubility and the bulky ethylene oxide side chain prohibits the polymer chains from agglomerating by sheathing the hydrophobic backbone of the polymers.[52,59,64] Fully dried PPE-R_1 dissolves in pure water with a solubility exceeding approximately 1 mg ml^{-1} (80 μM).

Polymer-DNA bioconjugation Conventional carbodiimide chemistry using EDC/sulfo-NHS catalyst offers a facile and simple method for the coupling of amino-functionalized oligonucleotides to the carboxylic acid groups of the polymers. First we confirmed the reactivity of the carboxylic acid group at the end of PPE-R_1-COOH by successfully attaching the PPE-R_1-COOH to amine-functionalized PS resins by carbodiimide chemistry. After the coupling reaction, the mixture solution was filtered to remove any unbound residual polymer in the solution. The filtrate solution showed very little fluorescence, which indicated that almost all the polymer was chemically bound to the PS resin implying the high reactivity of the chain-end carboxylic group. We applied the reactivity of the polymer toward amines to the covalent bioconjugation between the polymer and amine-functionalized oligonucleotides. The oligonucleotide used was 5'-NH_2-C_6-ACA CAT CAC GGA TGT-3' (ssDNA-NH_2), with an amine group at the 5'

position. An excess amount of the DNA was added to the polymer solution to ensure binding of the polymer molecule to the amine. After the coupling reaction between the two molecules, polymer and oligonucleotide, it was possible to purify the excess unbound oligonucleotide by microcentrifugal washing, which can separate components with different molecular weights. The molecular weight of the 15-sequence oligonucleotide is 4,762.2 g/mol and the number average molecular weight of the PPE-R_1-COOH, which was characterized by ^{1}H NMR end-group analysis, is 13,000 g/mol. The molecular weight of the bioconjugated PPE-oligonucleotide molecule is approximately 22,000 g/mol, so a centrifugal filter with a molecular weight cut-off (MWCO) of 10,000 is small enough to selectively remove the unbound oligonucleotide only. This has been confirmed by monitoring the change of the filtrate's UV absorbance (260 nm) after each washing time. Washing by centrifugation was repeated until there was no more change in UV absorbance. For the longer sequence hairpin oligonucleotides (5'-NH_2-C_6-ACA CAT CAC GGA TGT-3'), the bioconjugated polymer-beacon was also purified in the same manner but with a larger molecular weight cut-off microcentrifuge tube (MWCO = 12,000 g/mol). Bioconjugation between the polymer and DNA was confirmed by DNA gel electrophoresis. Nusieve agarose gel (4%) was used to analyze the DNA-PPE bioconjugate after hybridization. In Figure 4-3, lane 1 has only 15 base DNA that was hybridized with its target complementary DNA. Ethidium bromide stained the double helix DNA and shows the corresponding band. In lane 2, PPE-R_1-COOH before DNA conjugation was mixed with target DNA as a negative control. No band is observed in lane 2 because PPE-R_1-COOH does not have DNA bioconjugation and ensuing the absence of DNA double helix formation. In contrast, in lane 3, the PPE-DNA

bioconjugate forms DNA double helix upon binding with the target DNA and shows the broad band in the higher molecular region. This indicates that polymer and DNA are successfully coupled since the new band has slower migration compared to DNA alone due to the large molecular weight of the polymer. The board feature of the band is likely to be the result of the polydispersity of the polymer.

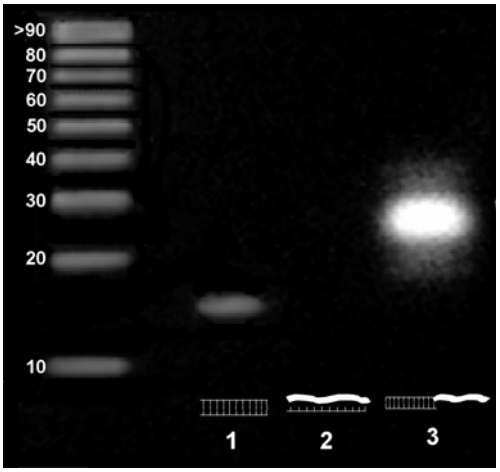

Figure 4-3. Gel electrophoresis of DNA (lane 1), PPE-R_1-COOH (lane 2), and PPE-DNA (lane 3) in the presence of c-DNA.

Signal Amplification by means of FRET Figure 4-4, which was obtained in 6×SSPE buffer at concentrations used in the DNA hybridization protocols, shows the absorption and emission spectra of PPE-R_1-COOH and HEX-labeled DNA. After coupling the DNA and PPE-R_1-COOH, the absorption and emission of the resulting PPE-DNA did not show any significant changes from those of PPE-R_1-COOH. The only difference was an increase in UV absorbance in the ca. 260 nm region, which is characteristic of the absorption of oligonucleotides indicating that oligonucleotide molecules were successfully bound to PPE-R_1-COOH. The emission spectra of the

polymers are narrow with well-defined 0-0 bands at λ_{max} = 460 nm and do not show any aggregation bands. The absolute quantum yields of PPE-R_1 and PPE-R_1-COOH in water, as analyzed by using an integrating sphere, were 53 % and 45 %, respectively. We used the PPE-DNA (15 base) bioconjugate as a model in order to investigate if the FRET mechanism from the emissive PPE to the HEX works upon hybridization.

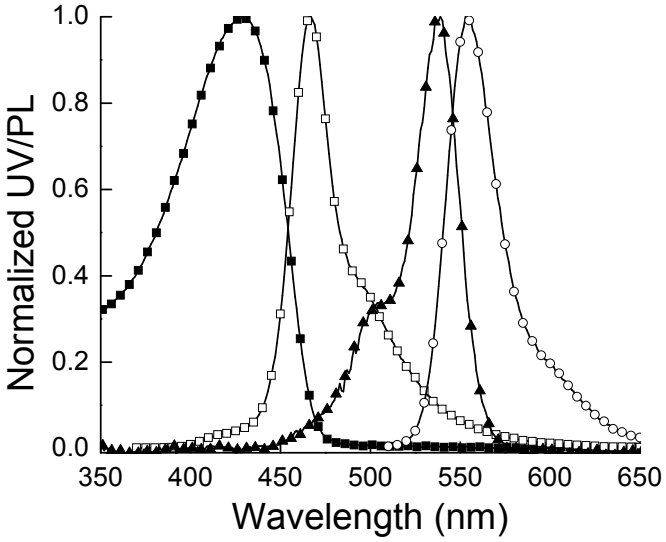

Figure 4-4. Normalized UV/PL spectra of PPE-R_1-COOH and HEX: absorption (■) and emission (□) spectrum of PPE, absorption (▲) and emission (○) spectrum of HEX.

As shown by Förster,[65-66] FRET is nominally the non-radiative transfer of energy from a donor to an acceptor molecule. Therefore, the signature of FRET is quenching of a high energy fluorophore followed by relatively high frequency light emission from an acceptor fluorophore. For this to occur, donor and acceptor molecules must be in close proximity (typically 1-10 nm). The FRET efficiency (F) is dependent on the inverse sixth power of the intermolecular separation, making it useful over distances comparable with

the dimensions of biological macromolecules. In addition, the fluorescence spectrum of the donor must be overlapped with the absorption spectrum of the acceptor. As one can clearly see in Figure 4-4, there is an excellent overlap between the emission of PPE-R_1-COOH and the absorption of HEX in the 450-600 nm range, which should make efficient FRET from PPE to HEX. Because the absorption spectra of the PPE and HEX are well separated selective excitation of PPE and HEX should be feasible for FRET study.

To demonstrate FRET, hybridization tests were conducted with HEX-labeled complementary ssDNA. The complementary ssDNA used in the study was HEX-DNA (5'-HEX-ACA CAT CAC GGA TGT-3'), with HEX (hexachlorofluorescein) at the 5' position. FRET experiments for HEX-DNA were carried out in 6×SSPE buffer and the results are shown in Figure 4-5. After hybridization, the PPE-DNA/DNA-HEX complex was selectively excited by 365 nm wavelength UV irradiation, which is not significantly absorbed by HEX. During this excitation experiment the fluorescence intensity from PPE was decreased and emission from HEX at 561 nm was largely increased as demonstrated in Figure 4-6. There was a slight red-shift of the emission maxima of HEX from λ= 555 nm without the polymer donor molecule to λ= 561 nm when HEX complexed with the polymer. A change in the charge density around HEX due to the close proximity of the negatively charged polymer induces a polarity change in the HEX molecule and likely causes the red-shift. The fluorescence intensity of HEX of the PPE-DNA/DNA-HEX complex was amplified more than 13 times compared to the emission intensity of the complex when HEX was directly excited at 500 nm as shown in Figures 4-5 and 4-6. The energy harvesting/transport properties of PPE after hybridization make it possible to achieve a highly amplified fluorescence signal by direct energy flow from the polymer to

the dye. Therefore, these results confirmed the signal amplification of HEX by energy transferred from PPE, indicating that our strategy of FRET from the PPE to dye was effective upon hybridization.

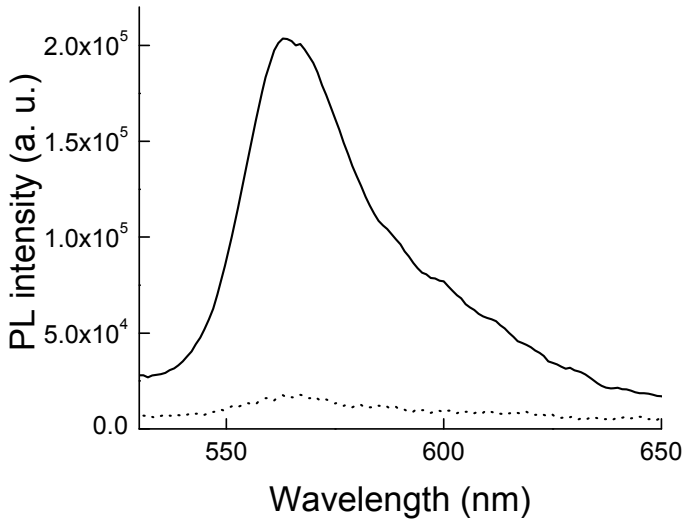

Figure 4-5. Emission spectra of PPE-DNA (1.0×10^{-7} M) upon hybridization with a complementary target HEX-DNA (4.0×10^{-7} M) when HEX was directly excited at 500 nm (dotted line) and when the PPE was excited at 365 nm (solid line) followed by FRET to HEX.

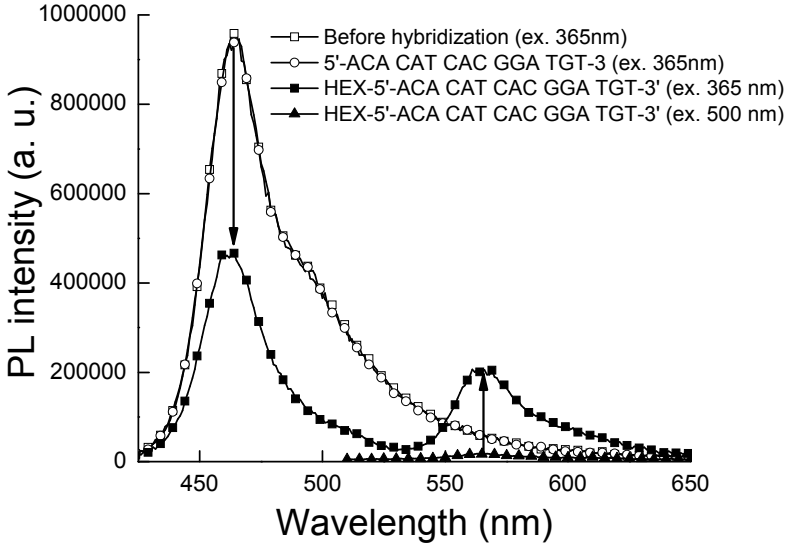

Figure 4-6. Comparison of PL change before (□) and after hybridization between HEX-labeled complementary target (excitation at 365 nm ■ ; at 500 nm ▲) and non-labeled complementary target (○).

Control experiments were also performed with the same sequence of complementary DNA but without HEX (Figure 4-6). Polymer emission at 460 nm did not show any change after hybridization with non-labeled target DNA, denoting that FRET is not observed in the absence of an energy acceptor molecule. This supports our interpretation that effective FRET from the polymer to HEX occurs upon hybridization. We also prepared completely water-soluble and cationically charged poly(phenyleneethynylenes) (Figure 4-7) as a control. The control polymer was mixed with HEX-labeled DNA to determine if FRET occurs from the polymer to HEX because of the attraction between the two oppositely charged fluorophores. After adding DNA, the fluorescence intensity from PPE significantly decreased. However, we observed very little signal amplification around HEX emission (Figure 4-8). Fluorescence quenching of

the polymer or HEX is believed to be due to the guanine (G) group in the oligonucleotides. Since G is the most electron-donating base of all four bases, the fluorescence drop can take place via electron transfer.[67-70] Also, the instability of DNA/polymer complex due to non-specific binding provides more conformational degrees of freedom to G, resulting in fluorescence drop of PPE and/or HEX. Even though the two fluorophores are oppositely charged, the bulky side chains of PPE-R_1 likely inhibit HEX from approaching the PPE backbone at a proximity close enough to see effective FRET. These results indicate that effective FRET from the polymer to HEX can be only achieved by stable polymer-DNA complex formation through hybridization with target complement at the polymer chain ends and not by simply mixing the two fluorophores. We endeavored to trace the emission source of the HEX molecules after hybridization. Figure 4-9 shows the excitation spectrum of the post-hybridized PPE-DNA/DNA-HEX complex and HEX-labeled DNA only. The result reveals that HEX emission originated not from the HEX itself but from the PPE emission. This result also demonstrates that FRET from the conjugated PPE to HEX was accomplished.

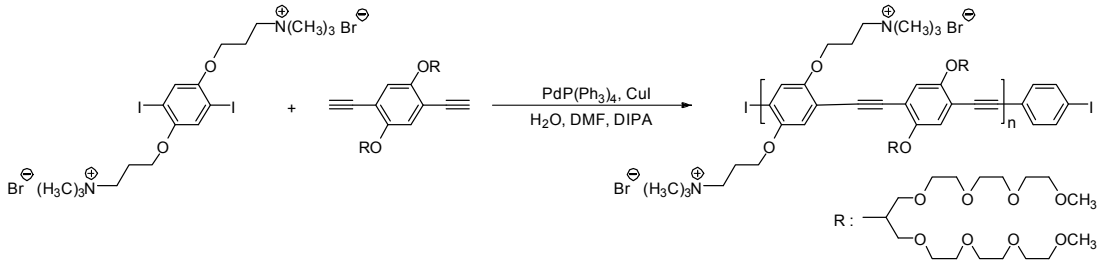

Figure 4-7. Chemical structure of positively charged PPE (PPE-$N(CH_3)_3^+$).

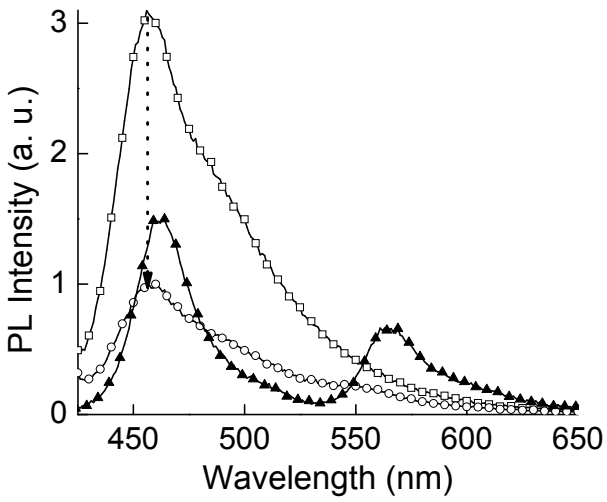

Figure 4-8. Comparison PL enhancement of HEX before (□) and after (○) adding HEX-labeled ssDNA in positively charged PPE (PPE-$N(CH_3)_3^+$). Compared with the PPE-DNA/DNA-HEX complex case (▲), increment of HEX emission in PPE-$N(CH_3)_3^+$/DNA-HEX are negligible.

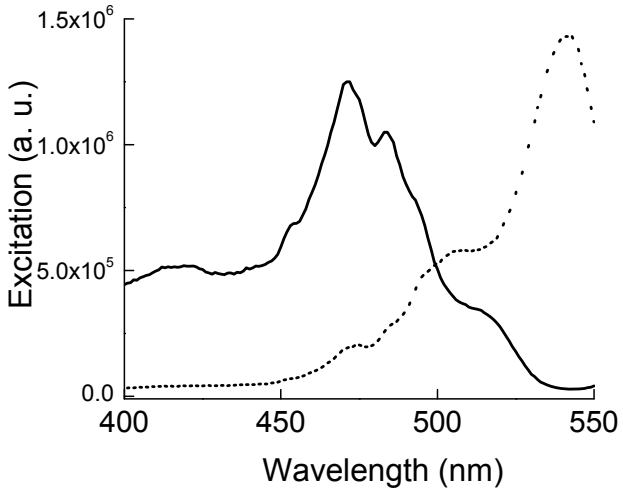

Figure 4-9. Excitation spectrum of PPE-DNA/HEX-DNA (solid) and HEX-labeled DNA only (dotted) corresponding to the emission wavelength of 556 nm.

Self-signaling Design for Label-free Detection Successful FRET by PPE-DNA/HEX-DNA hybridization allowed us to expand the sensor system to polymer-beacon conjugates. The molecular beacon, developed by Tyagi et al, is a self-signaling probe that eliminates the cost and time consuming procedures of DNA fluorescence labeling.[68,71-73] A traditional molecular beacon is a hairpin ssDNA in which a fluorescence dye and a quencher molecule located at opposite ends of the hairpin are in close contact. In a hairpin-shaped state (closed form), the stem keeps these two moieties in a close proximity to each other and fluorescent energy from the fluorophore is absorbed by the quencher through a FRET mechanism. However, when a target complementary ssDNA is introduced into the solution, hybridization opens the hairpin, thus moving the fluorescent dye away from the quencher and allowing the dye to emit a fluorescence signal. The rigidity and the length resulting from DNA double helix formation prevents the fluorophore and the quencher from being in close proximity. We applied the molecular beacon concept to our sensor design by replacing the conventional dye with conjugated PPE. Conjugated polymer can be considered a macromolecular chromophore that operates as a one-dimensional wire-like molecule that amplifies the fluorescence signal and the two molecular beacon at the ends of the polymer are two switch to turn off and on the amplified fluorescence signal of the polymer. In closed form, polymer fluorescence is completely quenched through amplified quenching mechanism of polymers. Fluorescent sensory signal amplification is induced upon opening of the hairpin by DNA/DNA hybridization, thus providing high sensitivity and label-free detection.

We have directly bioconjugated PPE-R_1-COOH to an amine functionalized oligonucleotide attached to a quencher by standard carbodiimide coupling and purified them in the same manner as used for the PPE-HEX experiments. A 25 base (5'-NH_2-CGC TCG AAG GAG GAA GGA GGG AGC G -DABCYL-3') oligonucleotide that forms a stem and loop structure was used in the reaction. The 15-mer loop of the beacon used for these studies was designed to bind specifically to a sequence in the left side of the TC1 tract of the human c-Src proto-oncogene.[74] According to theoretical calculations, this oligonucleotide sequence forms a stable hairpin (dG = -4.6 Kcal/mol).[75-76] 4-(4-(dimethylamino)phenyl-azo)benzoic acid) (DABCYL) was used as the quencher due to the good overlap of its UV absorption spectrum (λ_{max} = 478 nm) with PPE emission. After purifying the PPE-DNA-DABCYL beacon with centrifugal washing, UV absorbance from the PPE-DNA-DABCYL solution shows a shoulder at 460-500 nm, a typical characteristic of DABCYL absorbance, revealing that PPE was successfully conjugated to NH_2-DNA-DABCYL (Figure 4-10).

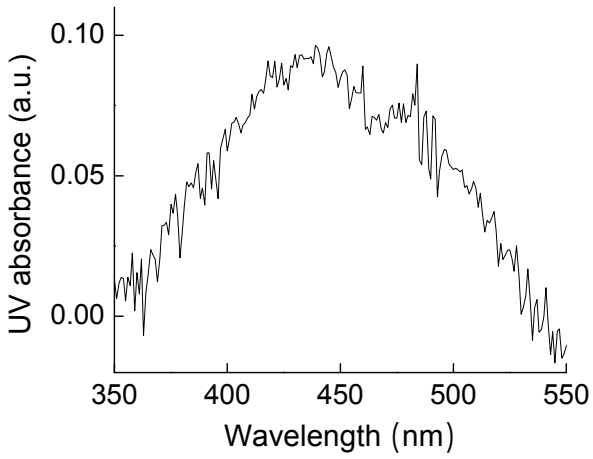

Figure 4-10. UV absorbance of PPE-DNA beacon (1.0 x 10^{-6} M)

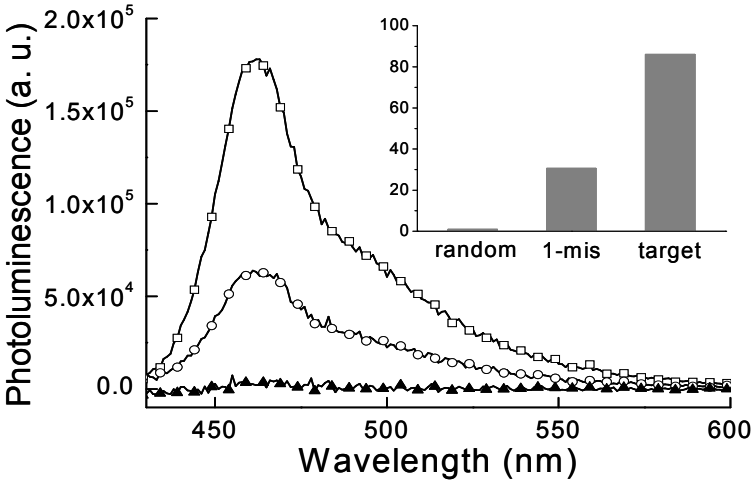

Figure 4-11. Overall fluorescence enhancement in polymer-beacon (1.0×10^{-6} M) after hybridization: complementary ssDNA (4×10^{-6} M, □), 1-mismatch (○), non-complementary ssDNA (▲), Excitation wavelength was 420 nm. Measurements were performed in Tris-HCl buffer (Tris-HCl 20 mM, NaCl 50 mM, $MgCl_2$ 5 mM, EDTA 2 mM). All curves are background (prehybridization) subtracted. Inset: Normalized fluorescence increase in 1-mismatch and perfect target DNA with respect to the emission in non-complementary DNA.

Figure 4-11 shows the fluorescence enhancement of PPE from post-hybridization with a series of DNA molecules including complementary ssDNA (5'-CGC TCC CTC CTT CCT CCT TCT TT-3'), 1-mismatch ssDNA (5'- CGC TCC CTC CAT CCT CCT TCT TT-3'), and noncomplementary ssDNA (5'GTG AGG GAG GAA GTA AAA AGA TT-3'). The hybridization experiments were conducted in a 20 mM Tris-HCl buffer (pH=8.0). The fluorescence intensity in the presence of target DNA was almost two orders of magnitude higher than the fluorescence intensity in the presence of the non-complementary target (Figure 4-11, inset). Polymer fluorescence was quenched in the closed form as the fluorescence energy of the polymer was effectively absorbed by

DABCYL. Opening of the beacon loop through hybridization with complementary ssDNA caused DABCYL to move far away from PPE, resulting in prevention of FRET from PPE to DABCYL and the restoration of the polymer emission. The results demonstrate that the PPE-DNA beacon can provide not only signal amplification but also self-signaling property.

4.5. Conclusion

We developed hybrid bio/-synthetic sensory conjugated polymers to selectively and sensitively detect target DNAs in aqueous solution. A completely water-soluble and highly emissive conjugated poly(*p*-phenyleneethynylene) (PPE) was synthesized and covalently bonded to amine functionalized DNA through chain-end modification. Upon DNA/DNA hybridization the PPE-DNA hybrid system demonstrated efficient Förster energy transfer from PPE to the fluorescent dye attached to the complementary DNA. A large signal amplification through the use of engineered conjugated polymers was convincingly demonstrated. We also bioconjugated a DNA molecular beacon to a newly developed conjugated polymer to achieve label-free and signal-amplifying detection of target DNAs and demonstrated self-signaling and signal amplifying property. The results presented in this contribution can give a design principle to develop completely water-soluble and highly emissive conjugated polymers and their bioconjugation with biological molecules for the development of high performance synthetic/bio- hybrid molecular biosensors and functional materials.

4.6. References

1. Shirakawa, H.; Louis, E. J.; MacDiarmid, A. G.; Chiang, C. K. and Heeger, A. J. *Chem.*

Commun. **1977**, 578.

2. Kim, J.; McQuade, D. T.; Rose, A.; Zhu, Z.; Swager, T. M. *J. Am. Chem. Soc*. **2001**, *123*, 11488.

3. Sato, T.; Jiang, D.-L.; Aida, T. *J. Am. Chem. Soc*. **1999**, *121*, 10658.

4. Schenning, A. P. H.; peters, E.; Meijer, E. W. *J. Am. Chem. Soc*. **2000**, *122*, 4489.

5. Pinto, M. R.; Schanze, K. S. *Proc, Natl. Acad.* Sci. USA **2004**, 101, 7505.

6. Chrisstoffels, L. A. J.; Adronov, A.; Fréchet, M. J. *Angew. Chem. Int. Ed*. **2000**, *39*, 2163.

7. Ho, H.-A.; Boissinot, M.; Bergeron, M. G.; Corbeil, G.; Doré, K.; Boudreau, D.; Leclerc, M. *Angew. Chem., Int. Ed.* **2002**, *41*, 1548.

8. Brédas, J.-L.; Beljonne, D.; Coropceanu, V.; Cornil, J. *Chem. Rev*. **2004**, *104*, 4971.

9. Baldo, M. A.; O'Brien, D. F.; You, Y.; Shoustikov, A.; Sibley, S.; Thompson, M. E; Forrest, S. R. *Nature* **1998**, *395*, 151.

10. Kraft, A.; Grimsdale, A. C.; Holmes, A. B.; *Angew. Chem. Int. Ed*. **1998**, *37*, 402.

11. Friend, R. H.; Gymer, R. W.; Holmes, A. B.; Burroughes, J. H.; Marks, R. N.; Taliani, C.; Bradley, D. D. C.; DosSantos, D. A.; Brédas, J.-L.; Logdlund, M.; Salaneck, W. R. *Nature* **1999**, *397*, 121.

12. Cao, Y. ; Parker, I. D. ; Yu, G. ; Zhang, C. ; Heeger, A. J. *Nature* **1999**, *397*, 414.

13. Klarner, G.; Davey, M. H.; Chen, W. D.; Scott, J. C.; Miller, R. D. *Adv. Mater*. **1998**, *10*, 993.

14. Huang, F.; Hou, L. T.; Wu, H. B.; Wang, W. H.; Shen, H. L.; Cao, W.; Yang, W.; Cao, Y. J.*J. Am. Chem. Soc*. **2004**, *126*, 9845.

15. Jones, R. M.; Bergstedt, T. S.; McBranch, D. W.; Whitten, D. G. *J. Am. Chem. Soc*. **2001**, *123*, 6726.

16. Culter, C. A.; Bouguettaya, M.; Reynolds, J. R. *Adv. Mater*. **2002**, *14*, 684.

17. Halls, J. J. M.; Cornil, J.; Santos, D. A.; Silbey, R.; Hwang, D. H.; Holmes, A. B.; Brédas, J.-L.; Friend, R. H. *Phys. Rev. B* **1999**, *60*, 5721.

18. Guldi, D. M.; Swartz, A.; Luo, C.; Gómez, R.; Segura, J.; Martín, N. *J. Am. Chem. Soc*. **2002**, *124*, 10875.

19. Kulkarni, A. P.; Tonzola, C. J.; Babel, A.; Jenekhe, S. A. *Chem. Mater*. **2004**, *16*, 4556.

20. Turro, N. J. Modern *Molecular Photochemistry*: University Science Books: Sausalito, CA, 1991.

21. Hong, J. W.; Hemme, W. L.; Keller, G. E.; Rinke, M. T.; Bazan, G. C. *Adv. Mater*. **2006**, *18*, 878.

22. Wosnick, J. H.; Swager, T. M. *Curr. Opin. Chem. Biol*. **2000**, *4*, 715.

23. McQuade, D. T.; Pullen, A. E.; Swager, T. M. *Chem. Rev*. **2000,** *100*, 2537.

24. Swager, T. M. *Acc. Chem. Res*. **1998**, *31*, 201.

25. Heeger, P. S.; Heeger, A. J. *Proc. Natl. Acad. Sci. USA* **1999**, *96*, 12219.

26. Kim, J.; McQuade, D. T.; McHugh, S. K.; Swager, T. M. *Angew. Chem. Int. Ed*. **2000**, *39*, 3868.

27. Pinto, M. R.; Kristal, B. M.; Schanze, K. S. *Langmuir* **2003**, *19*, 6523.

28. Marsella, M. J.; Swager, T. M. *J. Am. Chem. Soc*. **1993**, *115*, 12214.

29. Harrison, B. S.; Ramey, M. B.; Reynolds, J. R.; Schanze, K. S. *J. Am. Chem. Soc*. **2000**, *122*, 8561.

30. Chen, L. H.; McBranch, D.; Wang, R.; Whitten, D. *Chem. Phys. Lett*. **2000**, *330*, 27.

31. Wang, D. L.; Wang, J.; Moses, D.; Bazan, G. C.; Heeger, A. J.; Park, J. H.; Park, Y. W. *Synth. Met*. **2001**, *119*, 587.

32. McQuade, D. T.; Hegedus, A. H.; Swager, T. M. *J. Am. Chem. Soc*. **2000**, *122*, 12389.

33. Song, J.; Cisar, J. S.; Bertozzi, C. R. *J. Am. Chem. Soc*. **2004**, *126*, 8459.

34. Shoji, E.; Freund, M. S. *J. Am. Chem. Soc*. **2001**, *123*, 3383.

35. Yang, J. S.; Swager, T. M. *J. Am. Chem. Soc*. **1998**, *120*, 5321.

36. Yang, J. S.; Swager, T. M. *J. Am. Chem. Soc*. **1998**, *120*, 11864.

37. Liu, Y.; Mills, R. C.; Boncella, J. M.; Schanze, K. S. *Langmuir* **2001**, *17*, 7452.

38. Kuroda, K.; Swager, T. M. *Macromolecules* **2004**, *37*, 716.

39. Levitsky, I. A.; Krivoshlykov, S. G.; Grate, J. W. *J. Phys. Chem. B*. **2001**, *105*, 8468.

40. Zhang, S.-W.; Swager, T. M. *J. Am. Chem. Soc*. **2003**, *125*, 3420.

41. Gaylord, B. S.; Heeger A. J.; Bazan G. C. *Proc. Natl. Acad. Sci.U.S.A.* **2002**, *99*, 10954.

42. Nilsson, K. P. R.; Inganäs, O. *Nat. Mater*. **2003**, *2*, 419.

43. Pun, C.-C.; Lee, K.; Kim, H.-J.; Kim, J. *Macromolecules* **2006**, *39*, 7461.

44. Lee, K.; Rouillard, J.-M.; Pham, T.; Gulari, E.; Kim, J. *Angew. Chem. Int. Ed*. **2007**, *46*, 4667.

45. Wang, S.; Bazan, G. C. *Adv. Mater*. **2003**, *15*, 1425.

46. Chen, L.; McBranch, D. W.; Wang, H.; Helgeson, R.; Wudl, F.; Whitten, D. G. *Proc. Natl. Acad. Sci. USA* **1999**, *96*, 12287.

47. Wosnick, J. H.; Mello, C. M.; Swager, T. M. *J. Am. Chem. Soc.***2005**, *127*, 3400.

48. Pinto, M. R.; Schanze, K. S. *Synthesis-Stuttgart*. **2002**, *9*, 1293.

49. Lavigne, J. J.; Broughton, D. L.; Wilson, J. N.; Erdogan, B.; Bunz, U. H. F. *Macromolecules* **2003**, *36*, 7409.

50. Tan, C.; Atas, E.; Müller, J. G.; Pinto, M. R.; Kleiman, V. D.; Schanze, K. S. *J. Am. Chem. Soc*. **2004**, *126*, 13685.

51. Stork, M.; Gaylord, B. S.; Heeger, A. J.; Bazan, G. C. *Adv. Mater*. **2002**, *14*, 361.

52. Lee, K.; Cho, J. C.; Deheck, J.; Kim, J. *Chem. Commun*. **2006**, 1983.

53. Ho. H. A.; Doré, K.; Boissinot, M.; Bergeron, M. G.; Tanguay, R. M.; Boudreau, D.; Leclerc, M. *J. Am. Chem. Soc*. **2005**, *127*, 12673.

54. Abérem, M. B.; Najari, A.; Ho, H.-A.; Gravel, J.-F.; Nobert, P.; Boudreau, D.; Leclerc, M. *Adv. Mater*. **2006**, *18*, 2703.

55. Ho, H.-A.; Béra-Abérem, M.; Leclerc, M. *Chem. Eur. J*. **2005**, *11*, 1718.

56. Gaylord, B. S.; Heeger A. J.; Bazan, G. C. *J. Am. Chem. Soc*. **2003**, *125*, 896.

57. Liu, B.; Bazan, G. C. *Chem. Mater*. **2004**, *16*, 4467.

58. Yang, C. J.; Pinto, M.; Schanze, K.; Tan, W. *Angew. Chem. Int. Ed*. **2005**, *44*, 2572.

59. Khan, A.; Müller, S.; Hecht, S. *Chem. Commun*. **2005**, 584.

60. Chen, L.; Xu, S.; McBranch, D.; Whitten, D. *J. Am. Chem. Soc*. **2000**, *122*, 9302.

61. Burrows, H. D.; Lobo, V. M. M.; Pina, J.; Ramos, M. L.; Seixas de Melo, J.; Valente, A. J. M.; Tapia, M. J.; Pradhan, S.; Scherf, U. *Macromolecules* **2004**, *37*, 7425.

62. Tapia, M. J.; Burrows, H. D.; Valente, A. J. M.; Pradhan, S.; Scherf, U.; Lobo, V. M. M.; Pina, J.; Seixas de Melo, *J. Phys. Chem. B* **2005**, *109*, 19108.

63. Tan, C.; Pinto, M. R.; Schanze, K. S. *Chem. Commun*. **2002**, 446.

64. Jiang, D.-L.; Choi, C.-K.; Honda, K.; Li, W.-S.; Yuzawa, T.; Aida, T. *J. Am. Chem. Soc*. **2004**, *126*, 12084.

65. Förster, T. *Ann. Phys*. **1948**, *2*, 55.

66. Lakowicz, J. R. In *Principles of Fluorescence Spectroscopy;* Kluwer Academic/Plenum Publisher: New York, 1999.

67. Seidal, C. A.; Schuz, A.; Sauer, M. H. M. *J. Phys. Chem*. **1996**, *100*, 5541.

68. Marras, S. A. E.; Kramer, F. R.; Tyagi, S. *Nucleic Acids Res*. **2002**, *30*, e122.

69. Steenken, S.; Jovanovic, V. *J. Am. Chem. Soc*. **1997**, *119*, 617.

70. Heinlein, T.; Knemeyer, J.-P.; Piestert, O.; Sauer, M. *J. Phys. Chem. B* **2003**, *107*, 7957.

71. Bonnet, G.; Tyagi, S.; Libchaber, A.; Kramer, F. R. Proc. *Natl. Acad. Sci. USA* **1999**, *96*, 6171.

72. Tyagi, S.; Bratu, D. P.; Kramer, F. R. *Nat. Biotechnol*. **1998**, *16*, 49.

73. Tyagi, S.; Marras, S. A. E.; Kramer, F. R. *Nat. Biotechnol*. **2000**, *18*, 1191.

74. Antony, T.; Subramaniam, V. *J. Biomol. Struct. Dyn*. **2001**, *19*, 497.

75. Zuker, M. *Nucleic Acid Res*. **2003**, *31*, 3406.

76. Mathews D. H.; Sabina, J.; Zuker, M.; Turner, D. H. *J. Mol. Biol*. **1999**, *288*, 911.

CHAPTER 5

Conjugated Polyelectrolyte-Antibody Hybrid Molecules for Live Cell-Imaging

Parts of this chapter appear in: Lee, K.; Kronk, A.; Seiler, C. E.; Elenitoba-Johnson, K.; Lim, M. S.; Kim. J. Manuscript in preparation.

5.1. Abstract

We presented the design, synthesis, and application of highly-fluorescent and water-soluble conjugated poly(p-phenyleneethynylene) (PPE) derivatives (PPE-B and PBZ2) as fluorescent probes to image human B-cell lymphoma (SUDHL-4) and human T-cell leukemia (Jurkat) that play a crucial role in human immunology research. The two PPEs, PPE-B and PBZ2, having blue and red emission, respectively, were prepared by Pd-catalyzed polymerization. The emission maximum of PPE-B in water was at 460 nm and that of PBZ2 was at 630 nm. The conjugated polymers were bioconjugated with antibodies (CD3 or CD20) by means of carbodiimide chemistry between a carboxylic group of the polymers and an amine group in the antibodies to prepare the conjugated polymer-labeled antibodies, PPE-B-CD3 and PBZ2-CD20. The conjugated polymer-labeled antibodies were incubated with the suspension cells. PPE-B-CD3 selectively stained B-cells only while PBZ2-CD20 showed excellent specificity toward T-cells (or Jurkat), demonstrating excellent cross-selectivity. The cytotoxicity of the polymers was also examined and the results showed that the polymers did not have any harmful effects on the cell viability. Due to the larger molecular weight and high extinction coefficient of the conjugated polymers, the conjugated PPE-B-CD3 showed much brighter cell imaging compared to conventional FITC-labeled CD-3. The results imply that biocompatible and water-soluble conjugated polymers are superior to small organic dyes and toxic inorganic quantum-dots as a fluorescent signaling reporter for live cell imaging.

5.2. Introduction

Convenient and cost-effective methods for bioimaging in real time particularly with high sensitivity are highly desired in medical diagnosis, identification of cancer cells, immunofluorescent techniques, catalytic pathway monitoring, drug delivery monitoring through membrane or cytoplasm, and identification of cell mutations.[1-4] Conventional cell staining techniques for immunofluorescence microscopy require time and cost consuming multiple steps in sample preparation such as, fixation of cells, blockings, and primary and secondary antibodies treatments. On the contrary, direct labeling not only greatly reduces required preparation steps but also, and more importantly, can avoid the common problems of cross-reactivity and high-level background. Small fluorescent molecules and inorganic quantum dots have been extensively studied in labeling biological entities such as bacteria, viruses, cells, and tissues.[5-20] However, small organic fluorescent molecules often suffer from photo-bleaching and the much more stable inorganic quantum dots such as CdSe and CdTe are not free from potential cytotoxicity due to possible heavy metal reaching from the nanoparticles. Another potentially critical issue in the application of inorganic quantum dots to *in-vivo* bioimaging is their aggregation resulting from the disruption of the passivation layer of the quantum dots induced by environmental change.[6,13,21,] Therefore, there is a great need to devise a bioimaging method that is simple, nontoxic, and can provide high sensitivity.

Conjugated polyelectrolytes (CPEs) are conjugated polymers having ionic or non-ionic water soluble side chains for the solubility of the polymers in water. The molecular design of highly fluorescent and water-soluble CPEs and their application for novel biosensors are a topic of much scientific interest.[23-25] The large molecular weight and a

high extinction coefficient of CPEs provide a unique energy harvesting property to the CPEs. Therefore, if the side chain of the CPEs is rationally designed to efficiently prevent aggregation of the hydrophobic backbone of CPEs in water, CPEs become a bright emitter in aqueous environment. Abundant side chains and the two chain ends of CPEs are available to introduce a reactive functional group for additional modifications and bioconjugation.[24-26]

To the best of our knowledge, there were no systematic studies on cell staining using chemically synthesized fluorescent conjugated polyelectrolytes and its conjugation with antibody, universal biomarker, where more sensitive fluorescent detection of cell targeting could be readily employed. Here, we report novel CPE-antibody conjugates for fast, convenient, and highly sensitive live cell imaging. It is advantageous to use primary antibodies directly labeled with a fluorophore without an introduction of secondary antibody. Therefore, the hybrid CPE-antibody conjugates were prepared by means of direct bioconjugation between a membrane antibody (CD3 or CD20) and a conjugated poly(*p*-phenyleneethynylene) (PPE) derivative (PPE-B or PBZ2) having blue or red fluorescent emission (Figure 5-1). CD3 is an antibody which selectively recognizes B-cells only while CD20 will bind to T-cells (or Jurkat) specifically. The two CPEs, PPE-B and PBZ2, were prepared by Pd-catalyzed polymerization and have carboxylic acids on the side chains or the two chain ends of the CPE. The CPE was covalently linked to the antibody as a macromolecular fluorescent reporter through carbodiimide chemistry between the carboxylic acid of the CPE and amine groups of the antibody. Sensitivity, cross-selectivity, cell viability, and dilution tests were systematically conducted. The

developed CPEs and the method for bioconjugation of the CPEs with antibodies virtually can be applied for the direct labeling of any biological molecules.

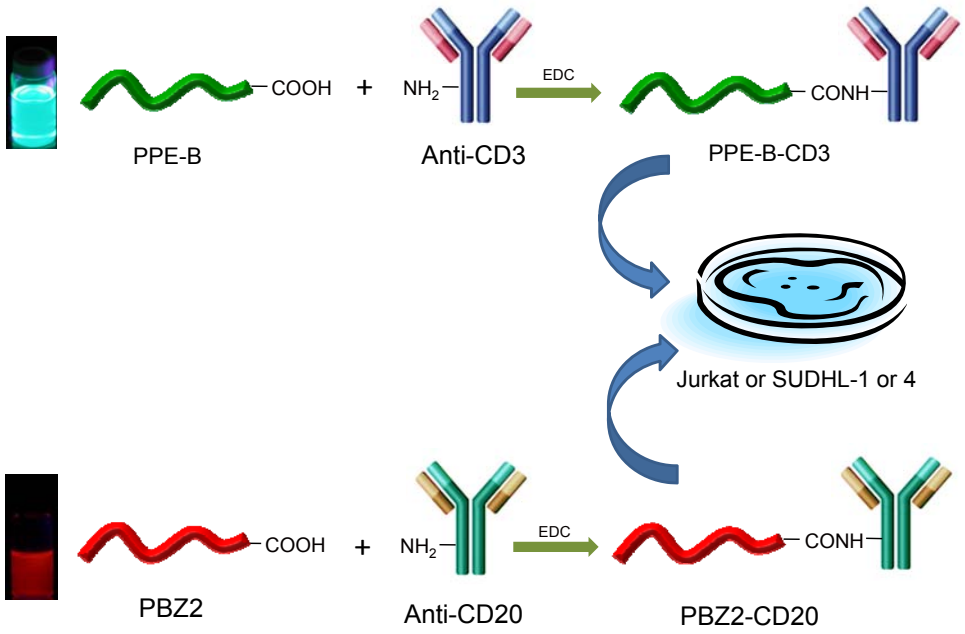

Figure 5-1. Overall strategy of cell imaging with water-soluble fluorescent polymer-antibody conjugates.

5.3. Experimental Section

Materials and Method. All solvents and reagents for polymer preparation were used without further purification as purchased from Fisher Scientific or Sigma-Aldrich Chemical Co. Detailed synthetic routes for 2,5-diiodo-1,4-hydroquinone (1), 4,7-dibromo-2,1,3-benzothiadiazole (2), M2 and M4 was previously published.[25-27] NMR characterization of polymers was conducted by Varian Inova 500 (11.7 Tesla, oxford magnet). The following materials and chemicals for conjugation and cell study were used as received. 1-ethyl-3-(3-dimethylaminopropyl) carbodiimide hydrochloride (EDC), N-

hydroxysulfosuccinimide (Sulfo-NHS), 2-(N-morpholino)ethanesulfonic acid (MES) buffer and phosphate buffer saline (PBS) buffer were purchased from Pierce Biotechnologies for bioconjugation. Mouse monoclonal anti-CD3 and CD20 were purchased from GeneTex, Inc. and BD Biosciences, respectively. Functional grade purified anti-human CD3 and FITC anti-human CD20 was purchased from eBioscience, Inc. Human anaplastic large cell lymphoma (SUDHL-1), Human B cell lymphoma (SUDHL-4) and human T cell leukemia (Jurkat) were purchased from Deutsche Sammlung von Mikroorganismen und Zellkulturen (DSMZ) GmbH (Braunschweig, Germany). RPMI1640 for cell culture experiment to grow SUDHL-1 (T cell), SUDHL-4 (B cell), or Jurkat cells and HyQ PBS buffer (pH=7.0) for cell staining using polymer-antibody conjugates were purchased from HyClone, Thermo Fisher Scientific Inc.

Synthesis of Diethyl 4,4'-(2,5-diiodo-1,4-phenylene)bis(oxy)-dibutanoate (M1)

To a solution of 2,5-diiodo-1,4-hydroquinone (**1**, 1.0 g, 2.76 mmol) were added a potassium carbonate (1.615 g, 8.28 mmol), ethyl 4-bromobutyrate (1.615 g, 8.28 mmol) and dimethylformamide (DMF, 15 ml). The reaction mixture was stirred at 80 ºC for 48 hr. After the reaction, the reaction mixture was cooled down to room temperature and filtered through a filter paper. DMF was removed by rotary evaporator at a reduced pressure. Crude mixture was re-dissolved in chloroform and extracted twice with deionized water. After drying over $MgSO_4$ and filtering, chloroform was removed in vacuo. Further purification was done by column chromatography (ethyl acetate : hexane = 1 : 1 v/v) and the following recrystallization in methanol at −18 ºC gave white waxy powder (yield: 0.65 g, 41 %). ^{1}H-NMR (500 MHz, $CDCl_3$): δ/ppm 7.10 (s, 2H, aromatic),

4.20 (m, 4H, -OC$\underline{H}_2$$CH_3$), 4.01 (t, 4H, -OC$\underline{H}_2$-), 2.60 (t, 4H, -C$\underline{H}_2$COO-), 2.15 (m, 4H, -C$\underline{H}_2$-), 1.27 (t, 6H, -$CH_3$).

Synthesis of 4.7-bis((trimethylsilyl)ethynyl)benzothiadiazole (3). To a 50 ml Schlenck flask with a stir bar were added 4,7- dibromo-2,1,3-benzothiadiazole (**2**, 1.55 g, 5.27 mmol), trimethylacetylene (1.79 ml, 12.65 mmol), $Pd(PPh_3)_4$ (61 mg, 52.7 μmol) and CuI (10.0 mg, 52.7 μmol). After purging with Ar for 2 min, 20 ml of toluene and 5 ml of diisopropylamine were added respectively. The mixture was stirred at 65 ºC for 7 hr after cycles of argon purging and degassing by vacuum several times. Solvent was evaporated at 32 ºC with reduced pressure and the crude mixture was purified by a short column of silica gel with ether as an eluent. Further purification was done by column chromatography (methylene chloride : hexane = 2 : 3 v/v). Recrystallization in methylene chloride and hexane (2:7) at – 18 ºC gave yellow-white fluffy powder (yield: 1.03 g, 60 %) ^{1}H-NMR (500 MHz, $CDCl_3$): δ/ppm 7.71 (s, 2H, aromatic), 0.341 (s, 18H, -Si(C$\underline{H}_3$)$_3$). ^{13}C-NMR (500 MHz, $CDCl_3$) δ/ppm 154.22, 133,16, 117.26, 103,65, 99.99, 0.11. HRMS (Voltage ES+, electrospray with Na+ added): calculated m/z of [M+Na]+ 351.0783; measured m/z 351.0777.

Synthesis of 4.7-diethynylbenzodthiadiazole (M3). In a 100 ml 2-neck round bottom flask with Ar purging was added compound **3** (0. 361 g, 1.098 mmol) and tetrahydrofuran (5 ml). After stirring for 5 min for complete dissolution, potassium hydroxide (0. 247 g, 4.4 mmol) in methanol (5 ml) was dropwise added and the solution became brown immediately. The solution was left at room temperature with stirring for 1 hr and the reaction completion was confirmed by thin layer chromatography. The solvent was evaporated at 32 ºC with reduced pressure and the crude compound was redissolved

in chloroform and purified by silica gel-based flash column chromatography (methylene chloride : hexanes = 1 : 1 v/v) to give M3 as a yellow powder (air unstable, 0.20 g, 98 %) ^{1}H-NMR (500 MHz, $CDCl_3$): δ/ppm 7.77 (s, 2H, aromatic), 3.70 (s, 2H, C≡C-H) HRMS (EI+ voltage): calculated m/z of [M+] 184.0095; measured m/z 184.0098.

Polymerization for PPE-B. Monomer M1 (40.8 mg, 69.1 μmol), monomer M2 (61.6 mg, 69.1 μmol), toluene (1.0 ml), and diisopropylamine (2 ml) were placed into a 50 ml Schlenck flask. After complete dissolution of the two monomers, the solution was degassed by three times of vacuum and argon purging. In a separate Schlenck flask, tetrakistriphenylphosphine palladium (0) (3 mol % of total monomers) and copper (I) iodide (3 mol % of total monomers) were transferred under a nitrogen atmosphere of a glove box and argon was purged in the Schlenck flask for 10 min. Two catalysts were dissolved in toluene (1.0 ml) and degassed by three times of vacuum and argon purging. The degassed solution containing catalyst was cannulated into the monomer solution. After transfer of the catalyst solution to monomer solution, three cycles of degassing to a polymer solution was finally done again. The polymer solution was allowed to stir under argon purging at 55 ºC for 48 hr. The reaction mixture was filtered through a 0.8 micrometer membrane syringe. The mixture solution was concentrated at reduced pressure and precipitated in diethylether (15 ml). The crude polymer was redissolved in 15 ml of dioxane and the solution was mixed with 10 % aqueous NaOH solution (15 ml). Solution was stirred under argon atmosphere at room temperature for 12 h. Polymer solution was centrifuged to remove insoluble impurity and dialyzed (Spectra/Por, Spectrum Laboratories, Inc., 12,000-14,000 MWCO) against deionized water for 2 days (10 x 4 L water exchanges). The polymer solution was lyophilized to yield a yellow solid

(51 mg, 60 %). ^{1}H-NMR (500 MHz, D_2O): δ/ppm 7.27 (s, 2H, aromatic), 7.15 (s, 2H, aromatic), 4.03 (broad m, 6H, -$CH_2C\underline{H}_2O$-, -$OC\underline{H}$-), 3.81-3.21 (broad m, 56H, -$OC\underline{H}_2C\underline{H}_2$), 3.18 (broad s, 12H, -$OC\underline{H}_3$), 2.25 (broad t, 4H, -$CH_2C\underline{H}_2COO$-), 1.87 (broad m, 4H, -$CH_2C\underline{H}_2CH_2$-), GPC (THF-based, it was measured before deprotection of an ethyl group) M_n= 73,100 $gmol^{-1}$, Mw= 214,200 $gmol^{-1}$, PDI = 2.93.

Polymerization for PBZ-2. To a 25 ml Schlenck flask with a stir bar were added M3 (68.5 mg, 0.372 mmol) and M4 (230.2 mg, 0.354 mmol). The flask was placed under argon atmosphere and 3.5 ml of dimethylformamide, 4 ml of deionized water, and 1 ml of diisopropylamine (DIPA) were added to the flask after degassing. To a separate flask were added tetrakis(triphenylphosphine)palladium, Pd(0) (17.2 mg, 11.5 μmol), and CuI (2.84 mg, 11.5 μmol) and the flask was also degassed. Pd(0) catalyst was successively added to the monomer mixture by cannular transfer and degassed by argon purging and vacuum recycles several times. The mixture was stirred at 55 ºC for 24 hr. 4-ethynylbenzoic acid (54.4 mg, 0.372 mmol), Pd catalyst (8.6 mg), CuI (1.4 mg), DIPA (0.5 ml) were added to the solution and further reacted at 55 ºC for additional 24 hr for the end-capping reaction. The cooled polymer solution was filtered, concentrated, precipitated in acetone (40 ml), and filtered again. The polymer was redissolved in water and precipitated again in acetone/ether/methanol (3:3:1, total 63 ml), filtered and dried. The polymer powder was dissolved in 1 M NaOH solution (50 ml) and, dialyzed (Spectra/Por, Spectrum Laboratories, Inc., 12,000-14,000 MWCO) against several changes of deionized water for 2 days. Lyophilization of the resulting red solution gave PBZ2 as a red fiber. Yield: 37 %, ^{1}H NMR (500MHz, D_2O) δ 8.2-7.2 (broad, aromatic C-

H), 4.2-3.3 (broad, aliphatic broad C-H), 2.90-2.50 (broad, aliphatic C-H). GPC (DMF-based) M_n = 49,500, PDI = 3.81.

Synthesis of tert-butyl 3,3'-(2,5-diiodo-1,4-phenylene)bis(oxy)bis(propane-3,1-diyl)dicarbamate (**S1**) To a solution of 2,5-diiodo-1,4-hydroquinone (0.5 g, 1.40 mmol) were added a potassium carbonate (0.77 g, 5.6 mmol), tert-butyl N-(3-bromopropyl)carbamate (1.00 g, 4,2 mmol, TCI America, Co.) and dimethylformamide (DMF, 10 ml) and reaction mixture was stirred at 50 ºC for 18 hr. After the reaction, reaction mixture was cooled down and filtered. DMF was removed with rotary evaporator at reduced pressure. Crude mixture was re-dissolved in chloroform and extracted twice with deionized water. After drying over $MgSO_4$ and filtering, chloroform was removed in vacuo. Further purification was done by column chromatography (ethyl acetate : hexane = 2 :5 v/v) and the product was precipitated in the presence of column eluent at -18 ºC to give white powder (yield: 0.4 g, 42 %). ^{1}H-NMR (500 MHz, $CDCl_3$): δ/ppm 7.19 (s, 2H, aromatic), 5.05 (broad s, 2H, -N<u>H</u>COO-), 4.02 (t, 4H, -OC<u>H</u>$_2$CH$_3$), 3.39 (t, 4H, -NC<u>H</u>$_2$-), 2.03 (m, 4H, --NCH$_2$C<u>H</u>$_2$-), 1.45 (s, 18H, -C(CH$_3$)$_3$). ^{13}C-NMR (500 MHz, $CDCl_3$) δ/ppm 156.04, 152.71, 122.55, 86.08, 79.13, 68.58, 38.34, 29.29, 28.45.

Preparation for PBZ-NBoc. To a 25 ml Schlenck flask with a stir bar was added **3** (35.5 mg, 0.108 mmol), **S1** (73.04 mg, 0.108 mmol). The flask was placed under argon atmosphere and 1 ml of toluene was added to the flask after degassing. To a separate flask was added tetrakis(triphenylphosphine)palladium, $Pd(PPh_3)_4$ (7.5 mg, 6.48 μmol), and CuI (0.82 mg, 4.32 μmol) and the flask was also degassed $Pd(PPh_3)_4$ catalyst was successively added to the monomer mixture by cannular transfer and degassed by argon

purging and vacuum recycles several times. At first, some insoluble parts exist, but the mixture became completely soluble and transparent at 70 ºC. The mixture was stirred at 75 ºC for 72 hr. As time went by, solution color became red shift (blue → green → yellow → yellow orange → red-orange). Polymer solution was precipitated in 20 ml of methanol, gravity-filtrated and rinsed with 10 ml of methanol, acetone, and hexane, respectively. Polymer was dried in vacuo to give PBZ-NBoc. Yield: 43 mg, ^{1}H NMR (500MHz, $CDCl_3$) δ 7.85 (broad s, 2H), 7.20 (broad s, 2H), 5.20 (broad s, 2H), 4.24 (s, 4H), 3.50 (broad m, 2H), 2.15 (broad s, 4H), 1.38 (broad s, 18H). ^{13}C-NMR (500 MHz, $CDCl_3$) δ/ppm 156.13, 154.32, 153.74, 132.59, 117.30, 116.99, 114.33, 99.99, 91.64, 79.16, 67.50, 38.09, 29.17, 28.47. M_n based on NMR-end analysis = 5,500.

Photophysical Analysis of CPEs. UV/Vis absorption spectra were recorded with a Varian Cary50 UV/Vis spectrophotometer in various solvents. Photoluminescence spectra and quantum yield were taken on a PTI QuantaMaster^{TM} spectrofluorometer, QM4 (Photon Technology International, Birmingham, NJ). Absolute quantum efficiencies of all polymers were obtained from an integrating sphere.

Polymer-Antibody Bioconjugation (PPE-B-CD3 and PBZ2-CD20). All reagents are immediately handled and used before bioconjugation. 1 mg of PBZ2 was dissolved in 100 μl MES buffer (0.1 M, pH=4.7). 200 mM (or 50 mM in PBZ2-CD20 case) of EDC (100 μl) and 200 mM (50 mM in PBZ2-CD20 case) of sulfo-NHS (100 μl) (Pierce Biotechnologies, Thermo-scientific, Inc) in MES buffer were prepared respectively. 10 μl (final concentration 18 mM) of EDC was directly added to 100 μl of PBZ2 solution, which was based on a 13 kDa PPE-B-CD3, results in a 30-fold molar excess of EDC to polymer. To the reaction mixture 25 μl of sulfo-NHS was also added to

the final concentration of 37 mM. Reaction components were mixed well and stirred for 15 minutes at room temperature for reaction. Activated PPE-B or PBZ2 was separated from excess EDC, EDC-byproducts, and sulfo-NHS using Zeba^{TM} Desalt Spin Columns (5 ml) and the medium buffer (final volume: 400 μl) was exchanged to phosphate-buffered saline (PBS, 0.1 M sodium phosphate, 0.15 M NaCl, pH 7.4). Purification of solution containing sulfo-NHS after the separation was fractionally confirmed by UV absorbance peak at 280 nm that was significantly decreased. Different amount of activated polymer solution (67 μl, 33 μl, 7 μl, and 3 μl) was added to 100 μl (1 mg/ml) of an antibody, respectively (final volume of each sample: 500 μl). The solution was mixed well and then reaction was allowed to proceed for 2 hr at room temperature. Reaction was quenched by adding base to raise the pH above 8 to promote autohydrolysis of the NHS esters, thereby regenerating the original carboxylic groups. Medium was finally exchanged to cell buffer (PBS, pH=7.0, HyQ^{TM}, HyClone, UT) and used for cell staining immediately (final concentration: 3.3 μM based on a 150 kDa antibody). The synthesis of CPE-antibody conjugates was verified by reducing 10.0 % Tris-HCl SDS PAGE (stacking gel pH=6.8, separating gel pH=8.8) at denaturating conditions after boiling in the SDS loading buffer for 5 min and stained with coomassie blue dye. Images were obtained from Fotodyne Foto/convertible Dual transilluminator with Foto/Analyst software with coomassie blue filter. Images were obtained from Fotodyne Foto/convertible Dual transilluminator with Foto/Analyst software with coomassie blue filter. Dot intensity from an image was measured by ImageJ software provided by National Institutes of Health (NIH) and the mean intensity value of a certain area was calculated.

Cell Culture. Human B cell lymphoma (SUDHL-4) and human T cell leukemia (Jurkat) cell line were cultured in 75 cm^2 flasks at 37 ºC in a humidified atmosphere with 5 % CO_2. The medium contained 10 % fetal bovine serum (FBS, 50mls heat deactivated) in RPMI-1640 supplemented with a proprietary brand of Glutamine called Glutamax^{TM}-I Supplement (Invitrogen^{TM}, 5 ml of this stuff dissolved in 500 ml of RPMI - 10%) and antibiotic-antimycotic mix for antibiotics (InvitrogenTM, 100x, liquid). It contains 10,000 units of penicillin (base), 10,000 μg of streptomycin (base), and 25 μg of amphotericin B/ml utilizing penicillin G (sodium salt), streptomycin sulfate, and amphotericin B as Fungizone® Antimycotic in 0.85% saline. Before use, 5ml of this stuff was diluted in 500ml of RPMI 1640 with 10% FBS. The medium was changed every third day and cell viability was checked every day.

Cytotoxicity and Proliferation Assay of Cell against the CPEs. Cell viability and proliferation of cells against the conjugated polyelectrolytes were evaluated in different concentrations. All cells were cultured in 75 cm^2 flasks briefly 96 hr prior to the cytotoxicity test and confirmed 99 % viability of cells before use. Arbitrary concentrations (mM to nM range) of PPE-B solutions were prepared to find a kill curve. 2000 μl of RPMI buffer with 2×10^5 cells were replated on each well of a 24 well-plate (the plate in triplicate, which means 3 wells of cells for each concentration to try and control for any error) and 20 μl of a various concentrations of polymer solutions to this cell mixture was added. Also, additional control was also prepared by adding same amount of water to cells as a diluent without the polymer solution. Cytotoxicity was evaluated every 24 hr using a hemacytometer as a cell-counting method after dead cells were stained with trypan blue dye.

Fluorescence Microscopy and Confocal Microscopy. Fluorescence images were acquired by Olympus BX41 fluorescence microscope (Optical Analysis corporation, Nashua, NH 03063) equipped with metal halide lamp, various optical filters (approximate excitation/emission in nm = 400/420, 420/475, 470/500 or 560/620 with narrow or wideband emission) DP71 digital camera, and Microsuite5 biological suite software. For actual comparison of the intensity of CPE-antibody conjugates with FITC-labeled antibody, the microscope was used with the same setup condition. The amount of antibody adsorbed on cell surfaces was quantified by fluorescence intensity measurements. Confocal Images were obtained from a Leica TCS SP2 confocal microscope operating with a 63× oil immersion objective (numerical aperture 1.4).

Cell Imaging with CPE-Antibody Conjugate 100 μl of each cell suspension (ca. 1 million cells /each tube) was prepared in PBS (pH=7) and 10 μl of polymer-antibody conjugates (final concentration: 0.3 μM, based on 150kDa antibody) prepared were incubated to suspension cell at room temperature for 30 min. Unbound antibody was removed by spin-down of cell (HyQ^{TM} PB, RCF, 400 × g, 7 min) for three recycling times. Cells were resuspended in 50 μl of PBS (Hyclone, UT) and 10 μl cells suspension stained was diluted with PBS (1 to 10 times) and placed on a glass slide and a cover slip was mounted on the slide. Labeled cells were immediately visualized by fluorescence microscope or preserved in refrigerator (4 ºC) until 48 hr after fixation with formaldehyde (final concentration: 4 %).

Selectivity Test of CPE-Antibody Conjugates Dilution test to check a selectivity of polymer-antibody conjugates was also done in a same manner with cell staining test. 20 μl of PPE-B-CD3 and PBZ2-CD20 conjugates were incubated to one

millions of cells (100 μl) for 30 minute respectively and images were obtained from fluorescence microscope in same setup condition. Same concentration of Jukat and B cell were prepared and they were mixed in different ratios (100:0, 90:10, 80:20, 70:30, 60:40, 50:50, 40:60, 30:70, 20:80, 10:90, 0:100 in Jurkat : SUDHL-4 v/v) and PPE-B-CD3 and PBZ2-CD20 conjugates were incubated in each of cell mixture. After the unbound polymer-antibody conjugates were isolated, images were obtained from fluorescence microscope with two different optical filters having emission wavelength at 475 and 620 nm respectively.

5.4. Results and Discussion

For M1 synthesis for PPE-B copolymer, 2,5-diiodohydroquinone starts by reacting 1,4-dimethoxybenzene with iodine through the acid based electrophillic aromatic iodination in 85 % yield as previously reported in the literature (Scheme 5-1).[25] Demethylation reaction was achieved by means of BBr_3. The resulting 2,5-diiodohydroquinone was then reacted with ethyl 4-bromobutyrate by Williamson-ether synthesis to give ethyl-protected carboxylic group functionalized M1. In M3 synthesis for PBZ2, benzothiadiazole compound was reacted with bromine, followed by trimethylsilylacetylene and a subsequent deprotection reaction in base to give monomer 3 (M3). M3 was turned out to be very unstable so that it was immediately used for polymerization upon preparation. The copolymerization of M1 and M2 for PPE-B was carried out using conventional palladium-catalyzed Sonogashira-Hagihara copolymerization method (Scheme 5-2). We recently developed several different types of PPEs containing a carboxylic group that are more soluble in water and have improved

emissive properties compared with previously reported PPEs to investigate correlation between chemical structure and photophysical properties systematically (K. Lee, T. Yucel, H.-J. Kim, D. Pochan & J. Kim, unpublished data). It has been found out that a bulky bifurcated ethylene oxide group in polymer provides an excellent solubility in water.[24] A conjugated polymer should be water-soluble and have appropriate functional group for conjugation with biological moiety to be a good sensory reporter because any biological target must be handled in aqueous environment. Sometimes, a reagent dissolves in polar solvent like dimethyl sulfoxide or methanol and makes dilution in an aqueous buffer, however, it can also have detrimental effect on biological system due to their toxicity. Our conjugated polyelectrolyte, PPE-B prepared as dried state showed an excellent water solubility exceeding 10 mg/mL in deionized water.

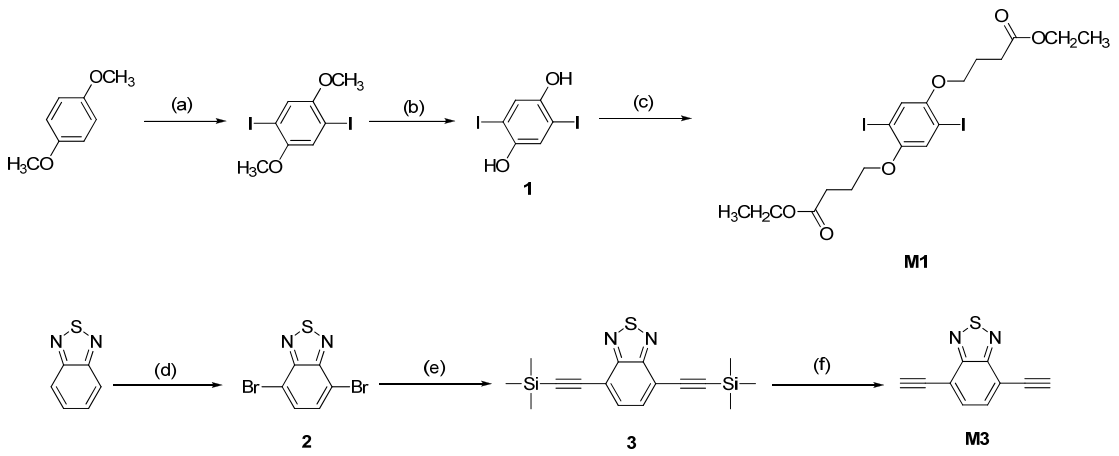

Scheme 5-1. Monomer synthesis (a) I_2, H_2SO_4, acetic acid, water, 100 ºC (b) BBr_3, dichloromethane, -60 ºC → r. t., 48 hr (c) K_2CO_3, ethyl 4-bromobutyrate, dimethylformamide (DMF), 80 ºC, 48 hr (d) Bromine, hydrobromic acid, 100 ºC overnight (e) trimethylacetylene, Pd3(PPh3)4, CuI, triethylamine, toluene. 65 ºC, 7 hr. (f) potassium hydroxide, methanol:tetrahydrofuran (1:1 v/v), room temperature, 1 hr.

Copolymerization of M3 and M4 for the red emissive PBZ1 was also conducted using Pd-catalyzed method. Our original design for red-emission polymers includes a large portion of a bulky ethylene oxide group and a carboxylic group as a side chain in the chemical structure like PPE-B structure to give a good water-solubility. However, our systematic investigation about the correlation between the emission color of PBZ derivatives (PPE-BT_x) and the portion of benzothiadiazole unit in the polymer structure revealed that the polymer must compose of more than 50 % of the benzothiadiazole unit to have pure red emission (Figure 5-2 and 5-3). However, in this case of having 50 % of benzothiadiazole units in the polymer structure a reduced solubility in water was observed due to the decreased amount of charged carboxylic group to incorporate the benzothiadiazole unit. The water-solubility of the copolymers was very good only when the charged pendent group exists in every other repeating unit. Unfortunately, however, the bioconjugation of the CPE with an antibody induced polymer aggregation in water due to the consumption of the carboxylic group. Therefore, we redesigned a red-emissive CPE to have alternating benzothiadiazole unit and non-reactive sulfonic acid unit as a charged group. The reactive carboxylic acid group was introduced at the two ends of the CPE for bioconjugation with an antibody. The *in-situ* end-modification of PBZ1 with 4-ethynylbenzoic acid and additional palladium catalyst provide end-carboxylic group functionalized CPE, PBZ2. It was fairly water-soluble (> 3 mg/ml in deionized water) and bright red-emissive.

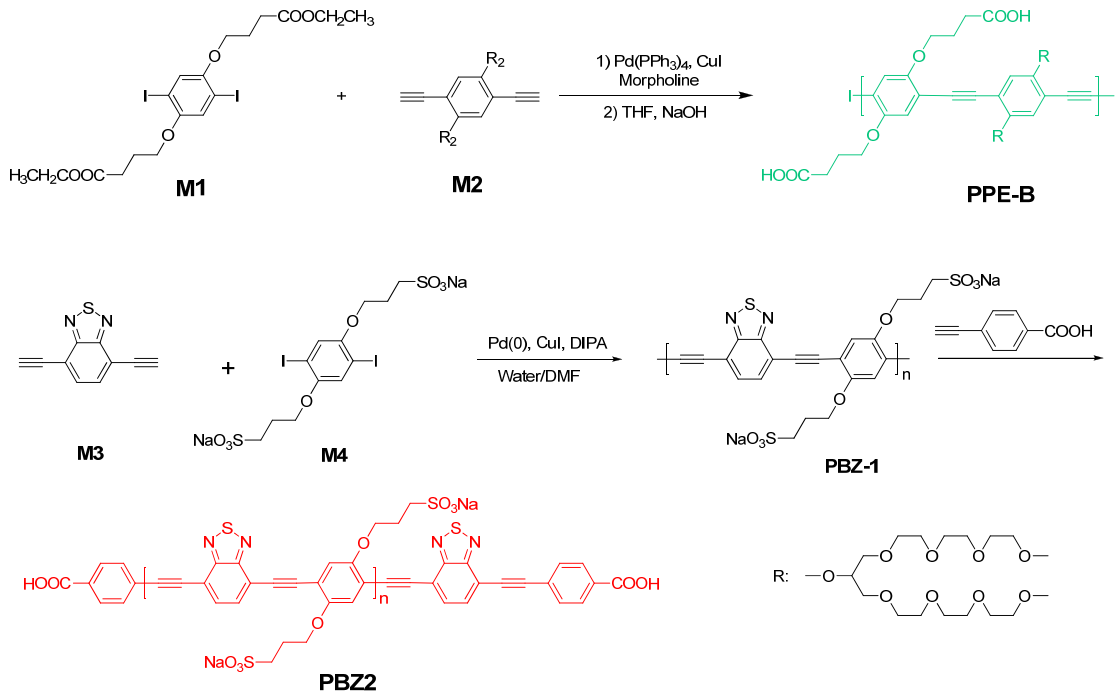

Scheme 5-2. Synthesis of the CPEs (PPE-B and PBZ2).

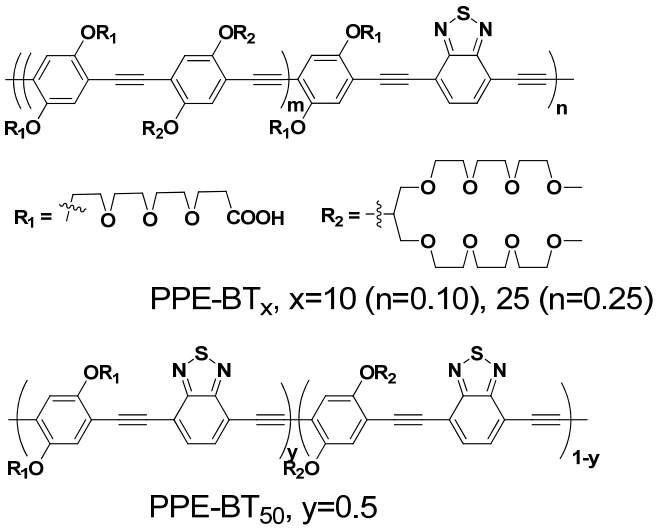

Figure 5-2. Chemical structure of PPE derivatives containing benzothiadiazole unit.

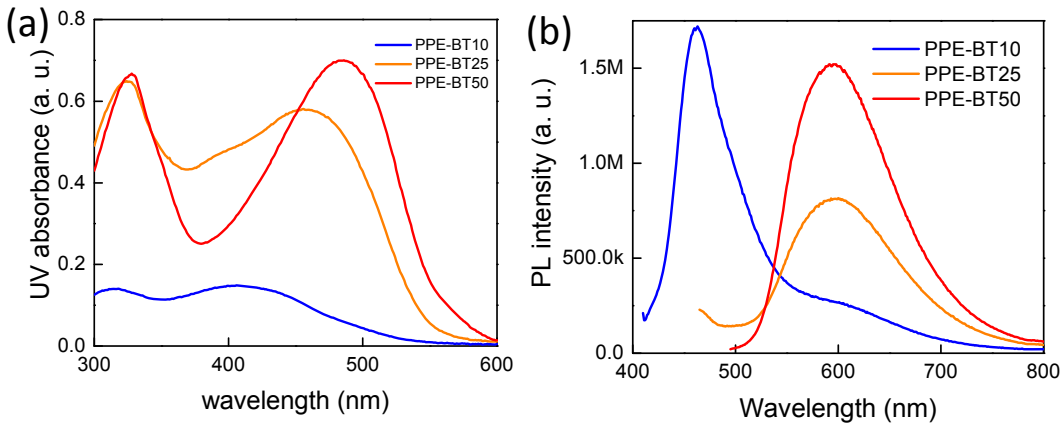

Figure 5-3. (a) UV absorption and (b) photoluminescence spectra of PPE-BT_x.

Figure 5-4, which was obtained in deionized water, shows the absorption and emission spectra of PPE-B and PBZ2. PPE-B and PBZ2 showed blue-green and red emission at 460 nm and red emission at 630 nm respectively. Absolute quantum yield of PPE-B in water measured by using an integrating sphere was the range of 0.38 – 0.57 depending on the concentration (10^{-4} – 10^{-7} M). On the other hand, PBZ2 showed a broad emission spectrum with a suppress 0-0 band and a long tail, implying some aggregation in water. An organic-soluble and highly emissive poly(benzothiadiazole) derivative (PBZ-NBoc, Scheme 5-3 and Figure 5-5 for its UV/PL spectra) showed a well-defined 0-0 emission band at 560 nm in non-polar solvent such as chloroform and tetrahydrofuran. However, in a polar solvent like DMF, PBZ-NBoc showed an emission shift to 590 nm due to the suppress 0-0 band at 560 nm. It is a characteristic typical of excimer/aggregation-like emission induced by polymer aggregation.[28-30] The quantum yield of PBZ2 (0.15 μM) was 1.1±0.6 % in water. We are currently investigating the effect of benzothiadiazole on the aggregation of CPE in water.

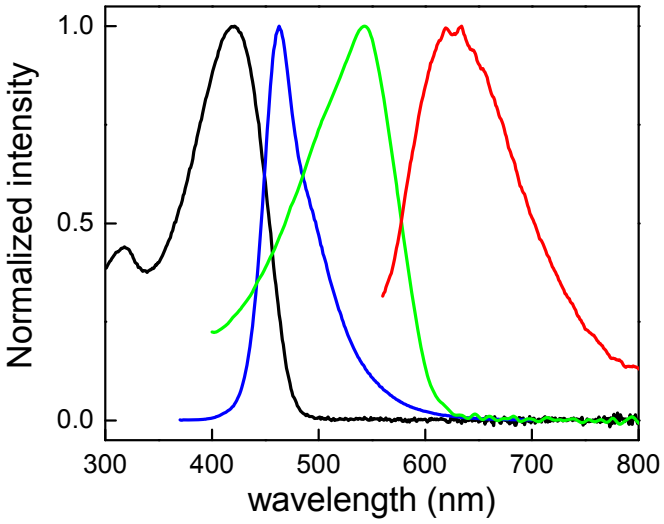

Figure 5-4. UV absorption and photoluminescence spectra of PPE-B (UV:black/PL:blue) and PBZ2 (UV:green/PL: red). PPE-B (100 nM) and PBZ (150 nM) in deionized water was excited at 365 nm and 540 nm, respectively.

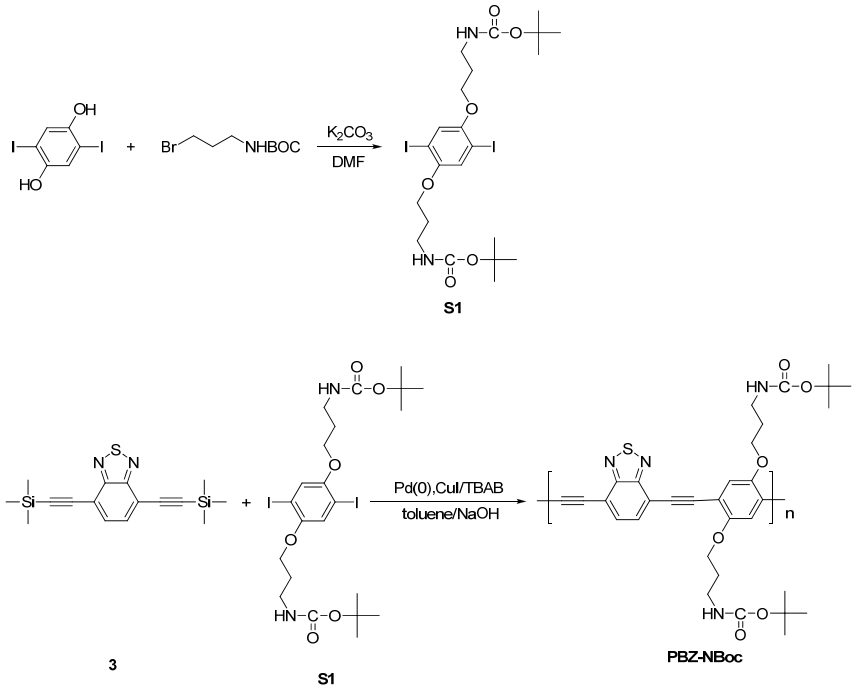

Scheme 5-3. Synthetic route of PBZ-NBoc.

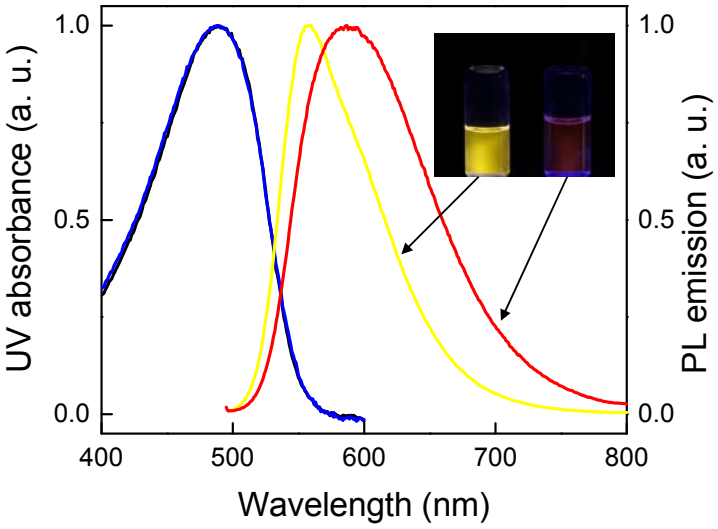

Figure 5-5. UV/PL spectra of PBZ-NBoc in chloroform (black/yellow) and DMF (blue/red) at 2 mg/L. Its quantum yields in chloroform and DMF are 92 % and 15 % respectively.

Labeling of proteins with a chromophore/fluorophore is a universal method in colorimetric assays and immunofluorescence. However, if many chromophores/fluorephores are attached to an antibody or enzyme such labeling can affect the function of the antibody and the enzyme. The molar mass of CPE is much larger than that of small chromophores and fluorephores. Therefore, by putting the same number of CPE instead of small molecular chromophores and fluorephores a much brighter CPE-antibody can be prepared and can achieve much more sensitive assays. With this in mind, we employed a covalent conjugation strategy in which carboxylic groups of the CPE is conjugated to lysine side chains of an antibody via an amide linkage. Using commercially available reagents (EDC and sulfo-NHS), a succinimide functionality was introduced to the carboxylated CPE via carbodiimide chemistry to facilitate the amide bond formation with amine groups of an antibody. We prepared CPE-

antibody conjugates having different number of CPE per antibody by controlling the stoichiometric amount of CPE per antibody during the bioconjugation reaction. The resulting CPE-antibody conjugates were verified by SDS-PAGE electrophoresis. The SDS-PAGE gel of PPE-B-CD3 conjugates is shown in Figure 5-6. We used the heat-induced denaturation proceeding gel electrophoresis (100 ºC) to consider only covalently bound CPE-antibody by minimizing the possible non-specific binding of CPE to the antibody. On the lane A only pure CD3 was run. There are two bands are shown in the lane A. One is corresponding to the heavy chain (60 KDa) of CD3 and the other is the F_{ab} light chain (23 KDa) of CD3, an IgG2-type antibody. On the lanes B through E we ran the resulting PPE-B-CD3 conjugates prepared with different amount of PPE-B per CD3 as indicated in the figure caption. After the conjugation with 5 times excess PPE-B (lane B), the heavy chain band at 60 KDa disappeared and instead a new band over 180 KDa appeared. Considering that the number average molecular weight of PPE-B is 73,100 the location of the PPE-B-CD3 conjugated in the gel is reasonable. The broad feature and the long tailing of the PPE-B-CD3 bands are likely due to the combination of the polydispersity of PPE-B and the distribution of the number of bound PPE-B per CD3. As the amount of PPE-B added to the bioconjugation increased from the lane C to E, the band of PPE-B-CD3 conjugate gradually moved to a higher molecular region. This result also confirms that PPE-B is predominantly conjugated to the heavy chain.

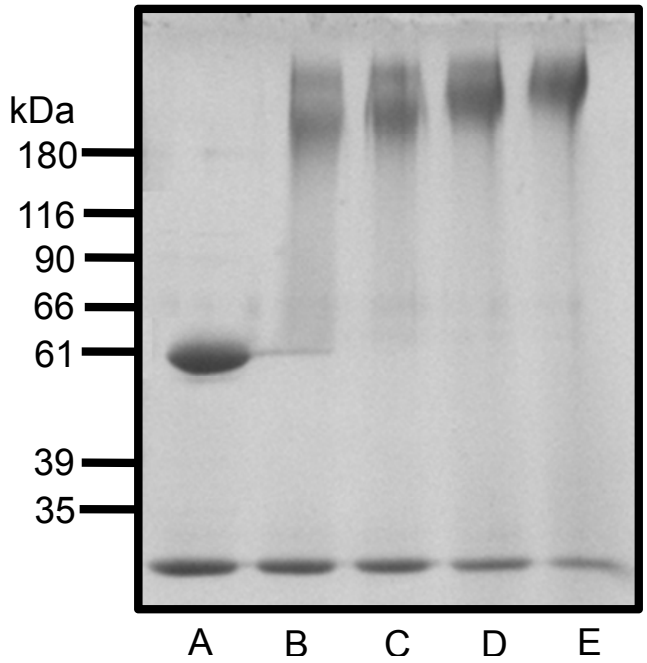

Figure 5-6. Coomassie Blue-stained 10% SDS-PAGE analysis of CD3 and PPE-B-CD3 conjugates having varying stoichiometric amount of PPE-B per antibody. Lane A: only CD3, no polymer, lane B-D corresponds to 5:1, 10:1, 50:1, 100:1 (PPE-B:CD3), respectively. Bands located at the bottom of the gel are corresponding to the F_{ab} light chain of 23 KDa.

We studied the selectivity of the CPE-antibody conjugates to see whether the CPE tethering to the antibodies affects the specificity of the antibodies. Immunofluorescence microscope images shown in Figure 5-7 clearly demonstrate that PPE-B-CD3 conjugates stained the Jurkat cells whereas SUDHL-4 (B cell) was not stained by the conjugates (Figure 5-7 a and b). The bright spots in Figure 5-7-a show that mainly the cell surface is stained with PPE-B-CD3 as expected. The few blue emissive dots in the fluorescence image of Figure 5-7-b are likely due to non-specifically bound PPE-B aggregates on the substrate that were not removed somehow through the purification step after the bioconjugation. The base of this postulation is the fact that in the DIC image there is no

cell at the locations where the blue dots are observed in the fluorescence image. Similarly, SUDHL-4 was selectively stained by PBZ2-CD20 but SUDHL-1 (T-cell) was not stained by the conjugate (Figure 5-7 c and d). These results imply that the CPE tethering to the antibodies does not affect the specificity of the antibodies. We also examined Jurkat cells after cell fixation with 4 wt% formaldehyde followed by incubation with the CPE–antibody conjugates. Interestingly, in this case we observed that not just the cell surface but the whole cell was stained. (Figure 5-8). It is likely that the cell membrane was disrupted during the cell fixation steps.

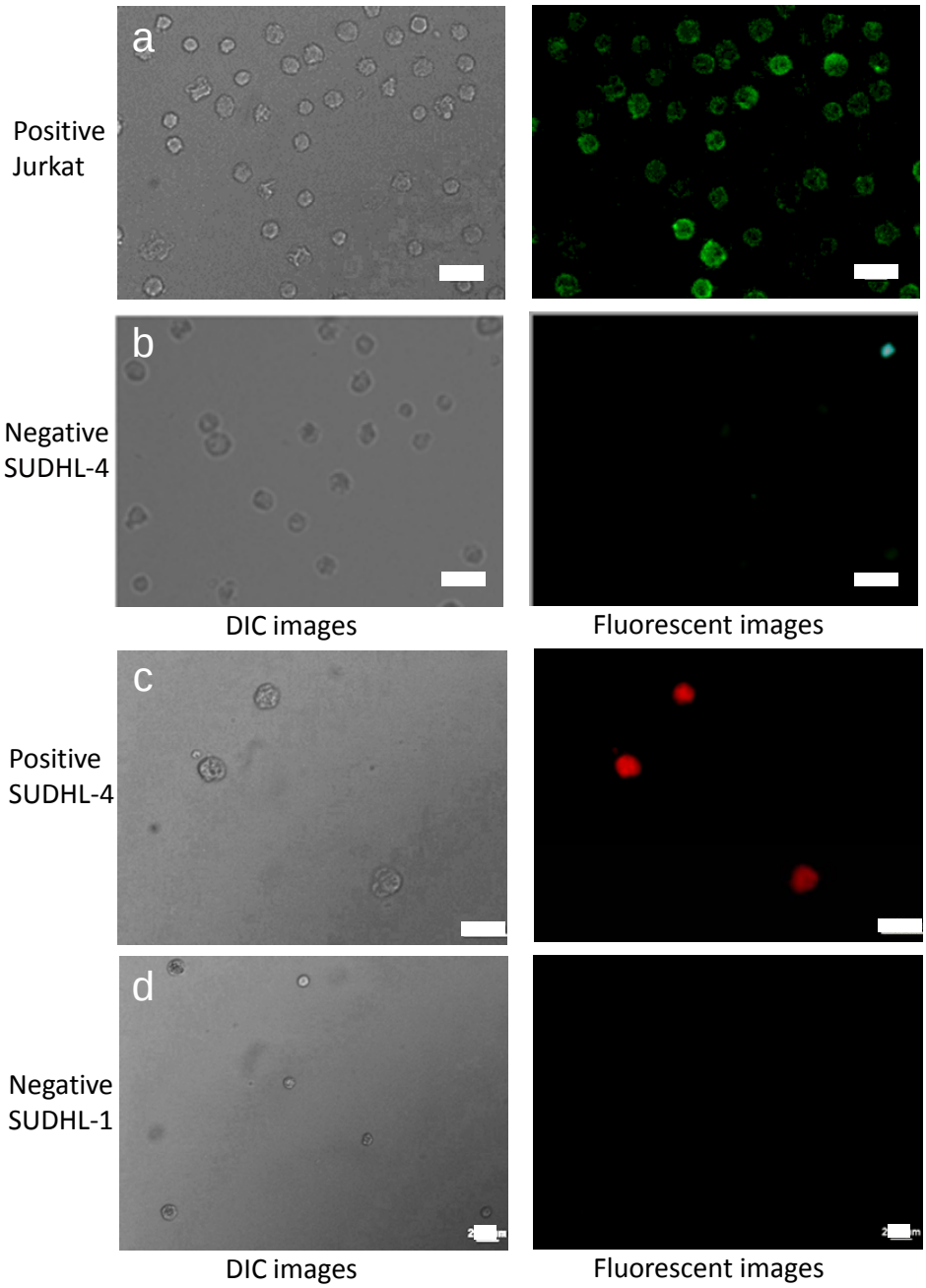

Figure 5-7. Fluorescence microscope images of live cells after the incubation with PPE-B-CD3 (a: Jurkat and b: B-cell) and PBZ2-CD20 (c: B-cell and d: T-cell) for 30 min. Differential interference contrast (DIC) images are shown in the left column and fluorescence images are in the right column. The images in the a and b low were obtained upon excitation at 470 nm and the images in the lows c and d were from 560 nm excitation. Scale bar: 20 μm.

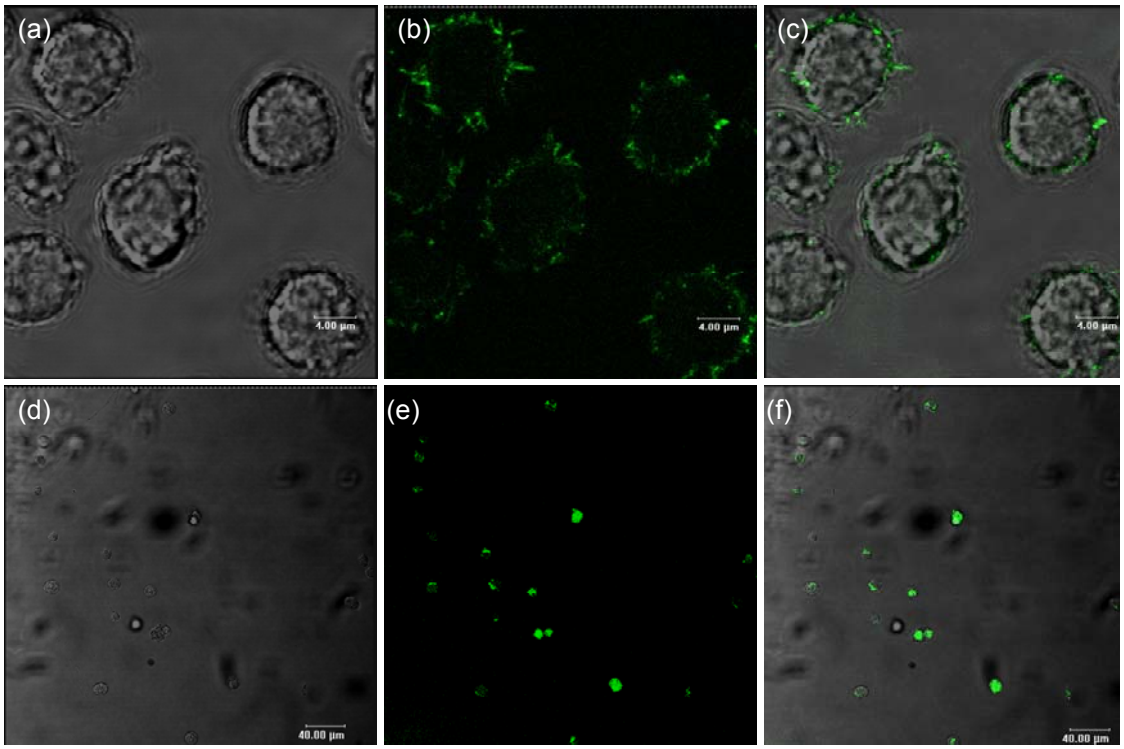

Figure 5-8. Confocal images of Jurkats stained with PPE-B-CD3. The cells were stained before fixation (a, b, c) and after fixation (d,e,f) with 3 % formaldehyde.

Having established that PPE-B-CD3 and PBZ2-CD20 can effectively target and stain the membranes of Jurkat and B-cell respectively, we then investigated the cross-selectivity of the CPE-antibody conjugates in the presence of both cells. Equal amount of Jurkat and SUDHL were mixed together as suspension in buffer and PPE-B-CD3 and PBZ2-CD20 conjugates were then added to the cell suspension. As shown in Figures 5-9 a and 5-9 b, only Jurkats were selectively stained with PPE-B-CD3 conjugates and B cells were stained with exclusively PBZ2-CD20. The fluorescence image in Figure 5-9 c clearly demonstrated that our CPE-antibody conjugates have excellent cross-selectivity and are suitable for immunofluorescence techniques. We also did the dilution tests to find if our CPE-antibody conjugates can be applicable to quantitative cell counting and cell

sorting. Mixed cells of SUDHL-4 and Jurkat having different mixing ratios were stained with the CPE-antibody conjugates. The ratio, the number of stained SUBHL-4/total number of stained cells, was plotted against the cell mixing ratio. The number of stained cells was counted from fluorescence microscope images in Figure 5-10. The linear correlation curve shown in Figure 5-10 implies that CPE-antibody conjugates are suitable for cell quantification applications such as fluorescence-activated cell sorting (FACS).

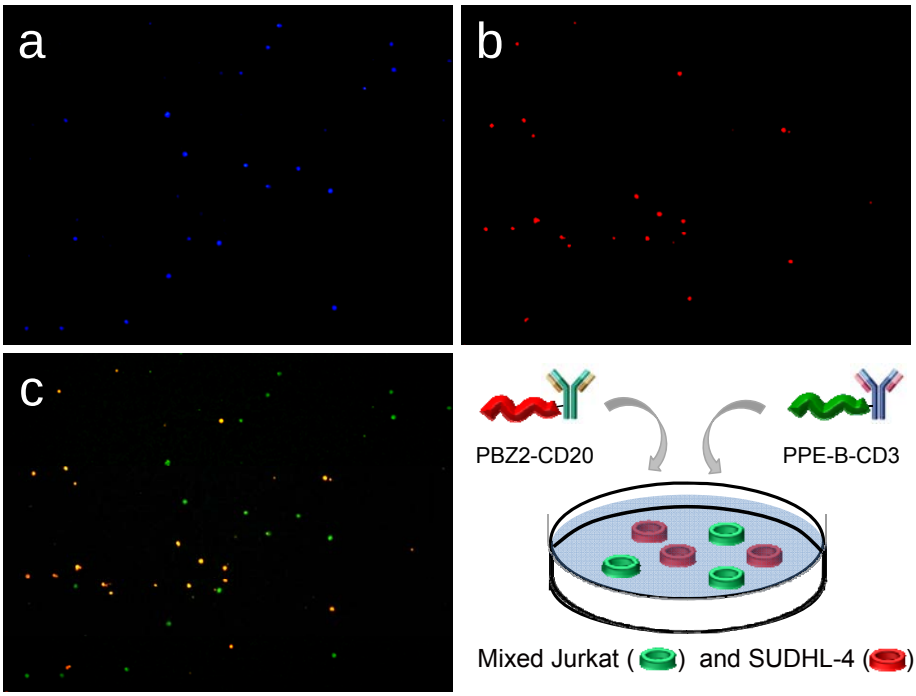

Figure 5-9. Fluorescence microscope images of the mixed Jurkat and SUDHL-4 after incubation with PPE-B-CD3 (1.0 μM) and PBZ2-CD20 (1.0 μM) together. Panel a shows blue emission (excitation: 395-415 nm, emission: 435-485 nm) of PPE-B-CD3-stained Jurkat. Panel b shows PBZ2-CD20-stained SUDHL-4 having red emission (excitation: 540-580 nm, emission: 590-650 nm). The panel c image shows both Jurkat and SUDHL-4 having difference emission color. The image was obtained by using a wideband emission filter (> 500 nm), exposure of wide excitation filter (450-490 nm), and an external incandescent light.

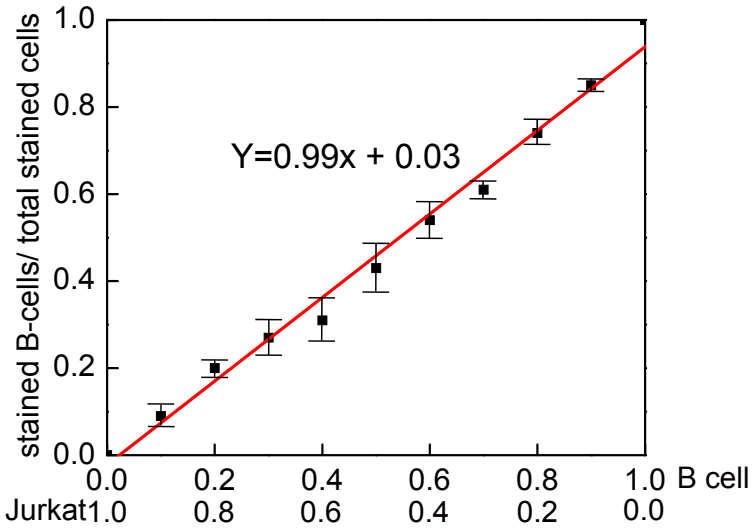

Figure 5-10. The correlation between the ratio (the number of stained SUBHL-4/total number of stained cells) and the cell mixing ratio.

The cytotoxicity of the CPEs to SUDHL-4 and Jurkat was investigated with various concentrations of PPE-B (nM – μM). We incubated living cells, Jurkat and SUDHL-4, in RPMI1640 cell media together with PPE-B for 72 hr and analyzed the viability and proliferation of the cells. As a control, the same cells were also incubated in the same conditions without adding PPE-B. Surprisingly, we did not observe any dead cell even from the batches incubated with 1×10^{-6} M PPE-B, the highest concentration. This means that the cells have more than 99 % viability even in micromolar concentration regime. At a concentration of 1×10^{-6} M of PPE-B, the proliferation of SUDHL-4 and Jurkat slightly decreased to 86 % and 80 % compared with the control cells after 72 hr of incubation (Figure 5-11 a and b). Total number of SUDHL-4 and Jurkat cells after incubation for 72 hr increased by 10 and 15 times of the number of the initial cells, respectively (Figure 5-11 c). Interestingly, the cell doubling time of both SUDHL-4 and Jurkat when incubated

with 1×10^{-6} M PPE-B was shorter than that reported previously (SUDHL: ~ 40 hr, Jurkat: 25-35 hr), implying that the metabolic activity of the cells in the condition we used is enhanced. Fluorescence microscopy was also applied after incubating SUDHL-4 with PPE-B to examine whether there is non-specific binding between them. As shown in Figure 5-11d, we did not observe any PPE-B emission from SUDHL-4 after incubation with PPE-B and subsequent washing, suggesting that there is a negligible non-specific binding between PPE-B and the cells. While positively charged molecules such as cationic toxins like antimicrobial peptides sometimes show penetration through the cell membranes, cell membranes are impermeable to negatively charged PPEs to due negligible electrostatic attractions between the PPEs and cell membranes.

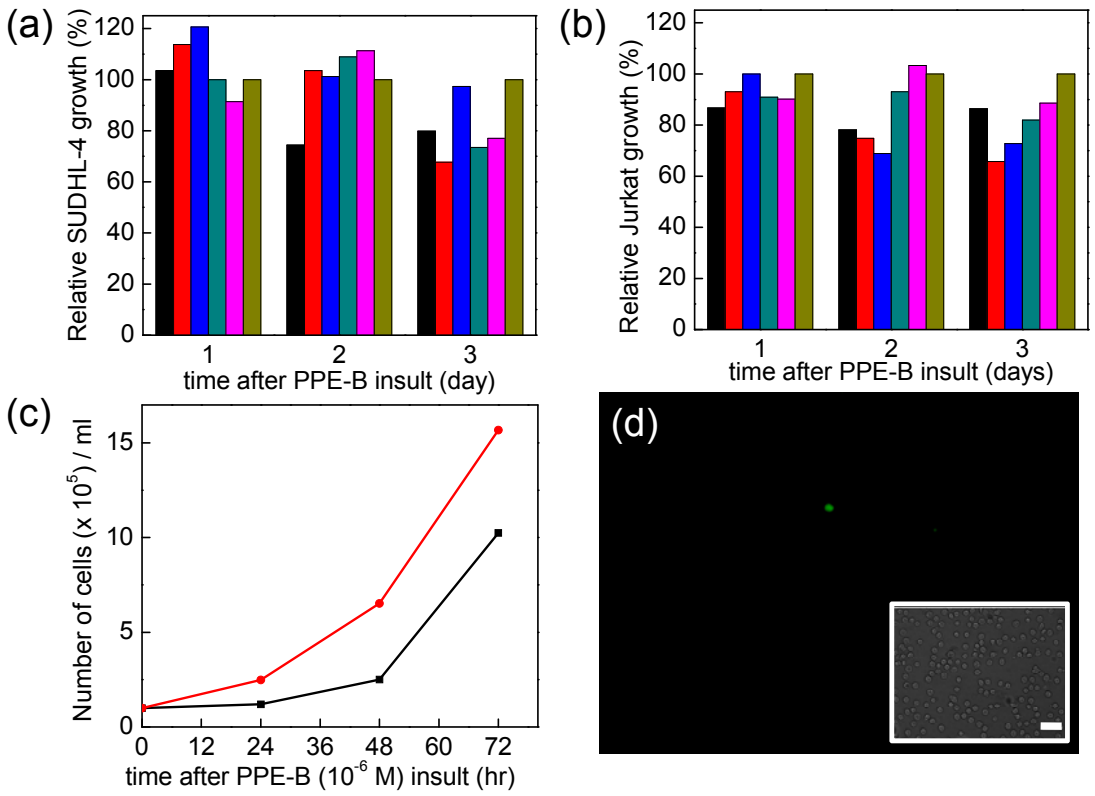

Figure 5-11. Cell viability and proliferation of (a) SUDHL-4 and (b) Jurkat incubated with different concentrations of PPE-B for 3 days. The concentration of PPE-B in the media was varied from 0.05 to 500 μg/mL (in μg/mL, 500: Black, 50: red, 5: blue, 0.5: turquoise, 0.05: pink, 0: khaki (positive control)). Trypan blue reagents were added to small aliquot of sample, and the number of dead cells and live cells were counted by a hemacytometer in every 24 hrs after the incubation with PPE-B. Relative cell growth (%) was calculated as (the number of live cells) / (the number of live cell in control) × 100. (c) A cell proliferation curve of SUDHL-4 (black) and Jurkat (red) upon incubation with the highest concentration of PPE-B (500 μg/mL). (d) A fluorescence microscope image of SUDHL-4 after 1 hr from the incubation with PPE-B. 100 μl of SUDHL-4 cell media (1 millions cells) was incubated with10 μl of 3 μM PPE-B. The image was obtained after unbound PPE-B was washed off by spinning with fresh cell media (500 × g, 6 min) several times. (Inset) An optical image corresponding to the fluorescence image.

5.5. Conclusion

We have demonstrated that rationally designed conjugated polyelectrolytes can be covalently attached directly to an antibody as a fluorescent reporter molecule without affecting the recognition specificity of the antibody. Two fluorescent and water-soluble CPEs having blue (PPE-B) and red (PBZ2) emission, respectively, were synthesized and bioconjugated with CD3 and CD20, respectively to form CPE-antibody conjugates. PPE-B-CD3 showed excellent specificity toward T-cells (Jurkat) and PBZ2-CD20 selectively bound to B-cells (SUDHL-4). Due to the energy harvesting property and a high extinction coefficient of CPEs, the developed CPE-antibody conjugates showed much higher sensitivity in the live cell imaging and visualization compared with a conventional FITC-labeled antibody. The cross-selectivity tests and the dilution tests confirmed that the developed CPE-antibody conjugates have excellent cross-selectivity and also suitable for quantitative cell counting and cell sorting such as fluorescence-activated cell sorting (FACS). Cell viability and proliferation study confirmed that the CPEs are not cytotoxic therefore, Jurkat and SUDHL-4 showed normal growth and proliferation when they were incubated with CPEs solution. The results demonstrate that as an fluorescent reporting molecule the biocompatible, water-soluble, and emissive CPEs are potentially superior to small molecular dyes and cytotoxic heavy-atom based quantum-dots. The developed CPEs and the convenient direct bioconjugation method are readily applicable to any other biological molecules.

5.6. References

1. Massoud, T. F.; Gambhir, S. S. *Genes Dev*. **2003**, *17*, 545.

2. Blasberg, R. G.; Tjuvajev, J. G. *J. Clin. Investig*. **2003**, *111*, 1620.

3. Weissleder, R.; Ntziachristos, V. *Nature Med*. **2003**, *9*, 123.

4. Wagenaar, D. J.; Weissleder, R.; Hengerer, A. *Acad. Radiol*. **2001**, *8*, 409.

5. Chan, W. C. W.; Maxwell, D. J.; Gao, X.; Bailey, R. E.; Han, M.; Nie, S. *Curr. Opin. Biotechnol*. **2002**, *13*, 40.

6. Chan, W. C. W.; Nie, S. *Science* **1998**, *281*, 2016.

7. Bruchez, M., Jr.; Moronne, M.; Gin, P.; Weiss, S.; Alivisatos, A. P. *Science* **1998**, *281*, 2013.

8. Mattoussi, H.; Mauro, J. M.; Goldman, E. R.; Anderson, G. P. Sundar, V. C.; Mikulec, F. V.; Bawendi, M. G. *J. Am. Chem. Soc*. **2000**, *122*, 12142.

9. Akerman, M. E.; Chan, W. C. W.; Laakkonen, P.; Bhatia, S. N.; Ruoslahti, E. *Proc. Natl. Acad. Sci*. **2002**, *99*, 12617.

10. Jaiswal, J. K.; Mattoussi, H.; Mauro, J. M.; Simon, S. M. *Nat. Biotechnol*. **2003**, *21*, 47.

11. Larson, D. R.; Zipfel, W. R.; Williams, R. M.; Clark, S. W.; Bruchez, M. P.; Wise, F. W.; Webb, W. W. *Science* **2003**, *300*, 1434.

12. Wu, X.; Liu, H.; Liu, J.; Haley, K. N.; Treadway, J. A.; Larson, J. P.; Ge, N.; Peale, F.; Bruchez, M. P. *Nat. Biotechnol*. **2003**, *21*, 41.

13. Dubertret, B.; Skourides, P.; Norris, D. J.; Noireaux, V.; Brivanlou, A. H.; Libchaber, A. *Science* **2002**, *29*, 1759.

14. Han, M.; Gao, X.; Su, J. Z.; Nie, S. *Nat. Biotechnol*. **2001**, *19*, 631.

15. Green M. *Angew. Chem. Int. Ed*. **2004**, *43*, 4129.

16. Gao, X.; Cui, Y.; Levenson, R. M.; Chung, L. W. K.; Nie, S. *Nat. Biotechnol*. **2004**, *22*, 969.

17. Kim, S.; Lim, Y. T.; Soltesz, E. G.; De Grand, A. M.; Lee, J.; Nakayama, A.; Parker, J. A.; Mihaljevic, T.; Laurence, R. G.; Dor, D. M.; Cohn, D. H.; Bawende, M. G.; Frangioni, J. V. *Nat. Biotechnol*. **2004**, *22*, 93.

18. Kim, I.-B.; Shin, H.; Garcia, A. J.; Bunz, U. H. F. *Bioconjugate Chem*. **2007**, *18*, 815.

19. Derfus, A. M.; Chan, W. C. W.; Bhatia, S. N. *Nano. Lett*. **2004**, *4*, 11.

20. Michalet, X.; Pinaud, F. F.; Bentolila, L. A.; Tsay, J. M.; Doose, S.; Li, J. J.; Sundaresan, G.; Wu, A. M.; Gambhir, S. S.; Weiss, S. *Science* **2005**, *307*, 538.

21. Pathak, S.; Choi, S.-K.; Arnheim, N.; Thompson, M. E. *J. Am. Chem. Soc*. **2001**, *123*, 4103.

22. Dahan, M.; Laurence, T.; Pinaud, F.; Chemla, D. S.; Alivisatos, A. P.; Sauer, M.; Weiss, S. *Opt. Lett*. **2001**, *26*, 825.

23. Thomas, S. W. III; Joly, G. D.; Swager, T. M. *Chem. Rev*. **2007**, *107*, 1339 and all references therein.

24. Lee, K.; Cho, J. C.; Deheck, J.; Kim, J. *Chem. Commun*. **2006**, 1983.

25. Lee, K.; Povlich, L. K.; Kim, J. *Adv. Funct. Mater*. **2007**, *17*, 2580.

26. Swager, T. M. *Acc. Chem. Res*. **1998**, *31*, 201.

27. DaSilveira Neto, B. A.; Sant'Ana Lopes, A.; Ebeling, G.; Gonçalves, R. S.; Gosta, V. E. U.; Quina, F. H.; Dupont, J. *Tetrahedron* **2005**, *61*, 10975.

28. Jenekhe, S. A. *Adv. Mater*. **1995**, *7*, 309.

29. Kim, J.; Swager, T. M. *Nature* **2001**, *411*, 1030.

30. Kim, J. Levitsky, I. A.; McQuade, T.; Swager, T. M. *J. Am. Chem. Soc*. **2002**, *124*, 7710.

31. Parker, B. W.; Kaur, G.; Nieves-Neira, W.; Taimi, M.; Kohlhagen, G.; Shimizu, T.; Losiewicz, M. D.; Pommier, Y.; Sausville, E. A.; Senderowicz, A. M. *Blood*, **1998**, *91*, 458.

CHAPTER 6

Chemically and Photochemically Stable Conjugated Poly(oxadiazole) Derivatives: A Comparison with Polythiophenes and Poly(*p*-phenyleneethynylenes)

Parts of this chapter appear in: Lee, K.; Kim, H.-J.; Cho, J. C.; Kim, J. Published in *Macromolecules* **2007**, *40*, 6457.

6.1. Abstract

We have designed and synthesized highly stable conjugated poly(oxadiazoles) derivatives (**PO1** and **PO2**). The oxadiazole-containing conjugated polymers have strong photoluminescent property and completely soluble in organic solvents. **PO1** and two commonly used conjugated polymers, PPE and P3HT, were tested under strong acidic condition and strong UV irradiation condition to investigate their chemical and photochemical stability. **PO1** turned out to be intact through the harsh treatments while the two control polymers were severely damaged in their conjugated backbone and lost their emissive property. Protonation of oxadiazole unit of **PO1** by acids induced backbone planarization of **PO1**, resulting in emission color change from blue to green. Reversible color change by adding and removing trifluoroacetic acid (TFA) to **PO1** and latent fluorescent patterning by using a photoacid generator and UV irradiation through a photomask were demonstrated. The results provide a design principle to develop highly stable conjugated polymers for various applications where photobleaching and oxidation are a common challenging problem.

6.2. Introduction

For the last three decades, organic conjugated polymers have attracted much attention as an active component for their potential applications such as organic transistors[1-4], polymer light-emitting devices[5-7], photovoltaic cells[8], and chemical and biological sensors[9-12]. A wide range of conjugated polymers, for example, polythiophenes[13-19], poly(p-phenylenes)[20-21], poly(*p*-phenylenevinylenes)[22-24], poly(*p*-phenyleneethynylenes)[25-29], and polyfluorenes[30-32], have been reported in the literature as promising materials for these applications. One of the greatest advantages of conjugated polymers over inorganic materials or heavy metal-based organic molecules are their easy processing and non-toxic property. However, the critical disadvantage found in currently available conjugated polymers is their poor stability compared to inorganic materials because they are vulnerable to photodegradation and oxidation in the presence of strong UV, oxygen, and acids. Unfortunately, these harsh conditions are required either as an operating condition or during the fabrication procedures of the above mentioned devices. For example, long time direct exposure to strong sunshine is the ideal condition to maximize energy harvesting and produce useful electricity in solar cell application but a least desirable condition in point of polymer stability. Many biological applications require bioconjugation with peptides or nucleotides and their synthetic procedures involve in UV irradiation, photoacid generator, and/or TFA (trifluoro acetic acid) deprotection. These are detrimental conditions for conjugated polymers.

In this research, we prepared the systematic investigation about the stability and pH sensitive properties of our newly developed poly(oxadiazole-co-phenylene-co-fluorene) derivatives (**POx, x=1, 2**). **POx** showed highly emissive and stable property

against long time UV exposure and strong acidic condition. In these harsh conditions, the emissive properties of **POx** was comparatively investigated with other two frequently used conjugated polymers, poly(*p*-phenyleneethynylene)s (**PPE**) and poly(3-hexylthophenes) (**P3HT**).

Oxadiazole-containing polymers and organic small molecules are a topic of interest due to their unique properties arising from the presence of its nitrogen-containing heterocyclic aromatic structure. The electron-deficient oxadiazole moiety has been used in the molecule design of organic optoelectronic materials to improve the electron mobility.[33] Incorporating oxadiazole-containing organic materials in the electroluminescence devices constituted of multi-layered organic thin films can greatly improve the overall device efficiency by making the balance of charge mobility in the active organic components.[34,35] Very recently we have synthesized a series of oxadiazole-containing organic molecules and investigated the role of the oxadiazole unit in terms of conjugation and emissive property as well.[36] Oxadiazole moiety is also known to provide enhanced thermal stability, redox stability, and good film-forming properties.[37,38]

Our oxadiazole-containing conjugated polymer is composed of three different units for their own role and designed for signal-amplifying DNA microarray development.[39] The amine functional group is for polymer tethering to a solid support and solid-state DNA synthesis at the same time. The fluorene unit is to improve the solubility and color tuning of the polymer. The oxadiazole unit is to enhance the stability of the polymer during the solid-state DNA synthesis that requires UV irradiation and strong photoacid generators.

6.3. Experimental Section

Materials and methods All solvents and reagents were used without further purification as received from Sigma-Aldrich Chemical Co. Compound **2** and **3** were prepared by the literature procedure with slight modification.[39,40] Gel permeation chromatography (GPC) was used to determine the number and weight average molecular weights and the molecular weight distributions with respect to polystyrene standards (Waters Corp.) in tetrahydrofuran as an eluent. UV/Vis absorption spectra were recorded with a Varian Cary50 UV/Vis spectrophotometer. Photoluminescence spectra and quantum yield in solution and the solid state were obtained by using PTI QuantaMaster^{TM} spectrofluorometers equipped with an integrating sphere. Fluorescence life-time of the **M1** were measured with PTI TimeMaster^{TM} fluorescence lifetime spectrometer. ^{1}H NMR spectra (400 MHz or 500 MHz) were obtained from Varian Inova 400 or 500 NMR instrumentation. Polymer film was coated by spincasting method (3000 rpm for 1 min) on the glass or HMDS coated glass using 1 mg/ml of polymer solution (**PO1** in chloroform, and **PPE** or **P3HT** in tetrahydrofuran).

Synthesis of compound 4 having C_{16} chain: To a 100 ml 2 neck round bottom flask were added compound **3** (0.29 g, 0.429 mmol), 4-bromobenzoyl chloride (0.198 g, 2.1 x 0.429 mmol), triethylamine (0.24 ml), and 25 ml of chloroform. During vigorous stirring precipitation was observed due to the limited solubility of **4** in chloroform. Even though 10 ml of tetrahydrofuran was added to the solution, the solution was still hazy. The reaction further continued overnight for completion. Solid product was filtered to collect dihydrazide compound (**4**). However, compound **4** showed a limited solubility in organic solvents, so reaction was proceeded without further characterization.

^{1}H-NMR (400 MHz, $CDCl_3$): δ/ppm 11.70, 10.40 (broad s, 4H, NH), 7.85 (s, 2H, aromatic), 7.75, 7.67 (dd, J= 32, 8 Hz, 8H, aromatic), 4.27 (t, 4H, CH_2), 2.02 (m, 4H, CH_2), 1.10-1.50 (m, 52H, CH_2), 0.83 (t, 6H, CH_3).

Monomer M2 C_{16} chain: The synthesis and characterization of monomer **M1** have been reported in other publication.[39] **M2** was prepared according to the same procedure as **M1**. 0.37 g of compound **4** was dissolved in 150 ml of phosphorus oxychloride and the solution was refluxed for 24 hr. The mixture was poured into 1500 ml water and the appearing solids were collected by filtration and drying in vacuo. White powder product (**M2**) was obtained from recrystallization in benzene (Yield: 87 %). ^{1}H-NMR (500 MHz, $CDCl_3$): δ/ppm 8.04, 7,69 (dd, J= 175, 11 Hz, 8H, aromatic), 7.80 (s, 2H, aromatic), 4.08 (t, 4H, CH_2), 1.88 (m, 4H, CH_2), 1.15-1.43 (m, 52H, CH_2), 0.85 (t, 6H, CH_3).

Synthesis of PO1 and PO2: **PO2** synthesis was done according to the synthetic route of polymer **PO1** in the literature reported previously with a slight modification.[39] To a 50 ml of Schlenk flask were added **M2** (50.0 mg, 49.75 μmol), **M3** (31.8 mg, 49.75 μmol), **M4** (42.4 mg, 100 μmol), THF (3 ml) and 1M K_2CO_3 (2 ml). Degassed tetrakis(triphenylphosphine)palladium(0) (5 mol%) in THF (1 ml), prepared in a separate Schlenk, was transferred to the monomer mixture by cannula and the monomer solution was degassed by several cycles of vacuum and argon purging. Polymerization was carried out at 80 °C for 36 h. The solution of the reaction mixture was precipitated in 30 ml of methanol and filtered. It was further wash with methanol, acetone, water, and hexane (3 x 10 ml each) and dried. Further purification was done by extraction with chloroform/water to give precursor polymer. 2.5 ml of trifluoroacetic acid (TFA) was

carefully added to the polymer in chloroform (5 ml) and the polymer solution was stirred at room temperature for 6 h to cleave *t*-BOC group. After evaporation of solvent and TFA, the polymer was re-dissolved in chloroform and washed with 1 M KOH solution, followed by NaCl, and deionized water to give yellow polymer (**PO2**) (Yield: 73 mg). ^{1}H-NMR (500 MHz, $CDCl_3$): δ/ppm 8.28 (d, 4H, aromatic), 7.91 (d, 4H, aromatic), 7.40-7.74 (broad m, 14H, aromatic), 7.36 (s, 2H, aromatic), 4.25 (t, 4H, CH_2), 4.00 (t, 4H, CH_2), 2.68 (m, 4H, CH_2), 2.11 (broad s, 4H, NH_2), 1.99 (m, 8H, CH_2), 1.90-1.01 (broad m, 100H, CH_2), 0.88 (t, 6H, CH_3), 0.78 (t, 12H, CH_3). The number/weight average molecular weight was calculated with the polymer before cleavage of *t*-BOC due to the limited solubility of **PO2** in tetrahydrofuran as a GPC eluent, M_n = 35,000, PDI = 3.7.

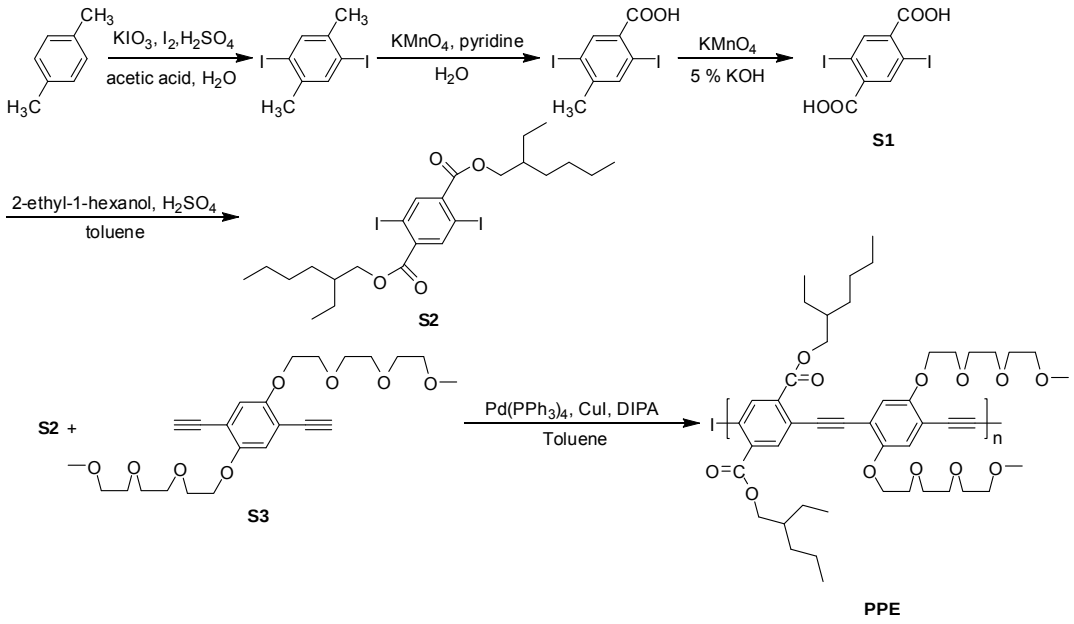

Scheme 6-1. Monomer and polymer synthesis for **PPE**.

Synthesis of Bis(2-ethylhexyl) 2,5-diiodoterephthalate (**S2**) 2,5-diiodoterephthalic acid (**S1**, 0.3 g, 0.72 mmol) prepared according to a previous

literature[41], 2-ethyl-1-hexanol (0.28 g, 2.16 mmol), toluene (20 ml), and 0.1 mL of concentrated H_2SO_4 were heated for 24 h to reflux, with separation of the water using a Dean-Stark trap. Reaction mixture was cooled down and the organic layer was washed with water and dried with $MgSO_4$. Further purification was done by column chromatography (ethyl acetate: hexane = 1: 15 v/v) to get viscous yellow oil (0.14 g, 30 %). ^{1}H-NMR (500 MHz, $CDCl_3$): δ/ppm 8.26 (s, 2H, aromatic), 4.27 (d, 4 H, -OC$\underline{H}_2$-), 1.79 (m, 2H, -C$\underline{H}$-), 1.55-1.30 (m, 16H, -C$\underline{H}_2$-), 0.95 (m, 12H, C$\underline{H}_3$).

PPE synthesis S2 (65 mg, 0.14 mmol) and **S3** (90 mg, 0.14 mmol) prepared according to a previous literature[29] were placed into a Schlenck flask (50 ml). Toluene (1.5 ml) and diisopropylamine (3 ml) were added. After complete dissolution of two monomers, the solution was degassed by three times of vacuum and argon purging. In a separate Schlenck flask, tetrakistriphenylphosphine palladium (0) and copper (I) iodide were dissolved in toluene (1.5 ml) under a nitrogen atmosphere in a glove box and degassed. The degassed solution containing catalyst was cannulated onto the monomer solution. After transfer of the catalysis solution to monomer solution, polymerization solution was finally degassed again and allowed to stir under argon purging at 55 ℃ for 2 days. The reaction mixture filtered with 0.45 ㎛ membrane syringe. The toluene solution was precipitated in methanol 2 times. ^{1}H-NMR (500 MHz, $CDCl_3$): δ/ppm 8.11 (s, 2H, aromatic), 7.10 (s, 2H. aromatic), 4.3-3.5 (broad m, 28H, -OC$\underline{H}_2$-), 3.35 (s, 6H, -OC$\underline{H}_3$), 1.78 (m, 2H, -C$\underline{H}$-), 1.7-1.2 (broad m, 16H, -C$\underline{H}_2$-), 1.85 (broad s, 12H, -C$\underline{H}_3$).

6.4. Results and Discussion

Monomer **M1** and **M2** were prepared according to the synthetic routes illustrated in Scheme 6-2. Ethylhexyl or hexadecane group was attached to diethyl 2.5 – dihydroxyterephthalate by Williams-ether synthesis to give a good solubility in organic solvents to the final polymer. A hydrazine reaction, followed by the 4-bromobenzoyl treatment gave a dihydrazide compound **4**. Compound **4** showed a limited solubility in organic solvents, so reaction was proceeded without further characterization. Compound **4** having a hydrazide group was converted to an oxadiazole group through intramolecular ring closure reaction by refluxing **4** at phosphorus oxychloride. We initially tried to make the conjugated polymer containing an oxadiazole unit by ring closing reaction of the hydrazide group after the polymerization of the linear polymer. However, we failed to make the conjugated polymer having oxadiazole units due to the solubility problem and side reaction during the ring closure reaction in phosphorus oxychloride. We overcame these problems by conducting the ring closure reaction in the monomer state. **M1** and **M2** were obtained as a pale yellow powder at a yield of ca. 75%. **M1** and **M2** showed a good solubility in organic solvents such as chloroform and tetrahydrofuran (>15 mg/ml). We also prepared several other monomers having different length of alkyl chains (hexyl or octyl group) and polymerized them to make polyoxadiazole derivatives (Data not included). However, we noticed that the polymers having short alkyl side chains showed limited solubility in organic solvents due to the strong backbone rigidity that is in a good agreement with the results from Wu et al.[40] To prepare **M3**, ethyl oxamate was first reacted with oxalyl chloride to give ethyloxalyl isocyanate. Isocyanate group was blocked with BOC group and introduction of bromopentyl group was achieved by the

nucleophillic reaction with t-butoxide. Finally, the removal of ethyloxalyl group gave **M3** having t-BOC protected di-amino group.

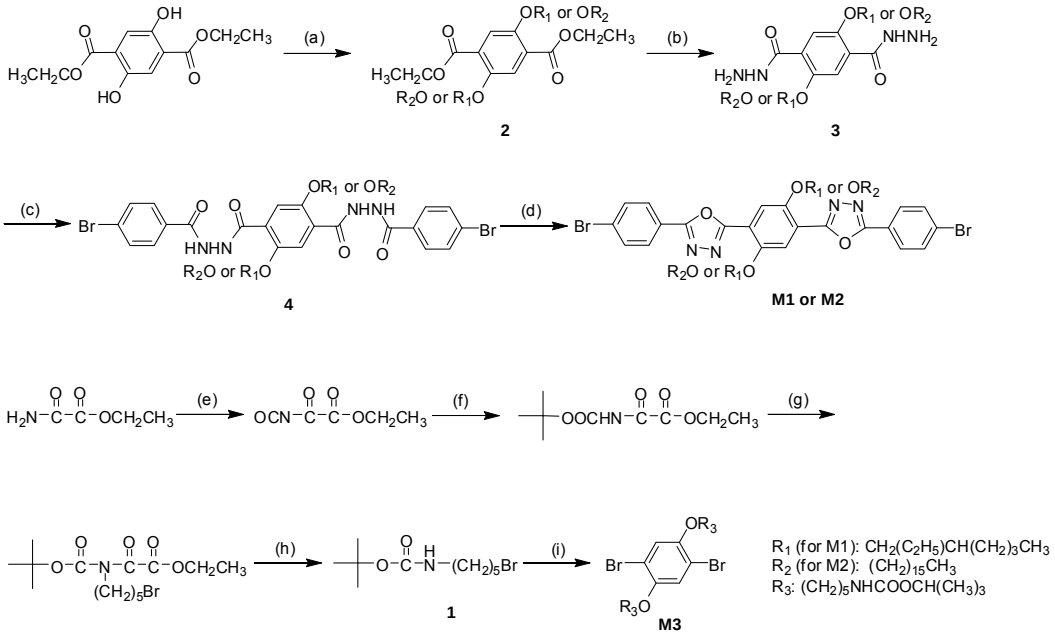

Scheme 6-2. Monomer synthesis: (a) 2-Ethylhexylbromide (for R_1) or 1-bromohexadecane (for R_2), K_2CO_3, DMF, 80 °C, 48 h. (b) H_2NNH_2, ethanol, 78 °C, 24 h. (c) 4-bromobenzoyl chloride, triethylamine, chloroform, 12 h. (d) $POCl_3$, reflux, 12 h. (e) oxalyl chloride, methylene chloride, 0 °C → 25 °C, 12 h. (f) *t*-butanol, toluene, 0 °C → 40 °C, 15 min. (g) 1, 5-dibromopentane, *t*-BuOK, DMF, 40 °C, 1 h. (h) LiOH, THF, water, r. t., 3 h. (i) 2, 5-dibromohydroquinone, K_2CO_3, DMF, 70 °C, 48 h.

Photophysical properties of **M1** and **M2** were investigated by means of UV-Vis and PL analysis. **M1** and **M2** showed similar physical and photophysical behaviors. In Figure 6-1(a), the UV-Vis spectrum of **M1** has two absorption maximums at 307 and 373 nm, respectively and the emission maximum of the photoluminescence spectrum was observed at 413 nm in chloroform. The main chain conjugation is responsible for the absorption peak at 373 nm and the central para-dialkoxy phenyl ring creates another

chromophore and produces the absorption peak at 307 nm.[36] Quantum yield of **M1** and **M2** was 44 % (ex. at 313 nm) and 76 % (ex. at 370 nm) in chloroform, respectively. We investigated the stability of **M1** by analyzing the effect of acidic environment on the photophysical property of **M1**. The emission spectrum of **M1** gradually red shifted without losing intensity as TFA was added into the **M1** solution in chloroform (Figure 6-1(b)). We believe that the observed red shift is due to the acid-induced planarization of **M1** mainchain as illustrated in Figure 6-2.[36,42,43] The nitrogen atoms in the oxadiazole ring are prone to be protonated in the presence of TFA because the lone pair electrons in nitrogen are not participated in the aromatic sextet. There are several works which revealed the relationship the planar structure and fluorescence life-time due to the keto-enol formation of heterocyclic ring.[42-44] The life-time of **M1** characterized by time-resolved fluorescence spectroscopy increased from 2.1 and 2.4 ns after adding TFA, showing a good agreement with the reported results that a planar structure induces the longer fluorescence life-time as shown in Figure 6-1(c). Moreover, we did not observe the bathochromic shifts from the oxadiazole derivatives without alkoxy side-chains which cannot form the proposed stable 6-membered ring structure, supporting our hypothesis.

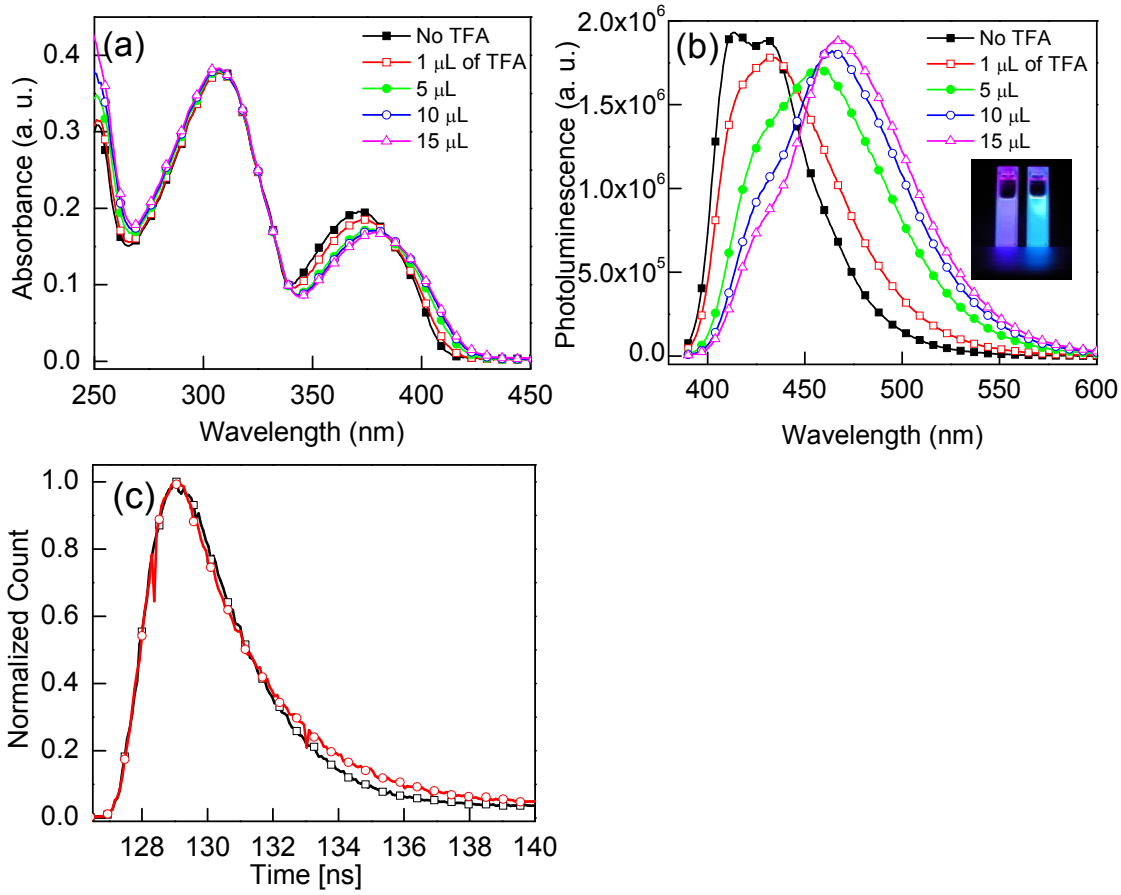

Figure 6-1. (a) UV-Vis and (b) PL spectrum profiles of **M1** in chloroform upon TFA treatment. (c) Fluorescence life time results of **M1** (1mg/L) characterized by time-resolved fluorescence spectroscopy before (□, emission at 413 nm) and after (○, emission at 468 nm) adding 10 μl of TFA in 3 ml of chloroform upon excitation at 386 nm. The protonation of the aromatic dioxadiazole unit induces the planarization of the structure by forming a stable 6-membered ring structure and causes the blue to green fluorescence shift.

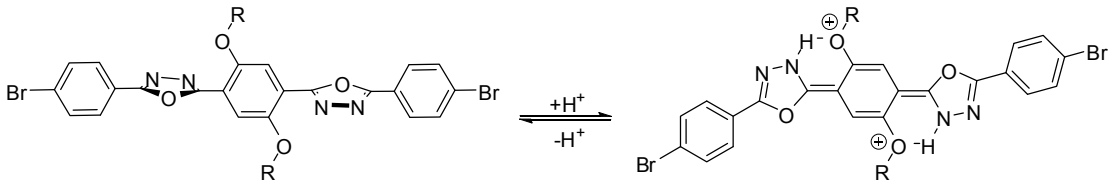

Figure 6-2. A proposed planarization mechanism induced by TFA.

The polymer **PO1** and **PO2** were prepared via the Suzuki cross-coupling reaction of the oxadiazole monomer **M1** (or **M2**), the di-amine monomer **M3**, and a fluorene monomer having borolene unit **M4** (or **M5**) as shown in Scheme 6-3.[39,45] The photophysical and chemical properties of the resulting oxadiazole-containing conjugated polymers turned out to be independent to the length of the alkyl side chain on the fluorene unit and the oxadiazole unit. **PO1** showed better solubility in chloroform than **PO2**. Therefore, we will focus the discussion on **PO1**. Molecular weights of these copolymers were determined by gel permeation chromatography (GPC) using monodisperse polystyrenes as the standard. The number (M_n)and weight (M_w) average molecular weight of **PO1** before cleavage of tert-BOC was 51,000 g/mol and 224,000 g/mol, respectively, and the polydispersity indices (PDI) was 4.4. **PO1** before deprotection of t-BOC had an off-white color and was soluble in organic solvents such as tetrahydrofuran (THF), and chloroform, but almost insoluble in polar solvents like N,N-dimethylformamide (DMF) and dimethylsulfoxide (DMSO). After deprotection of t-BOC, **PO1** was still soluble in chloroform but their solubility in THF was significantly decreased.

We compared the photophysical properties and particularly stability of **PO1** with poly(*p*-phenyleneethynylene)s (**PPE**) and poly(3-hexylthiophene) (**P3HT**), commonly used conjugated polymers (Figure 6-3). The PPE was synthesized by using palladium-catalyzed Sonogashira-Hagihara reaction and the P3HT was prepared by the conventional procedure.[27,46] Both conjugated polymers were soluble in THF and chloroform.

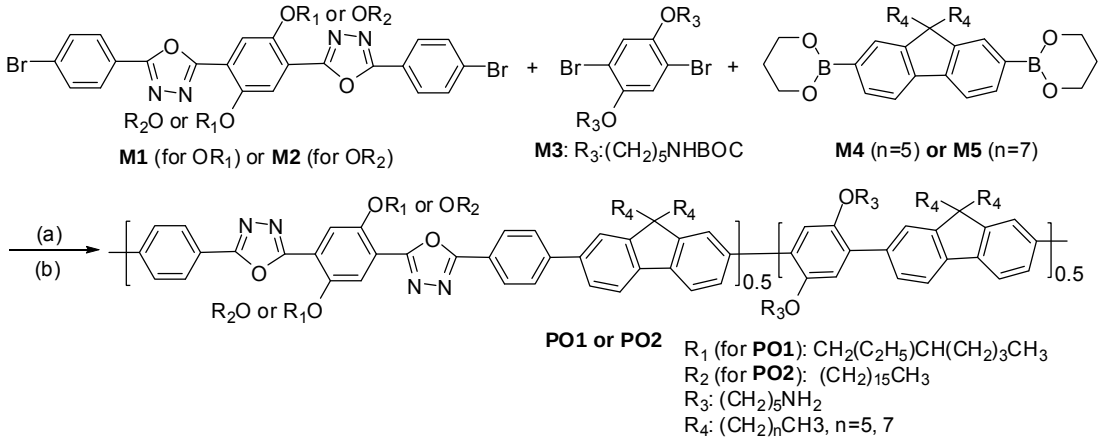

Scheme 6-3. Polymer synthesis (a) THF, water, $Pd(PPh_3)_4$, K_2CO_3, 80 °C, 36 h. (b) 50 % TFA in $CHCl_3$.

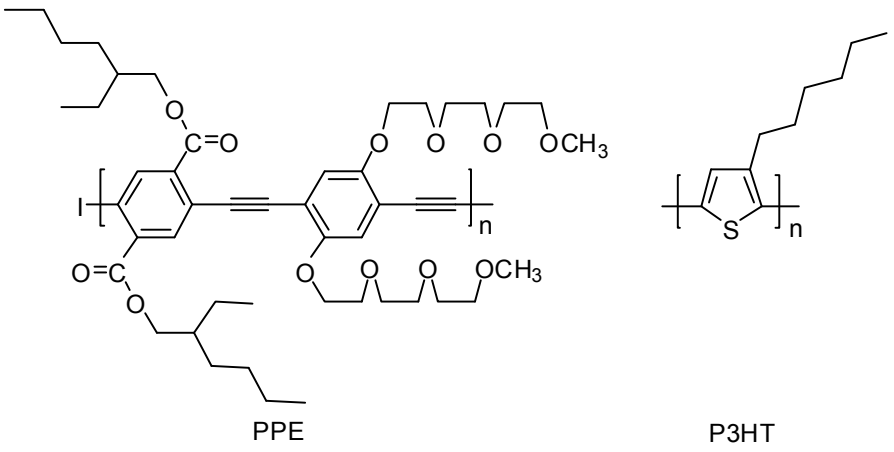

Figure 6-3. The chemical structure of poly(*p*-phenyleneethynylene)s (**PPE**) and polythiophene (**P3HT**).

Table 6-1. Photo-physical data of **PO1**, **PPE**, and **P3HT** used in this study.

poly	E_g/eV[b]	solution[a]		film		Φ ($CHCl_3$)[c]	Φ (film)[c]
		$\lambda_{max,abs}$/nm $\lambda_{max,em}$/nm	Stokes shift $cm^{-1,}$	$\lambda_{max,abs}$/nm $\lambda_{max,em}$/nm	Stokes shift cm^{-1}		
PO1	2.83	385 413	1760	385 425	2440	0.94	0.05
PPE	2.5	445 486	1900	482 546	2430	0.6	0.17
P3HT	2.25	430 567	5620	513 645	3990	0.12	0.00016

[a] UV-Vis and PL data were measured in chloroform (1 mg/L) for **PO1** and tetrahydrofuran (1 mg/L) for **PPE** and **P3HT**. [b] The optical HOMO-LUMO energy gap is based on the low-energy onset in the solution-state UV-Vis spectra [c] Quantum yield is absolute quantum value measured by using an integrating sphere.

The optical characteristic of the polymers were investigated by UV-Vis and PL spectra in the solution and the film state. Photophysical data of the conjugated polymers are summarized in Table 6.1. The polymers were spuncast to form optical quality films from the chloroform (**PO1,** 1mg/ml) or tetrahydrofuran (**PPE** or **P3HT**, 1mg/ml) solution. As shown in Figure 6-4 (a), the absorption λ_{max} of **PO1** was observed at 385 nm both in chloroform and in the film while the emission λ_{max} was located at 413 nm in chloroform solution and 425 nm in the film. We also observed the broad tailing band from the solid film, which implies that **PO1** aggregated in the solid state likely due to π-π backbone stacking. Figure 6-4 (b) and (c) show the absorption and emission spectra of **PPE** and **P3HT**. The absorption (emission) maximum of **PPE** and **P3HT** in THF was at 445 nm (486 nm) and 430 nm (567 nm), respectively. One can see the significant red shift from the solution to the film. The quantum yield in the solid state decreased accordingly.

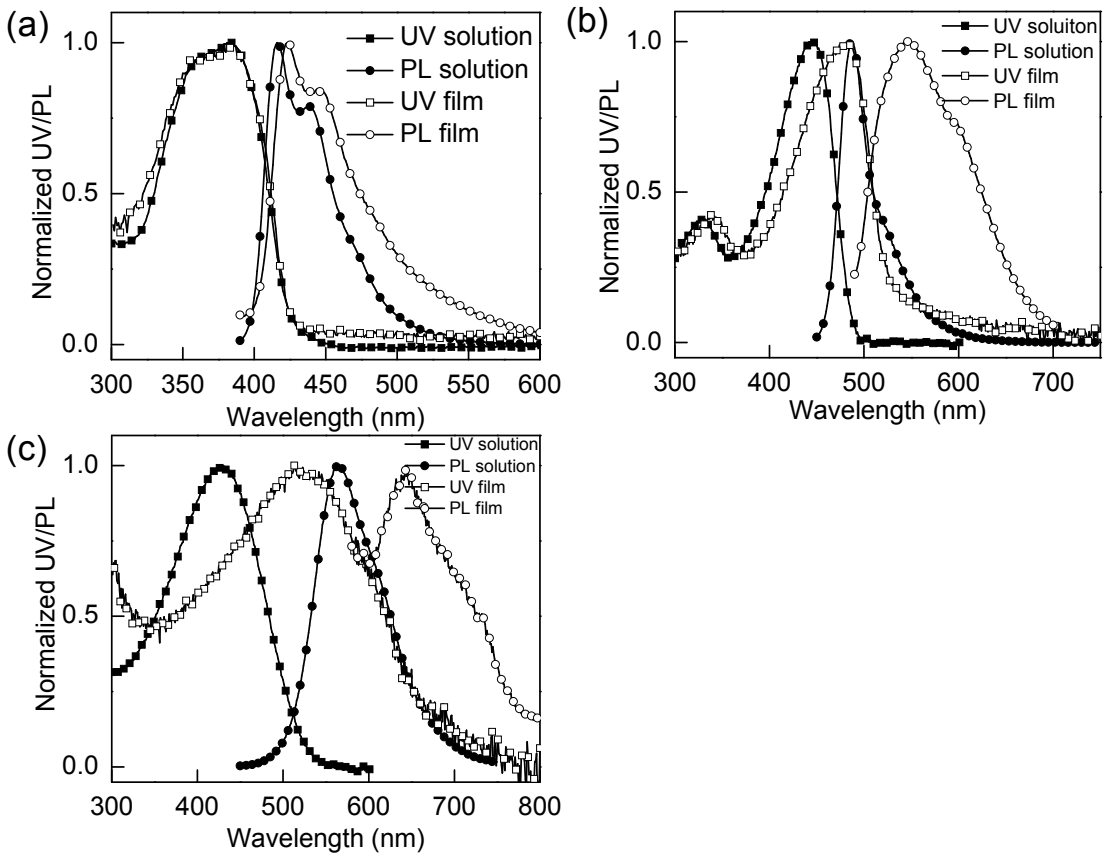

Figure 6-4. UV-Vis (■: solution, □: film) and PL (●: solution, ○: film) spectra of (a) **PO1**, (b) **PPE** (c) **P3HT** in solution and in the film.

We investigated the stability of **PO1** films in acidic condition and under strong UV illumination condition, respectively, and used PPE and P3HT as a control. First, the polymer films were placed in 1 M hydrochloric acid (HCl) solution at room temperature for 1 hour. The UV-Vis spectra of the polymers before and after the HCl treatment are shown in Figure 6-5 (a). **PO1** showed slight decrease in absorption intensity while the absorption intensity of PPE and P3HT decreased significantly to 74 % and 86 % of the original value, respectively. Absorption λ_{max} of PPE and P3HT also blue shifted, from 482nm to 464nm for PPE and from 513nm to 499nm for P3HT, implying a backbone

damage by the strong acid. Moreover, the fluorescence emission spectra in Figure 6-5 (b) clearly demonstrate that the emissive property of **PO1** is intact during the HCl treatment but that of PPE and P3HT is severely damaged by the strong acid treatment: **PPE** showed 41 % quenching and **P3HT** showed 74 % quenching.

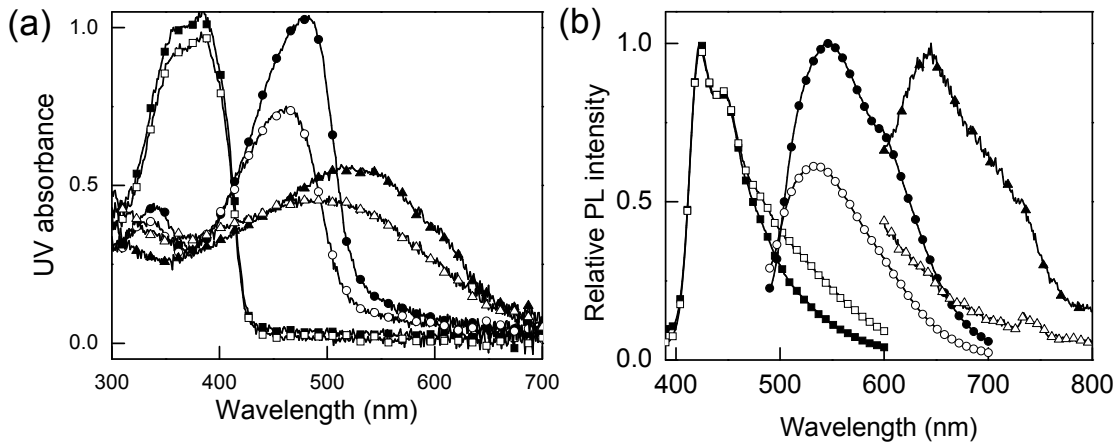

Figure 6-5. (a) UV-Vis and (b) PL spectra of the polymer films before (■: **PO1**, ●: **PPE**, ▲: **P3HT**) and after (□: **PO1**, ○: **PPE**, Δ: **P3HT**) the HCl treatment. All polymer-coated slides were dipped in 1 M HCl solution at room temperature for 1 hr.

We also tested stability of each polymer in the presence of a strong acid and under UV irradiation condition. 1 wt% of triphenylsulfonium triflate, a photo-acid generator (PAG), was added to each polymer solution in chloroform (**POx**) or tetrahydrofuran (**PPE** and **P3HT**). Thin layer films of the polymers were fabricated by spincasting, and subsequently exposed to 254 nm of strong UV irradiation (4 W) for 1 hr to activate the PAG. The UV-Vis spectra of each film before and the after the UV irradiation are shown in Figure 6-6 (a). The absorption intensity of **PO1** decreased 16 %, while that of **P3HT** decreased 27 %. **P3HT** also showed a blue-shift of its absorption λ_{max} from 510nm to 490nm likely due to the reduced conjugation length resulting from backbone damage. As

for **PPE**, its main chain looked to be completely degraded by UV irradiation because the film essentially did not show any chromophore absorption. It is believed that the weak backbone triple bond was completely photo-bleached by UV irradiation. Furthermore, the photoluminescence (PL) spectra in Figure 6-6 (b) clearly show that the main chain conjugation of **PPE** and **P3HT** is significantly damaged by UV irradiation and the acid. The fluorescence emission of PPE was completely quenched and that of P3HT was 77 % quenched. However, interestingly after the UV irradiation the PL intensity of **PO1** at 425 nm remained constant and surprisingly a new even stronger band emerged at 500 nm. We believe that the oxadiazole unit was protonated by the strong acid generated upon UV irradiation and the protonation induced backbone planarization and produced the new emission band at 500nm. The reason why we did not observe a strong new emissive band formation from the same **PO1** film upon HCl treatment is likely that aqueous HCl cannot penetrate into the **PO1** while PAG was evenly distributed in the **PO1** film. In fact, the PL spectrum of the **PO1** film after the HCl treatment shows only small shoulder formation above 480nm. (Figure 5(b). Interestingly we could pattern a fluorescent image on a spincast film of **PO1** by using a photomask (Figure 6-6 (b) inset). The UV-exposed letter area shows green emission while the unexposed background emits blue fluorescence.

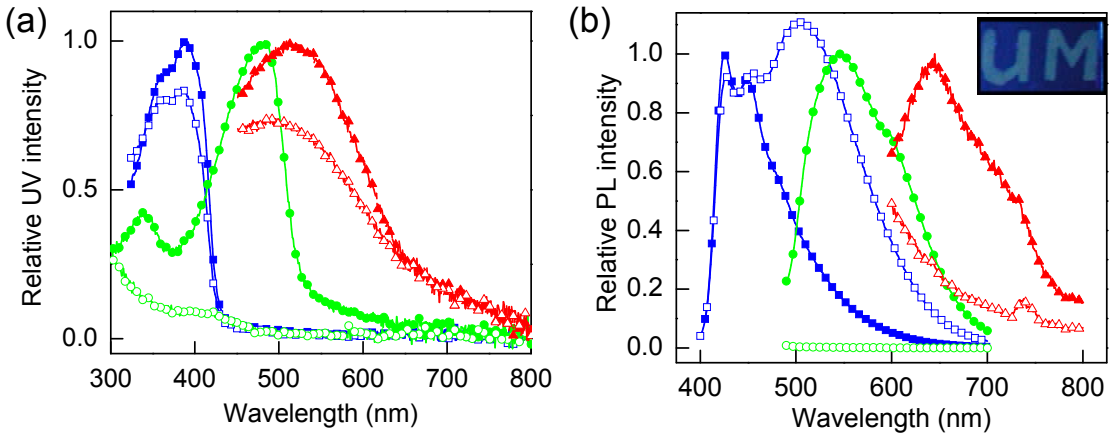

Figure 6-6. Change in (a) UV and (b) PL spectra before (■: **PO1**, ●: **PPE**, ▲: **P3HT**) and after (□: **PO1**, ○: **PPE**, Δ: **P3HT**) UV irradiation (254 nm, 6W, 1hr) in the presence of photogenerated acid (PGA), UV irradiation condition: 254 nm, 6W, 1hr. (Inset) patterned images of **PO1** after 1 hr UV exposure. The area of the character "UM" was exposed to 254 nm of UV light for 1 hour.

To confirm the stability of **PO1** and our acid-induced planarization hypothesis, we additionally investigated the absorption and emission properties of **PO1** in chloroform solution by using TFA. TFA was added and homogeneously mixed into the **PO1** solution. Figure 6-7 shows the UV-Vis and PL spectra of the solution upon addition of TFA. From Figure 6-7 (a) we can see slight red shift as TFA was gradually added. The solution color was changed from transparent to light yellow an indication of aggregation/planarization.[47-51] Consistently, PL spectra also show a new band formation at 500nm and significant fluorescence quenching by TFA. It is believed that the quinoid structure of **PO1** due to the protonation of oxadiazole unit induces backbone planarization (Figure 6-2). The protonation also charges **PO1** and decrease the solubility of **PO1** in chloroform. Therefore, the planarization and the decreased solubility of **PO1** cause polymer aggregation in the solution and resulting fluorescence quenching.

However, in the film structure the mobility of the chain is suppressed by adjacent polymer chains and therefore we did not observe fluorescence quenching but an emerging new strong band in Figure 6-6 (b). Another evidence supporting our hypothesis is the reversibility test we conducted. We removed TFA from the **PO1** chloroform solution by vacuum and the fluorescence emission of the solution was completely recovered. We repeated the addition and removal of TFA and observed completely reversible increase and decrease of the emission λ_{max} at 415nm as shown in Figure 6-7 (c).

The presented strong acid and UV irradiation studies evidently show that **PO1** is remarkably stable in harsh conditions such as under strong acidic and UV irradiation conditions. Particularly, because all the experiments were conducted in ambient condition we can emphasize that **PO1** is not vulnerable to oxidation that is the common degradation mechanism of conjugated polymers. The unique stability of **PO1** made its application for our recent development of signal-amplifying DNA microarrys.[39]

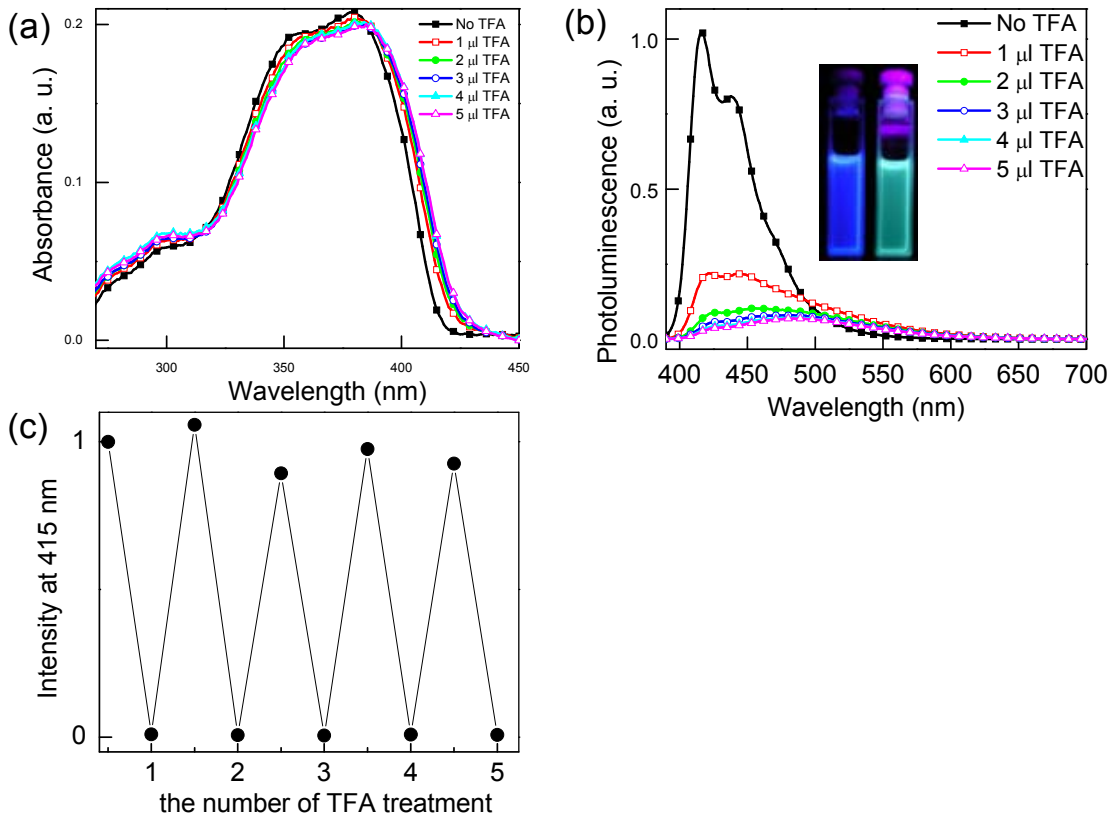

Figure 6-7. (a) UV-Vis and (b) photoluminescence spectra of **PO1** solution in chloroform (1 mg/L) upon addition of TFA, (c) Reversible feature of the emission change of **PO1** in chloroform by adding and removing of TFA (TFA was added and removed by vacuum repeatedly).

6.5. Conclusion

We have synthesized conjugated polymers containing oxadiazole moiety and examined the stability of the polymers in harsh conditions like strong acid and prolonged UV exposure. The poly(oxadiazole) derivative, **PO1**, showed an exceptional stability in the harsh conditions and its emissive property was intact while the two control polymers, PPE and P3HT, were significantly damaged and their emissive property was completely ruined. The oxadiazole unit of **PO1** is believed to be protonated in a strong acidic

environment and induces backbone planarization of **PO1**. Cycles of addition and removal of TFA in **PO1** solution produced completely reversible fluorescence emission change from blue to green due to the protonation and subsequent planarization of the conjugated polymer backbone, demonstrating the chemical stability of **PO1**. Latent fluorescence patterning on a **PO1** film was also demonstrated by using a photoacid generator and UV irradiation through a photomask. The outstanding chemical and photochemical stability of **PO1** can provide a molecular design principle to develop conjugated polymers having unique stability for various optoelectronic device applications and biosensor array development.[39]

6.6. References

1. Dhoot, A. S.; Yuen, J. D.; Heeney, M.; McCulloch, I.; Moses, D.; Heeger, A. J. *Proc. Nat. Acad. Sci.* **2006**, *103*, 11834-11837.

2. Siddons, G. P.; Merchin, D.; Back, J. H.; Jeong, J. K.; Shim, M. *Nano Lett.* **2004**, *4*, 927-931.

3. Rogers, J. A.; Bao, Z.; Makhija, A.; Braun, P. *Adv. Mater.* **1999**, *11*, 741.

4. Chua, L. L.; Zaumseil, J.; Chang, J. F.; Ou, E. C. W.; Ho, P. K. H.; Sirringhaus, H.; Friend, R. H. *Nature* **2005**, *434*, 194-199.

5. Hebner, T. R.; Wu, C. C.; Marcy, D.; Lu, M. H.; Sturm, J. C. *Appl. Phys. Lett*. **1998**, *280*, 1741.

6. Jin, S.-H.; Kim, M.-Y.; Kim, J. Y.; Lee, K.; Gal, Y.-S. *J. Am. Chem. Soc*. **2004**, *126*, 2474.

7. Müller, C. D.; Falcou, A.; Reckefuss, N.; Rojahn, M.; Wiederhirn, V.; Rudati, P.; Frohne, H.; Nuyken, O.; Becker, H.; Meerholz, K. *Nature*, **2003**, *421*, 829.

8. For recent review, see: Gunes, S.; Neugebauer, H.; Sariciftci, N. S. *Chem. Rev*. **2007**, *107*, 1324.

9. McQuade, D. T.; Pullen, A. E.; Swager, T. M. *Chem. Rev*. **2000**, *100*, 2537.

10. Thomas, S. W., III; Joly, G. D.; Swager, T. M. *Chem. Rev*. **2007**, *107*, 1339.

11. Nilsson, K. P. R.; Ingana¨s, O. *Nat. Mater.* **2003**, *2*, 419.

12. Xu, Q.-H.; Wang, S.; Korystov, D.; Mikhailovsky, A.; Bazan, G. C.; Moses, D.; Heeger, A. J. *Proc. Natl. Acad. Sci. U.S.A.* **2005**, *102*, 530.

13. McCullough, R. D.; Ewbank, P. E.; Loewe, R. S. *J. Am. Chem. Soc*. **1997**, *119*, 633.

14. Le Floch, F.; Ho, H. A.; Harding-Lepage, P.; Bedard, M.; Neagu-Plesu, R.; Leclerc, M. *Ad*v. *Mater.* **2005**, *17*, 1251.

15. Yang, H. C.; Shin, T. J.; Yang, L.; Cho, K.; Ryu, C. Y.; Bao, Z. N. *Ad*v. *Funct. Mater*. **2005**, *15*, 671.

16. Berggren, M.; Inganas, O.; Rasmusson, J.; Gustafsson, G.; Andersson, M. R.; Wennerstrom, O.; Hjertberg, T. *Nature* **1994**, *372*, 444.

17. Andersson, M. R.; Berggren, M.; Inganas, O.; Gustafsson, G.; Gustafsson-Carlberg, J. C.; Selse, D.; Hjertberg, T.; Wennerstrom, O. *Macromolecules***1995**, *28*, 7525.

18. Kim, Y.; Cook, S.; Choulis, S. A.; Nelson, J.; Durrant, J. R.; Bradley, D. D. C. *Chem. Mater.* **2004**, *16,* 4812.

19. Li, G.; Shrotriya, V.; Huang, J. S.; Yao, Y.; Moriarty, T.; Emery, K.; Yang, Y. *Nat. Mater.* **2005**, *4*, 864.

20. Harrison, B. S.; Ramey, M. B.; Reynolds, J. R.; Schanze, K. S. *J. Am. Chem. Soc*. **2000**, *122*, 8561.

21. Taylor, D. K.; Samulski, E. T. *Macromolecules* **2000**, *33*, 2355.

22. Burrourghes, J. H.; Bradley, D. D. C.; Brown, A. R.; Marks, R. N.; Mackay, K.; Friend, R. H.; Burns, P. L.; Holmes, B. *Nature (London)* **1991**, *347*, 539.

23. Sariciftci, N. S.; Braun, D.; Zhang, C.; Srdanov, V. I.; Heeger, A. J.; Stucky, G.; Wudl, F. *Appl. Phys. Lett.* **1993**, *62*, 585.

24. Geens, W.; Tsamouras, D.; Poortmans, J.; Hadziioannou, G. *Synth. Met.* **2001**, *122*, 191.

25. For the issue about poly(aryleneethynylene)s, see: Weder, C. *Ad*v. *Polym. Sci.* **2005**, *177*.

26. Zhao, X. Y.; Pinto, M. R.; Hardison, L. M.; Mwaura, J.; Muller, J.; Jiang, H.; Witker, D.; Kleiman, V. D.; Reynolds, J. R.; Schanze, K. S. *Macromolecules* **2006**, *39*, 6355.

27. Bunz, U. H. F. *Chem. Rev.* **2000**, *100*, 1605.

28. Breen, C. A.; Rifai, S.; Bulovic, V.; Swager, T. M. *Nano Lett*. **2005**, *5*, 1597.

29. Lee, K.; Cho, J. C.; Deheck, J.; Kim, J. *Chem. Commun*. **2006**, 1983.

30. Bemius, M. T.; Mike, I.; O'Brien, J.; Wu, W. *Adv. Mater.* **2000**, *12* 1737.

31. Scherf, U.; List, E. J. W. *Adv. Mater.* **2002**, *14*, 477.

32. Kraft, A.; Grimsdale, A. C.; Holmes, A. B. *Angew. Chem., Int. Ed.* **1998**, *37*, 402.

33. For recent review, see: Kulkarni, A. P.; Tonzola, C. J.; Babel, A.; Jenekhe, S. A. *Chem. Mater*. **2004**, *16*, 4556.

34. Adachi, C.; Tsutsui, T.; Saito, S. *Appl. Phys. Lett.* **1989**, *55*, 1489.

35. Hamada, Y.; Adachi, C.; Tsutsui, T.; Saito, S. *Jpn. J. Appl. Phys*. **1992**, *31*, 1812.

36. Bolton, O.; Kim, J. *J. Mater. Chem*. **2007**, *17*, 1981.

37. Levi, M. D.; Fisyuk, A. S.; Demadrille, R.; Markevich, E.; Gofer, Y.; Aurbach, D.; Pron, A. *Chem. Commun*. **2006**, 3299.

38. Buchwald, E.; Meier, M.; Karg, S.; Pösch, P.; Schmidt, H.-W.; Strohriegl, P.; Rieβ, W.; Schwoerer, M. *Adv. Mater*. **1995**, *7*, 839.

39. Lee, K.; Rouillard, J.-M.; Pham, T.; Gulari, E.; Kim. J. *Angew. Chem. Int. Ed*. **2007**. *46*, 4667.

40. Wu, T.-Y.; Sheu, R.-B.; Chen, Y. *Macromolecules* **2004**, *37*, 725.

41. Zhou, Q.; Swager, T. M. *J. Am. Chem. Soc*. **1995**, *117*, 12593.

42. Wu, Y.; Peng, X.; Fan, J.; Gao, S.; Tian, M.; Zhao, J.; Sun, S. *J. Org. Chem*. **2007**, *72*, 62.

43. Lee, J. K.; Kim, H.-J.; Kim, T. H.; Lee, C.-H.; Park, W. H.; Kim, J.; Lee, T. S. *Macromolecules* **2005**, *38*, 9427.

44. Chang, D. W.; Kim, S.; Park, S. Y.; Yu, H.; Jang, D.-J. *Macromolecules* **2000**, *33*, 7223.

45. Miyaura, N.; Suzuki, A. *Chem. Rev*. **1995**, *95*, 2457.

46. McCullough, R. D.; Lowe, R. D.; Jayaraman, M.; Anderson, D. L. *J. Org. Chem*. **1993**, *58*, 904.

47. Kim, J. *Pure Appl. Chem.* **2002**, *74*, 2031.

48. Kim, J.; Swager, T. M. *Nature* **2001**, *411*, 1030.

49. Kim, J.; Mcquade, D. T.; Mchugh, S. K.; Swager, T. M. *Angew. Chem. Int. Ed*. **2000**, *39*, 3868.

50. Kim, J.; Levitsky, I. A.; Mcquade, D. T.; Swager, T. M. *J. Am. Chem. Soc*. **2002**, *124*, 7710.

51. Jenekhe, S. A. *Adv. Mater*. **1995**, *7*, 309.

CHAPTER 7

Signal-Amplifying Conjugated Polymer-DNA Hybrid Chips

Parts of this chapter appear in: Lee, K.; Rouillard, J.-M.; Pham, T.; Gulari, E.; Kim, J. Published in *Angew. Chem. Int. Ed*. **2007**, *46*, 4667.

7.1. Abstract

DNA microarray allowing massively parallel gene discovery studies and gene expression is a powerful method to discover a target material with probes with known identity. However, such a tiny detection signal in proportion to the quantity of a target normally requires its proliferation through polymerase chain reaction (PCR). We prepared a newly developed conjugated polymer (**P1**) having unique stability in rigorous conditions and its application for signal amplifying DNA chips. Highly fluorescent **P1** polymers were covalently attached to a glass slide and oligonucleotides were directly synthesized on emissive polymer-coated microarray substrate using photogenerated acid. Target binding signal upon DNA/DNA hybridization was amplified through the fluorescence resonance energy transfer (FRET) mechanism. Energy-harvesting property of the conjugated polymer makes it possible to transfer larger amount of energy from the polymer to dye. This system represents the enhancement of the sensitivity and selectivity in DNA-chip.

7.2. Introduction

Bio-/synthetic hybrid materials have recently received considerable attention due to their potential biomedical applications.[1-3] The most reliable way of identifying any biological target is through its genetic code.[4-7] However, the current commercial DNA microarray requires costly and time consuming polymerase chain reaction (PCR) to multiply the number of analyte DNA and labeling of analyte DNA with a fluorescent dye because of the low detection limit. In this context, devising self-signal amplifying DNA microarrays can realize low cost, fast, and reliable detection of nucleic acids. One of our research thrusts is to develop the necessary tools for detecting up to tens of thousands of agents simultaneously in a short time with low false positive rate and using very small amount samples with DNA microarrays. Herein, we report signal amplifying DNA chips fabricated by on-chip DNA synthesis on a thin film of a newly developed conjugated polymer (Figure 7-1).

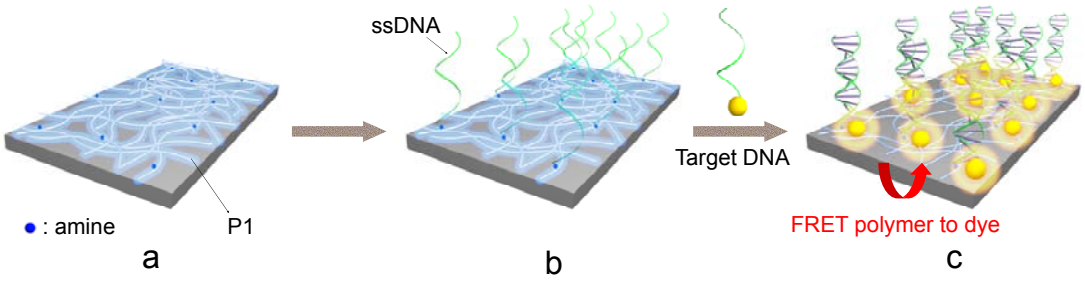

Figure 7-1. Schematic representation of the signal-amplifying conjugated polymer based DNA chip. a) **P1**-coated glass slide by covalent bonding, b) light-directed on-chip oligonucleotide synthesis, c) hybridization with a target DNA results in large emission enhancement of the fluorescent dye through efficient Förster resonance energy transfer.

Conjugated polymer-based biosensors are an attractive approach to improve the detection limit because an environmental change at a single site can affect the properties of the collective system, producing large signal amplification.[8-15] Therefore, if one devises a strategy combining the signal amplification scheme of conjugated polymers and the efficient on-chip DNA synthesis, signal amplifying DNA microarrays can be conveniently prepared. The on-chip oligonucleotide synthesis[7, 16-20] has a unique advantage of massively parallel fashion, flexible in sequence design, easy to manufacture, and having high sequence fidelity, compared to other recently developed methods, such as, the pin micro-dotting method,[6] the ink-jet micro-dropping method,[21] and the electrostatic addressing method.[22] Almost all the on chip DNA synthesis technologies, however, require harsh conditions such as long exposure to UV and/or to strong acids, polar and nonpolar solvents. Under these harsh conditions conventional conjugated polymers will be photo-bleached or chemically degraded.

7.3. Experimental Section

7.3.1. P1 synthesis

Materials and Methods for monomer and P1 synthesis. All solvents and reagents were used without further purification as received from Sigma-Aldrich Chemical Co. UV/Vis absorption spectra were recorded with a Varian Cary50 UV/Vis spectrophotometer. Photoluminescence spectra and quantum yield in solution and solid state were obtained by using PTI QuantaMaster™ spectrofluorometers equipped with an integrating sphere. Gel permeation chromatography (GPC) was used to determine number and weight average molecular weights and molecular weight distributions,

M_w/M_n, of the polymer samples with respect to polystyrene standards (Waters Corp.) in tetrahydrofuran as an eluent. ^{1}H NMR spectra (500 MHz) and ^{13}C NMR spectra (125 MHz) were obtained from Varian Inova 500 NMR instrumentation. High-resolution mass spectra were obtained from VG (Micromass) 70-250-S magnetic sector mass spectrometer. Melting point was measured by PerkinElmer differential scanning calorimetry (DSC7). Scheme 7-1 represents the overall synthetic routes for M1 and M3.

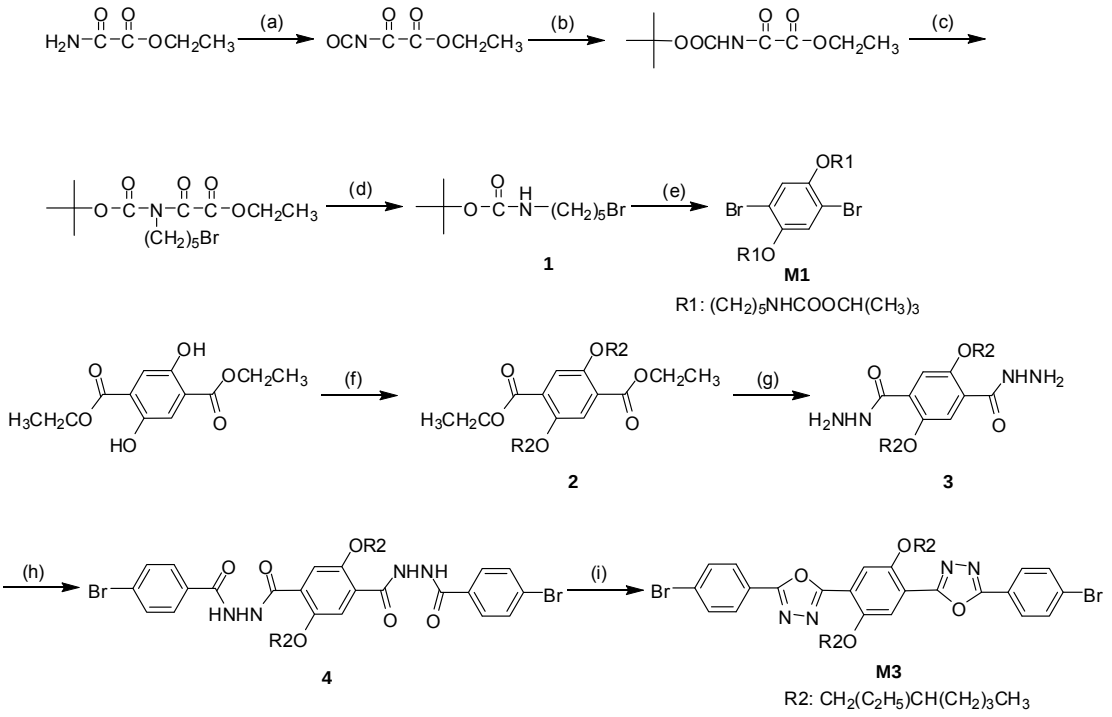

Scheme 7-1. Monomer synthesis: (a) Oxalyl chloride, methylene chloride, 0 °C → 25 °C, 12 h. (b) *t*-butanol, toluene, 0 °C → 40 °C, 15 min. (c) 1, 5-dibromopentane, *t*-BuOK, DMF, 40 °C, 1 h. (d) LiOH, THF, water, r. t., 3 h. (e) 2, 5-dibromohydroquinone, K_2CO_3, DMF, 70 °C, 48 h. (f) 2-Ethylhexylbromide, K_2CO_3, DMF, 80 °C, 48 h. (g) H_2NNH_2, ethanol, 78 °C, 24 h. (h) 4-bromobenzoyl chloride, pyridine, NMP, 12 h. (i) $POCl_3$, reflux, 12 h.

***N*-5-Bromopentyl *tert*-butyl carbamate (1).** The compound 1 was prepared by previous literature with slight modification of the length of alkyl side chain.[23] 25.6 mL Oxalyl chloride solution (50 mmol, 2 *M* in methylene chloride) was added to a 100 mL flask and it was cooled to 0 ^{o}C. Then, 5 g ethyl oxamate (43 mmol) was added to the reactor. The solution was refluxed overnight. After the removal of solvent and unreacted oxalyl chloride, the product was purified by vacuum distillation at 65-70 ^{o}C. The obtained product was 2.38 g (yield 39 %). To 2.38 g ethyloxalyl isocyanate dissolved in 20 mL toluene was added dropwise 1.7 g *tert*-butanol dissolved in 4 mL toluene at 0 ^{o}C. The solution was heated to 40 ^{o}C for 15 min. After the removal of solvent and remaining *tert*-butanol, the crude product was dried in vacuum. The obtained product was 3.55 g (yield 96 %). To a 100 mL flask were added 35 mL DMF, 3.55 g *N*-*tert*-butoxycarbonyl ethyl oxamate, and 1.83 g potassium *tert*-butoxide (16.3 mmol). The solution was stirred at 60 ^{o}C for 1 h, and then the solution was added dropwise to the reactor containing 37.6 g 1,5-dibromopentane (10 equiv to ethyl oxamate). The solution was stirred at 60 ^{o}C for 1 h. After the removal of the unreacted 1,5-dibromopentane under vacuum, the product was extracted with methylene chloride. The solution was washed with water and dried with $MgSO_4$. The crude product was purified by column chromatography using ethyl acetate/hexanes (1/4, v/v). The obtained product was 3.9 g (yield 81 %). To a 100 mL flask were added 50 mL THF, 3.9 g *N*-*tert*-butyloxycarbonyl *N*-5-bromopentyl ethyl oxamate, and 1.66 g LiOH (39.7 mmol) dissolved in 20 mL water. The solution was stirred at room temperature for 3 h. The solution was diluted with water and extracted with methylene chloride. The organic layer was dried with $MgSO_4$ and concentrated to give product. The obtained product was 2.9 g (yield 83 %). ^{1}H-NMR (500 MHz, $CDCl_3$):

δ/ppm 4.55 (broad s, 1H, N-H), 3.40 (t, 2 H, CH_2), 3.13 (m, 2H, CH_2), 1.5-1.85 (m, 6H, CH_2), 1.41 (s, 9H).

Synthesis of *tert*-butyl 5.5'-(2,5-dibromo-1,4-phenylene)bis(oxy)bis(pentane-5,1-diyl)dicarbamate (M1). To a 250 mL 2-neck round-bottomed flask equipped with condenser were added compound **1** (5.00 g, 18.8 mmol), 2,5-dibromohydroquinone (1.69 g, 6.26 mmol), and potassium carbonate (3.46 g, 25.0 mmol) in 20 ml of dimethylformamide (DMF). The flask was purged with extra pure Ar gas and placed in a 75 °C constant temperature oil bath. The reaction was carried out for 48 h with continuous stirring, and then cooled down. DMF was removed at reduced pressure by a rotary evaporator. The crude mixture was dissolved in chloroform and washed with water by extraction (4 times). The organic layer was dried by stirring with $MgSO_4$ and then filtered. The mixture was concentrated by the removal of chloroform. An additional purification was conducted by column chromatography. (ethyl acetate : hexane = 2 : 5 v/v). ^{1}H-NMR (500 MHz, $CDCl_3$): δ/ppm 7.07 (s, 2H, aromatic), 4.58 (broad s, 2H, N-H), 3.95 (t, 4H, CH_2), 3.15 (m, 4H, CH_2), 1.5-1.85 (m, 12H, CH_2), 1.41 (s, 18H). ^{13}C-NMR (125 MHz, $CDCl_3$): δ/ppm 160.0, 150.0, 118.5, 111,1, 79.1, 70.0, 40.4, 29.7, 28.7, 28.4, 23.2. HRMS (Voltage ES+) : calculated m/z of [M+Na]+ 659.1307; measured m/z 659.1315. Melting point: 98 °C.

Synthesis of 2,5-bis(2-ethylhexyloxy)terephthalohydrazide (**3**) 11.43 g of diethyl 2,5-bis(2-ethylhexyloxy)terephtalate (**2,** liquid at 25 °C, ^{1}H-NMR (500 MHz, $CDCl_3$): δ/ppm 7.34 (s, 2H, aromatic), 4.37 (q, 4H, -COOC<u>H</u>$_2$-), 3.89 (d, 4H, -OC<u>H</u>$_2$CH-), 1.73 (m, 2H, -C<u>H</u>-), 1.57-0.91 (m, 26H, alkyl), 0.90 (t, 6H). ^{13}C-NMR (125 MHz, $CDCl_3$): δ/ppm 166.4, 151.7, 124.5, 116.1, 71.8, 61.3, 39.5, 30.4, 29.1, 23.7, 23.0, 14.3,

14.1, 11.1. HRMS (Voltage ES+) : calculated m/z of [M+H]+ 479.3373; measured m/z 479.3361.), prepared with slight modification by previous literature[24], and hydrazine monohydrate (17 ml) were added into 100 ml anhydrous ethanol (99.5 %) and the mixture was stirred at 78 ^{o}C for 24 h. The mixture solution was cooled down and poured into 1800 ml water. Solids was collected by filtration and dried in vacuo. Additional recrystallization was done by ethanol to give a white cotton-like products of **3** (Yield: 46 %). ^{1}H-NMR (500 MHz, $CDCl_3$): δ/ppm 9.18 (s, 2H, NH), 7.85 (s, 2H, aromatic), 4.17 (s, 4H, NH_2), 4.08 (d, 4H, CH_2), 1.83 (m, 2H, CH), 1.21-1.54 (m, 16H, CH_2), 0.97 (s, 12H, CH3). ^{13}C-NMR (125 MHz, $CDCl_3$): δ/ppm 165.5, 151.0, 123.0, 115.7, 72.2, 39.4, 30.8, 29.0, 24.2, 23.0, 14.0, 11.1. HRMS (Voltage ES+) : calculated m/z of [M+H]+ 451.3284; measured m/z 451.3278. Melting point: 65 °C.

Synthesis of 5,5'-(2,5-bis(2-ethylhexyloxy)-1,4-phenylene)bis(2-(4-bromophenyl)-1,3,4-oxadiazole) (**M3**) To a 250 ml 2 neck round bottom flask were added compound **3** (4, 81 g, 10.7 mmol), 4-bromobenzoyl chloride (4,92 g, 22.47 mmol), pyridine (5 ml), and NMP 135 ml. After vigorous stirring for a while, the solution became a gel and the reaction continued overnight. The mixture was poured into 3000 ml of water and filtered to collect dihydrazide compound (**4**). Additional purification was done by recrystallization in chloroform. However, compound **4** showed a limited solubility in organic solvents, so reaction was proceed without further characterization. 7.63 g of compound **4** was dissolved in 150 ml of phosphorus oxychloride and the solution was refluxed for 24 hr. The mixture was poured into 1500 ml water and the appearing solids were collected by filtration and drying in-vacuo. White powder product (**M3**) was obtained from recrystallization in benzene (Yield: 76 %). ^{1}H-NMR (500 MHz,

$CDCl_3$): δ/ppm 8.04, 7,69 (dd, J= 175, 11 Hz, 8H, aromatic), 7.86 (s, 2H, aromatic), 4.08 (d, 4H, CH_2), 1.84 (m, 2H, CH), 1.29-1.67 (m, 16H, CH_2), 0.96 (t, 6H, CH_3), 0.90 (t, 6H, CH_3). ^{13}C-NMR (125 MHz, $CDCl_3$): δ/ppm 164.7, 163.6, 151.0, 132.4, 128.4, 126.5, 122.9, 116.4, 114.4, 71.8, 39.7, 30.4, 29.1, 23.8, 23.0, 14.1, 11.2. HRMS (Voltage ES+) : calculated m/z of [M+H]+ 779.1808; measured m/z 779.1835. Melting point: 168 °C.

Polymer Synthesis (**P1**) To a 50 ml of Schlenk flask were added **M1** (132.8 mg, 0.208 mmol), **M2** (232.3 mg, 0.416 mmol), **M3** (162.4 mg, 0.208 mmol), THF (9ml) and 1M K_2CO_3 (5 ml). Degassed tetrakis(triphenylphosphine)palladium(0) (5 mol%) in THF (1 ml), prepared in a separate Schlenk, was transferred to the monomer mixture by cannula and the monomer solution was degassed by several cycles of vacuum and argon purging. Polymerization was carried out at 80 °C for 36 h. The solution of the reaction mixture was precipitated in 100 ml of methanol and filtered. Solid product was washed by water and acetone 3 times. Further purification was done by extraction with chloroform/water to give precursor polymer. 10 ml of trifluoroacetic acid (TFA) was carefully added to polymer in chloroform (10 ml) and the polymer solution was stirred at room temperature for 6 h to cleave *t*-BOC group. After evaporation of solvent and TFA, the polymer was re-dissolved in chloroform and washed with 1 M KOH solution, followed by NaCl, and deionized water to give yellow polymer (**P1**) (Yield: 120 mg). ^{1}H-NMR (500 MHz, $CDCl_3$): δ/ppm 8.29 (d, 4H, aromatic), 7.93 (d, 4H, aromatic), 7.5-7.9 (m, 14H, aromatic), 7.10 (s, 2H, aromatic), 4.15 (d, 4H, CH_2), 3.95 (t, 4H, CH_2), 3.08 (m, 4H, CH_2), 2.09 (broad s, 4H, NH_2), 1.91 (m, 2H, CH), 1.12-1.83 (m, 84H, CH_2), 1.01 (t, 6H, CH_3), 0.93 (t, 6H, CH_3), 0.80 (t, 12H, CH_3). The number/weight average molecular

weight was calculated with the polymer before cleavage of *t*-BOC due to the limited solubility of **P1** in tetrahydrofuran as a GPC eluent, M_n = 51,000, PDI = 4.4.

7.3.2. DNA Chip Fabrication

Polymer immobilization onto a glass substrate. A glass slide (25 mm × 75 mm) was dipped in $NH_4OH/H_2O_2/H_2O$ (40 ml/40 ml/160 ml) at 80 °C for 1 h and rinsed with DI water (30 ml). After drying, the slide was soaked in pirahna solution (H_2SO_4 : H_2O_2 = 35 ml : 15 ml) for overnight, washed with DI water (30 ml) and dried with a stream of air. It was transferred into a solution of 97% aminopropyltrimethoxysilane (APTMS) (2 ml), DI water (2 ml), and methanol (48 ml) and sonicated for 30 min. It was rinsed with methanol (30 ml) and water (30 ml), and then dried with a stream of air. The slide was baked at 120 °C for 30 min. Amino-functionalized glass slide was reacted with 1,4-diphenylenediisothiocyanate (100 mg) in dimethylformamide (DMF) (54 ml) and pyridine (6 ml) for 2 h. It was washed with 30 ml of DMF, 30 ml of methylenechloride and dried. Only one side of the slide was reacted with **P1** (2 mg) in pyridine (0.5 ml) and chloroform (9 ml). The slide was subsequently washed with chloroform, methylene chlorides, and DI water. Further cleaning steps of the slide were achieved by sonication in chloroform for 5 min and drying in a vacuum oven. For comparison of FRET efficiency, an amine functionalized glass slide without **P1** (a glass after step in Scheme 7-2) was used as a control slide.

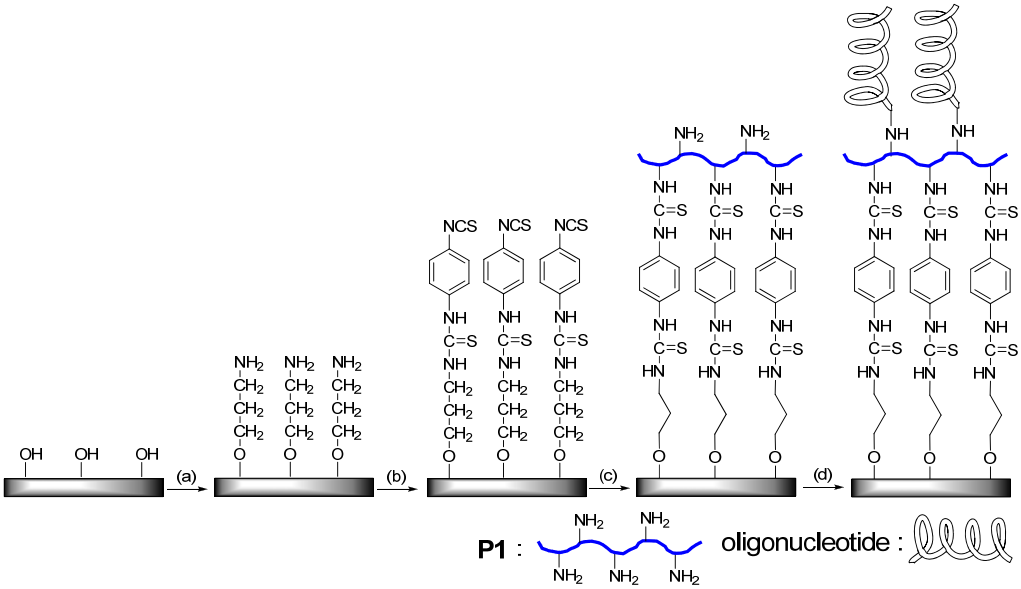

Scheme 7-2. Light-directed parallel on-chip DNA synthesis on P1-immobilized glass: a) APTMS, b) 1,4-phenylenediisothiocyanate, c) polymer (**P1**), and d) cyclic procedures of oligo synthesis.

Light directed on-chip oligonucleotide synthesis. The glass slide was enclosed in a holder connected to a DNA synthesizer. Oligonucleotide synthesis was performed using the standard phosphoramidite chemistry[25] except for the deprotection step, where a photogenerated acid (PGA) was used to deprotect the terminal dimethoxytrityl protecting group at selected reaction sites (Figure 7-2).[17,26] The synthesizer is coupled to an optical unit for digital photolithographic projection using a Digital Light Projector (Texas Instruments). At each deprotection step, the slide holder was filled with the PGA precursor solution in CH_2Cl_2 and a predetermined light pattern was projected onto the device surface to trigger the formation of acid. The DNA synthesis reagents were obtained from Glen Research. A DNA patterned image after hybridization was obtained from a GenePix 4000B microarray scanner (Molecular Devices Corp.) with dual lasers (532 nm/17 mW, 635 nm/10mW).

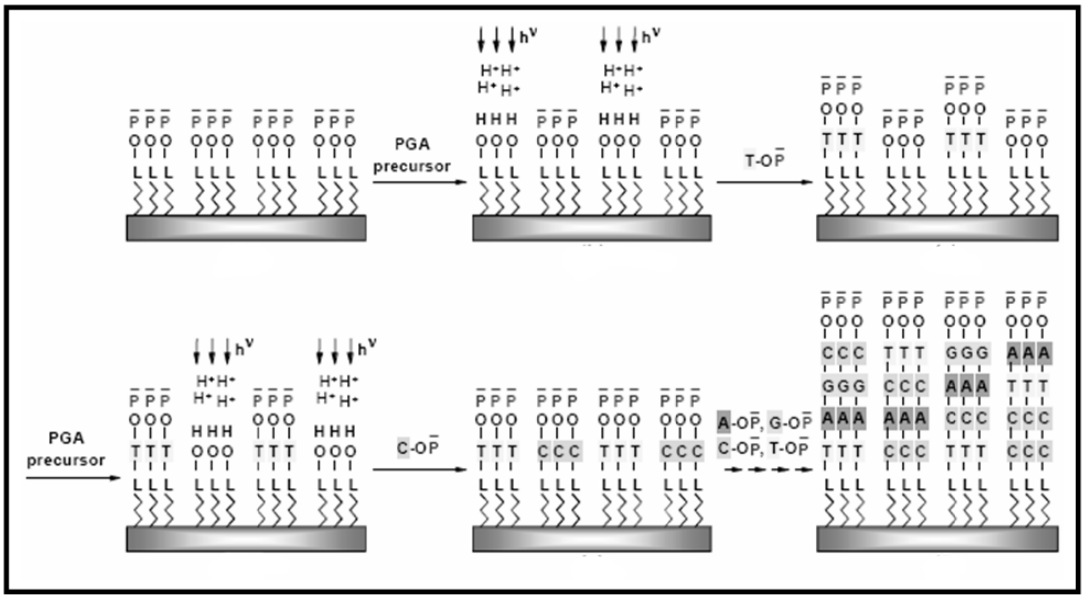

Figure 7-2. Schematic representation of light directed on-chip oligonucleotide synthesis.

7.3.3. Hybridization Test

Hybridization Test and Analysis. 1 ml of 6×SSPE (900 mM sodium chloride, 60 mM sodium hydrogen phosphate, 6 mM EDTA, pH 7.4) was added onto the slide and removed after 5 min. 150 µl (20×SSPE/Acetylated BSA/water = 3/1/6) of SSPE solution was dropped onto the slide and removed. Hybridization solution (20×SSPE: 15 µl, Acetylated BSA: 5 µl, water: 29 µl, HEX-labeled DNA, 5'-HEX-aca cat cac gga tgt-3': 0.5 µl, Cy5-labeledDNA, 5'-gaa ata atg ctt cgt cga tat tag act tct act gcg gat cat aca-Cy5-3': 0.5 µl) was heated to 65 °C to prevent loop formation of the target oligo. 2-3 drops of the hybridization solution of analyte DNA were applied onto the slide. The slide was kept in a humid chamber and incubated at 25 °C for 1 h. The slide was rinsed with 6×SSPE and iced water and dried with a stream of air. The slide was examined by using a

fluorescence scanner and PL intensity before and after hybridization was investigated by using a fluorescent spectrophotometer (PTI QuantaMaster™ Spectrofluorometers with an integrating sphere). Hybridization tests with 1-mismatch (5'-HEX-aca cat ctc gga tgt-3') and a non-complementary DNA (5'-HEX-tgt gta gtg cct aca-3') were also conducted in the same condition as for the complementary DNA. The fluorescence images in Figure 7-7 inset were obtained by using BX41 Fluorescence microscope, DP71 digital camera (Olympus), and Microsuite 5 Biological Suite Software (Olympus) and are background (prehybridization) subtracted. Direct excitation of the dye and **P1** excitation for amplification were carried out at 500 nm and 405 nm, respectively.

Dimethyltrityl (DMT) quantification to measure the density of DNA on chips. The amount of DMT, cleaved from the final cycle of oligo synthesis was measured by UV spectroscopy in order to compare the density of oligonucleotides synthesized on the P1-coated glass with the oligo density on the control (amine modified glass without **P1**). 0.1 M of *p*-toluenesulfonic acid monohydrate (TSA) (4 ml) was prepared in anhydrous acetonitrile and was treated to glass slides for 1 min. The DMT solution was measured by UV spectroscopy in order to quantify DMT concentration. This solution is easier to pipet than solutions containing methylene chloride and is acidic enough to neutralize any residual base. DMT absorption was determined by scanning from 400 nm to 600 nm by UV (Figure 7-3). A major peak corresponding to a DMT cation appears at 500 nm. There is a second peak at 410 nm with an extinction coefficient of 28,690.

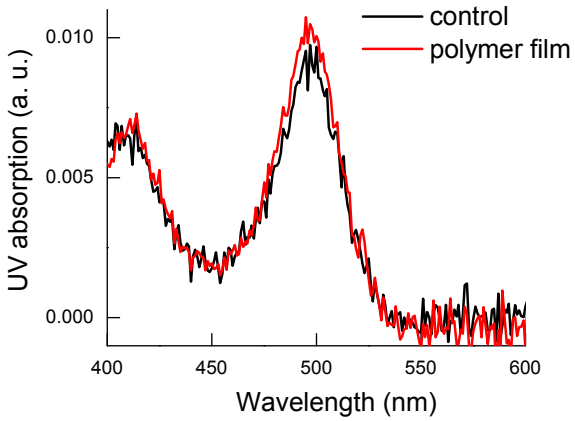

Figure 7-3. UV absorbance for DMT quantification

In Beer's law, the molar absorptivity (or extinction coefficient) is constant and the absorbance is proportional to concentration for a given DMT dissolved in a given solvent and measured at a given wavelength (410 nm).

$$A=\varepsilon \cdot b \cdot c$$

where A is the absorbance (no units, since $A=\log_{10}P_0/P$)

ε is the molar absorptivity with units of $L \cdot mol^{-1} \cdot cm^{-1}$

b is the path length of the sample (cm, 1 cm cuvette)

c is the concentration of the DMT in acetonitrile, expressed in $mol \cdot L^{-1}$.

The surface concentration of oligonucleotide in the slides (20 cm x 20 cm) measured using this equation is 2.44 $pmol \cdot cm^{-2}$. Both the polymer and control slide have similar numbers in oligo concentration.

Detection limit study. Figure 7-4 showed the result of our detection limit study. In the picomolar concentration regime the fluorescence intensity from the target DNA slightly increases. From 10^{-10} molar concentration the signal intensity becomes

significantly larger than the baseline. Therefore, the detection limit should be about 10^{-10} M or 20 picogram of the target DNA in 50 μl solution.

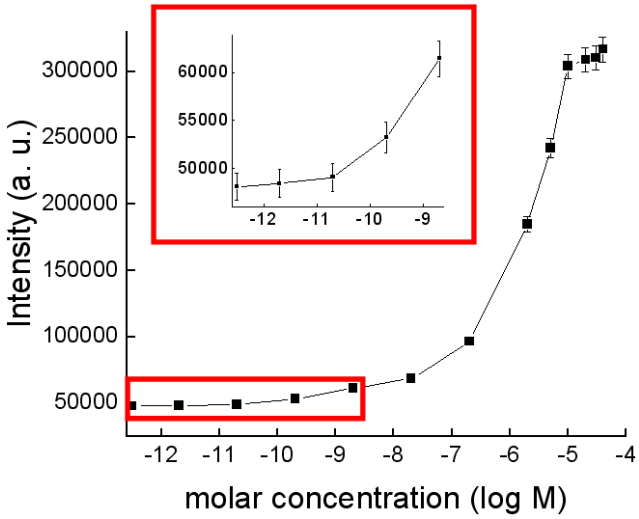

Figure 7-4. Profile of fluorescence intensity upon change of target DNA concentration.

7.4. Results and Discussion

We have developed a novel conjugated polymer having a strong fluorescent emission and unique stability under the above-mentioned harsh conditions. Scheme 7-3 shows the chemical structure of the poly(oxadiazole-co-phenylene-co-fluorene) (**P1**) with oxadiazole units and amine side chains. All monomer units of **P1** were designed to have their own contribution to the final property of **P1** and synthesized through multiple synthetic steps. Oxadiazole is an electron-poor heterocyclic molecule that has been used in polymer design in which the improvement of electron transport and/or stability of the polymer are required.[27-29] We designed an oxadiazole-containing monomer (**M3**) and incorporated this unit into the conjugated polymer backbone by using Pd-based Suzuki coupling method.[30] The oxadiazole-containing monomer unit **M3** of **P1** has an intense

blue fluorescence emission at 413 nm in a chloroform solution and is stable when exposed to strong UV irradiation and a strong acidic environment. The amine groups on the phenylene unit (**M1**) of **P1** serve as functional groups for immobilization of **P1** on a glass substrate as well as linkers for direct on-chip synthesis of oligonucleotides on the resulting thin-layer film of **P1**. The fluorene unit (**M2**) of **P1** is incorporated to provide a good solubility in organic solvents and to ensure a good spectral overlap with commonly used organic dyes for an efficient fluorescent resonance energy transfer (FRET).

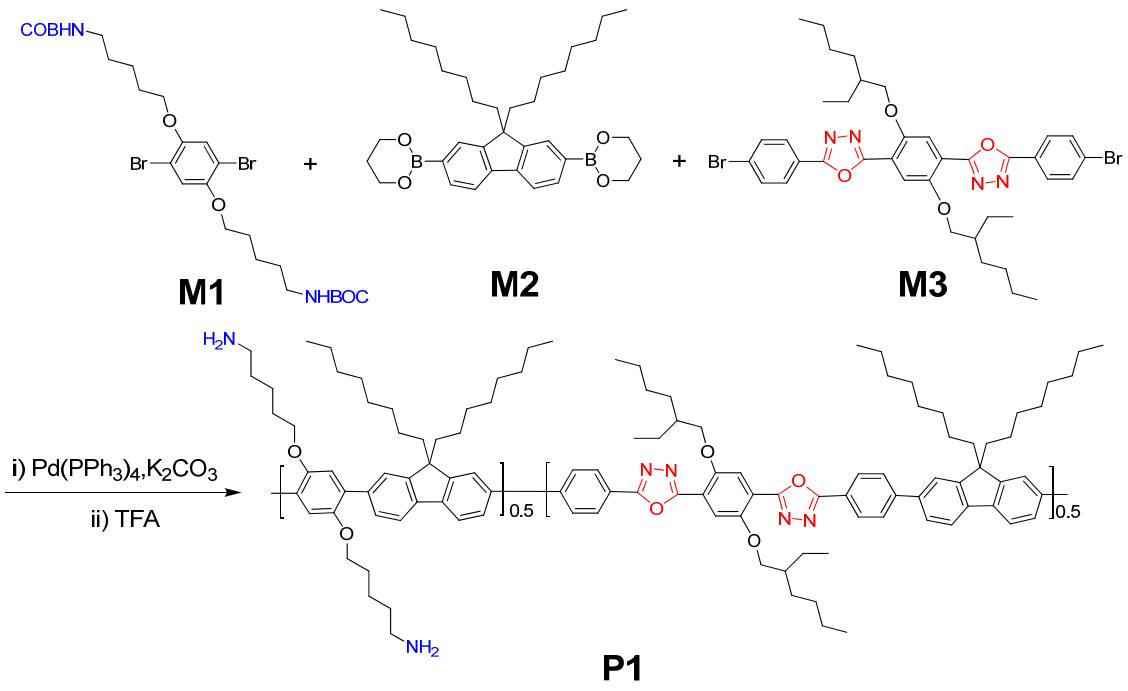

Scheme 7-3. Chemical structure of **P1**.

Figure 7-5 shows the absorption (UV) and photoluminescence spectra (PL) of **P1** in chloroform and incorporated in the film. The absolute quantum yield of **P1** solution in chloroform (1 mg L^{-1}), measured in an integrating sphere (PTI technologies, Inc.), was 94

%. We investigated the stability of **P1** compared with commonly used conjugated polymers, such as, poly(*p*-phenyleneethynylene)s and poly(3-hexyl thiophene), under strong UV and highly acidic conditions. None of the compounds except **P1** survived these tests (See Chapter 6). The fluorescence of the conventional conjugated polymers was completely quenched by degradation of polymers under these harsh conditions. However, **P1** showed unique stability against the exposure to UV irradiation and acid treatments both in the solution and solid state. The unique stability of **P1** made possible on-chip DNA synthesis directly on a thin film of the conjugated polymer.

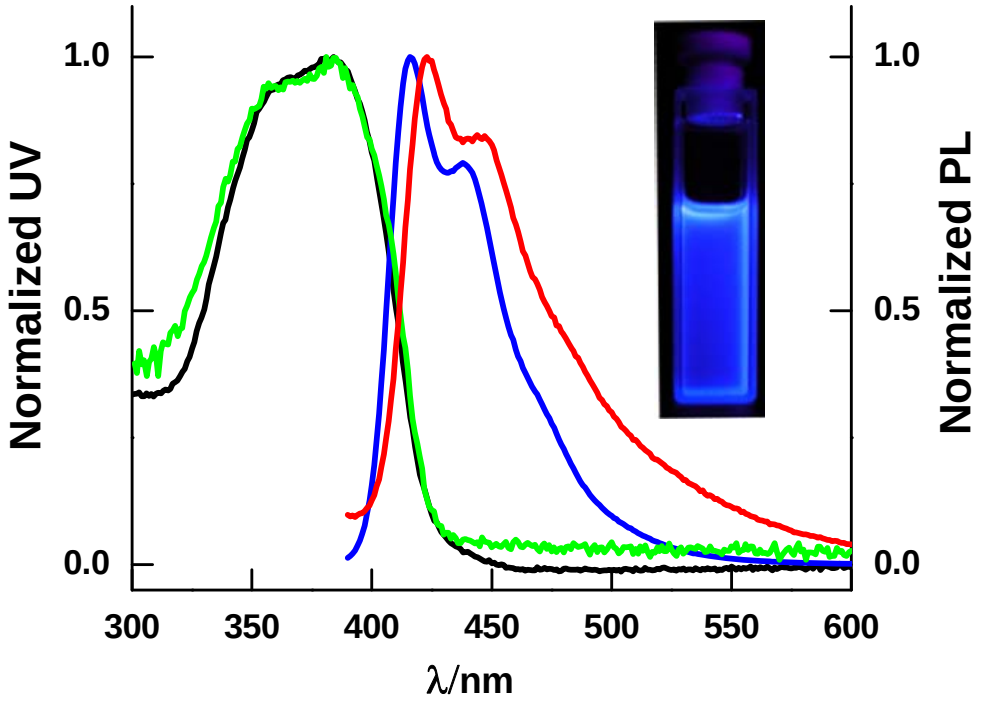

Figure 7-5. UV and PL spectra of **P1** in chloroform (black = UV, blue = PL) and solid film (green = UV, red = PL).

The Preparation of **P1**-coated glass substrates is described in Scheme 7-2. We covalently linked **P1** to a glass substrate to prevent any loss of **P1** during the on-chip DNA synthesis. To do so, isothiocyanate-functionalized glass substrates were prepared by using a slightly modified literature procedure.[12] First, aminopropyl groups were introduced onto a glass substrate by first cleaning with pirahna solution (H_2O_2 : H_2SO_4 3:7 (v:v)), followed by aminopropyltrimethoxysilane (APTMS) coating. 1,4-phenylenediisothiocyanate was then reacted with the amine of APTMS to form a reactive linker for **P1**. Finally, **P1** was chemically bound onto the glass substrate. After immobilization of **P1**, the derived UV spectrum of the glass substrate showed a new broad band at 350-400 nm, which corresponds to **P1** absorption. Fluorescence spectroscopy also showed a well-defined fluorescence emission spectrum of **P1** from the glass substrate.

The light-directed on-chip DNA synthesis on the **P1**-coated glass substrate was conducted. In this research, we used the efficient phosphoramidite chemistry developed in the early 1980s by Caruthers for the oligonucleotide synthesis.[31] This method has been proven to be robust, reliable, scalable, and most efficient. The on-chip DNA synthesis was conducted by using a modified automatic oligo-synthesizer equipped with a UV patterning device. The synthesis is carried out using 5'-(4,4'-dimethoxytrityl) (DMT) nucleophosphorarmidite monomers as the building blocks and each synthesis cycle consists of a deprotection step by using photogenerated acids, coupling of a DMT-protected monomer, capping of unreacted terminal OH groups, and oxidation of the phosphite to phosphatetriester at internucleotide linkages.[17,32] Various sequences of DNA can be synthesized at different locations on the chip by generating a strong acid at the

desired locations by UV-induced decomposition of a photo-acid-generator (PAG). The photogenerated acid (PGA) then catalyzes the deprotection reaction, producing a 5'-OH group, which is available for the next monomer. We synthesized two different sequences. The first sequence was 5'-ACA TCC GTG ATG TGT T-glass-3' (the 3' T is a spacer), which was used for hybridization with the complementary sequence with HEX (hexachloro-fluorescein) dye and the second sequence was 5-ACG AAG CAT TAT TTC T-glass-3' for the Cy5-labeled complementary sequence.

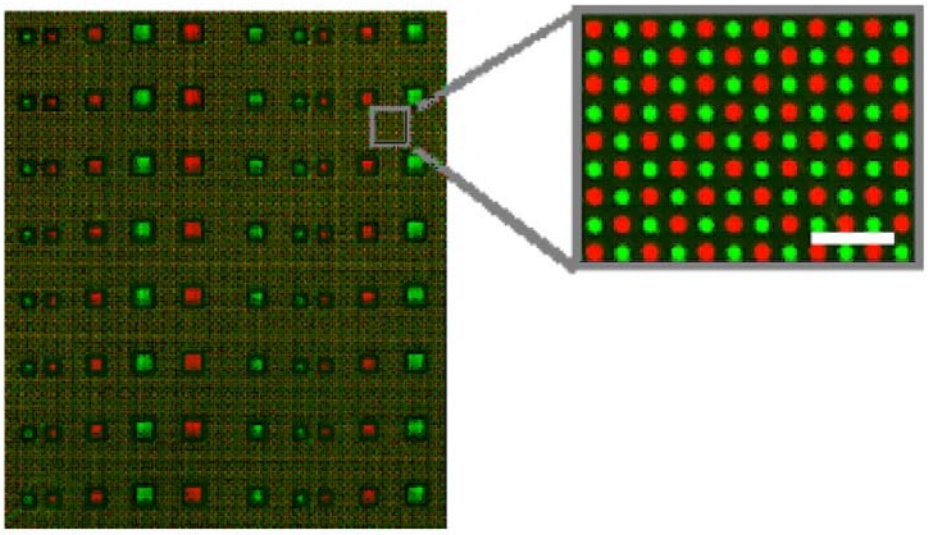

Figure 7-6. A fluorescence image of a patterned signal-amplifying DNA microarray with two different DNA sequences after hybridization with a mixture of c-DNA-HEX (green) and c-DNA-Cy5 (red; scale bar: 200 um).

Figure 7-6 shows the fluorescent image of the synthesized DNA on the **P1**-coated glass substrate after hybridization with two different dye-labeled complementary DNA molecules. Selective fluorescent patterns of green (HEX) and red (Cy-5) dots are clearly shown in the Figure 7-6. This result demonstrates that direct on-chip DNA synthesis onto

a **P1**-coated glass slide was macroscopically accomplished. Moreover, during the harsh DNA synthesis procedures, the emissive property of **P1** was maintained. We prepared a control sample to conduct quantitative analysis of signal amplification by **P1**. The control sample had the same 16 base DNA sequence (5'-ACA TCC GTG ATG TGT T-glass-3', the 3' T is a spacer) as was synthesized on an amine-functionalized glass slide, but without **P1**. The density of the synthesized oligonucleotide (2.44 pmol·cm^{-2}) on the conventional control slide was the same as that of the oligo on the P1-coated slide. This was confirmed by UV absorption at 410 nm.

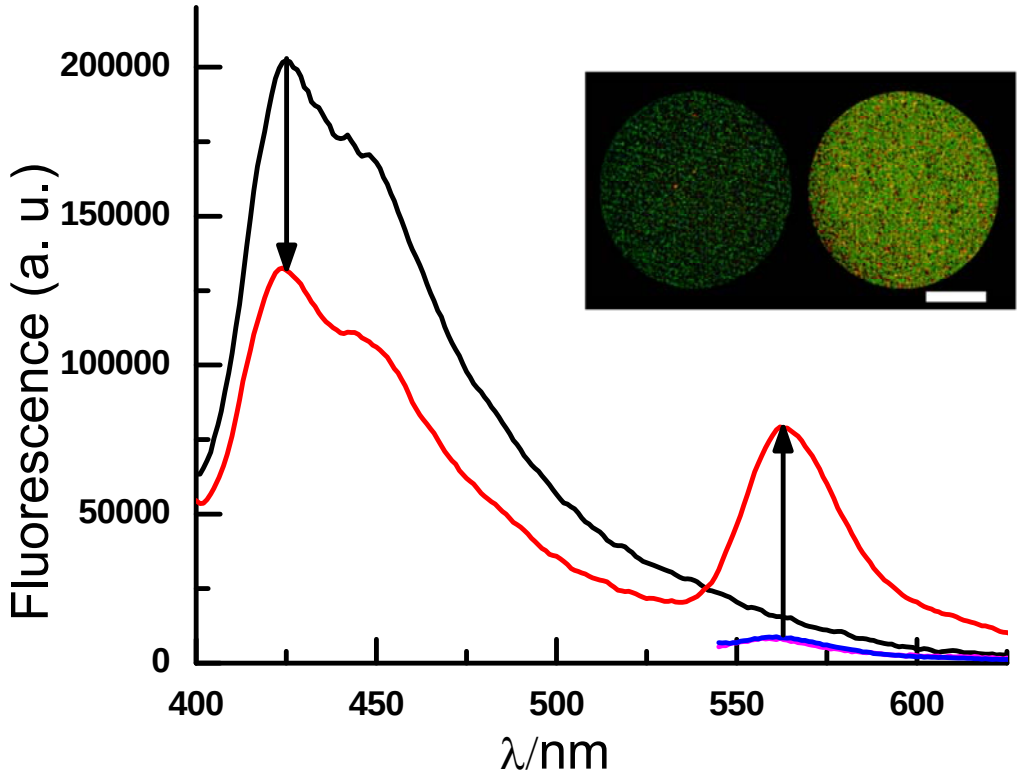

Figure 7-7. PL emission spectra of P1 substrate before (black) and after hybridization when excited at 380 nm (red) and 535 nm (blue); PL emission of the control (pink, excited at 535 nm). Note that the blue and pink lines are essentially superimposed and

appear around 550-625 nm. Inset: comparison of fluorescence intensity upon excitation at 535 nm (left) and 405 nm (right). Scale bar: 25 μm.

We used a 15 base HEX-labeled complementary DNA sequence to observe the FRET effect from **P1** to HEX dye. FRET involves a nonradiative transmission of fluorescence energy from a donor molecule to the acceptor molecule. Therefore, the signature of FRET is quenching of the higher energy fluorophore followed by amplified emission from the acceptor fluorophore having the lower energy. FRET is also influenced by the spectral overlapping between the donor emission and the acceptor absorption. **P1** has a good spectral overlap with HEX, satisfying the requirement for efficient FRET. Figure 7-7 shows the fluorescent emission spectrum of the **P1**- coated DNA chip and the control slide before and after hybridization with the HEX-labeled complementary DNA (c-DNA-HEX). Upon hybridization tests with c-DNA-HEX on the signal amplifying **P1**-immobilized DNA chip, one can observe a large signal amplification. The fluorescence emission of **P1** was decreased when excited at 380 nm, whereas the emission of HEX was significantly amplified. Direct excitation of HEX at 535 nm produced only a weak fluorescence emission as shown in Figure 7-7. This large signal amplification clearly indicates an efficient fluorescence resonance energy transfer from **P1** to HEX. The detection limit of our signal-amplifying DNA microarray is 10^{-10} M. We conducted the same hybridization test on the control slide. Direct excitation of HEX at its absorption maximum (λ_{max}) of 535 nm produced the same weak fluorescence emission as obtained from the direct excitation of the **P1**-immibilized DNA chip at 535 nm. This result also indicates that the density of DNA on the **P1**-immibilized DNA chip is the same as that of the conventionally prepared control slide.

Selectivity test was also done with HEX-labeled one-mismatch DNA (5'-HEX-ACA CAT CTC GGA TGT-3') and a HEX-labeled non-complementary DNA (5'-HEX-TGT GTA GTG CCT ACA-3'). Figure 7-8 shows the relative fluorescence intensity of HEX on the complementary and one-mismatch DNA compared to that of the noncomplementary DNA, demonstrating the selectivity of the signal amplifying conjugated polymer-based DNA microarray.

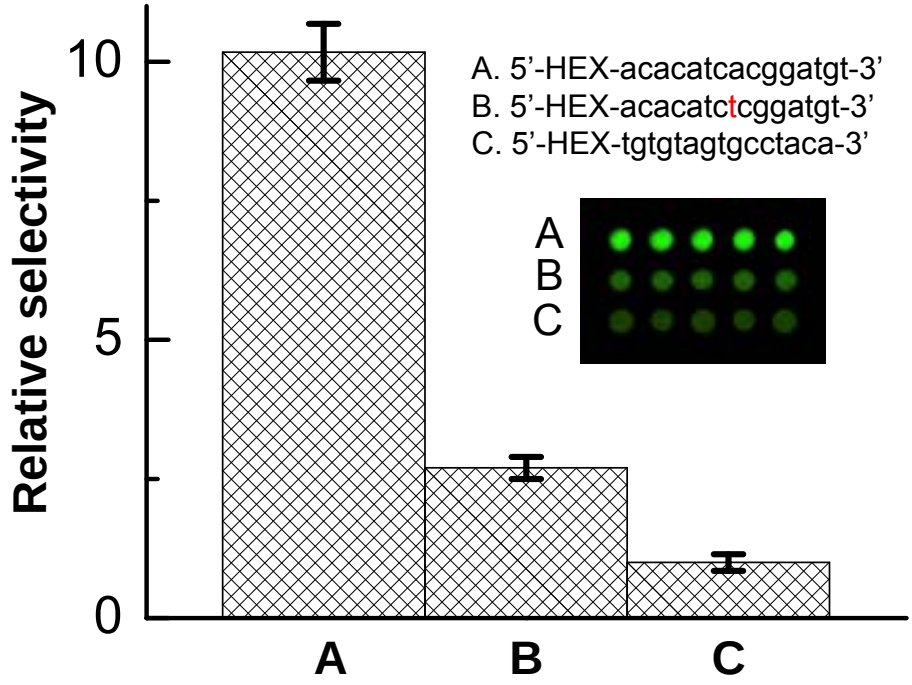

Figure 7-8. Selectivity test: A) perfect match, B) one mismatch, and C) random sequence. Inset: A microscanned image, from the top row down: perfect match, one mismatch, and random sequence. The spot diameter is 55 μm. I_f = fluorescence intensity.

7.5. Conclusion

We have established a fast and readily applicable strategy to make a signal amplifying DNA microarray by developing a novel conjugated polymer and combining

the efficient and convenient on-chip DNA synthesis. The newly developed conjugated poly(oxadiazole-co-phenylene-co-fluorene) is highly emissive and has unique stability in harsh environments. DNA hybridization tests showed a good selectivity and a large signal amplification achieved by an efficient FRET from the emissive conjugated polymer to the dye-labeled target DNA. The results provide a design principle for further development of self-signal amplifying DNA microarray that possibly allow PCR-free DNA detection through a large signal amplification. Based on the developed signal amplifying strategy we are discussing a design strategy to achieve self-signaling property for label-free detection by combining intercalating dye (Chapter 8) the molecular beacon (Chapter 9) concept and the newly developed conjugated poly(oxadiazole-co-phenylene-co-fluorene).

7.6. References

1. Langer, R.; Tirrell, D. A. Designing materials for biology and medicine. *Nature* **2004**, *428*, 487.

2. Storhoff, J. J.; Mirkin, C. A. *Chem. Rev*. **1999**, *99*, 1849.

3. Sanghvi, A. B.; Miller, K. P.-H.; Belcher, A. M.; Schmidt, C. E. *Nature Mater*. **2005**, *496*, 496.

4. Breaker, R. B. *Nature*, **2004**, *432*, 838.

5. Service, R. F. *Science* **1998**, *282*, 396.

6. Schena, M.; Shalon, D.; Davis, R. W.; Brown, P. O. *Science* **1995**, *270*, 467.

7. McGall, G.; Labadie, J.; Brock, P.; Wallraff, G.; Nguyen, T.; Hinsberg, W. *Proc. Natl. Acad. Sci. USA* **1996**, *93*, 13555.

8. McQuade, D. T.; Pullen, A. E.; Swager, T. M. *Chem. Rev*. **2000**, *100*, 2537.

9. Heeger, P. S.; Heeger, A. J. *Proc. Natl. Acad. Sci. USA* **1999**, *96*, 12219.

10. Peter, K.; Nilsson, R.; Inganäs, O. *Nature Mater*. **2003**, *2*, 419.

11. Ho, H.-A.; Boissinot, M.; Bergeron, M. G.; Corbeil, G.; Doré, K.; Boudreau, D.; Leclerc, M. *Angew. Chem. Int. Ed*. **2002**, *41*, 1548.

12. Liu, B.; Bazan, G. C. *Proc. Natl. Acad. Sci. USA* **2005**, *102*, 589.

13. Chen, L.; McBranch, D. W.; Wang, H.-L.; Helgeson, R.; Wudl, F.; Whitten, D. G. *Proc. Natl. Acad. Sci. USA* **1999**, *96*, 12287.

14. Haskin-Glusac, K.; Pinto, M. R.; Tan, C.; Schanze, K. S. *J. Am. Chem. Soc*. **2004**, *126*, 14964.

15. Pun, C. C.; Lee, K.; Kim, H.-J.; Kim, J. *Macromolecules*, **2006**, *39*, 7461.

16. Fodor, S. P.; Read, J. L.; Pirrung, M. C.; Stryer, L.; Lu, A. T.; Solas, D. *Science* **1991**, *251*, 767.

17. Gao, X.; LeProust, E.; Zhang, H.; Srivannavit, O.; Gulari, E.; Yu, P.; Nishiguchi, C.; Xiang, Q.; Zhou, X. *Nucleic Acids Res*. **2001**, *29*, 4744.

18. Komolpis, K.; Srivannavit, O.; Gulari, E. *Biotechnol. Prog*. **2002**, *18*, 641.

19. Rouillard, J.-M.; Zuker, M.; Gulari, E. *Nucleic Acids Res*. **2003**, *31*, 3057.

20. Gao, X.; Zhou, X.; Gulari, E. *Proteomics* **2003**, *3*, 2135.

21. Blanchard, A. P.; Kaiser, R. J.; Hood, L. E. *Biosens. Bioelectron*. **1996**, *11*, 687.

22. Cheng, J.; Sheldon, E. L.; Wu, L.; Uribe, A.; Gerrue, L. O.; Carrino, J.; Heller, M. J.; O'Connell, J. P. *Nat. Biotechnol*. **1998**, *16*, 541.

23. Berree, F.; Bazureau, J.-P.; Michelot, G.; Le Corre, M. *Synth. Commun.* **1999**, *29*, 2685.

24. Wu, T.-Y.; Sheu, R.-B.; Chen, Y. *Macromolecules* **2004**, *37*, 725.

25. McBride, L. J.; Caruthers, M. H. *Tetrahedron Letters* **1983**, *24*, 245.

26. Hornbeck, L. J. *SPIE Eur. Proc*. **1996**, *2783*, 135.

27. Bolton, O. J.; Kim, J. *J. Mater. Chem*. **2007**, *17*, 1981.

28. Li, X.-C.; Spencer, G. C. W.; Holmes, A. B.; Moratti, S. C.; Cacialli, F.; Friend, R. H. *Synth. Met*. **1996**, *76*, 153.

29. Peng, Z.; Bao, Z.; Galvin, M. E. *Adv. Mater*. **1998**, *10*, 680.

30. Miyaura, N.; Suzuki, A. *Chem. Rev*. **1995**, *95*, 2457.

31. McBride, L. J.; Caruthers, M. H. *Tetrahedron Letters* **1983**, *24*, 245.

32. Gao, X.; Yu, P.; Proust, E.; Sonigo, L.; Pellois, J. P.; Zhang, H. *J. Am. Chem. Soc*. **1998**, *120*, 12689.

CHAPTER 8

Sensitive and Selective Label-free DNA Detection by Conjugated Polymer-based Microarray and Intercalating Dye

Parts of this chapter appear in: Lee, K.; Maisel, K.; Rouillard, J.-M.; Gulari, E.; Kim, J. Published in *Chem. Mater*. **2008**, *20*, 2848.

8.1. Abstract

DNA microarray has a great deal of potential due to several features of which microarray technology are advantageous to its use, which are fast, facile, relatively chip to use, and simultaneously detectable for many genes. However, for clinically-convenient application, it is desirable to invent a method that is sensitive, label-free, and readily applicable to the detection of all un-labeled genomes. We developed a label-free and signal amplifying DNA microarray detection method using highly fluorescent conjugated polymers (POX1) and an intercalating dye SYBR green I. A conjugated polymer (POX1) having unique stability in rigorous conditions and its application for signal amplifying DNA chips has been previously prepared. Highly fluorescent POX1 polymers were covalently attached to a glass slide and oligonucleotides were directly synthesized on emissive polymer-coated microarray substrate using photogenerated acid. Efficient fluorescence resonance energy transfer (FRET) from POX1 to SYBR green I was clearly shown in order to amplify the signal upon hybridization with complementary target DNA in the presence of SYBR green I. Selectivity test results with 1-mismatch and non-complementary DNA presents that this polymer-DNA hybrid chip can enhance efficiently signal of a conventional DNA chip to lower the false signal from target analytes.

8.2. Introduction

DNA microarrays are a unique and powerful tool in biomedical research for sequencing the human genome, understanding the gene expression, and developing diagnostic tests of genetic diseases by means of selective detection of specific DNA sequences.[1-5] Convenient solid-state, on-chip DNA synthesis has contributed significantly to the fast progress of DNA microarray development. There has also been recent effort to improve sensitivity by applying the energy harvesting and signal transduction property of conjugated polymers to DNA detection.[6-10] A label-free detection strategy also has gained much interest because it can provide fast and cost-effective DNA detection.[11-16] Among the label-free detection methods are protease-based detection, molecular beacon system, and the use of intercalating dyes.[15,17-20]

Intercalating dyes are fluorescent molecules that preferably bind to the major groove of a double helix DNA over single strand DNA (ssDNA). SYBR green I, an intercalating dye, is an asymmetrical cyanine dye having a high quantum yield of 0.80 that is 100 times larger than that of ethidium bromide, a commonly used intercalating dye, and is also much less mutagenic than ethidium bromide. However, SYBR green I like other intercalating dyes can also stain ssDNA as the amount of SYBR green I required for double stranded DNA detection increases because its specificity toward double helix DNAs is not perfect. Hence, this non-specific binding is a critical problem when only a trace amount of analyte DNA is available for detection. In this case, a large amount of the dye is required to produce a distinguishably strong signal but the large amount of dye can reduce specificity.

We have developed a series of uniquely stable oxadiazole-containing conjugated polymers toward photo-bleaching and chemical degradation and established an on-chip DNA synthesis strategy on thin-layers of these oxadiazole-containing conjugated polymers.[12,21] By achieving efficient fluorescence resonance energy transfer (FRET) from the polymer layer to the dye-labeled DNA we have shown a large signal amplification. Energy-harvesting property of the conjugated polymer made it possible to transfer larger amount of energy from the polymer to dye. The system represented the enhancement of the sensitivity and selectivity in DNA-chip. In all of these cases, the resulting synthesized probing single stranded oligonucleotides is not able to generate sensory signal by itself. Therefore, the intensity of a sensory signal absolutely relies on the number of bound analyte ssDNA with fluorescent dye labeling, limiting the sensitivity. Therefore, a label-free detection technique rendering self-signaling and signal amplification is desirable for accurate and fast analysis particularly when the analyte concentration is low. Based on the previous result, in this Chapter, we present signal amplifying DNA microarrays having label-free DNA detection capability by combining the signal amplification scheme of the conjugated polymer (POX1)-based DNA microarray and the intercalating dye, SYBR green I. Because the emission signal from SYBR green I can be largely amplified by the FRET-based signal amplification mechanism, even a small amount of SYBR green I can produce a strong enough emission signal without losing the specificity as schematically illustrated in Scheme 8-1.

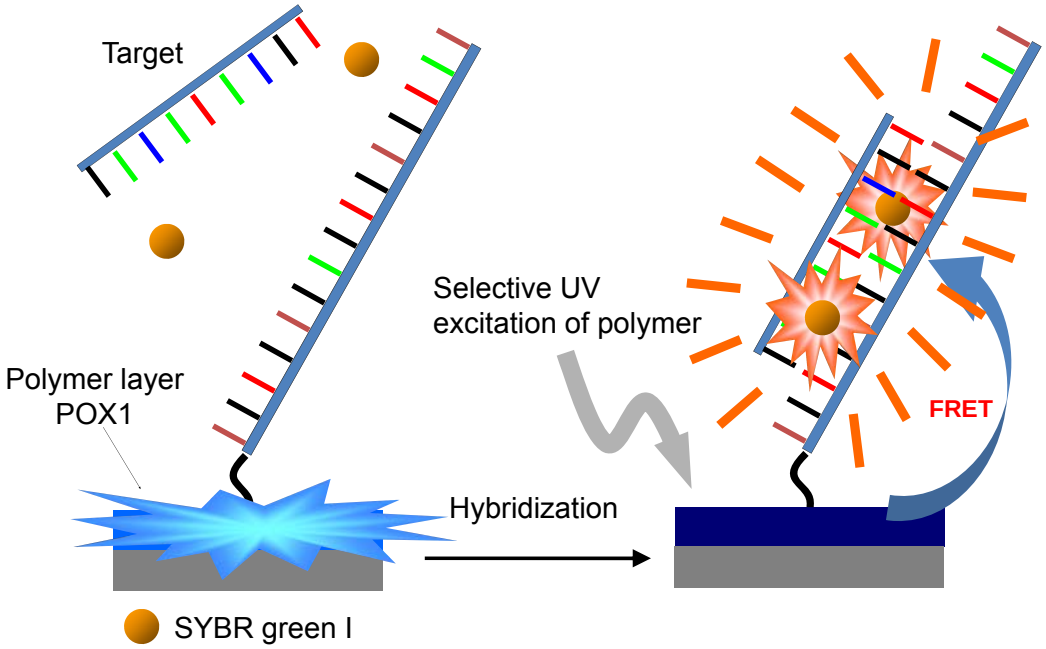

Scheme 8-1. A label-free conjugated polymer-DNA hybrid microarray.

8.3. Experimental Section

Materials and Methods The chemicals and reagents from Sigma-Aldrich Chemical Co. and Glen Research were used without further purification. Varian Cary50 UV/Vis spectrophotometer was used to conduct the absorption study and PTI QuantaMaster^{TM} spectrofluorometer with an integrating sphere was used to find the quantum yields as well as photoluminescence spectra. SYBR green I, the intercalating dye was purchased from Invitrogen worldwide and also used without further purification. Detail synthetic route and characteristic data for conjugated polymers (POX1) was previously reported in Chapter 7.

Light directed on-chip oligonucleotide synthesis. The glass slide was inserted into a holder attached to a DNA synthesizer. Standard phosphoramidite chemistry was used for all steps of oligonucleotide synthesis except for the deprotection step. In this

step, the terminal dimethoxytrityl protecting group was deprotected using a photoacid generator (PAG), which was put into the holder containing the slide. The digital photolithographic projection unit from a Digital Light Project (Texas Instruments) was attached to the synthesizer and used to project a preset light pattern onto the slide to activate PAG. For each deprotection step, PGA and CH_2Cl_2 were filled into the slide holder and activated to remove the terminal dimethoxytrityl protecting group. The deprotection step followed by the attachment of a base unit was repeated until the desired DNA sequence was obtained, as illustrated in Scheme 8-2. Patterned DNA synthesis was confirmed by GenePix 4000B microarray scanner (Molecular Devices Corp.) with dual lasers (532 nm/17 mW and 635 nm/10mW).

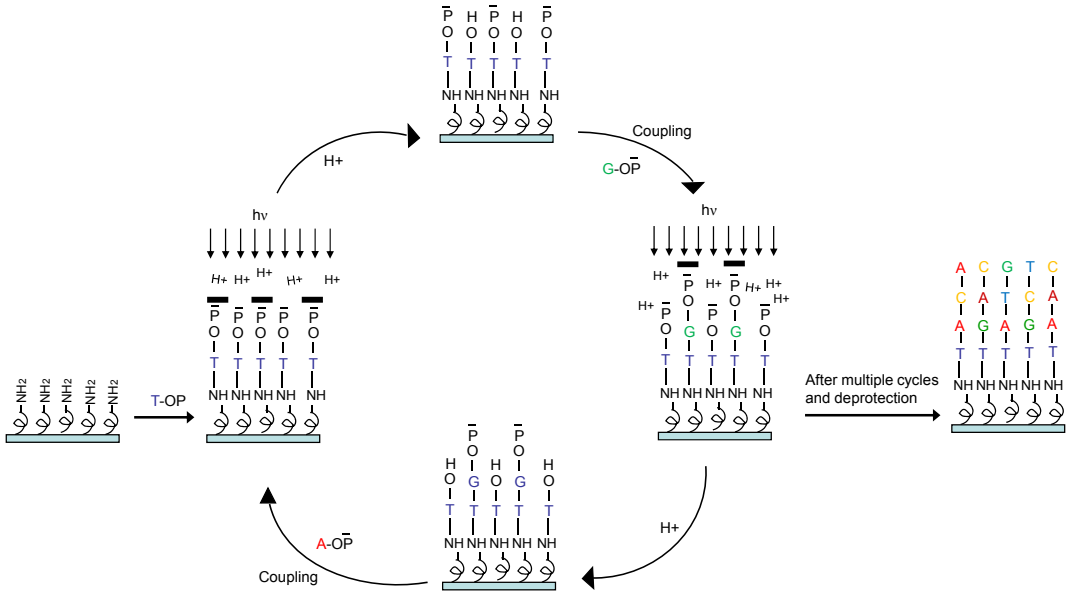

Scheme 8-2. Schematic illustration of the on-chip DNA synthesis.

Determination of SG1 concentration. SG1 concentration was calculated by using the Beer's law and the molar absorptivity of 73,000 $L \cdot mol^{-1} \cdot cm^{-1}$ reported

previously by Vitzthum and co-workers.[22] The absorbance of SG1 dissolved in a TE buffer (pH = 7.5) was measured at 495 nm.

$$A=\varepsilon \cdot b \cdot c$$

where A is the absorbance (no units, since $A=\log_{10}P_0/P$)

ε is the molar absorptivity with units of $L \cdot mol^{-1} \cdot cm^{-1}$

b is the path length of the sample (cm, 1 cm cuvette)

c is the concentration of the DMT in acetonitrile, expressed in $mol \cdot L^{-1}$.

Hybridization After the light directed on-chip oligonucleotide synthesis, the glass slides were washed with 5 mL of 6×SSPE. Prehybridized solution (30 μL, 20×SSPE, 15 μL acetylated bovine serum albumin (ac-BSA), 90 μL water) was then added to the glass slides and washed away after 3 minutes. Hybridization solution (15μL 20×SSPE, 28.5 μL water, 5 μL ac-BSA, 0.5 μL target DNA with sequence 5'-ACA CAT CAC GGA TGT-3', and 1 μl of SG1 with various concentration) was heated to 95 ºC. To hybridize the DNA, we added the hybridization solution and covered the slides with a second glass slide, not allowing any air to be trapped between the two glass slides. Hybridization was induced by slowly decreasing temperature. We incubated the slides for one hour at 37 ºC. After removing the solution from the slides, the slides were rinsed with 6×SSPE and iced water and dried with a stream of air. The quality of the slides was examined by using a fluorescence scanner and the PL intensity of the slides before and after hybridization was investigated by using a fluorescent spectrophotometer. Alternatively we conducted the dye intercalating separately after the hybridization. This method also gave the same results that we obtained from the simultaneous hybridization

and dye intercalation method. Selectivity tests with a single-mismatch DNA (5'-ACA CAT CTC GGA TGT-3') and a random target sequence (5'-TGT GTA GTG CCT ACA-3') were also performed by using the same condition. The fluorescence images in Figure 2(b) inset were obtained by using BX41 Fluorescence microscope, DP71 digital camera (Olympus), and Microsuite 5 Biological Suite Software (Olympus). The background (prehybridization) was subtracted. Direct excitation of SYBR green I and **POX1** excitation for amplification were carried out at 500 nm and 405 nm, respectively.

8.4. Results and Discussion

Figure 8-1 and 8-2 shows the chemical structures, and the absorption and emission spectra of SYBR green I and POX1, respectively. As one can see, there is a large spectral overlap between the emission spectrum of POX1 and the absorption spectrum of SYBR green I, satisfying a requirement for efficient FRET. Moreover, the absorption λ_{max} of POX1 is well separated from that of SYBR green I, allowing exclusive excitation of either the donor or the acceptor for the energy migration study between POX1 and SYBR green I.

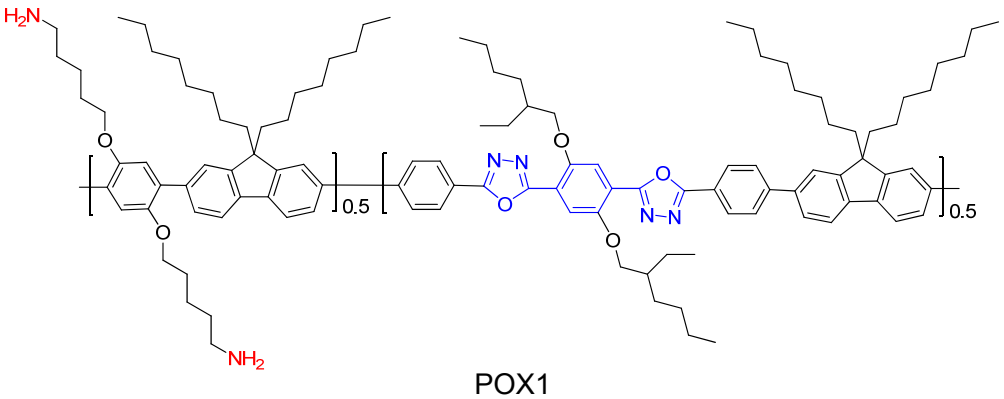

POX1

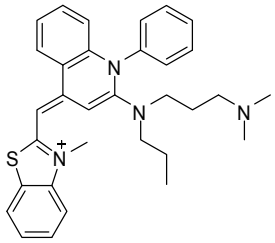

SYBR green I (SG1)

Figure 8-1. The chemical structures of POX1 and SYBR green I.

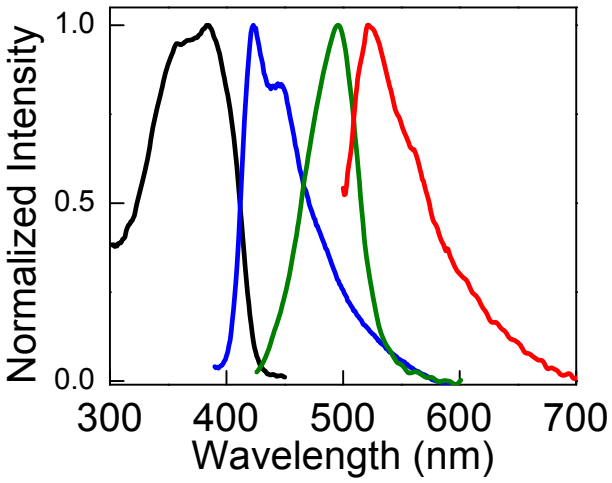

Figure 8-2. UV-Vis/PL spectra (black/blue for POX1 and green/red for SYBR green I) in the solid film (POX1) and in 0.5 μM 6 x SSPE solution at pH = 7.4 (SYBR green I).

We first studied the specificity of SYBR green I toward double stranded DNAs at three different concentrations: 5×10^{-7} M that is the manufacturer's recommended concentration, 5×10^{-8} M, and 5×10^{-9} M.[22] The concentration of SYBR green I recommended by the manufacturer was 5×10^{-7} M, which was calculated based on the molar absorption coefficient (~73,000 $M^{-1}cm^{-1}$ in TE buffer pH 7.5) of SYBR green I at the absorption maximum at 494 nm. For the study 50 μL of 1×10^{-5} M (0.5 nmol) aqueous solution of the complementary DNA sequence (5'-ACA CAT CAC GGA TGT-3'), an 1-mismatch sequence (5'-ACA CAT CTC GGA TGT-3'), and a random sequence (5'-TGT GTA GTG CCT ACA-3') was spread, respectively, onto a DNA microarray without POX1 and incubated at 37°C together with SYBR green I. As shown in Figure 8-3, 5×10^{-8} M and 5×10^{-9} M concentrations gave a good specificity but the signal was very weak and not well distinguishable due to the relatively large error range. As the concentration of SYBR green I increased to 5×10^{-7} M, the emission intensity became much stronger. However, the specificity of the intercalating dye toward the double strand DNA significantly decreased and we could hardly distinguish the target, 1-mismatch, and even the random sequence.

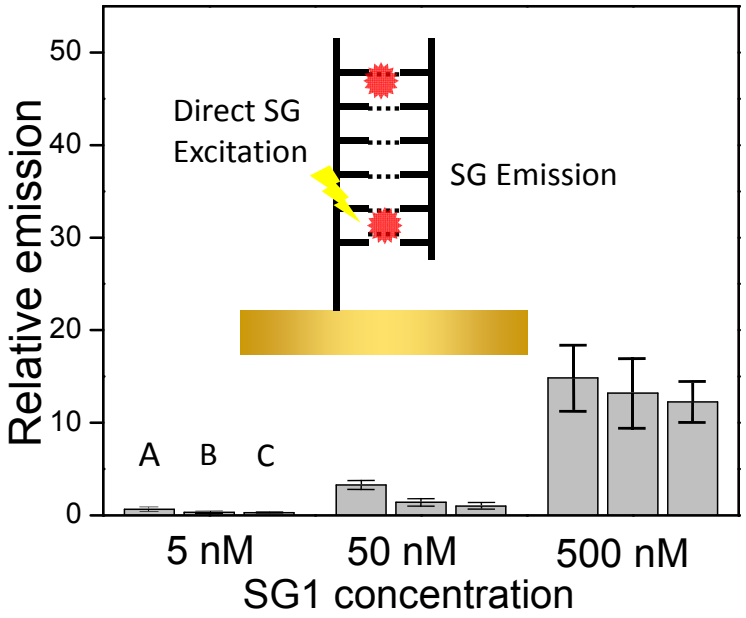

Figure 8-3. Selectivity test of conventional control slides without POX1. A: perfect match (5'-ACA CAT CAC GGA TGT-3'), B: 1-mismatch (5'-ACA CAT CTC GGA TGT'3'), C: random sequence (5'-TGT GTA GTG CCT ACA -3').

We built the signal amplifying and self-signaling DNA microarray by means of covalent immobilization of POX1 on a glass substrate having isothiocyanato groups as a linker and the subsequent light-directed on-chip DNA synthesis. Detail procedure is in the experimental section above. After the DNA synthesis, the resulting DNA patterns were confirmed by a UV scanner. The spot diameter was 55 μm and the density of the synthesized DNA was 0.243 nmol/cm^2. We systematically investigated the signal amplifying property of our DNA microarrays by hybridizing 50 μl of 1.0×10^{-5} M of the complementary DNA sequence (5'-ACA CAT CAC GGA TGT-3') to the DNA microarrays together with SYBR green I at various concentrations. POX1 was selectively excited at 380 nm and the emission of POX1 at 425 nm and the emission of SYBR green I at 525 nm were monitored. As shown in Figure 8-4, as the concentration of SYBR green

I increased, the emission from POX1 at 425 nm decreased and instead the emission from SYBR green I at 525 nm gradually increased due to efficient energy transfer from POX1 to SYBR green I . One can clearly see the discrete SYBR green I emission when 5 nM or higher concentration of SYBR green I was used. However, when SYBR green I concentration increased from 50 nM to 100 nM, the emission of SYBR green I was broadened and bathochromic shifted. We found from the binding study of SYBR green I to ssDNAs that the peak broadening and bathochromic-shift indicate non-specific binding of SYBR green I to ssDNA, its aggregation, and the resulting fluorescence quenching.

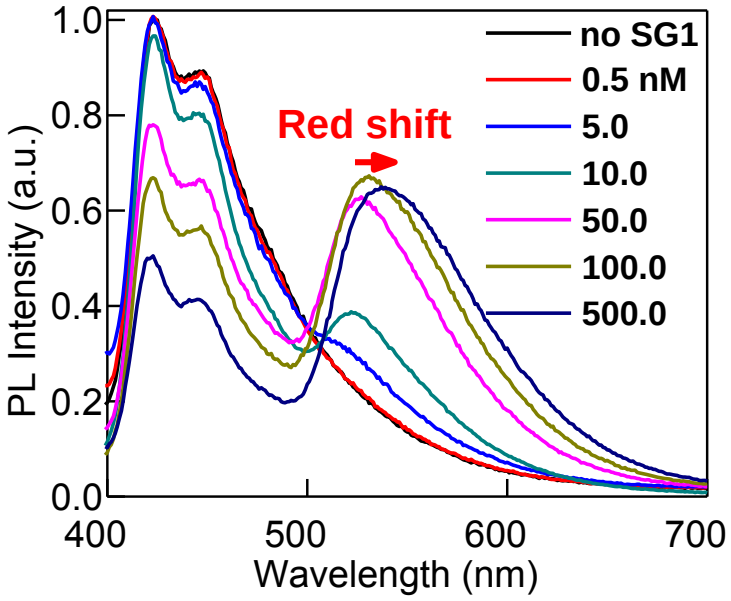

Figure 8-4. Emission profile in various SYBR green I concentrations. The excitation wavelength was 380 nm.

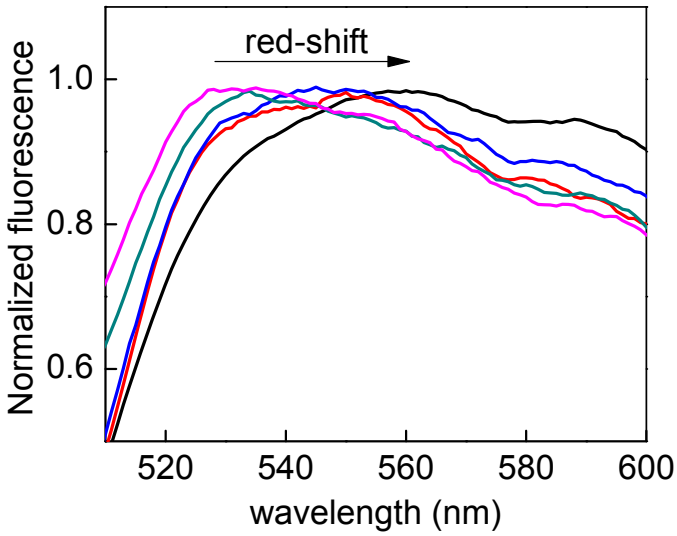

Figure 8-5. Normalized photoluminescence of SG1 solution (5 μM) in the presence of 15 base-pair ssDNA (0.1 nM; pink, 0.05 nM; green, 0.02 nM; blue, 0.01 nM; red, noDNA; black) in 6×SSPE buffer (pH = 7.4).

The fluorescence emission band of SYBR green I complexed with ssDNA was significantly broader and the emission maximum was shifted to a longer wavelength (525 nm to 560 nm) as the SG1/ssDNA ratio increased as shown in Figure 8-5. It is known that the fluorescence intensity of SYBR green I when attached to ssDNA is significantly lower than that of the dye complexed with a double strand DNA due to aggregation-induced self-quenching. Vitzthum and co-workers reported a bathochromic shift of the emission maximum of SYBR green I when it binds to ssDNA.[22] They reported that the emission maximum of SYBR green I was at 525 nm when the dye/base pair ratio was 1. However, the emission maximum shifted to 535 and 552 nm when the dye/base pair ratio increased to 2 and 10, respectively. Therefore, the bathochromic shift of SYBR green I emission in the higher concentrations (100 nM or 500 nM) and the negligible increase in

its emission intensity in the experiment are direct evidence of non-specific binding of SYBR green I to ssDNA.

The FRET efficiency calculated by the equation, 1-(intensity of donor with acceptor)/(intensity of donor without acceptor) was 0.04, 0.22, 0.33, and 0.55 for 10, 50, 100 and 500 nM of SYBR green I, respectively. With the SYBR green I concentration of 50 nM, which has the best FRET efficiency without non-specific binding to ssDNA, we achieved 15 times signal amplification from our signal amplifying DNA microarray as shown in Figure 8-6. The SYBR green I emission was largely amplified when POX1 was excited at 380 nm compared to the SYBR green I emission from the direct excitation of the intercalating dye at 490 nm. This large signal amplification stems from a much larger absorption intensity of POX1 layer (0.015 at 380 nm) compared to that of SYBR green I (0.001 at 490 nm). Therefore, POX1 layer absorbs a much larger amount of photon than SYBR green I can absorb and gives its energy as the FRET donor to the FRET acceptor, SYBR green I. Figure 8-6 inset shows fluorescence microscope images of a DNA microarray spot for comparison. There is large contrast difference between the two images confirming the efficient signal amplification. When 50 nM SYBR green I on the signal amplifying microarray was directly excited at 500 nm (right image) the spot was too dim. Conventional microarrays without the POX1 layer also showed the same dim spots. On the contrary, the POX1-coated signal amplifying DNA microarray showed strong emission with high contrast when POX1 was excited at 405 nm. The detection limit of the POX1-coated signal amplifying DNA microarray was in the sub-picomolar regime. The excitation spectrum of the amplified SYBR green I emission at 525nm in Figure 8-7 clearly presents that the origin of the 525nm emission is from POX1.

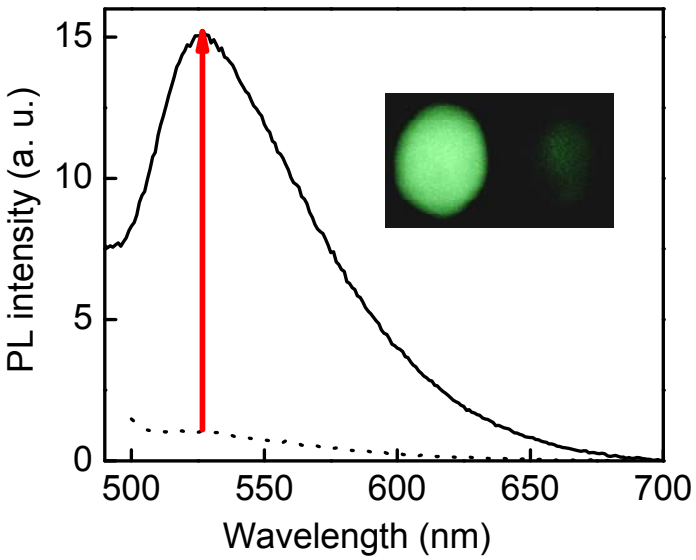

Figure 8-6. PL emission spectra of SYBR green I after hybridization with a target DNA ([c-DNA] = 1.0 x 10-5 M, 5'-ACA CAT CAC GGA TGT-3', [SYBR green I] = 50 nM) when excited at 380 nm (solid), 490 nm (dotted).

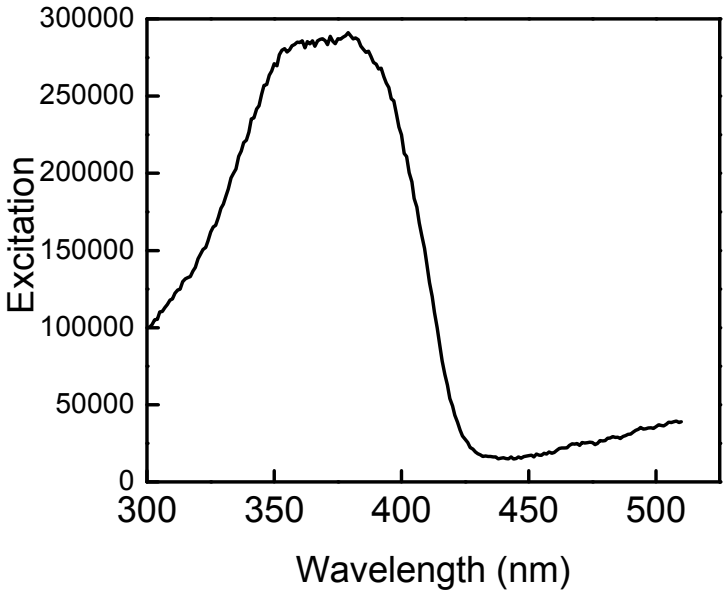

Figure 8-7. Excitation spectrum for the SYBR green I emission at 525 nm.

Selectivity tests were conducted by using 1.0×10^{-5} M one-mismatch DNA (5'-ACA CAT CTC GGA TGT-3') and random mismatch DNA (5'-TGT GTA GTG CCT ACA-3'). We also tested non-specific binding of SYBR green I (50 nM) to the ssDNA probes on the microarrays without having the complementary DNA and to the glass slide having only POX1 without ssDNA synthesis, respectively. Figure 4 shows the relative fluorescence intensity of each case and demonstrates the good specificity of the DNA microarrays. One can clearly see that the signal intensity of the 50 nM SYBR green I on our signal amplifying DNA microarray (Figure 8-8) is largely amplified compared to the signal intensity of the same 50 nM SYBR green I on the conventional DNA microarray (Figure 8-3) due to an efficient FRET.

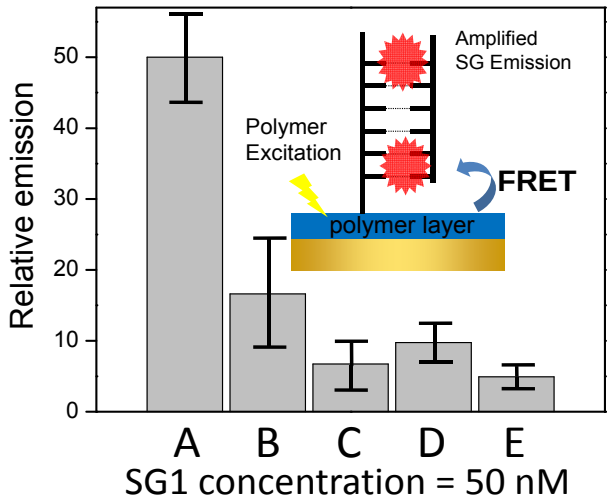

Figure 8-8. Selectivity test of the signal amplifying DNA microarray having the POX1 layer. A: perfect match (5'-ACA CAT CAC GGA TGT-3'), B: 1-mismatch (5'-ACA CAT CTC GGA TGT-3'), C: random sequence (5'-TGT GTA GTG CCT ACA-3'), D: prehybridized control, E: only POX1-coated slide. Hybridization condition: incubation in 6×SSPE at 37 °C for 20 min, each [DNA] = 1.0×10^{-5} M, [SYBR green I] = 50.0 nM.

8.5. Conclusion

In this chapter, we have demonstrated a label-free and signal amplifying DNA microarray using a conjugated polymer and an intercalating dye SYBR green I. The newly developed conjugated poly(oxadiazole-co-phenylene-co-fluorene) (POX1) is highly emissive and has unique stability in harsh environments. POX1 was covalently attached to a glass slide and oligonucleotides were directly synthesized on POX1 immobilized-glass substrate using photogenerated acid and UV irradiation. Efficient FRET from the conjugated polymer to the dye produced large signal amplification so that without losing good selectivity, sensitive detection of sub-picomolar concentrations of the target DNA was achieved.

8.6. References

1. Drmanac, S.; Kita, D.; Labat, I.; hauser, B.; Schmidt, C.; Burczak, J. D.; Drmanac, R. *Nature Biotechnology*, **1998**, *16*, 54.

2. Schena, M.; Shalon, D.; Davis, R. W.; Brown, P. O. *Science*, **1995**, *270*, 467.

3. Yershov, G.; Barsky, V.; Belgovskiy, A.; Kirillov, E.; Kreindlin, E.; Ivanov, I.; Parinov, S.; Guschin, D.; Drobishev, A.; Dubiley, S.; Mirzabekov, A. *Proc. Natl. Acad. Sci. USA*, **1996**, *93*, 4913.

4. Lockhart, D. J.; Winzeler, E. A. *Nature*, **2000**, *405*, 827.

5. Sassolas, A.; Leca-Bouvier, B. D.; Blum, L. J. *Chem. Rev*. **2008**, *108*, 109.

6. Gao, X.; LeProust, E.; Zhang, H.; Srivannavit, O.; Gulari, E.; Yu, P.; Nishiguchi, C.; Xiang, Q.; Zhou, X. *Nucleic Acids Res*. **2001**, *29*, 4744.

7. Komolpis, K.; Srivannavit, O.; Gulari, E. *Biotechnol. Prog*. **2002**, *18*, 641.

8. Rouillard, J.-M.; Zuker, M.; Gulari, E. *Nucleic Acids Res*. **2003**, *31*, 3057.

9. Gao, X.; Zhou, X.; Gulari, E. *Protenomics* **2003**, *3*, 2135.

10. Mukherjee, S.; Berger, M. F.; Jona, G.; Wang, X. S.; Muzzey, D.; Snyder, M.; Young, R. A.; Bulyk, M. L. *Nat. Genet*. **2004**, *36*, 1331.

11. Liu, B.; Bazan, G. C. *Chem. Mater*. **2004**, *16*, 4467.

12. Lee, K.; Rouillard, J.-M.; Pham, T.; Gulari, E.; Kim, J. *Angew. Chem. Int. Ed*. **2007**, *46*, 4667.

13. Ho, H.-A.; Béra-Abérem, M.; Leclerc, M. *Chem. Eur. J*. **2005**, *11*, 1718.

14. Thomas, S. W., III; Joly, G. D.; Swager, T. M. *Chem. Rev*. **2007**, *107*, 1339.

15. Lee, K.; Povlich, L. K.; Kim, J. *Adv. Funct. Mater*. **2007**, *17*, 2580.

16. Pun, C.-C.; Lee, K.; Kim, H.-J.; Kim, J. *Macromolecules* **2006**, *39*, 7461.

17. Wosnick, J. H.; Mello, C. M.; Swager, T. M. *J. Am. Chem. Soc*. **2005**, *127*, 3400.

18. He, F.; Tang, Y.; Yu, M.; Feng, F.; An, L.; Sun, H.; Wang, S.; Li, Y.; Zhu, D.; Bazan, G. C. *J. Am. Chem. Soc*. **2006**, *128*, 6764.

19. Yang, C. J.; Pinto, M.; Schanze, K.; Tan, W. *Angew, Chem. Int. Ed*. **2005**, *44*, 2572.

20. Xu, H.; Wu, H.; Huang, F.; Song, S.; Li, W.; Cao, Y.; Fan, C. *Nucleic Acids Res*. **2005**, *33*, e83.

21. Lee, K.; Kim, H.-J.; Cho, J. C.; Kim, J. *Macromolecules* **2007**, *40*, 6457.

22. Zipper, H.; Brunner, H.; Bernhagen, J.; Vitzthum, F. *Nucleic Acids Res*. **2004**, *32*, e103.

CHAPTER 9

Label-Free and Self-Signal Amplifying "Molecular Beacon" Biosensors using Conjugated Polymers

Parts of this chapter appear in: Lee, K.; Rouillard, J.-M.; Gulari, E.; Kim, Manuscript in preparation.

9.1 Abstract

We have developed a conjugated polymer and molecular beacon-based solid state DNA sensing system to achieve sensitive label-free detection. The novel conjugated poly(oxadiazoles) derivative (POX-SH) having amine and thiol functional groups was designed to have unique chemical and photochemical stability for the development. POX-SH was soluble in most non-polar organic solvents and had intense blue fluorescence and a high quantum yield. By means of the thiol group POX-SH was covalently immobilized onto a maleimido-functionalized glass slide followed by direct on-chip oligonucleotide synthesis of molecular beacons by using the amine side chain of the POX-SH layer. The molecular beacon synthesis was terminated by a fluorescent dye or quencher molecules as the FRET acceptor to establish efficient FRET from POX-SH. The molecular beacon probes selectively opened upon hybridization with the target DNA sequence and affected the FRET between the polymer and the dye or the quencher, producing sensitive and label-free sensory signal. The molecular design parameters such as the size of the stem and the loop of the molecular beacon, choice of dye, and the number of quencher molecules were systematically controlled and their effects on the sensitivity and selectivity were investigated.

9.2. Introduction

DNA microarrays have become a powerful tool in gene sequencing and gene expression studies.[1-8] Principally, DNA microarrays are collections of microscopic DNA spots, commonly representing many different kinds of single genes, arrayed on a microscope slide or a chip by covalent attachment for high-throughput screening. Thousands of individual genes can be spotted or directly synthesized on a single square inch slide at a time. Analyte DNA or RNA molecules are then labeled with a fluorescent dye and then spread out onto the DNA microarray. Complementary sequences will be hybridized with the probing DNA on the DNA microarray. After washing off non-specifically bound analyte DNA the microarray is scanned to visualize the bound DNA by means of the labeled fluorescent dye. The fluorescent dye labeling is necessary because the conventional DNA microarray does not have any capability to generate sensory signal by itself. However, the dye tagging on analyte DNA requires time and cost. Therefore, a self-signaling DNA microarray that allows label-free detection is highly desirable. There have been several new generation of responsive probes having optical or electrical signal upon binding with a label-free target. Among these are surface plasmonic resonance (SPR)[9-12], quartz crystal microbalance[12-18], label-free electronic detection of DNA[19-20], the use of intercalating dye[21-24], and molecular beacon concept[25-30].

Conjugated semiconducting polymers have received a wide attention as signal-transducing elements for sensory applications. In particular, the extraordinary signal amplification is originated from the exciton migration along the 1-dimensional wire-like conjugated polymer backbone and a considerable effort has been inspired by this unique phenomenon to apply this concept toward the detection of biological targets.[31] For

example, recently we have developed signal-amplifying molecular DNA sensors in homogeneous aqueous solution state and solid-state microarrays by uniquely combining rationally designed conjugated polymers and probing DNA molecules.[24,32-34] The signal amplifying DNA microarrays were achieved by developing a chemically and photochemically stable conjugated polymer and covalent bonding of the polymer to a solid substrate followed by convenient on-chip DNA synthesis.

To the developed signal-amplifying concept, herein, we added a self-signaling concept by using a molecular beacon probe and conjugated polymers to achieve label-free DNA detection (Figure 9-1). The molecular beacon was devised as a self-signaling probe to eliminate the time consuming fluorescence labeling of analyte DNAs. A traditional molecular beacon is a hairpin structured ssDNA in which a fluorescent dye and a quencher molecule located at the two ends of the hairpin form close contact. Due to the adjacent quencher molecule the dye cannot emit any fluorescence unless the molecular beacon hybridizes with a complementary ssDNA. Hybridization with a complementary ssDNA opens the hairpin, moving the fluorescent dye away from the quencher thus allowing the dye to emit its fluorescence signal. However, the challenge is that immobilization of molecular beacons on solid surfaces requires specific chemical design limiting the practical application of the molecular beacon. We covalently tethered a newly developed conjugated polymer by using its thiol side chain to a maleimide modified solid substrate and then synthesize molecular beacons from the amine functional group of the polymer through the on-chip DNA synthesis. The molecular beacon probes were terminated by a quencher or a fluorescent dye to build a turn-on and a turn-off type of self-signaling and signal amplifying DNA microarrays. We

systematically studied the effects of the variation in the probe size, stem length, and the number of quencher per molecular beacon probe on the sensitivity of the microarrays.

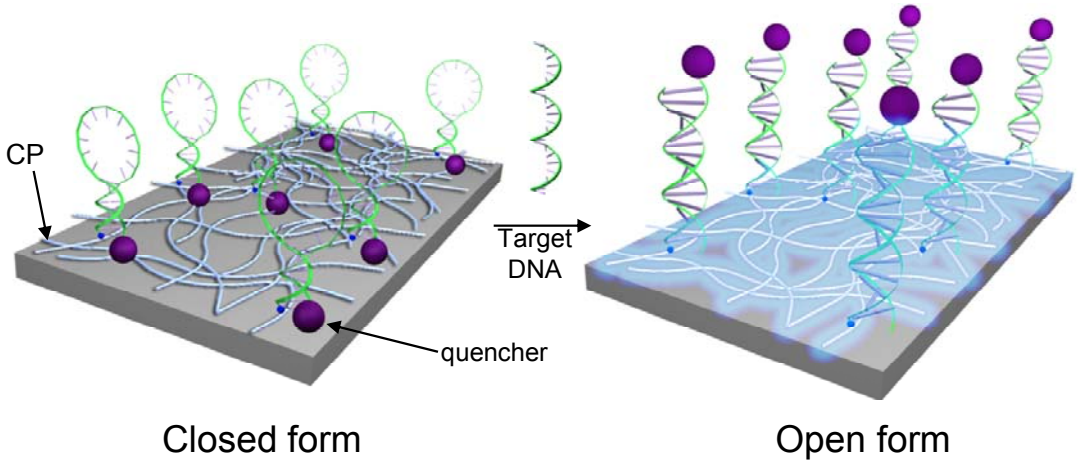

Figure 9-1. Schematic representation of label-free and signal amplifying DNA microarray using a molecular beacon.

9.3. Experimental Section

Materials and methods All solvents and reagents for monomer and polymer synthesis were used without further purification as received from Sigma-Aldrich Chemical Co. or Fischer Scientific Co. An amine-functionalized polymer (POX, Figure 9-2) and monomer **2** and **3** were reported previously and monomer **4** was purchased from Sigma Aldrich.[32] All the chemicals for the on-chip oligonucleotide synthesis such as phosphoramidites, 5'-DABCYL phosporamidite, 5'-hexachlorofluorescein phosphoramidite, and trebler phosphoramidite were purchased from Glen Research Co. A cross linker, succinimidyl 4-[*N*-maleimidomethyl]cyclohexane-1-caroboxylate (SMCC) was purchased from Pierce Inc. (Fisher Scientific Co.) Synthesis and characterization of POX were reported previously.[32] ^{1}H NMR spectra (400 MHz or 500 MHz) were obtained

from Varian Inova 400 or 500 NMR instrumentation. UV/Vis absorption spectra were obtained using a Varian Cary50 UV/Vis spectrophotometer. Photoluminescence spectra and quantum yield in the solid state were recorded by using PTI QuantaMaster™ spectrofluorometer equipped with an integrating sphere. The number and weight average molecular weights and the molecular weight distributions were determined by gel permeation chromatography (GPC) with respect to polystyrene standards (Waters Corp.) in THF as an eluent.

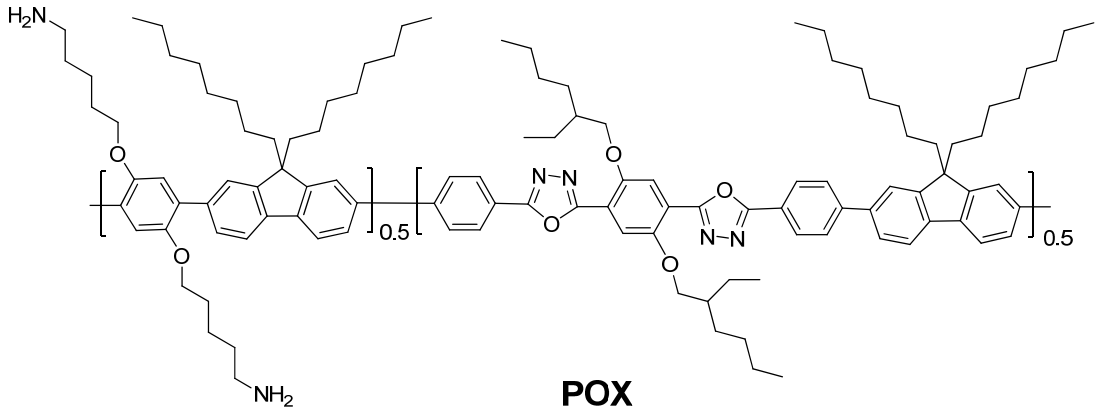

POX

Figure 9-2. Chemical Structure of **POX**.

Synthesis of 1,4-dibromo-2,5-bis(6-bromohexyloxy)benzene (**1**): To a 1000 ml 2 neck round bottom flask were added 2,5-dibromohydroquinone (13.8 g, 51.5 mmol), 1,6-dibromohexane (151 g, 618 mmol), potassium carbonate (56.9 g, 412 mmol) and 600 ml of acetone. The mixture was stirred at 50 ºC for 72 hr. The crude mixture was filtered to remove any insoluble salt and impurities. Solution was concentrated at reduced pressure and precipitated in 800 ml of methanol. Product was filtrated and dried in vacuo. Additional purification was done by recrystallization in chloroform and hexane mixture.

Yield: (16.8 g, 55 %, dibromoalkane residue slightly remained according to NMR analysis, reaction went without further purification), ^{1}H-NMR (500 MHz, $CDCl_3$): δ/ppm 7.00 (s, 2H, aromatic), 3.96 (t, 4H, -OC$\underline{H}_2$), 3.43 (t, 4H, -C$\underline{H}_2$Br), 1.97 (m, 4H, -C$\underline{H}_2$-), 1.92 (m, 4H, -C$\underline{H}_2$-), 1.52 (m 4H, -C$\underline{H}_2$-). ^{13}C-NMR (125 MHz, $CDCl_3$): δ/ppm 150.1, 118.7, 111.3, 69.8, 33.9, 32.5, 28.9, 27.7, 27.3.

Synthesis of 6,6'-(2,6-dibromo-1,4-phenylene)bis(oxy)dihexane-1-thiol (**2**): Compound **1** (8.22 g, 13.8 mmol) was dissolved in 70 ml of ethanol and stirred for 30 min in argon purging. Thiourea (2.11 g, 27.6 mmol) was slowly added to the solution and the solution was heated under reflux overnight. The crude mixture was poured into 10 % sodium hydroxide solution (50 ml) and stirred for 4 hr at room temperature. The solution was neutralized with 10 % HCl (32 ml). The mixture was filtered at reduced pressure. The solid was extracted with methylene chloride/water (3 times). Combined organic phase was again washed with deionized water (2 times). The methylene chloride solution was dried with sodium sulfate, filtered, and evaporated at reduced pressure at room temperature. Compound was additionally dried in vacuo. The product obtained was unstable in the air due to disulfide formation and showed the decreased solubility in organic solvents. The reaction was proceeded to the next step without further purification. Yield (6.5 g, 94 %), ^{1}H-NMR (500 MHz, $CDCl_3$): δ/ppm 7.09 (s, 2H, aromatic), 3.98 (t, 4H, -OC$\underline{H}_2$), 2.56 (t, 4H, -C$\underline{H}_2$Br), 1.83 (m, 4H, -C$\underline{H}_2$-), 1.67 (m, 4H, -C$\underline{H}_2$-), 1.53 (m 4H, -C$\underline{H}_2$-), 1.46 (m 4H, -C$\underline{H}_2$-), 1.36 (t, 2H, -S$\underline{H}$).

Synthesis of (6'6'-(2,5-dibromo-1,4-phenylene)bis(oxy)bis(hexane-6,1-diyl))bis(tritylsulfane) (**M1**): To a 250 ml 2 neck round bottom flask were added compound **2** (5.00 g, 10 mmol) and 40 ml of anhydrous methylene chloride. After stirring

the mixture for 10 min under argon purging, trityl chloride (11.14 g, 40.0 mmol) in methylene chloride (10 ml) was slowly added and the mixture was stirred under argon purging at room temperature for 24 hr. The solution was extracted with 10 % NaOH and washed again with deionized water. The solution was dried over magnesium sulfate, filtered and concentrated by rotary evaporator at reduced pressure. Additional purification was done by silica gel column chromatography (ethyl acetate : hexane = 1 : 9) and the product was dried in vacuo to give a white powder (yield: 7.4 g, 75 %). ^{1}H-NMR (500 MHz, $CDCl_3$): δ/ppm 7.42 (m, 12 H, aromatic), 7.30 (dd, 12 H, aromatic), 7.22 (m, 6H, aromatic), 7.09 (s, 2H, aromatic), 3.91 (t, 4H, -OC$\underline{H}_2$), 2.17 (t, 4H, -C$\underline{H}_2$Br), 1-50-1.20 (m, 16H, -C$\underline{H}_2$-). ^{13}C-NMR (125 MHz, $CDCl_3$): δ/ppm 150.05, 145.06, 130.05, 127.84, 126.55, 118.49, 111.16, 70.11, 66.44, 31.91, 28.88, 28.65, 28.52, 25.54.

Polymerization synthesis (**POX-SH**): To a 50 ml of Schlenk flask were added **M1** (39.3 mg, 39.9 μmol), **M2** (76.4 mg, 119.7 μmol), **M3** (93.4 mg, 119.7 μmol) **M4** (140.3 mg, 279.3 μmol), THF (7 ml) and 1M K_2CO_3 (7 ml). Degassed tetrakis(triphenylphosphine)palladium(0) (6.46 mg, 5.6 μmol) in THF (1 ml), prepared in a separate Schlenk, was transferred to the monomer mixture by cannula and the monomer solution was degassed by several cycles of vacuum and argon purging. Suzuki type-polymerization was carried out at 75 °C for 48 h. Polymer solution was precipitated in 100 ml of methanol and filtered by gravity force. Solid product was washed with water (2 x 20 ml) and acetone (2 x 20 ml). Polymer pellet was redissolved in chloroform and washed with deionized water (2 times). Solution was dried over $MgSO_4$, filtered and evaporated by rotary evaporator at reduced pressure to give precursor polymers. 10 ml of trifluoroacetic acid (TFA) was carefully added to polymer in chloroform (10 ml) and the

polymer solution was stirred at room temperature for 8 h in order to cleave *t*-BOC and trityl blocking group. After evaporation of solvent and TFA, the polymer was re-dissolved in chloroform and washed with 1 M KOH solution, followed by NaCl solution, and deionized water to give yellow polymer (**P1**) (Yield: 180 mg, 63 %). The number and weight average molecular weight were calculated for the polymer before the cleavage of *t*-BOC due to the limited solubility of P1 in tetrahydrofuran as a GPC eluent, M_n = 19,500, M_w = 76,000. ^{1}H-NMR (500 MHz, $CDCl_3$): δ/ppm 8.3-6.8 (m, aromatic C-H), 4.18-3.95 (m, aliphatic -OC$\underline{H}_2$-), 2.75-2.65 (two t, aliphatic -C$\underline{H}_2$SH and -C$\underline{H}_2$NH$_2$), 2.2-0.6 (broad m, aliphatic C$\underline{H}_2$ and C$\underline{H}_3$).

Glass substrate modification and polymer immobilization: A slide glass (1 × 3 inches) was incubated into ammonium hydroxide/water/35% hydrogen peroxide (1:4:1 v/v) solution at 80 ºC for 1 hr. A slide was rinsed with sufficient amount of deionized (DI) water (ca. 50 ml) and dried with nitrogen gas. Slides were dipped into Pirahna solution (caution: H_2SO_4 : 35 % hydrogen peroxide = 3 : 7 v/v, highly exothermic, H_2SO_4 must be poured slowly into hydrogen peroxide) and incubated for overnight. It is rinsed with 100 ml of DI water and dried with a stream of nitrogen gas. It is transferred into 97 % aminopropyltrimethoxysilane (APTMS)/methanol/water (1 : 24 : 1 v/v) and sonicated for 30 min. The solution temperature was elevated from 20 ºC to 37 ºC. The slide was washed with methanol (30 ml) and DI water (30 ml) and dried with nitrogen gas. It was baked in a convection oven at 120 ºC for 30 min. Amino-functionalized glass slide was incubated with 7.5 mg of succinimidyl 4-[N-maleimidomethyl]cyclohexane-1-caroboxylate (SMCC) in anhydrous dimethylformamide (DMF) (200 μl) at room temperature for 2 hr. Excess SMCC was washed out with 50 ml of anhydrous DMF and

anhydrous chloroform and dried with a stream of air. Only one side of the slide was reacted with **POX-SH** in chloroform (9 ml) with a variety of incubation time (0.5 h, 1 h, 3 h and overnight) and subsequently washed with chloroform, methylene chloride, and DI water. Further cleaning step was conducted by the sonication of glass slide in chloroform for 5 min to remove any physically bounded polymer chain to substrate. After drying the slide by a stream of nitrogen, it was preserved in glove box (-35 ºC) for further DNA synthesis. Slide preparation and POX immobilization have been reported previously.[32]

On-chip oligonucleotide synthesis and oligonucleotide density measurement: The light-directed on-chip oligonucleotide reactions were carried out using apparatus described previously.[24,32,35] On-chip oligonucleotide synthesis was performed using the standard phosphoramidite chemistry except for the deprotection step, where a 2 % trichloroacetic acid (TCA)/methylene chloride (single sequence) or iodium PGA-P solution (multi sequences by arrayal patterns) to deprotect the terminal dimethoxytrityl protecting group at selected reaction sites. DABCYL, Dye (fluorescein or HEX), or trebler phosphoramidite was also used at the end of oligo synthesis to introduce single/multi quenchers and dye as an energy acceptor. Oligonucleotide synthesis was confirmed by UV/Vis spectra and a fluorescence image after hybridization with dye-labeled DNA, obtained from a GenePix 4000B microarray scanner (Molecular Devices Corp.) with dual lasers (532 nm/17 mW, 635 nm/10mW). To measure the density of DNA on polymer coated glass, dimethyltrityl (DMT) quantification method was used. A glass slide having oligonucleotide was treated with 0.1 M of *p*-toluenesulfonic acid monohydrate (TSA) (4 ml) in anhydrous acetonitrile for 1 min. DMT molecules cleaved from the final cycle of oligo synthesis was collected. UV absorption of the DMT solution

was measured by UV spectroscopy to quantify DMT concentration. A major peak corresponding to a DMT cation appears at 500 nm. We used a second peak at 410 nm with an extinction coefficient of 28,690. According to the Beer's law below, the concentration for a given DMT solution is proportional to UV absorbance and the molar extinction coefficient is constant.

$$A=\varepsilon \cdot b \cdot c$$

where A is the absorbance (no units, since $A=\log_{10}P_0/P$)
ε is the molar absorptivity with units of $L \cdot mol^{-1} \cdot cm^{-1}$
b is the path length of the sample (cm, 1 cm cuvette)
c is the concentration of the DMT in acetonitrile, expressed in $mol \cdot L^{-1}$.

Hybridization Test and Fluorescence Detection: Hybridization buffer contained 20 mM Tris-HCl, NaCl 55 mM, 10.8 mM KCl, 2mM EDTA and 100 mM $MgCl_2$ at pH 8.0. All DNA hybridization tests were conducted at 25 ºC. Complementary DNAs and non-complementary DNAs having different lengths of hairpin loop or stem were used for hybridization test. (See Table 9-1). Slides are firstly rinsed with hot water sufficiently and immersed in hybridization buffer. Hybridization DNA solutions (1×10^{-5}M, hybridization buffer above: 49.5 μl, complementary DNA: 0.5 μl) were heated to 90 ºC to prevent non specific loop formation of the target oligo and were applied onto the slide. The slide was covered with blank slide and kept in a humid chamber and incubated for 1 h. The slide was rinsed blank hybridization buffer and cold water (3 ºC) by quick dipping. FRET tests were performed by checking UV absorbance and photoluminescence emission changes before and after hybridization upon the excitation of POX (POX-SH) at 380 nm or the dye excitation at 490 nm (fluorescein) or 535 nm (HEX). Relative fluorescence increase in fluorescein test was calculated by $(I_{target}-I_{polymer})/(I_{probe}-I_{polymer})$, where I_{probe} and I_{target}

are the photoluminescence intensity of dye before and after hybridization respectively and $I_{polymer}$ is the photoluminescence intensity of polymer before DNA synthesis.

Table 9-1. DNA hairpin probes, P1 and P2; their Target (C1 and C2) and non-complementary DNAs (N1 and N2) used in this study.

Name	sequence
P1 (probe)	5'-DABCYL or dye-CCA CGC TCA TCA TAA CCT TCA GCA AGC TTT AAC TCA TAG TGA GCG TGG T -3' -glass
P2 (probe)	5'-DABCYL or dye-CGC TCC TAA AAC GAC GGC CAG TGG AGC GT -3' -glass
C1 (P1 complement)	5'-ACG CTC ACT ATG AGT TAA AGC TTG CTG AAG GTT ATG A-3'
C2 (P2 complement)	5'-ACT GGC CGT CGT TTT AGG AGC G-3'
N1 (non complement)	5'-TGA GAA TGA TAC TCA ATT TCG AAC GAC TTC CAA TAC T-3'
N2 (non complement)	5'-TGA CAA ACA GCA AAA TCC TAA C-3'

9.4. Results and Discussion

The chemical structure of the polymer was carefully designed by considering the required properties for covalent immobilization of the polymer as well as the hash reaction condition of the on-chip DNA synthesis. We previously developed an oxadiazole-containing and amine functionalized conjugated polymer. The oxadiazole unit was for chemical and photochemical stability and the amine side chain was a functional group for the immobilization of the polymer to a solid substrate and the on-chip DNA synthesis at the same time.[32] We kept the same oxadiazole unit for the stability but additionally added another unit having a thiol unit solely for the polymer immobilization so that we can precisely control the amount of the amine-containing unit for only on-chip DNA synthesis. **M1** synthesis for **POX-SH** was illustrated in Scheme 9-1. 2,5-dibromohydroquinone was reacted with 1,6-dibromohexane by Williamson-Ether synthesis. To prevent the formation of cross-linked by-product between dibromoalkyl compound and hydroquinone, hydroquinone was very slowly dropwise added into the excess amount of dibromohexane solution. However, we found out from systematic

additional studies that if the dibromoalkane molecule has a longer than C_5 and once the dibromoalkane is attached to the phenol group the reactivity of the bromine group at the other end of the alkyl chain significantly decreased. Therefore, Williamson-ether synthesis reaction of dibromohexyl compound with a phenolic group can be done in one-pot synthesis with a reasonable yield in the presence of excess dibromoalkyl (C_n n>4) compound. The resulting compound **1** was reacted with thiourea to give dithiol compound 2. This compound turned out to be very unstable in the air due to the disulfide formation. Therefore the thiol group was protected by trityl chloride. In trityl protection, the mixture was initially hazy due to the limited solubility of compound **2** in methylene chloride. However, the solution became completely transparent after the thiol group was protected with trityl group. Monomer **M2** having amine group and **M3** having oxadiazole unit were prepared according to our previous literature.[32,34] **M1** to **M3** prepared showed a good solubility in organic solvents such as chloroform and tetrahydrofuran (> 15 mg/ml).

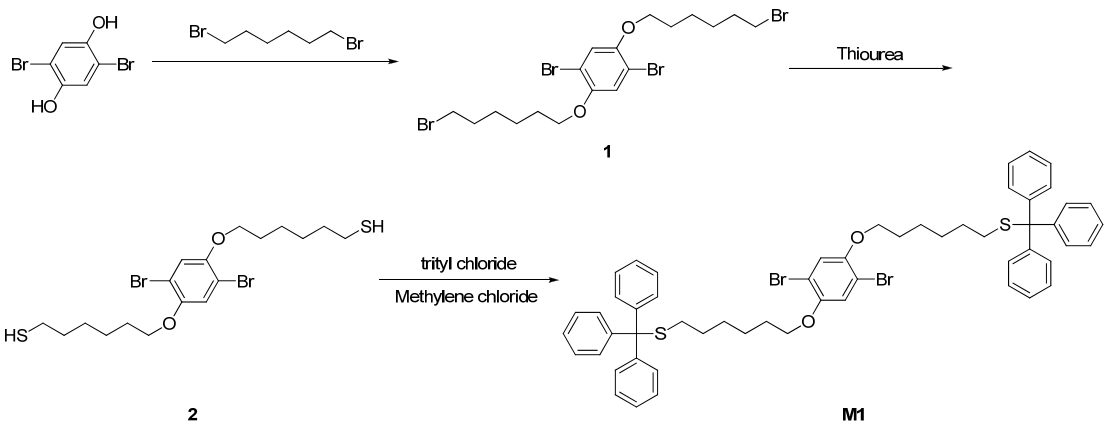

Scheme 9-1. Monomer synthesis for **M1**.

As shown in Scheme 9-2, the copolymerization was carried out by means of Suzuki cross-coupling polymerization of the aryl halide monomers **M1**, **M2**, and **M3** and a fluorine monomer **M4** having borolene unit in the presence of a palladium catalyst.[36] We have controlled the monomer ratios to obtained conjugated polymers having various compositions. As summarized in Table 9-2, there is a strong inverse correlation between the molecular weight of the resulting polymers and the fraction of M1 in the aryl halide monomers. It is likely that the chain propagation rate decreases once **M1** having the bulky side chain is reacted at the end of polymer chain. The number (M_n) and weight (M_w) average molecular weight of the polymers determined by gel permeation chromatography (GPC) using monodisperse polystyrene as the standard before cleavage of protecting groups were 19,500 g/mol and 76,000 g/mol, respectively, and the polydispersity indices (PDI) was 3.9. The polymer before deprotection of t-BOC and trityl group was favorably soluble in non-polar organic solvents like chloroform and tetrahydrofuran (THF) but almost insoluble in polar solvent and had a white-yellow color.

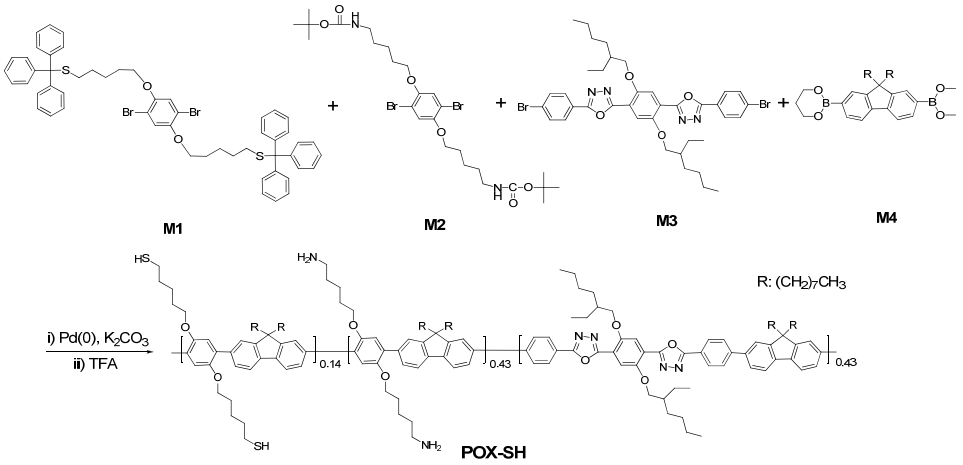

Scheme 9-2. Polymerization for **POX-SH**.

Table 9-2. Monomer ratio and its corresponding molecular weight.

M1	*M2*	*M3*	*M4*	M_n[a]	M_w[a]
1	1	1	3	2,700	15,400
1	2	2	5	4,700	23,000
1	3	3	7	19,500	76,000

a. unit: g/mol, molecular weight is calculated by polystyrene-based gel-permeation chromatography (GPC) as tetrahydrofuran eluent.

Deprotection reaction of the trityl and t-BOC group was conducted in 50 % trifluoroacetic acid (TFA) in chloroform to give **POX-SH**. The cleavage of trityl group and t-BOC group was monitored by ^{1}H-NMR analysis. For t-BOC cleavage, two peaks at 4.50 ppm and 1.43 ppm corresponding to proton of carbamate group and tertiary butyl group respectively disappeared and a new single peak at 1.97 ppm corresponding to the primary amine was observed. Also, a peak corresponding to alkyl protons next to –NH- group shifted from 3.13 ppm to 2.67 ppm. For the cleavage of trityl group, peak intensities at 7.40-7.20 ppm corresponding to aromatic protons significantly decreased and we observed a new band at 2.55 ppm and 1.35 ppm corresponding to alkyl protons and free thiol protons, respectively. After the deprotection the solubility of **POX-SH** in chloroform was slightly decreased but significantly decreased in THF.

Polymer immobilization on a glass substrate is described in Figure 9-3. In order to prevent any loss of polymer during the on-chip DNA synthesis, **POX-SH** was covalently bound to a glass substrate. Amino group was firstly introduced on a glass by aminopropyltrimethoxysilane (APTMS), followed by treatment of heterofunctional crosslinker, succinimidyl 4-[*N*-maleimidomethyl]cyclohexane-1-caroboxylate (SMCC), to conjugate the amino group of the substrate and the thiol group of **POX-SH**. After introduction of maleimido group which has a high affinity to a thiol group, **POX-SH** was

covalently linked onto the glass substrate. After immobilization of **POX-SH** and subsequent sonication for the removal of unbound polymer from the glass surface, a new broad absorption band at 350-400 nm corresponding to POX-SH absorption clearly appeared and the polymer in the film showed intense blue photoluminescence at 350-400 nm (Figure 9-3 and 9-4). We also prepared the same types of polymers having different length of the alkyl side chain on the fluorine unit (C_6) and the oxadiazole unit (C_{16}) but their chemical and photophysical properties were almost identical to **POX-SH** (Data not shown).

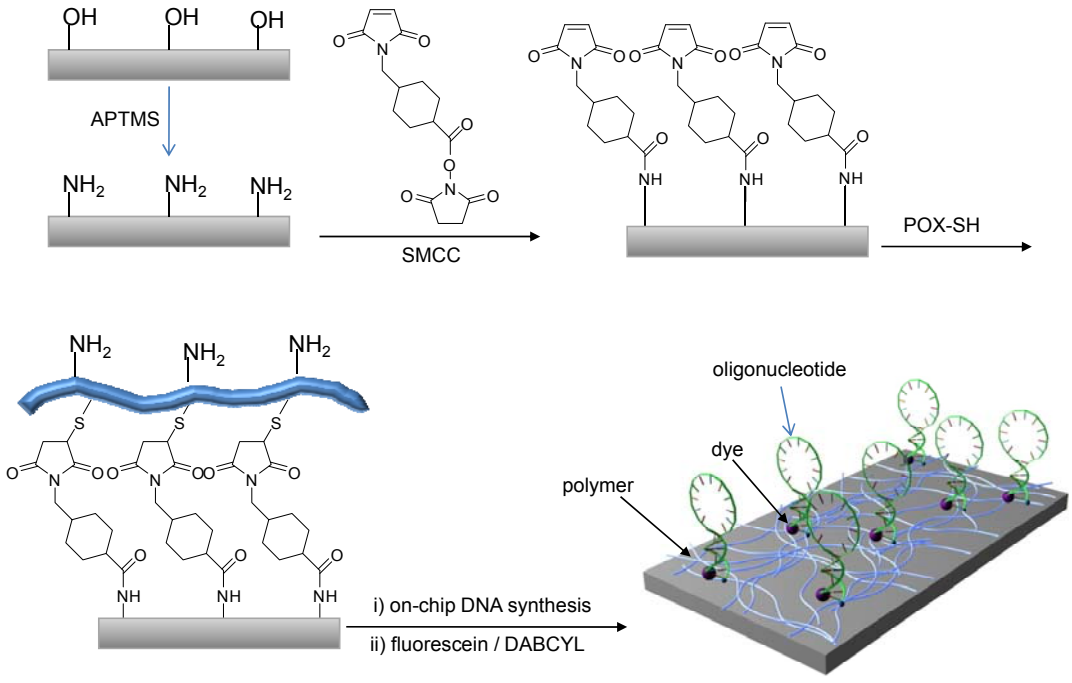

Scheme 9-3. Surface modification and polymer immobilization.

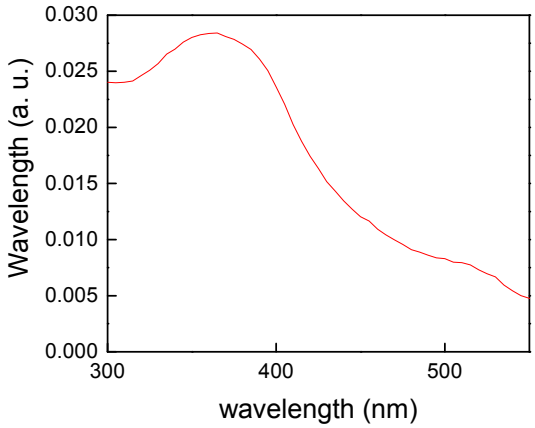

Figure 9-3. UV absorption spectrum of POX-SH on glass substrate.

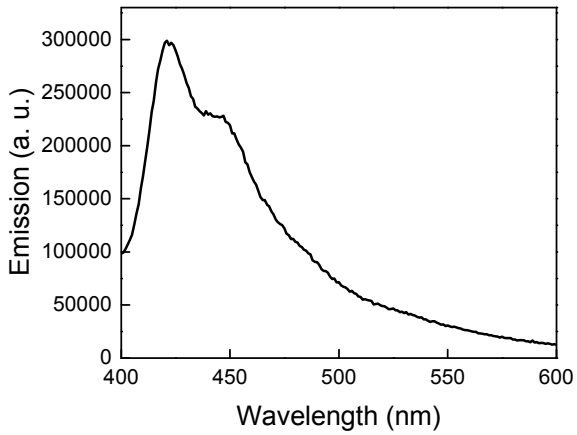

Figure 9-4. PL spectrum of of POX-SH on glass substrate.

On-chip oligonucleotide synthesis was conducted by applying the phosphoramidite chemistry to the amine group of POX-SH. The density of oligonucleotides synthesized on the POX-SH coated glass was measured by quantification of dimethyltrityl (DMT) which was cleaved from the synthesized

oligonucleotides at the final cycle of the oligo synthesis. The surface concentration of the synthesized oligonucleotides for all cases was 2.8×10^{12} molecules/cm^2. This value is smaller than the surface density (5.0×10^{13} molecules/cm^2) of oligonucleotides of the conventional DNA microarrays. This is reasonably acceptable because the amine density on the POX-SH layer is presumably smaller than the highly packed amine surface used for conventional microarrays.

DNA hairpin probes P1 and P2 having different lengths were designed in this study (Table 9-1). Probe P1 was designed to match a portion of the *Staphylococcus aureus femA gene*[37] for a practical value. At the end of the oligonucleotide sequences, a nonfluorescent dark quencher (mono DABCYL or tri-DABCYL) or fluorescent dye (fluorescein or HEX) was introduced to complete the DNA microarray fabrication. In the case of DABCYL as a dark quencher, the closed form of the beacon probe enables FRET from POX-SH to the quencher and as a result the emission from POX-SH will be significantly suppressed. Hybridization of a target complementary DNA to the loop region of the molecular beacon moves DABCYL from POX-SH layer and the emission of POX-SH will be recovered. The DABCYL synthesis was confirmed by UV absorption spectrum (Figure 9-5) showing the new band at 460 nm corresponding to DABCYL absorption.

Because the FRET efficiency is strongly dependent on the inverse sixth power of the intermolecular distance between the donor and the accepter DABCYL should be closely located at the POX-SH surface to sufficiently quench the POX-SH emission. We controlled the length of the loop, stem, and the number of DABCYL in the molecular beacon design and studied the effects of these parameters on the sensitivity of the DNA

microarray. Figure 9-6 show the emission spectra of POX-SH having the molecular beacon P1 with two different linkers and different number of quenchers before (square) and after hybridization (triangle). First we added two thymine (T) units as a spacer between the P1 sequence and the POX-SH to provide a better mobility to the molecular beacon. Therefore, there are three thymine between the POX-SH and the base where DABCYL is attached as shown in Figure 9-6 (a) and the distance is 10.2 Å. In this case the POX-SH emission was quenched only 52% by DABCYL while the emission was fully recovered when the complementary DNA sequence was introduced. The control slide without the quencher did not show any fluorescence quenching in the closed form, confirming the 52% quenching is induced by DABCYL (Figure 9-6 (d)). Because the sensitivity of this type of turn-on sensors is determined by the level of the emission intensity increase relative to the initial intensity, the initial emission intensity of POX-SH should be quenched as much as possible. To achieve this we removed the TT spacer even though this may reduce the mobility of the molecular beacon. As we can see in Figure 9-6 (b), the emission of the molecular beacon in the closed form was further suppressed due to the smaller distance between DABCYL and POX-SH.

We applied super-quenchers (SQs), an array of multiple quenchers, to our DNA microarrays to further suppress the background signal. Tan *at el*. synthetically assembled a solution-state molecular beacon having two or three DABCYLs at the end of the probe to get better quenching efficiency and achieved relatively large enhancement of fluorescent signal due to super-quenching.[38] We synthesized two types of SQs (three DABCYLS, 3Q and nine DABCYLs, 9Q, Scheme 9-4) directly on POX-SH. As we can see in Figure 9-6 (c), however, the quenching efficiency of the supper quenchers was

even worse than that of the mono quencher. The 3Q showed only 47% quenching and the 9Q had 57% quenching. This is likely that the molecular beacon having the SQs does not form a stable closed state in the solid state due to the steric hindrance the bulky super quencher experiences at the solid surface.

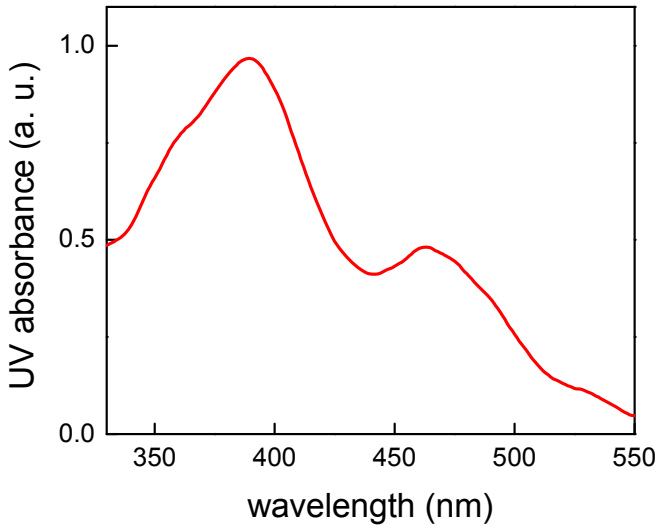

Figure 9-5. UV absorption spectra after DNA synthesis on polymer coated surface.

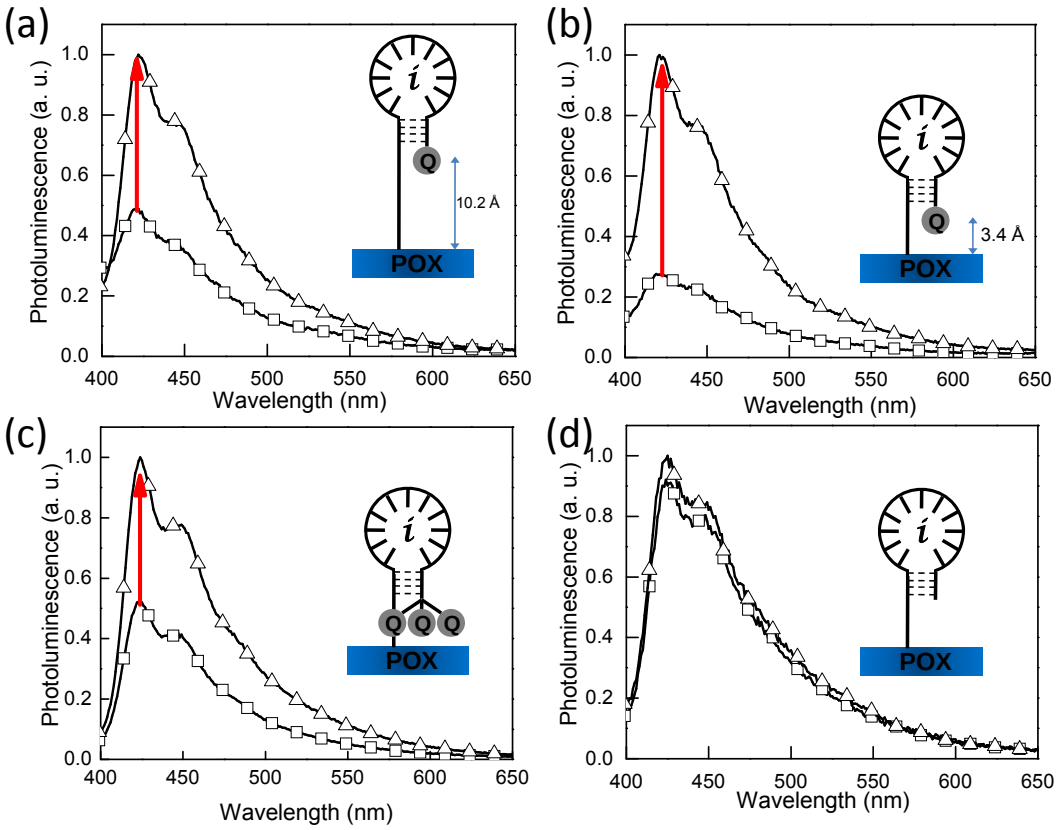

Figure 9-6. Polymer fluorescence before (square) and after hybridization (triangle) in various types of molecular beacons.

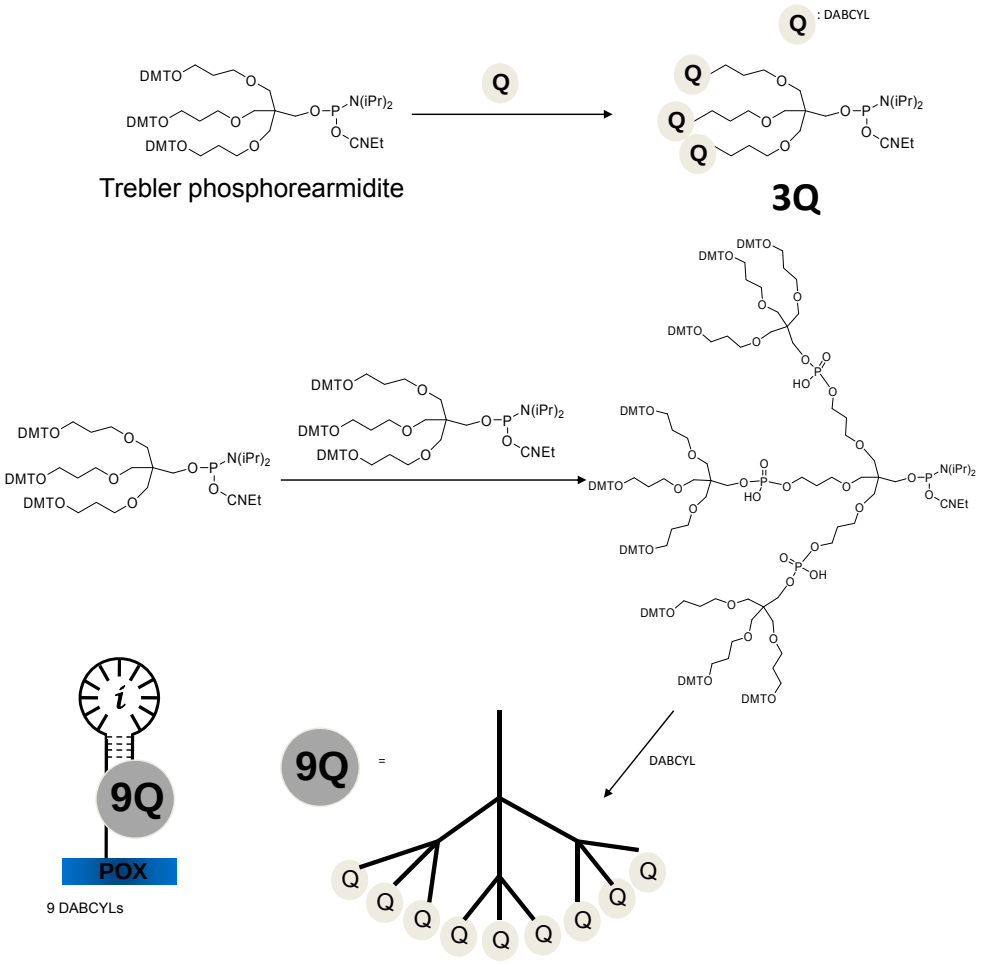

Scheme 9-4. SQ synthesis using trebler phosphorearmidite.

We also investigated the effect of the size of the loop on the quenching. Figure 9-7 shows the fluorescence spectra of two different probes, P1 and P2 before and after hybridization with target DNA C1 and C2, respectively. Emission of POX-SH having P1 and P2 were completely recovered upon hybridization. However, initial quenching efficiency of DABCYL on the shorter P1 was better than that of the longer P2. In the on-chip DNA synthesis of the probes P1 and P2, the overall synthesis yield of

oligonucleotide P1 and P2 are 74.0 % and 60.5 %, respectively. Therefore, the density of DABCYL of P1 is higher than that of P2. This is presumably the reason for the better quenching efficiency of the shorter probe P1.

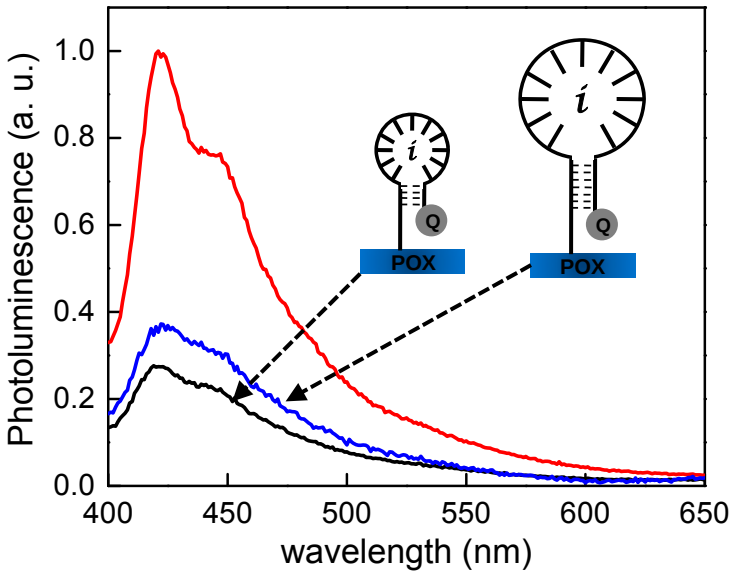

Figure 9-7. Photoluminescence of polymer-DNA chips having two different probe (P1 and P2) upon hybridization with target complement C1 and C2 respectively.

In addition to the 'turn-on' strategy discussed above, we have extended the molecular beacon-based label-free and signal amplifying DNA microarray concept to a 'turn-off' sensor by incorporating a fluorescent dye instead of DABCYL quencher (Figure 9-8). As the FRET accepter a fluorescein (green dye) or a HEX (yellow dye) was placed at the end of the molecular beacon. In the closed form, the fluorescent dye is located close to the POX-SH layer and efficiently takes fluorescence resonance energy transfer from the FRET donor, POX-SH. The emission signal from the dye is largely amplified (turn-on) through the FRET process because POX-SH as a macromolecule

absorbs much large amount of photon than a small molecular dye and the absorbed energy can be effectively transferred to the dye. When the molecular probe recognize its target sequence it forms a stable probe-target double helix by DNA hybridization. This recognition event moves the dye away from the POX-SH layer preventing FRET from the donor POX-SH to the dye, the FRET acceptor. Therefore the dye emission should be quenched (turn-off).

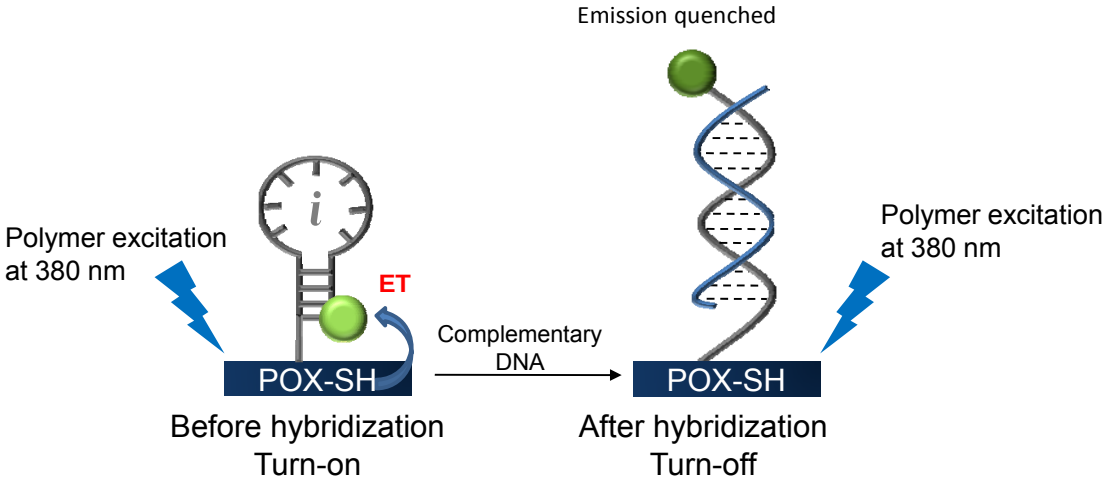

Figure 9-8. Schematic representation of turn-off sensor using fluorescence dye.

Figure 9-9 shows the fluorescence spectra of POX-SH having the molecular probe P1 or P2 with a fluorescein dye (5'-fluorescein-CCA CGC TCA TCA TAA CCT TCA GCA AGC TTT AAC TCA TAG TGA GCG TGG T-3') before and after hybridization with the complementary DNA sequence. Figure 9-9 (a) shows the signal amplification of the fluorescein dye of the closed form of P1. While the direct excitation of the fluorescein at 490 nm produced a weak emission the selective excitation of POX-SH at 380 nm generated much stronger emission from the fluorescein. Upon binding with a

complementary DNA (C1), the emission of fluorescein decreased due to the prevention of FRET (solid triangle) between POX-SH and fluorescein while the emission from fluorescein decreased only slightly (solid circle) in the presence of noncomplementary DNA (N1) (Figure 9-9 (b)). As shown in Figure 9-9 (c) and (d), P2 having the shorter sequence (5'-fluorescein-CGC TCC TAA AAC GAC GGC CAG TGG AGC GT-3') showed a slightly better amplification and emission quenching upon hybridization with the target sequence (C2).

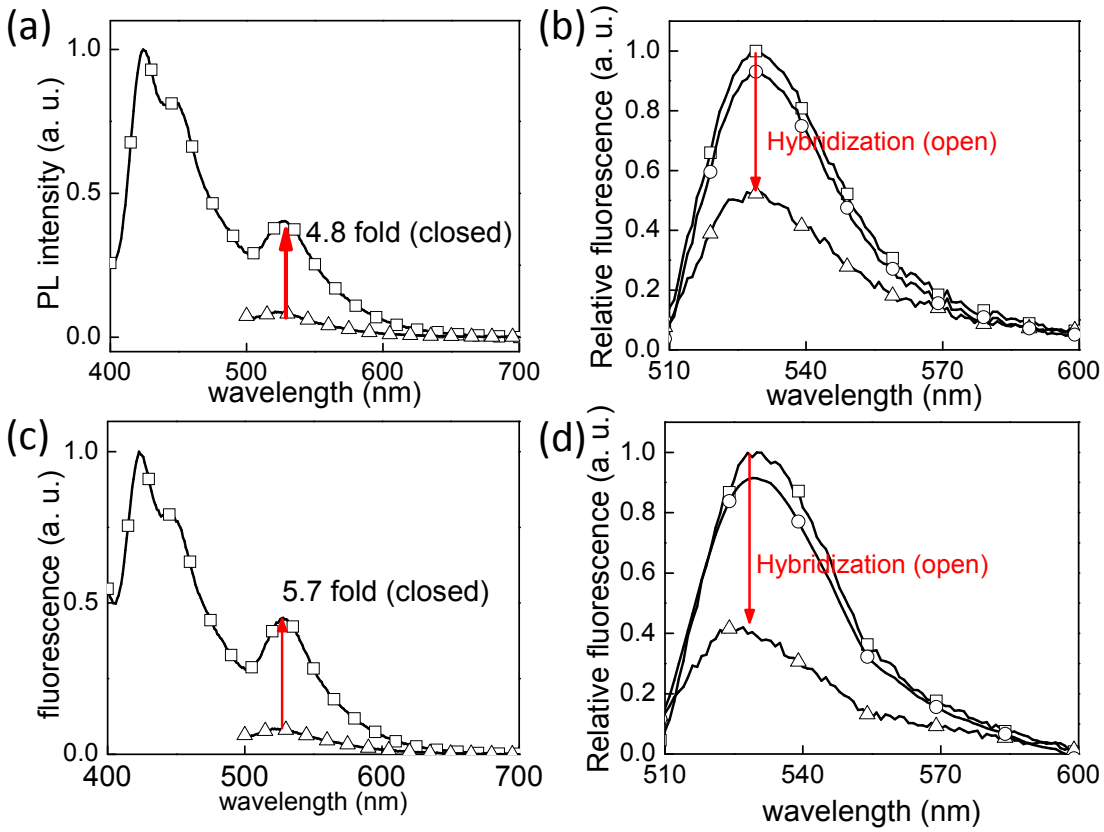

Figure 9-9. PL spectra in fluorescein dye case: Prehybridization state emission of (a) P1 and (c) P2 when excited at 380 nm (square) and 490 nm (triangle); relative fluorescence change after hybridization of P1 (b) and P2 (d) with target complement (C1 and C2, triangle) and random DNA (N1 and N2, circle) (excitation wavelength: 380 nm).

We also used HEX dye instead of fluorescein. The absorption and emission of HEX are in a longer wavelength compared to those of fluorescein, making the dye emission more discrete from the POX-SH emission. Overall the degree of amplification and the signal quenching by hybridization in the HEX system are similar to those of the fluorescein system (Figure 9-10).

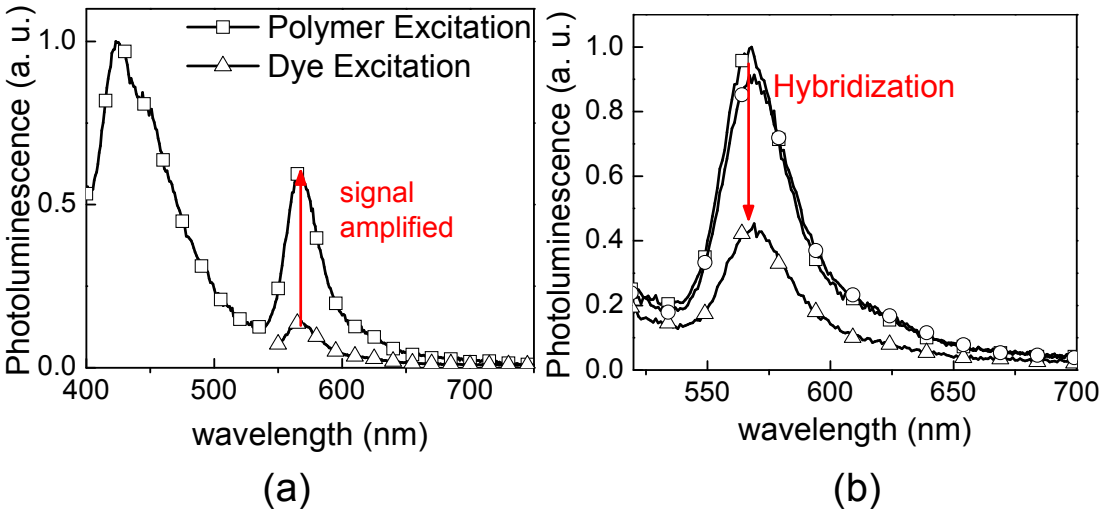

Figure 9-10. PL spectra when HEX dye was used: (a) emission in prehybridization state when excited at 380 nm (square) and 535 nm (triangle); (b) fluorescence change after hybridization with target DNA (triangle) and non-complementary DNA (circle) (square: prehybridization state, excitation wavelength: 380 nm).

9.5. Conclusion

In this chapter, we designed and synthesized POX-SH having oxadiazole unit for stability, thiol group for covalent tethering of POX-SH to a solid substrate, and amine unit for solid-state on-chip DNA synthesis. We developed self-signaling DNA microarray by synthesizing molecular beacons directly on a POX-SH layer by applying the on-chip DNA synthesis. A turn-on system with DNA hairpin probes having a nonfluorescent

quencher (DABCYL) and a turn-off system with a fluorescent dye (fluorescein or HEX) were developed. The turn-on sensor case, the fluorescent signal of POX-SH originally quenched by DABCYL was recovered upon binding with the complementary DNA while a nonspecific DNA sequence resulted in a minimal change in fluorescence emission. We controlled the length of the loop, stem, and the number of DABCYL in the molecular beacon design and studied the effects of these parameters on the sensitivity of the DNA microarray. In the turn-off system, as the FRET accepter a fluorescein (green dye) or a HEX (yellow dye) was placed at the end of the molecular beacon. In the closed form, the fluorescent dye is located close to the POX-SH layer and efficiently takes fluorescence resonance energy transfer from the FRET donor, POX-SH, and produced amplified emission. When the molecular probe recognize its target sequence it forms a stable probe-target double helix by DNA hybridization. This recognition event moved the dye away from the POX-SH layer preventing FRET from the donor POX-SH to the dye and quenched the dye emission. We demonstrated the self-signaling and signal amplifying DNA microarray by combining rational molecular design of emissive conjugated polymer, POX-SH, and solid-state DNA synthesis of molecular beacons.

Our preliminary experiments designed to prove the concept of self-signaling and signal amplifying DNA microarray have been successfully demonstrated. We anticipate that the optimization of the appropriate selection of a quencher and its size, a probe size, surface density, and better instrument design can improve the selectivity and sensitivity. Efforts to optimize and implement this design in a microarray format are in progress along these lines.

9.6. References

1. Langer, R.; Tirrell, D. A. Designing materials for biology and medicine. *Nature* **2004**, *428*, 487.

2. Lipshutz, R. J.; Fodor, S. P. A.; Gingeras, T. R.; Lockart, D. J. *Nat. Genet*. **1999**, *21*, 20.

3. Wolcott, M. J. Clin. *Microbiol. Rev*. **1992**, *5*, 370.

4. Breaker, R. B. *Nature*, **2004**, *432*, 838.

5. Schena, M.; Shalon, D.; Davis, R. W.; Brown, P. O. *Science* **1995**, *270*, 467.

6. Service, R. F. *Science* **1998**, *282*, 396.

7. Ramsay, G. *Nat. Biotechnol*. **1998**, *16*, 40.

8. Southern E. M. *Trends Genet*. **1996**, *12*, 110.

9. Smith, E. A.; Kyo, M.; Kumasawa, H.; Nakatani, K.; Saito, I.; Corn, R. M. *J. Am. Chem. Soc.* **2002**, *124*, 6810.

10. Brockman, J. M.; Frutos, A. G.; Corn, R. M. *J. Am. Chem. Soc*. **1999**, *121*, 8044.

11. Chen, Y.; Munechika, K.; Ginger, D. S. *Nano Lett*. **2007**, *7*, 690.

12. Wang, J. *Nucleic Acids Res*. **2000**, *28*, 3011.

13. Okahata, Y.; Matsunobo, Y.; Ijiro, K.; Murakami, A.; Makino M. *J. Am. Chem. Soc*. **1992**, *114*, 8299.

14. Bardea, A.; Dagan, A.; Ben-Dov, I.; Amit, B.; Willner, I. *Chem. Comm*. **1998**, 839.

15. Patolsky, F.; Lichtenstein, A.; Willner, I. *J. Am. Chem. Soc*. **2000**, *122*, 418.

16. Johnston, A. P. R.; Read, E. S.; Caruso, F. *Nano Lett.* **2005**, *5*, 953.

17. Johnston, A. P. R.; Mitomo, H.; Read, E. S.; Caruso, F. *Langmuir* **2006**, *22*, 3251.

18. Nguyen, T. H.; Elimelech, M. *Biomacromolecules* **2007**, *8*, 24.

19. Shiigi, H.; Tokonami, S.; Yakabe, H.; Nagaoka, T. *J. Am. Chem. Soc*. 2**005,** *127*, 3280.

20. Park, S.-J.; Taton, T. A.; Mirkin, C. A. *Science* **2002**, *295*, 1503.

21. He, F.; Tang, Y.; Yu, M.; Feng, F.; An, L.; Sun, H.; Wang, S.; Li, Y.; Zhu, D.; Bazan, G. C. *J. Am. Chem. Soc*. **2006**, *128*, 6764.

22. Maruyama, T.; Takata, T.; Ichinose, H.; Kamiya, N.; Kuma, H.; Hamasaki, N.; Morita, H.; Goto, M. *Biotechnol. Prog*. **2005,** *21*, 575.

23. Maruyama, T.; Park, L. C.; Shinohara, T.; Goto, M. *Biomacromolecules* **2004**, *5*, 49.

24. Lee, K.; Maisel, K.; Rouillard, J.-M.; Gulari, E.; Kim, J. *Chem. Mater.***2008** in press.

25. Bockisch, B.; Grunwald, T.; Spillner, E.; Bredehorst, R. *Nucleic Acids Res*. **2005**, *33*, e101.

26. Du, H.; Strohsahl, C. M.; Camera, J.; Miller, B. L.; Krauss, T. D. *J. Am. Chem. Soc*. **2005**, *127*, 7932.

27. Culha, M.; Stokes, D. L.; Griffin, G. D.; Vo-Dinh, T. *J. Biomed. Opt*. **2004**, *9*, 439.

28. Tan, W.; Wang, K.; Drake, T. J. *Curr. Opin. Chem. Biol*. **2004**, *8*, 547.

29. Broude, N. E. *Trends Biotechnol*. **2002**, *20*, 249.

30. Goel, G.; Kumar, A.; Puniya, A. K.; Chen, W.; Singh, K. *J. Appl. Microbiol*. **2005**, *99*, 435.

31. Thomas, S. W., III; Joly, G. D.; Swager, T. M. *Chem. Rev*. **2007**, *107*, 1339.

32. Lee, K.; Rouillard, J.-M.; Pham, T.; Gulari, E.; Kim, J. *Angew. Chem. Int. Ed*. **2007**, *46*, 4667.

33. Lee, K.; Povlich, L. K.; Kim, J. *Adv. Funct. Mater*. **2007**, *17*, 2580.

34. Lee, K.; Kim, H.-J.; Cho, J. C.; Kim, J. *Macromolecules* **2007**, *40*, 6457.

35. Gao, X.; LeProust, E.; Zhang, H.; Srivannavit, O.; Gulari, E.; Yu, P.; Nishiguchi, C.; Xiang, Q.; Zhou, X. *Nucleic Acids Res*. **2001**, *29*, 4744.

36. Miyaura, N.; Suzuki, A. *Chem. Rev*. **1995**, *95*, 2457.

37. Du, H.; Disney, M. D.; Miller, B. L.; Krauss, T. D. *J. Am. Chem. Soc*. **2003**, *125*, 4012.

38. Yang, C. J.; Lin, H.; Tan, W. *J. Am. Chem. Soc*. **2005,** *127*, 12772.

CHAPTER 10

Label-Free Identification of Prostate-Specific Antigen using Conjugated Polymer-Peptide Hybrid Chips

Parts of this chapter appear in: Lee, K.; Mandal, S.; Morry, J.; Srivannavit, O.; Gulari, E.; Kim. J. Manuscript in preparation.

10.1. Abstract

A fast and readily applicable detection strategy has been established through the development of label-free Prostate Specific Antigen (PSA) chips by designing a novel conjugated polymer (P1) and combining it with on-chip peptide synthesis. A layer of P1 was covalently anchored to a glass substrate through a polyethyleneglycol linker. A probing peptide sequence that is known to be efficiently cleaved by PSA was synthesized directly from P1 by means of a solid-state peptide synthesis. The end of the peptide was terminated either by a reporter (a fluorescent dye or a quencher) so that an efficient fluorescence energy resonance transfers (FRET) can be established between P1 and the reporter. The selective cleavage of the probing peptide sequence by PSA affected the FRET and produced a sensitive and selective fluorescence sensory signal.

10.2. Introduction

For decades, proteomics involving the large-scale study of proteins, particularly comprehensive view of the structure, function and regulation of biological systems have formed the core technologies for protein analysis.[1-7] A promising application of proteomics is for the development of specific protein biomarkers for disease diagnostics. There is also an increasing potential for spatially addressable peptide libraries by means of the on-chip peptide synthesis in proteomics because of the increasing demand of simultaneous detection of diverse range of biomolecular interaction and sequence specific bioactivity. However, the most current methods for biomarker detection require target labeling which is a costly and time-consuming process and requires subsequent stringent purification after the labeling. For example, commonly used separation and detection techniques are highly quantitative electrophoresis[8], high pressure liquid chromatography (HPLC) separation[9], mass spectroscopy[10], enzyme linked immunosorbent assay (ELISA)[11-13], and blotting techniques[14]. These fastidious steps make it difficult to perform real-time organism detection and fast diagnosis of cancer-related diseases.

Prostate cancer is a disease in which cancer develops in the prostate, a grand in the male reproductive system, and has become the most commonly diagnosed cancer in men. Many men who develop prostate cancer never have any symptoms, undertake no therapy, and eventually die of other causes.[15] Even though it can be treated with cryosurgery, radiation therapy, androgen deprivation therapy, chemotherapy, and proton therapy, currently there is no effective treatment that significantly prolongs in the life expectancy of a prostate cancer patient. The mortality rate of the prostate cancer has increased steadily. National Cancer Institute estimated in 2007 that one out of three men

turned out to be a new patient and one in every eighteen men died of prostate cancer. In fact prostate cancer is responsible for more male deaths than any other cancers except lung cancer. Therefore, an early detection is critically important to save the life of prostate cancer patients. Clinically, diagnosis of prostate cancer was firstly conducted by the measurement of a protein called prostate specific antigen (PSA) in the blood. PSA, a member of tissue chymotrypsin family of protease, is a 34kD glycoprotein produced almost exclusively by epithelium cells in the prostate gland. Increased levels of PSA may suggest the presence of prostate cancer and it has been recently used as a biomolecular marker for prostate cancer screening.[16-18]

Conjugated polymers are promising active materials to devise future generations of biosensors for the detection of biological molecules due to their environmental sensitive and signal amplifying properties.[19,20] Many recent papers have reported the use of amplified fluorescence signal of conjugated polymers as a sensitive signaling reporter for the detection of a number of biological analytes.[21,22] Upon binding with a target biological molecule, conjugated polymer-based sensory systems showed a remarkable fluorescence change by means of efficient electron transfer or fluorescence resonance energy transfer (FRET).

Herein, we report a label-free and sensitive protein chips using a highly fluorescent conjugated polymers to detect prostate cancer in early stage (Figure 10-1). A hexapeptide molecule which can be enzymatically cleaved by PSA has been selected and was directly synthesized on amine functionalized conjugated poly(oxadiazoles) (P1). After parallel peptide synthesis on polymer-coated slide followed by labeling with a

quencher or dye, the sample slide was incubated into PSA solution to observe FRET induced signal-amplified fluorescence change upon peptide cleavage.

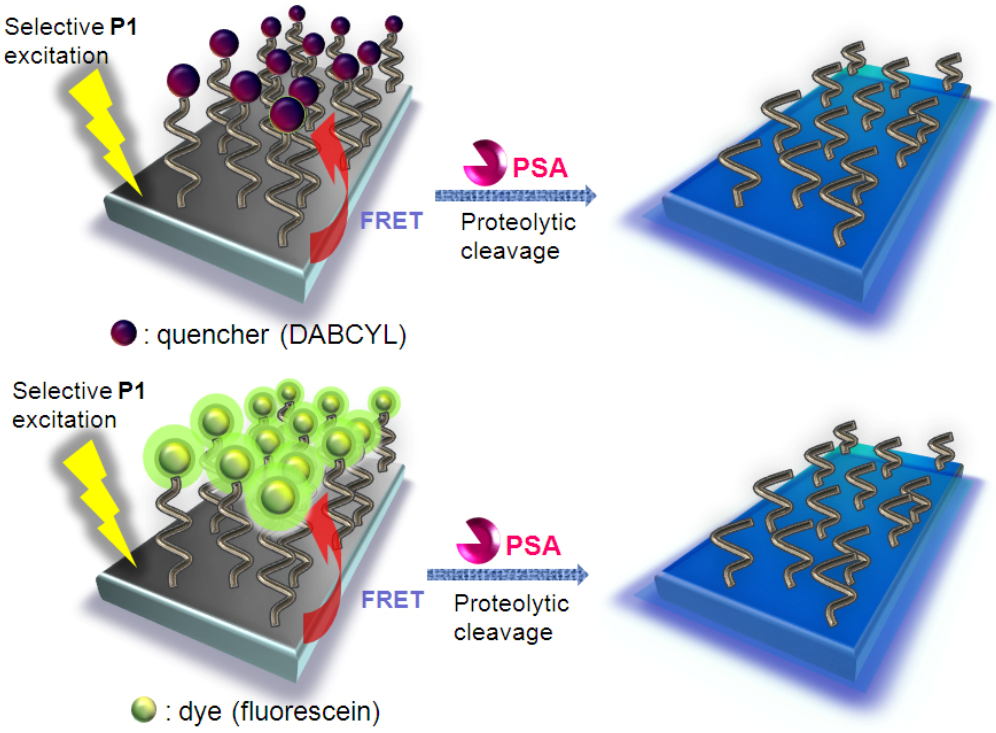

Figure 10-1. Schematic representation of PSA detection using conjugated polymer-peptide hybrid chips.

10.3. Experimental Section

Materials and Methods All solvents and reagents for polymer (P1) preparation were used without further purification as received from Sigma-Aldrich Co. UV/Vis absorption spectra were recorded with a Varian Cary50 UV/Vis spectrophotometer. Photoluminescence spectra and quantum yield in solution and in the solid state were obtained by using PTI QuantaMaster^{TM} spectrofluorometer equipped with an integrating sphere. The quencher, dimethylaminoazosulphonic acid (DABCYL), and the fluorescent

dye, 4,5-carboxyfluorescein (FAM), used in labeling the peptide sequence were purchased from AnaSpec, Inc and Molecular Probes, Co. respectively. The detail synthetic route and characteristic data of the conjugated polymer, poly(oxadiazole-co-phenylene-co-fluorene) (P1), has been previously reported.[20] Glass substrates used in this study were prepared by using a slightly modified literature procedure.[20]

Slides preparation Glass slides (25 mm × 75 mm) were dipped in $NH_4OH/H_2O_2/H_2O$ (40 ml/40 ml/160 ml) at 80 °C for 1 h and rinsed with DI water (30 ml). After drying, the slide was soaked in pirahna solution (H_2SO_4 : H_2O_2 = 35 ml : 15 ml) overnight, washed with DI water (30 ml) and dried with a stream of air. The glass slides were then transferred into a jar containing 97% aminopropyltrimethoxysilane (APTMS, 2ml), DI water (2ml) and high-purity methanol (48ml) and sonicated for 30 minutes. Finally, the slides were washed with methanol, followed by water, and then dried under a stream of air. The slides were baked at 135^{o}C for 30 minutes before the addition of polyethylene glycol (PEG) linker.

Addition of PEG linker SCM−PEG−Fmoc was reacted with the hydroxyl group of the APTMS to form a reactive linker for P1. The glass slides were then washed with ethanol and DMF and placed in 20% piperidine in dimethylformamide (DMF) for 2 hours.

P1 immobilization onto the glass slides The glass slides were reacted with 1,4-diphenylenediisothiocyanate (100 mg) in DMF (54 ml) in for 2 hours. The slides were then washed with dimethylformamide and dichloromethane before drying under a stream of air. Only one side of the slide was reacted with **P1** (2 mg) in pyridine (0.5 ml) and chloroform (9 ml). The slides were subsequently washed with chloroform,

dichloromethane, and DI water. Further cleaning steps of the slide were achieved by sonication in chloroform for 5 min and drying in a vacuum oven.

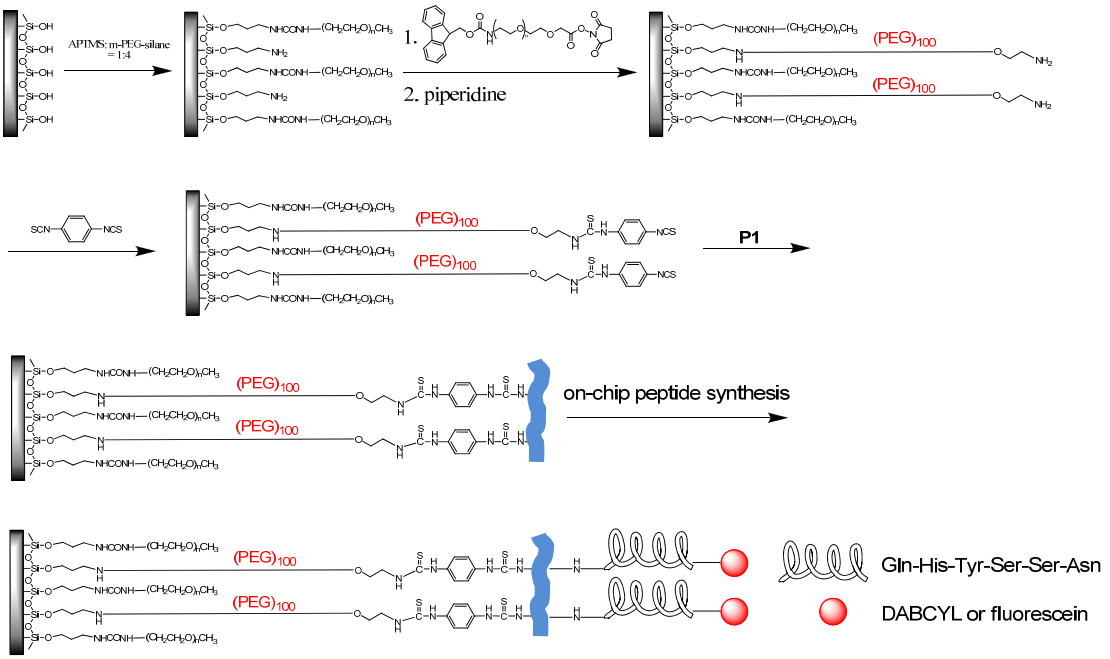

Scheme 10-1. Schematic representation of polymer immobilization onto glass substrate and on-chip peptide synthesis.

Direct peptide synthesis onto the glass slides[21] The glass slide was enclosed in a holder connected to a peptide synthesizer. Standard Fmoc (9-fluorenylmethyloxycarbonyl) was used for all steps. The glass slides were treated with a solution of 0.4 mmol of Fmoc protected amino acid, 0.4 mmol of 0.6 M solution of 2-(1h-7-azabenzotriazole-1-yl)-oxy-1,1,3,3,-tetramethyluroniumhexafluorophosphate (HATU) and 0.5 mmol of diisopropylethylamine (DIEA) in DMF. An activation time of 3 minutes and coupling time of 10 minutes was allowed for completion of coupling. Unsuccessful

couplings were capped with a 20% solution of acetic anhydride in DMF for 2 minutes. This was followed by extensive washing with DMF. Deprotection of Fmoc protecting group was done by flushing the glass substrate with a solution of piperidine in DMF for 20 minutes. The removal of side-chain protecting groups and the peptide from the resin at the end of the synthesis was achieved by incubating in a solution of trifluoromethanesulfonic acid, trifluoroacetic acid (TFA), dichloromethane, ethanedithiol, and thioanisole.

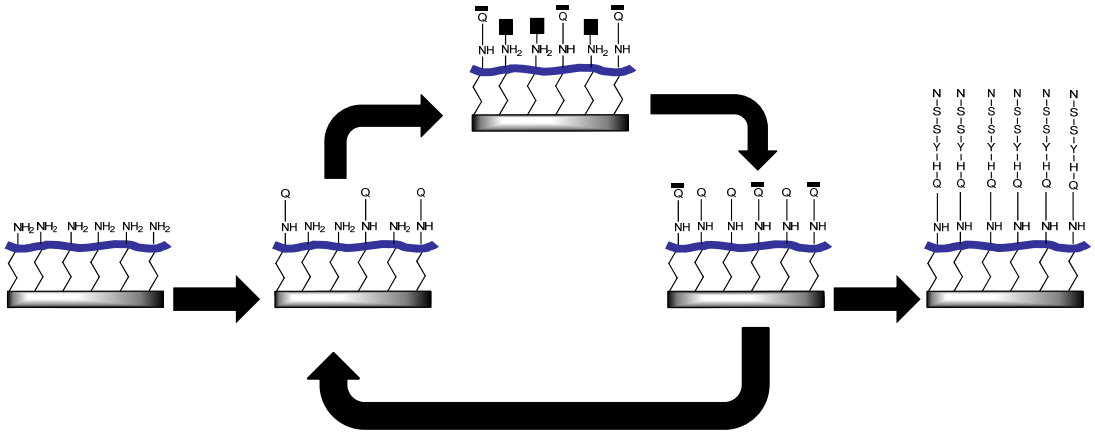

Scheme 10-2. Fmoc solid phase peptide synthesis.

Fluorescent labeling with carboxyfluorescein[21] The solution of FAM labeling was prepared by mixing 5ml of FAM stock solution (0.5 mM in DMF) with 0.3 gm of hydroxybenzotriazole (HOBT) and 500µl of diisopropylcarbodiimide (DIC). The glass substrates were incubated in this solution for 2 hours. Finally, the slides were washed with DMF and ethanol consecutively. DABCYL labeling was done in a same manner as fluorescein labeling.

PSA cleavage test 10μL of PSA was added onto the peptide coated region of the glass slides and incubated with 90μL of PSA buffer (100mM Tris, 0.5M NaCl) in a petridish at 37^{o}C for 4 hours. After washing the glass with the buffer and DI water, the photoluminescence spectra of each glass slide were examined by using PTI QuantaMaster^{TM} Spectrofluorometer before and after the incubation.

10.4 Results and Discussion

There are two strategies being employed in this study as shown in Figure 10-1. In the first strategy, a quencher-tagged peptide substrate is synthesized on P1 on the glass substrate. We used DABCYL (4-{[4-(Dimethylamino)-phenyl] azo}-benzoic acid) whose absorption has a good overlap with the polymer emission, satisfying the requirement for efficient FRET. The energy transfer from P1 to DABCYL will reduce the fluorescence emission intensity of P1. After the cleavage, however, the fluorescence emission of P1 should be recovered due to the removal of the quencher from the peptide. In the second strategy, fluorescein, a green dye, instead of the quencher is tagged at the end of the peptide sequence. Fluorescein was chosen to establish an efficient FRET from the energy donor (P1) to the acceptor (fluorescein). The attachment of the fluorescein at the end of the peptide grown from the P1-immobilized substrate will result in emission quenching of P1 and amplified dye emission simultaneously. The selective cleavage of the peptide sequence by PAS will remove the dye and induce the recovery of the P1 emission and the suppression of the amplified dye emission. The same peptide without DABCYL on P1-coated substrates was prepared as a negative control.

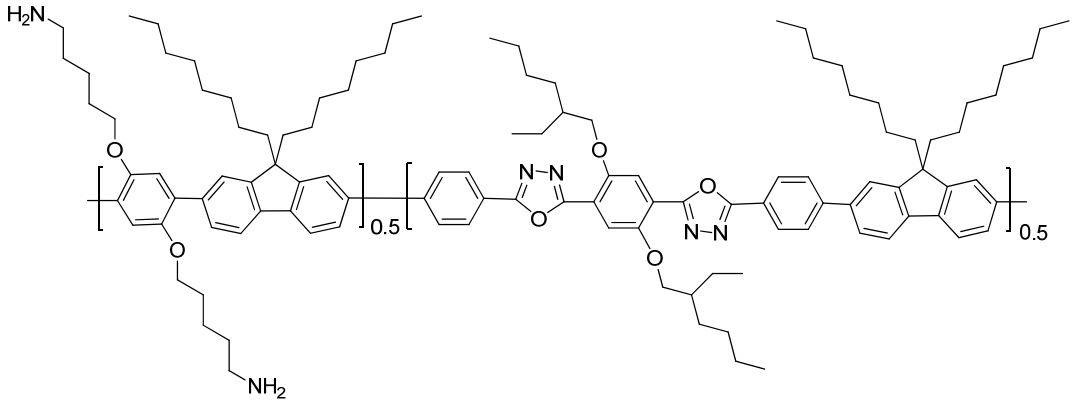

Figure 10-2. Chemical structure of P1.

As indicated in Scheme 10-1, a glass slide was firstly treated with a mixture of APTMS and m-polyethyleneglycol (PEG) silane (1:4 v/v) in ethanol/toluene solution to derivate amine group on the surface. The m-PEG chain was used to control the density of the amine functional groups on the surface by interspersion of the reactive amine group. After curing for 1 hr, it was dipped into a sodium phosphate buffer solution of the succinimide ester functionalized PEG5000 linker having Fmoc-amine (SCM-$(PEG)_{100}$-Fmoc). We introduced the long PEG linker between the slide and the P1 to increase the accessibility of PSA to the peptide sequence and to reduce non-specific adsorption of PSA to the substrate at the same time. As we concerned about the steric hindrance of PSA to the surface-tethered peptide sequence, the long PEG linker later turned out to be necessary for a successful peptide cleavage by PSA. After deblocking of Fmoc-amine by treatment of piperidine, 1,4-phenylenediisothiocynate was then reacted with free amine to form a reactive isothiocyanato group and followed by P1 tethering. Each step was confirmed by a characteristic peak in UV absorbance and photoluminescence spectra. It has been previously noted that P1 containing the oxadiazole unit is uniquely stable in UV

and strong acid treatment therefore suitable for the on-chip oligonucleotide synthesis in solid state.[22] The amine groups on P1 were used to anchor P1 to the glass substrate and as the reaction group for the peptide synthesis at the same time. The fluorene unit was introduced to increase P1 solubility in organic solvents and to facilitate solution-based film fabrication.

An *in-situ* integrated parallel peptide synthesis using solid-phase peptide chemistry and photogenerated acid chemistry were conducted by using an Expedite 8909 DNA synthesizer modified for peptide synthesis and equipped with an optical setup. PSA acts as a protease that semenogelins (namely I and II) in the seminal coagulum. Several peptide sequences corresponding to the cleavage map for semenogelin-I and semenogelin-II have been proposed in the literature. A preferred subsite occupancy was previously defined for peptide cleavage by PSA using phage display and iterative optimization of native substrate sequences.[23,24] The peptide sequence was chosen from a list of hexapeptide substrates found by Yang and co-workers.[23,25,26] The sequence, QHY−SSN, appears to have the highest relative cleavage rates (1.00) among all other hexapeptides and is therefore, used in this study. For the synthesis of the peptide sequence, conventional Fmoc chemistry by means of (*O*-(7-Azabenzotriazol-1-yl)-*N,N,N',N'*-tetramethyluronium hexafluorophosphate) (HATU) reagent was used. Side chain protecting groups were removed before attaching a dye or a quencher. P1 maintained its emissive property through the treatment of a blend of strong acids necessary for the side-chain removal. Finally, 4,5-carboxyfluorescein as a fluorescent dye or DABCYL as a quencher was labeled using carboxy-fluorescein and Lys(DABCYL), respectively (Figure 10-3).

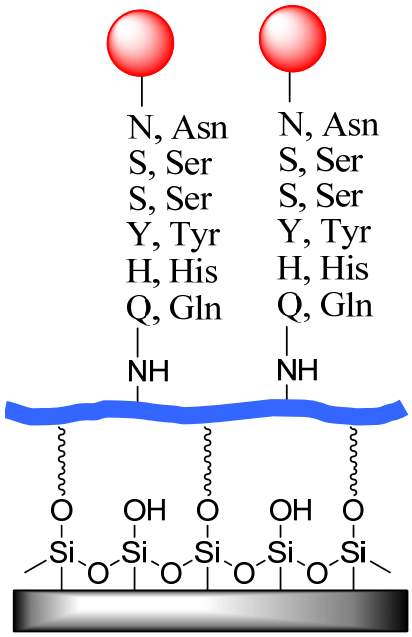

Peptide synthesis

1. **Coupling:**
   - I. HATU(2-(1H-7-azabenzotriazole-1-yl)-oxy-1,1,3,3-tetramethyluroniumhexafluorophosphate)
   - II. DIEA (Diisopropylethylamine), Fmoc amino acid
2. **Capping:** Acetic anhydride in DMF
3. **Deprotection:** Piperidine in DMF
4. **Side chain removal:**
   - I. Trifluoromethanesulfonic acid
   - II. Trifluoroacetic acid
   - III. Dichloromethane
   - IV. Ethanidithiol
   - V. Thioanisole
5. **FAM labelling:**
   - I. 4, 5 carboxyfluorescein
   - II. HOBT
   - III. Diisopropylcarbodiimide.

Figure 10-3. The synthetic procedure of the on-chip peptide synthesis on the P1-coated substrate and the reagents used for the synthesis.

The fluorescence spectrum of the P1-coated peptide slides before and after the incubation with PSA was obtained from a photoluminescence spectrometer. First, in the case DABCYL attached first strategy, fluorescence emission of P1 was significantly quenched by FRET from P1 to DABCYL before addition of PSA (Figure 10-4). After the proteolytic cleavage of the hexapeptide sequence by PSA, the emission intensity of P1 was fully recovered. The negative control in Figure 10-5 made use of the same hexapeptide sequence but without the attachment of DABCYL. No quenching of the P1 emission was observed of course and therefore there was no difference in the P1 emission intensity before and after the incubation with PSA. This result demonstrates that direct

on-chip peptide synthesis onto the P1-coated glass slide and the cleavage of the hexapeptide substrate by PSA were successfully accomplished.

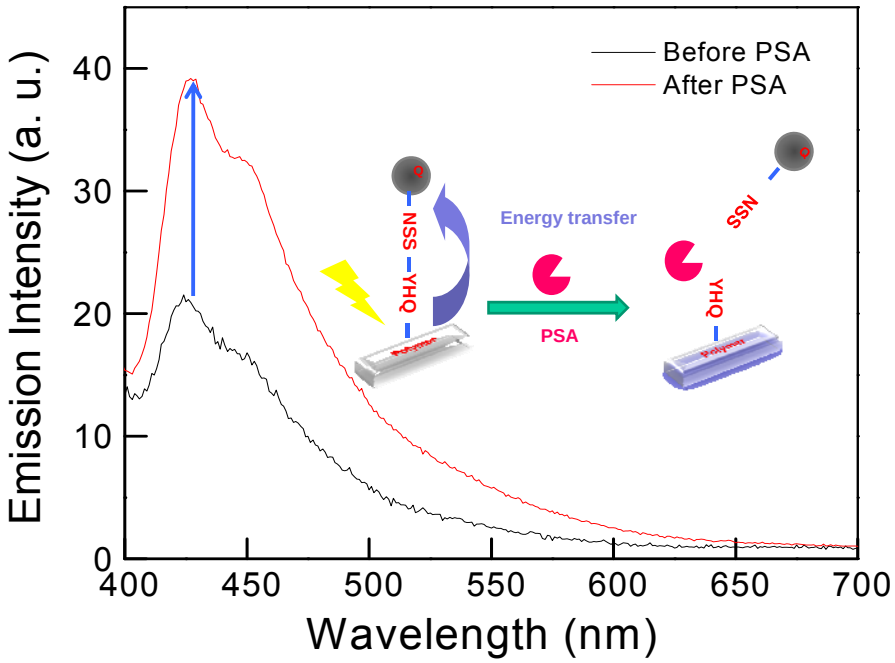

Figure 10-4. Photoluminescence spectra of P1-DABCYL system before (black) and after (red) PSA incubation. The slide was excited at 380 nm, a characteristic excitation wavelength of P1.

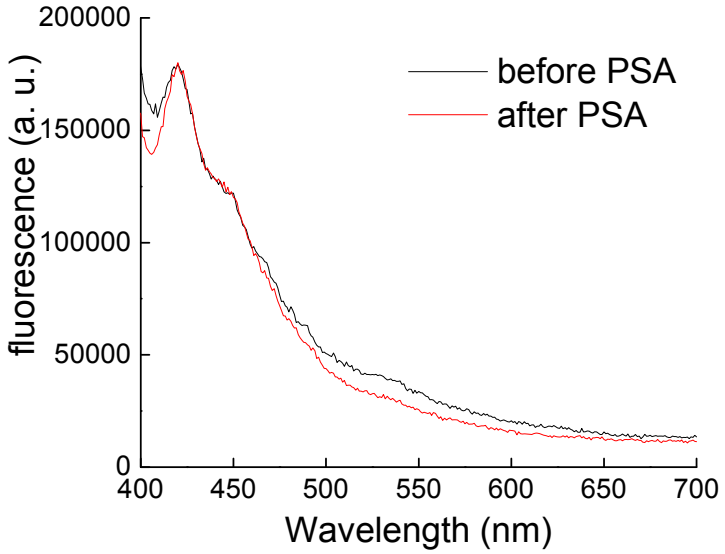

Figure 10-5. Photoluminescence of the same hexapeptide without DABCYL quencher on the P1-coated substrate as a control before and after the incubation with PSA. The excitation wavelength was 380 nm.

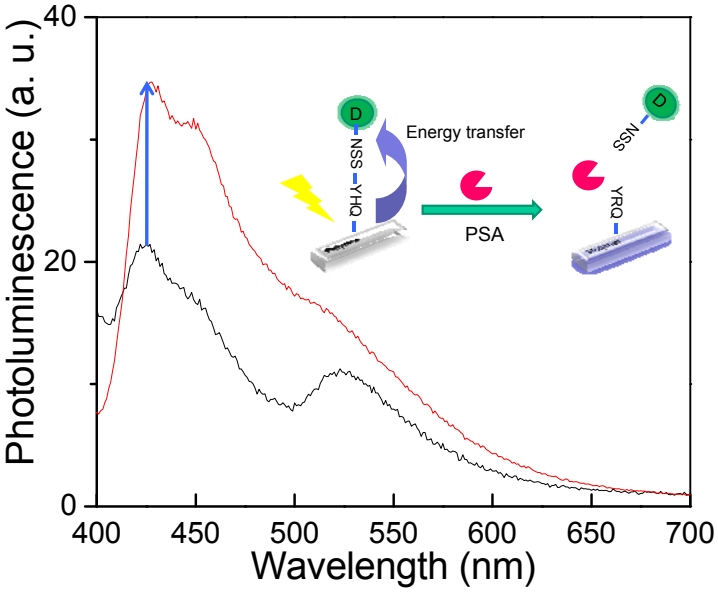

Figure 10-6. Photoluminescence spectra of P1-fluorescein before (black) and after (red) the PSA incubation. The slide was excited at 380 nm, a characteristic excitation wavelength of polymer.

In the second approach as illustrated in Figure 10-6 a fluorescein dye was attached to the end of the hexapeptide instead of DABCYL quencher. Figure 10-6 also shows the emission spectra of P1 before and after the incubation with PSA. Before the PAS treatment the discrete fluorescein emission peak was observed at 520 nm when P1 was selectively excited at 380 nm because the fluorescein emission was amplified through an effective FRET from P1 to fluorescein. Upon the release of fluorescein dye when the hexapeptide was cleavage by PSA, the emission from fluorescein was almost completely disappeared, whereas the P1 emission was restored. This signal conversion from fluorescein and P1 clearly indicates an efficient förster energy transfer from P1 to fluorescein. The FRET efficiency calculated by the equation, 1-(PL intensity after PSA at 525 nm)/(PL before PSA at 525 nm) was 0.78 when the long PEG spacer was used, whereas it was only 0.2 when PEG linker was not used. This confirms that the long and flexible PEG linker enables PSA to be fully accessible to the hexapeptide probe. We also checked the specificity of the hexapeptide sequence toward the enzymatic cleavage of PSA by constructing a P1-coated peptide chip having one mismatch in the peptide sequence, QRY-SSN, as a negative control. This sequence was reported to have a much lower cleavage rate due to the perturbed electrostatic potential of the catalytic triad in the literature.[25] The results presented in Figure 10-7 show no change in the P1 emission before and after the incubation with PSA due to the single-mismatch in the peptide sequence. In the same figure, direct excitation of fluorescein at 490 nm produced only much weaker fluorescence emission, confirming that the fluorescein emission was largely amplified by FRET from P1 to fluorescein when P1 was selectively excited at 380 nm.

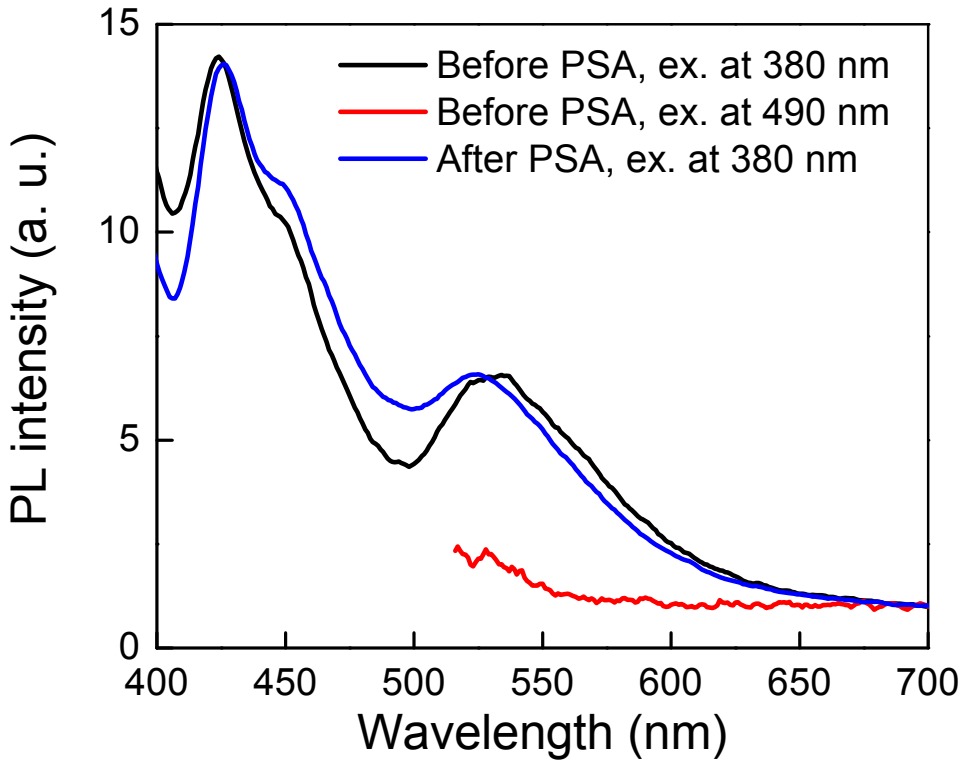

Figure 10-7. Photoluminescence of the P1-fluorescein having the single-mismatch sequence QRY-SSN before and after the PSA incubation. Excitation wavelength: 380 nm for P1 excitation (black and blue lines) and 490 nm for direct fluorescein excitation (red).

10.5. Conclusion

In this chapter, we have demonstrated a label-free and signal amplifying peptide microarray using a conjugated polymer as a FRET donor and a DABCYL quencher or fluorescein dye as a FRET acceptor. The FRET donor and the acceptor were connected through a hexapeptide sequence, QHY-SSN, for which PSA is a specific protease. The specific enzymatic cleavage of QHY-SSN sensitively affected on the FRET between the polymer to the reporter and produced fluorescence sensory signal. A negative control having no reporter and a single-mismatch sequence of QRY-SSN, respectively, showed no signal generation, confirming the specificity of the peptide microarray for PSA

detection. A long and flexible PEG linker turned out to be necessary to keep the protease activity of a free PSA toward the hexapeptide probe tethered to the P1-coated substrate. Currently we are investigating the detection limit of this system. The cleavage test results were very encouraging for the development of clinical test of a patient serum. Further studies are in progress.

10.6. References

1. Anderson, N. L.; Anderson, N. G. *Electrophoresis*, **1998**, *19*, 1853.

2. Blackstock, W. P.; Weir, M. P. *Trends Biotechnol*. **1999**, *17*, 121.

3. Hanash, S., Ed. Special Issue: Protein microarrays. *Proteomics* **2003**, 3 (11 and all papers therein).

4. MacBeath, G.; Schreiber, S. L. *Science* **2000**, 289, 1760.

5. Houseman, B. T.; Huh, J. H.; Kron, S. J.; Mrksich, M. *Nat. Biotechnol*. **2002**, *20*, 270.

6. Haab, B. B. *Proteomics* **2003**, *3*, 2116.

7. Angenendt, P.; Glokler, J.; Sobek, J.; Lebrach, H.; Cahill, D. J. *J. Chromatogr. A* **2003**, *1009*, 97.

8. Berg, J. M.; Tymoczko, J. L.; Stryer, L. Molecular Cell Biology, , 5th ed., W. H. Freeman, 2002.

9. Kennedy, R. T.; German, I.; Thompson, J. E.; Witowski, S. R. *Chem. Rev*. **1999**, *99*, 3081.

10. Kassel, D. B. *Chem. Rev*. **2001**, *101*, 255.

11. Lequin, R. *Clin. Chem*. **2005**, *51*, 2415.

12. Engval, E.; Perlman, P. *Immunochemistry*, **1971**, *8*, 871.

13. Ward, A. M.; Catto, J. W.F.; Hamdy, F. C. *Ann. Clin. Biochem*. **2001**, *38*, 633.

14. Burnette, W. N. *Anal. Biochem*. **1981**, *112*, 195.

15. Bostwick, D. G.; Crawford, E. D.; Higano, C. S.; Roach, M. Eds. *American Cancer*

Society's Guide to Prostate Cancer; Atlanta, GA: American Cancer Society, 2005.

16. Sahab, Z. J.; Semaan, S. M.; Sang, Q.-X. A. *Biomarker Insights* **2007**, *2*, 21.

17. Sokoll, L. J.; Chan, D. W. *Urologic Clinics North America* **1997**, *24*, 253.

18. Paul, B.; Dhir, R.; Landsittel, D.; Hitchens, M. R.; Getzenberg, R. H. *Cancer Res*. **2005**, *65*, 4097.

19. Zhou, Q.; Swager, T. M. J. Am Chem. Soc. **1995**, *117*, 12593.

20. Swager, T. M. *Acc. Chem. Res*. **1998**, *31*, 201.

21. Thomas, S. W. III; Joly, G. D.; Swager, T. M. *Chem. Rev*. **2007**, *107*, 1339 and all references therein.

22. Lee, K.; Rouillard, J.-M.; Pham, T.; Gulari, E.; Kim, J. *Angew. Chem. Int. Ed*. **2007**, *46*, 4667.

23. Mandal, S. R., "*Parallel Peptide Synthesis of Microfluidic Microarrays for Identification of Protein and Cell Binding Ligands*", Ph. D. dissertation, University of Michigan, 2007

24. Lee, K.; Kim, H.-J.; Cho, J. C.; Kim, J. *Macromolecules* **2007**, *40*, 6457.

25. Coombs, G. S.; Bergstrom, R. C.; Pellequer, J.-L.; Baker, S. I.; Navre, M.; Smith, M. M.; Tainer, J. A.; Madison, E. L.; Corey, D. R. *Chem. Biol.* **1998**, *5*, 475.

26. Réhault, S.; Brillard-Bourdet, M.; Bourgeois, L.; Frenette, G.; Juliano, L.; Gauthier, F.; Moreau, T. *Biochimica et Biophysica Acta* **2002**, *1596*, 55.

27. Yang, C. F.; Porter, E. S.; Boths, J.; Kanyi, D.; Hsieh, M.; Cooperman, B. S. *J. Peptide Res*. **1999**, *54*, 444.

28. Schechter, I.; Berger, A. *Biochem. Biophys. Res. Commun*. **1967**, *27*, 162.

CHAPTER 11

Summary and Future Prospective

11.1. Research Summary

Main theme of this thesis is to understand and develop highly sensitive and selective biosensors based on rationally designed conjugated polymers to detect clinically important biological targets such as DNA, protein, or cancerous cells. Conjugated polymer-based biosensors have recently received wide attention due to their signal amplification property and resulting orders of magnitude higher sensitivity compared to monomeric sensors. For a feasible application of conjugated polymers to biosensors, it is indispensible to establish molecular design principles that combine receptor molecules for specific detection of target molecules with conjugated polymers for signal transduction and amplification. In addition, many molecular design parameters such as intra-/intermolecular structure in constructing a sensory film must be understood to achieve high performance solid-state biosensors.

To prove the concept of the self-signal amplifying biosensors we initially made solution versions of conjugated polymer-based DNA sensory systems. We needed a water-soluble and highly emissive conjugated polymer having a versatile functional group for bioconjugation with oligonucleotides as receptors. Developing a water-soluble fluorescent conjugated polymer has been a challenging task due to the intrinsic hydrophobic nature of the conjugated polymer backbone, which causes strong aggregation of conjugated polymers in water even after modifying conjugated polymers with ionic side chains. We have tackled this problem through a systematic molecular design strategy and established the correlation between polymer aggregation and its chemical structure (Chapter 2). Systematic study regarding completely water-soluble and strongly fluorescent conjugated polymers have been successfully proposed for bio-

conjugation by introducing alternating bulky nonionic and ionic side chains to a conjugated polymer. We also successfully developed a method to bioconjugate the water-soluble conjugated polymers to proteins and DNA by modifying the chain ends of conjugated polymers with a carboxylic acid group (Chapter 3). End-functionalized PPE, prepared by *in situ* chemical modification during polymerization, was successfully attached to a model peptide, pentatyrosine on a 4-chloro-trityl PS resin. These studies provided a promising design guideline of the facile and fast preparation method of functionalized, water-soluble, and highly fluorescent conjugated polymers for bioconjugation.

Based on this method, hybrid bio/-synthetic sensory conjugated polymers were developed to achieve selective label-free detection of target oligonucleotides with amplified fluorescence signaling in solution state (Chapter 4). Upon DNA/DNA hybridization the PPE-DNA hybrid system demonstrated efficient Förster-type energy transfer from PPE to the fluorescent dye or quencher attached to the complementary DNA. Furthermore, this conjugation technique was successfully confirmed by conjugated polymer-antibody hybrid materials and its cell-staining applications (Chapter 5). We confirmed that the conjugated polymers are biologically safe against living cells and various types of cells were selectively stained after bioconjugation between a red or blue emissive CP and human immunoglobin G. Opportunity regarding the application of a highly fluorescent and completely water-soluble conjugated polymer as a signaling reporter has been successfully addressed by utilizing the conjugation technique to any antibody as a universal biomarker in bioimaging technology.

Since a solid-state sensor has many advantages over a solution version for actual applications, we applied the design principle of the signal-amplifying DNA sensor to the development of a solid-state sensor and sensor arrays (Chapter 7). We developed a much faster and versatile fabrication strategy to make signal-amplifying DNA microarrays by developing a novel conjugated polymer and adapting the convenient on-chip DNA synthesis technique. This method allows easy and efficient detection of up to several thousand agents simultaneously in a short time with a very low false positive rate and using very small amounts of samples. Newly-designed conjugated amine functionalized conjugated polymers containing oxadiazole group played an important role in this development. The polymers were highly emissive and showed unique stability in harsh environment such as a prolonged exposure to strong UV irradiation and highly acidic environments (Chapter 6). This stability made us enable to apply the on-chip direct DNA synthesis method to the conjugated polymers. DNA detection tests showed that both good selectivity and large signal amplification were achieved by efficient FRET from the emissive conjugated polymers to the dye-labeled target DNA.

We have further developed an intercalating dye-based system and a molecular beacon system to achieve a label-free detection in the solid state. Labeling a fluorescent dye to the analyte DNA requires a chemical reaction and subsequent purification, which can be time consuming and not quite cost effective. First, we developed intercalating dye-assisted label-free DNA microarrays using a poly(oxadiazole-co-phenylene-co-fluorene) derivative and on-chip DNA synthesis technique used in previous research (Chapter 8). Specificity of an intercalating dye was not perfect and when used in a large quantity it also binds to single strand DNA. However, when only small amounts of analyte DNA are

available, the amount of intercalating dye bound to the double helix DNA is too small to be confidently detected. Adding more intercalating dye to produce a stronger signal, however, causes a specificity problem since intercalating dye also binds to single strand DNA. Our signal-amplifying DNA microarray can overcome this issue because the conjugated polymer layer harvests energy and transfers the energy to the intercalating dye, thus amplifying the emission of the dye. Based on this technique, we also have developed a molecular beacon-based DNA microarray for label-free and amplifying detection (Chapter 9). We directly synthesized hairpin-shaped single strand oligonucleotides as a probe on the poly(oxadiazole-co-phenylene-co-fluorene) derivatives and completed the synthesis by placing a quencher unit at the end of the oligonucleotide. Since the two ends of the molecular beacon are designed to make a double helix the molecular beacon forms a hairpin structure and the hairpin formation locates the quencher close to the conjugated polymers and prevents the conjugated polymers from emitting light. Upon binding with a target DNA, the hairpin opens up and moves the quencher away from the conjugated polymers which restores the strong emission of the conjugated polymers and achieves a label-free signal amplifying detection.

We also have extended this concept to prostate cancer detection in the early stage (Chapter 10). Prostate specific antigen (PSA), cancer biomarker for prostate cancer was used for a target molecule in this study. PSA is known to cleave specific peptide sequences. Therefore, such a oligo-peptide sequence with a quencher or fluorescent dye as a PSA probe was successfully synthesized on the conjugated polymer substrate to prepare label-free and self-signal amplifying PSA sensor. Well-defined surface treatment provided free PSA activity toward peptide probe on polymer-coated film. PSA assay tests

showed excellent selectivity and sensitivity by means of the sequence specific cleavage of PSA and efficient FRET from conjugated polymer to the dye or quencher at the end of the peptide sequence.

In summary, rational molecular design of highly emissive conjugated polymers having unique stability combined with efficient bioconjugation and on-chip synthesis allowed us to establish the concept of self signal-amplifying molecular biosensors and sensor arrays. The informative results obtained through the thesis work are readily applicable to many other biosensor development.

11.2. Future Consideration

Some of the topics covered in this thesis are worthy of further investigations. For example, in solid state polymer-peptide hybrid sensor for prostate cancer, we are currently inspecting the detection limit of target PSA for feasible application of clinical diagnosis. Afterwards, we are planning to examine the device performance using human patient's serum. Aggregation behavior and morphology of the conjugated polyelectrolytes are also further being investigated by electron microscope and x-ray techniques. Also, preparation of a water-soluble and red-emissive conjugated polymer as a energy accepting moiety is an ongoing research project. To achieve this goal, a luciferin derivative, an enzyme-activated self-illuminating molecule, having a functional group for conjugation is under preparation now. The covalent coupling between the conjugated polymer and a luciferin derivative will provide the conjugated polymers with a self-illuminating property without photoexcitation. This self-illuminating hybrid material

based on bioluminescence resonance energy transfer (BRET) can be used as an *in-vivo* bioimaging probe for various tumor cells.